Intérêt des peptides bi-fonctionnels dans le traitement des cancers. Application au carcinome hépatocellulaire

Eric Savier

Sorbonne Université
Ecole Doctorale ED 394
Physiologie, Physiopathologie Thérapeutique

Centre de recherche Saint Antoine INSERM UMR S-938
Equipe Maladies fibro-inflammatoires d'origine métabolique et biliaire du foie
Faculté de médecine Saint Antoine
27 rue de Chaligny, Paris 75012

Unité de Technologies Chimiques et Biologiques pour la Santé (UTCBS)
INSERM U1267 - CNRS UMR8258
Université de Paris, Faculté de Pharmacie
4 Avenue de l'Observatoire
75270 PARIS CEDEX 06, FRANCE

INTERET DES PEPTIDES BI-FONCTIONNELS DANS LE TRAITEMENT DES CANCERS. APPLICATION AU CARCINOME HEPATOCELLULAIRE

Par Eric SAVIER

Thèse de doctorat de sciences
Dirigée par :

Dr Angelita REBOLLO
Pr Olivier SCATTON

Présentée et soutenue publiquement le 14 Avril 2023

Devant le jury composé de :

Pr Chang Zhi DONG, Président
Pr Olivier ROSMORDUC, Rapporteur
Pr Jean-Charles NAULT, Rapporteur
Pr Benoit BARROU, Examinateur
Dr Angelita REBOLLO, Co-Directeur
Pr Olivier SCATTON, Co-Directeur

1 Remerciements

Avant toute chose, je remercie vivement ma directrice de thèse, le Docteur Angelita REBOLLO qui m'a entrainé dans cette aventure, m'a replongé dans la biologie et la biochimie, en jachère depuis mon DEA et mon stage à Chapel Hill (NC, USA). Sa patience et sa rigueur m'ont évité tout découragement et ont permis l'aboutissement de cette thèse, qui j'espère, ne sera qu'une première étape dans la poursuite de notre collaboration entre cliniciens et chercheurs.

Je remercie mon co-directeur de thèse, le Professeur Olivier SCATTON qui m'a encouragé dans ce retour à la science fondamentale, dans un domaine qu'il connait bien pour avoir effectué sa thèse sur les modèles de xénogreffes. Il a favorisé les prélèvements tumoraux, mis en place un mini-laboratoire, permis les échanges avec les chercheurs et l'aboutissement de ce travail.

Je remercie mon chef de service le Professeur Jean-Christophe VAILLANT, enseignant hors pair en chirurgie, qui m'a permis de faire ce travail tout en restant praticien hospitalier dans son service.

Je remercie le Professeur Pr Chang Zhi DONG, spécialiste des peptides qui a accepté de présider le jury de cette thèse, dans un domaine où sa réputation n'est plus à faire.

Je remercie les Professeurs Olivier ROSMORDUC et Jean-Charles NAULT, d'avoir accepté d'être mes rapporteurs, étant chacun parmi les plus grands spécialistes français du carcinome hépatocellulaire.

Je remercie le Professeur Benoit BARROU d'être examinateur dans mon jury. Il est l'exemple du chirurgien-chercheur, acharné et passionné, digne au plus noble sens du terme de notre mission d'enseignement, de soin et de recherche.

Je remercie Pierre TUFFERY pour avoir réalisé les analyses *in silico* de ce travail, lui donnant ainsi une dimension présente et futuriste.

Je remercie le Professeur Filomena CONTI et Lynda AOUDJEHANE qui nous ont aidés pour disposer d'hépatocytes normaux à partir de la plateforme ICAN, le Docteur Frédéric CHARLOTTE pour sa constante disponibilité pour les prélèvements d'échantillons tumoraux.

Je remercie pour leur aide constante et leur soutien mes collègues chirurgiens, anesthésistes, le personnel du bloc opératoire IBODE, IADE, le personnel du laboratoire d'anatomie pathologique de la Pitié-Salpêtrière ainsi que le personnel de l'UTCBS.

Ce travail est dédié :
A Elisabeth, mon épouse qui m'accompagne depuis toujours dans la recherche pour le meilleur et pour le pire
A Edouard & Madeleine, Alexis, Paul, Benoît, nos 4 Dalton.

Au Docteur Charles-Henri SAVIER (1929-2022), mon premier maître

Au Docteur Etienne LEVY, maître de recherche à l'INSERM, pionnier de la réanimation chirurgicale digestive à l'hôpital Saint-Antoine, que j'ai eu la chance et le bonheur de croiser au début de mes études médicales comme étudiant hospitalier, et qui, au sein d'un service hospitalier de chirurgie, dans son unité de réanimation, nous montrait comment la science fondamentale était source de progrès et compatible avec l'exercice de la médecine.

2 Résumé

2.1 Résumé en français

Les tumeurs malignes sont la première cause de mortalité dans les pays industrialisés. Parmi les tumeurs solides, le carcinome hépatocellulaire (CHC) est la 4ème cause de décès dans le monde et son incidence progresse.

Les peptides sont de courtes chaines d'acides aminés dont les propriétés biologiques peuvent être utilisées en thérapeutiques. Ainsi les peptides interférants (IP) ont la propriété de bloquer l'interaction entre 2 protéines. D'autres peptides ont la propriété de franchir les membranes biologiques ou cellulaires, les *cell penetrating peptides* (CPP), parmi lesquels certains ne pénètrent que dans les tissus tumoraux, les *tumor-penetrating peptides* (TPP). La combinaison d'un TPP avec un IP produit un peptide bi-fonctionnel (TPP-IP).

Le but de cette thèse était d'étudier l'efficacité des TPP-IP dans des modèles de leucémie lymphoïde chronique humaine (LLC), *in-vitro* et *in-vivo* et des cellules humaines de CHC.

Les résultats obtenus, publiés dans 6 articles étaient les suivants :

- A partir de protéines dont les interactions sont connues, la technique du PEPscan, peu coûteuse et rapide, permettait d'identifier des candidats IP d'une part, en nombre relativement faible d'autre part. Les résultats du PEPscan ont été comparés à des modélisations *in silico*. Sous réserve des informations structurelles disponibles sur les protéines, ces 2 méthodes sont concordantes et encourageantes.
- Le site d'interaction entre les TPP et le récepteur membranaire NRP-1 est situé sur le domaine b1 de NRP-1 par modélisation *in silico*.
- C9h est un IP qui interfère entre les protéines PP2A et Caspase 9. La constante d'affinité entre C9h et PP2A a été mesurée et était proche de la constante d'affinité entre PP2A et Caspase 9.
- Les TTP (iRGD, LinTT1, TT1 et RPARPAR) avec ou sans un IP qui bloque l'interaction entre PP2A et SET, pouvaient pénétrer dans les cellules B des patients souffrants de LLC et dans les hépatocytes de CHC et induisaient une apoptose. Inversement,

l'internalisation était minime dans les cellules B ou hépatocytes normaux. Ces 4 TPP-IP étaient faiblement dégradés dans du sérum humain. L'iRGD-IP augmentait significativement la survie dans un modèle murin de xénogreffe de LLC.

- Les 4 peptides bi-fonctionnels (iRGD-IP, RPARPAR-IP, LinTT1-IP, TT1-IP) (IP bloque l'interaction PP2A/SET) ont été testés sur des hépatocytes malins ou non et l'internalisation peptidique était corrélée de manière logarithmique à la quantité de récepteur exprimée à la surface des cellules ainsi qu'à un score d'agressivité tumorale. L'internalisation induisait une apoptose des hépatocytes malins uniquement.
- TT1-IP et LinTT1-IP prolongeaient la survie de souris immunodéficientes greffées avec une lignée tumorale humaine de LLC, mais seul TT1-IP avait un effet significatif. La captation *in-vivo* de TT1-IP fluorescent après marquage par le Cy7, était plus importante chez une souris porteuse de cellules de LLC. Dans ce modèle, RPARPAR-IP n'avait pas d'effet sur la survie. Pourtant, l'apoptose induite sur les cellules tumorales par TT1-IP, LinTT1-IP et RPARPAR-IP était comparable. Aucun effet apoptotique n'a été observé avec IP seul ou TT1 seul ou sur des cellules saines. Ces derniers résultats démontraient les rôles complémentaires du TPP et de l'IP pour obtenir une apoptose spécifique des cellules tumorales. Sur les souris immunocompétentes nous n'avons pas observé de toxicité de TT1-IP. L'injection intra-péritonéale était suivie d'une concentration plasmatique maximale atteinte en 10 minutes puis d'une clairance plasmatique avec un temps de ½ vie de 28 minutes. Dans du sérum humain, la proportion de TT1-IP détectable était de 40% après 6h d'incubation montrant ainsi sa lente dégradation par protéolyse.

En résumé, les résultats obtenus dans cette thèse laissent penser que l'utilisation de peptides thérapeutiques dans le traitement des cancers est une possibilité réelle. La perspective immédiate est de tester ces peptides bi-fonctionnels sur des modèles murins de xénogreffes de CHC dans un but de validation pré-clinique.

Mots clefs

Cancer, leucémie lymphoïde chronique, carcinome hépatocellulaire, PP2A, SET, peptide, PEPscan, souris, xénogreffe.

2.2 Bi-functional peptides : interest in the cancer treatment. Application to hepatocellular carcinoma

2.3 Summary in english

Malignant tumours are the leading cause of death in industrialized countries. Among solid tumours, hepatocellular carcinoma (HCC) is the 4th leading cause of death worldwide and its incidence is increasing.

Peptides are small amino acids chains whose biological properties can be used in therapeutics.

As their name suggests, interfering peptides (IP) interfere between two proteins. Other peptides, named cell penetrating peptides (CPP), have the property of crossing biological or cellular membranes. In addition, some CPPs penetrate tumor tissues only and are therefore called tumor-penetrating peptides (TPP). The combination of a TPP with an IP produces bi-functional peptides (TPP-IP).

The purpose of this thesis was to study the efficacy of TPP-IP in models of human chronic lymphoid leukemia (CLL), *in-vitro* and *in-vivo* and human HCC cells.

The results were published in 6 articles, as follows:

- From proteins whose interactions are known, the PEPscan technique, inexpensive and fast, made it possible to identify a relatively small number of IP candidates. PEPscan results were compared to an *in silico* modelling system. Subject to the available structural information about proteins, these two methods are consistent and encouraging.
- The site of interaction between TPP and the NRP-1 membrane receptor is located on the b1 domain of NRP-1 through *in silico* modelling.
- C9h is an IP that interferes between PP2A and Caspase 9 proteins. The affinity constant between C9h and PP2A was measured and was close to the affinity constant between PP2A and Caspase 9.
- TTPs (iRGD, LinTT1, TT1, and RPARPAR) with or without an IP that blocks the interaction between PP2A and SET, were internalized into the B cells of patients with

CLL and HCC hepatocytes and induced apoptosis. Conversely, internalization was minimal in normal B cells or hepatocytes. These 4 TPP-IPs were weakly degraded in human serum. iRGD-IP significantly increased survival in a murine xenograft model of LLC.

- The 4 bi-functional peptides (iRGD-IP, RPAR-IP, LinTT1-IP, TT1-IP) (IP blocked the PP2A/SET interaction) were tested on malignant or non-malignant hepatocytes and peptide internalization was logarithmically correlated with the amount of receptor expressed on the cell surface as well as with tumor aggressiveness score. Internalization led to apoptosis of malignant hepatocytes only.
- TT1-IP and LinTT1-IP (IP blocked the PP2A/SET interaction) extended the survival of immunodeficient mice grafted with a human LLC tumour line, but only TT1-IP had a significant effect. *In vivo* uptake of fluorescent Cy7 labelled TT1-IP was greater in a mouse with CLL cells. In this model, RPARPAR-IP had no effect on survival. However, tumour cell-induced apoptosis by TT1-IP, LinTT1-IP and RPARPAR-IP was similar. No apoptotic effect was observed with IP alone or TT1 alone or on healthy cells. This last result demonstrated the complementary roles of TPP and IP in achieving specific tumor cell apoptosis. In immunocompetent mice, no toxicity of TT1-IP was observed. Following an intraperitoneal injection, the plasma concentration reached a maximum peak within 10 minutes before a plasmatic clearance of 28 minutes half-time life. In human serum incubation, 40% of TT1-IP was detectable after 6h showing its slow degradation by proteolysis.

In summary, the results obtained in this thesis suggest that the use of therapeutic peptides in cancer treatment is a real possibility. The immediate prospect is to test these bi-functional peptides on a HCC murine xenograft models for pre-clinical validation.

Key words

Cancer, cancer targeting, liver cancer, hepatocellular carcinoma, chronic lymphocytic leukemia, interfering peptides, tumor-penetrating peptides, PEPscan, PP2A, SET, mouse, xenograft.

3 Sommaire

3.1 Table des matières

3.2 Liste des figures

3.3 Liste des articles en PDF

3.4 Liste des annexes

3.5 Liste des abréviations

Acronyme	Signification
AA	Acide aminé
ABM	Agence de la biomédecine
AC	Anticorps
AFP	α- foeto-protéine
AG	Acides gras
Ag HBs	Antigène de surface du VHB
AKT	Protein kinase B
Aldob	fructose 1-6 biphosphonate aldolase B
ASIR	age-standardized incidence rate
ASR	Age-standardized incidence rate
BCLC	Barcelona clinic for liver cancer
CHC	Carcinome hépatocellulaire
CPP	Cell penetrating peptide
Cycle TCA	Cycle acide tricarboxylique
DHAP	Dihydroxyacétone phosphate
ECM	Extracellular matrix
EMT	epithelial-mesenchymal transition
FGF	fibroblast growth factor
FLC	Fibrolamellar carcinoma
FMOC	Fluorénylméthoxycarbonyle
GSK3ß	Glycogène synthase kinase 3ß
HAPB1	Hyaluronic acid binding protein 1 (p32)
HAS	Haute autorité de santé
HGF	Hepatic growth factor
HK	Hexokinase
HTA	Hypertension artérielle
I2PP2A	Inhibiteur 2 de la protéine phosphatase 2A (SET)
ICAN	Institute of Cardiometabolism and Nutrition
ICI	immune-check point inhibitor
IHC	Immunohistochemistry
KEAP1	Kelch-like ECH-associated protein 1
LI-RADS	Liver Imaging Reporting and DataSystem
LLC	Leucémie lymphoïde chronique
LMC	Leucémie myéloïde chronique
MAP	Mitogen-activated protein
MELD	Model of end-stage liver disease
miRNA	microRNA
MOF	Maximally overlapping fragment
MTOR	mecanistic target of rapamycine
NAFLD	Non-alcoholic fatty liver disease
NASH	Non-alcoholic steatohepatitis
NRF2	Nuclear factor erythroid 2-related factor 2
NRP-1	Neuropilin-1 (récepteur)
PD-1	Programmed (cell) death protein 1

PDK1	Kinase 1 dépendante de l'ositide phosphoïne
PD-L1	Programmed death-ligand 1
PEG	Polyéthylène glycol
PHAPII	Putative histocompatibility leukocyte antigen class II-associated protein II
PI3K	phosphoinositide 3-kinase
PP2A	Protein phosphatase 2A
PPI	Protein-protein interaction
RAF	Rapidly Accelerated Fibrosarcoma
RAS	Rat Sarcoma
SMAP	Small-molecule activator of PP2A
TCGA	The Cancer Genome Atlas
TERT	Telomerase reverse transcriptase
TGF-β	Transforming growth factor β
TH	Transplantation hépatique
TKI	Tyrosine kinase inhibitor
TP53	Tumor protein 53
TPP	Tumor penetrating peptide
VEGF	Vascular endothelial growth-factor
VEGFR	Vascular endothelial growth-factor receptor
VHB	Virus de l'hépatite B
VHC	Virus de l'hépatite C
VHD	Virus de l'hépatite Delta
VIH	Virus de l'immunodéficience humaine
VLDL	Very low density lipoprotein

4 Introduction

Les cancers sont la première cause de mortalité, en particulier dans les pays développés (Sung *et al*, 2021). L'incidence dans ces pays devrait encore augmenter en raison de l'âge grandissant des populations et de l'importance des facteurs de risque (Vogelstein *et al*, 2013). La plupart des cancers sont secondaires à des altérations génétiques (Vogelstein *et al*, 2013) qui vont modifier les fonctions des protéines, donc des cellules. Elles vont finir par se multiplier sans contrôle avec la capacité de migrer et de s'implanter à distance sous forme de métastase. Ce processus aboutit à la mort de l'individu.

Pour contrôler la maladie cancéreuse, les axes thérapeutiques sont les suivants : prévention, dépistage et traitements à visée curative qui s'accompagnent d'effets secondaires. Les traitements incluent l'exérèse chirurgicale pour les tumeurs solides, la destruction locale par des agents physiques ou des radiations ionisantes, la destruction des cellules malignes par des drogues cytotoxiques (chimiothérapie) ou leur contrôle par des traitements hormonaux et plus récemment *via* le système immunitaire (immunothérapie).

L'objet de cette thèse concerne une nouvelle approche thérapeutique : l'utilisation de peptides qui vont interférer avec les voies métaboliques désorganisées par la maladie cancéreuse. Nous y reviendrons après quelques généralités sur le carcinome hépatocellulaire, également objet de cette thèse.

4.1 Carcinome hépato-cellulaire

Les cancers du foie sont en augmentation globale dans le monde et l'on estime qu'ils devraient concerner plus d'1 million de personne par an en 2025 (Sung *et al*, 2021). Le carcinome hépato-cellulaire (CHC) représente environ 90% des tumeurs primitives du foie et a plusieurs caractéristiques que nous développerons succinctement : épidémiologie, physiopathologie, diagnostic et traitement.

Epidémiologie du CHC

Le CHC est le 6ème cancer dans le monde, avec 841 080 nouveaux cas en 2018 et la 4ème cause mondiale de mortalité par cancer (Sung *et al*, 2021). Les taux d'incidence et de

mortalité les plus élevés sont observés en Asie de l'Est et en Afrique (Figure 1), bien que l'incidence et la mortalité des CHC augmentent dans différentes parties de l'Europe et aux États-Unis (McGlynn *et al*, 2015). Le CHC est la cause de décès par cancer qui progresse le plus rapidement aux États-Unis depuis le début des années 2000 et il devrait devenir la 3ème cause de décès par cancer d'ici 2030, si ces tendances se maintiennent (Rahib *et al*, 2014).

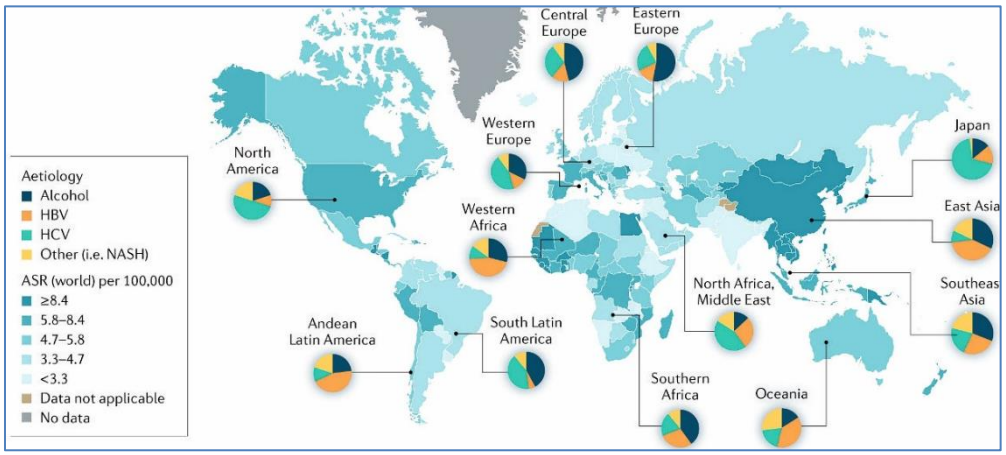

Figure 1: Incidence géographique et principaux facteurs étiologiques des carcinomes hépatocellulaires (CHC)

La plus forte incidence de CHC est observée en Asie de l'Est, la Mongolie présentant la plus forte incidence de CHC dans le monde. Le virus de l'hépatite B (VHB) est le principal facteur étiologique dans la plupart des régions d'Asie (sauf Japon), d'Amérique du Sud et d'Afrique; le virus de l'hépatite C (VHC) est le facteur causal prédominant en Europe occidentale, en Amérique du Nord et au Japon. La consommation d'alcool est le facteur étiologique en Europe centrale et orientale. La stéatohépatite non alcoolique (NASH), la principale étiologie incluse dans la catégorie « Other », est un facteur de risque qui augmente rapidement et qui devrait devenir la principale cause de CHC dans les régions à revenus élevés dans un proche avenir. ASR : age-standardized incidence rate. D'après Bray et al*, 2018; Llovet* et al*, 2021; Singal* et al*, 2020.*

En France, l'incidence annuelle en 2018 était de 12,5/100 000 chez l'homme et 2,5/100 000 chez la femme (rapport InVS 2020 http://lesdonnees.e-cancer.fr/). Le nombre de nouveau cas était estimé à 10 580 cas en 2018 et était en augmentation depuis 1980. L'augmentation de l'incidence est expliquée par l'épidémie d'hépatite C entre 1990 et 2015 (Global Burden of Disease Liver Cancer Collaboration *et al*, 2017), l'augmentation des cas de syndrome métabolique (Welzel *et al*, 2011) et par l'amélioration du dépistage (Costentin *et al*, 2018).

Physiopathologie et mécanismes d'apparition du CHC

Une particularité centrale du CHC est qu'il est lié à une inflammation chronique du foie, elle-même responsable de processus cicatriciels fibrosants, qui au long des années constituent

une cirrhose. C'est habituellement à ce stade (75-80% des CHC) que se développe le CHC avec des mécanismes de carcinogénèse multiples et intriqués (Figure 2) (D'souza *et al*, 2020; Mohr *et al*, 2021; Seen, 2021; Taniai, 2020). L'apparition d'un CHC au stade d'hépatite chronique non cirrhotique est possible, surtout en cas de NASH (Ioannou, 2021) mais cette éventualité est plus rare. Rappelons que le CHC sur foie sain est exceptionnel.

Les facteurs d'agression chronique du foie sont importants à connaître parce qu'ils influencent le dépistage, la prévention, la surveillance et la répartition géographique (Figure 1). Il s'agit principalement de la consommation excessive d'alcool, d'une NASH liée à un diabète ou une obésité, d'une infection par le VHB ou le VHC. Les autres facteurs de risque sont la surinfection par l'hépatite virale Delta (HDV) chez un patient porteur de l'antigène de surface du VHB (Ag HBs), l'âge (> 70 ans)(Rich *et al*, 2020), le sexe masculin (2 à 3 homme pour 1 femme), certaines ethnicités (hispanique) (Rich *et al*, 2019), certains toxiques (aflatoxine), les cholestases chroniques, des maladies génétiques héréditaires (hémochromatose, déficit en α1 anti-trypsine), le tabac (Lee *et al*, 2009). Inversement, d'autres facteurs pourraient être protecteurs comme le café ou l'aspirine (Bravi *et al*, 2013).

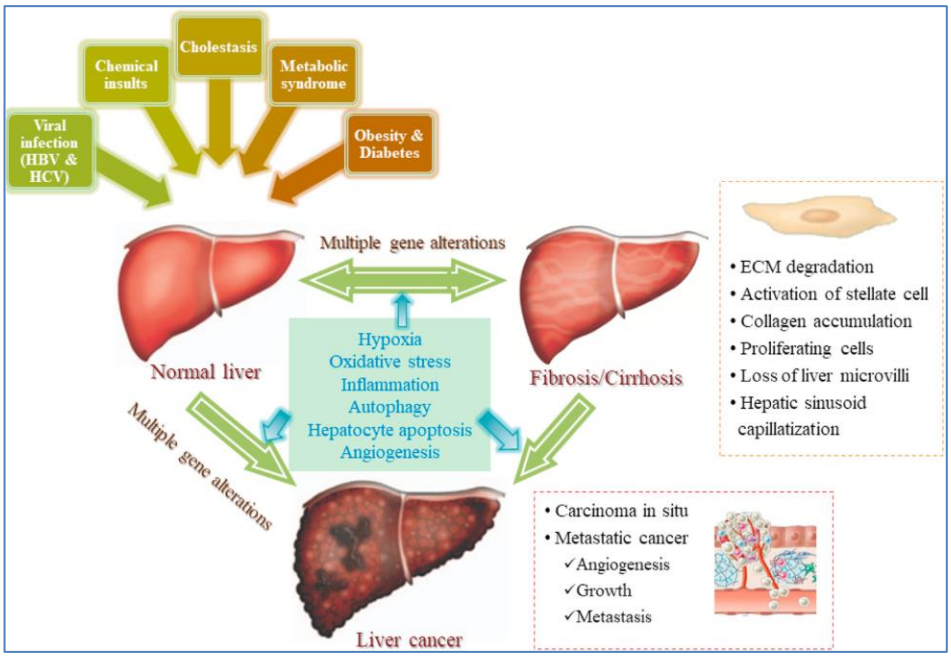

Figure 2: Représentation schématique des facteurs de risque et mécanismes d'apparition des CHC

Sous l'effet de facteur d'agression chronique des cellules hépatiques, une inflammation chroniques se pérennise et aboutit à une fibrose d'intensité croissante jusqu'au stade de cirrhose. Ce processus favorise l'apparition de cellules cancéreuses. Bien que plus rare, le passage rapide du foie normal au cancer est possible. EMC : Extracellular matrix. D'après Man et al, 2021.

Les dernières avancées dans le domaine, stimulées par l'épidémie de CHC associés aux maladies graisseuses du foie (NAFLD pour non-alcoholic fatty liver disease) font intervenir

dans la carcinogénèse la contribution de l'inflammation (NASH pour non-alcoholic steatohepatitis), de la cirrhose mais également du microenvironnement cellulaire, du système immunitaire (Figure 3) (Friedman *et al*, 2018).

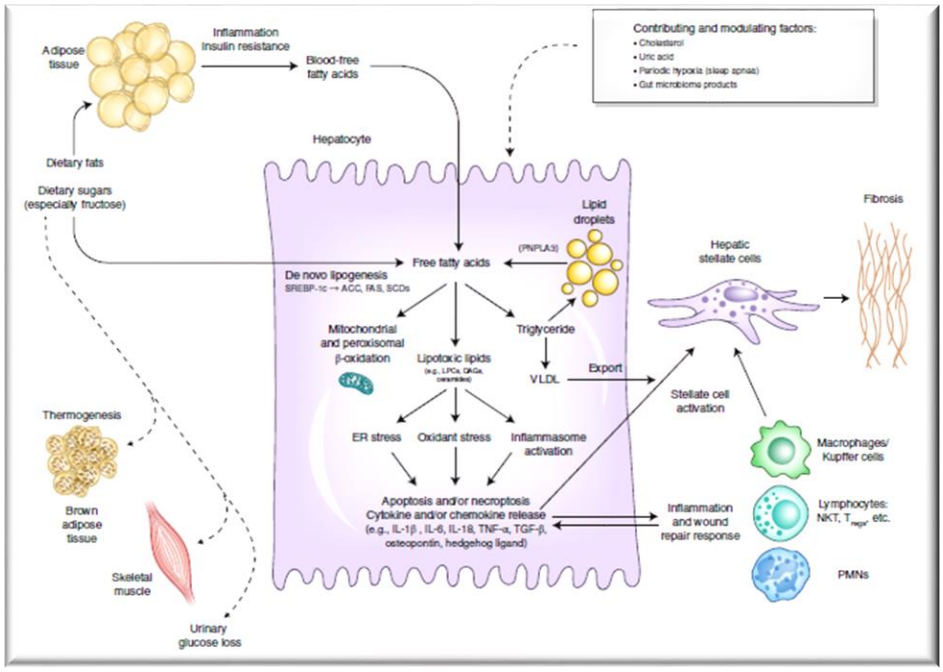

Figure 3: Représentation schématique de la pathogénie de la NAFLD.

Les acides gras libres qui proviennent de la lipolyse des triglycérides dans les tissus adipeux sont libérés dans le sang et captés par le foie. Une autre source majeure du flux d'acides gras (AG) sont les glucides en excès, en particulier le fructose, qui sont convertis en AG dans l'hépatocyte. Les deux grandes destinations des AG sont la bêta-oxydation mitochondriale et le stockage sous forme de gouttelette lipidique ou l'export sanguin sous forme de VLDL. Les triglycérides des gouttelettes de lipides subissent également une lipolyse régulée qui libère des AG dans d'hépatocytes. Le gène PNPLA3 intervient dans ce processus lipolytique. Une variante nucléotidique unique du PNPLA3 est fortement associée à la progression du NASH, ce qui souligne l'importance de la régulation de cette lipolyse. Lorsque l'élimination des acides gras par bêta-oxydation ou formation de triglycérides est dépassée, les acides gras peuvent contribuer à la formation d'espèces lipotoxiques qui entraînent le stress du reticulum endoplasmic, un stress oxydant et l'activation d'inflammasomes. Ces modifications sont responsables du phénotype de NASH avec lésion hépatocellulaire, inflammation, activation des cellules stellaires et accumulation progressive de matrice extracellulaire en excès. Les modifications du mode de vie qui comprennent des habitudes alimentaires saines et l'exercice régulier détournent les substrats métaboliques vers les tissus métaboliquement actifs et peuvent ainsi prévenir ou inverser la NASH. (Friedman et al*, 2018). Schéma : Marina Corral Spence/Springer Nature*

Principales altérations génétiques somatiques du CHC et classification

Les principaux gènes impliqués dans la cancérogenèse hépatique ont un impact sur 6 voies biologiques clefs (Campani *et al*, 2023) :

1. les mutations TERT (*Telomerase reverse transcriptase*) sont observées dans 60% des cas. La maintenance des télomères favorise l'immortalisation cellulaire ;
2. la dérégulation de la voie Wnt/β-caténine, secondaire à la mutation CTNNB1 (20-30%), est responsable d'une accumulation de β-caténine nucléaire, qui active des gènes de prolifération. CTNNB1 est plus fréquente avec l'abus d'alcool ;
3. la dérégulation du cycle cellulaire par mutation de TP53 (*tumor proteine 53*) (20-50%) conduit à une prolifération cellulaire et une résistance à l'apoptose. Elle est plus fréquemment associée au VHB ;
4. la dérégulation épigénétique intervient par modification de l'expression des gènes par divers mécanismes, notamment le remodelage de la chromatine, les modifications des histones et de la méthylation ;
5. une inflammation chronique ou une exposition à des agents cancérigènes expose les hépatocytes à un stress oxydatif. Le facteur 2 lié au NRF2 (nuclear factor erythroid 2-related factor 2), codé par NFE2L2 et l'activation de la voie KEAP1 (kelch-like ECH-associated protein 1) jouent un rôle clef dans la protection des cellules contre le stress oxydatif. Des mutations activatrices de NFE2L2 et des mutations inactivatrices de KEAP1 sont retrouvées dans environ 6 % et 4 % des CHC et confèrent aux cellules cancéreuses un avantage de résistance au stress oxydatif par l'inhibition de la dégradation médiée par KEAP1 de NRF2 (Zucman-Rossi *et al*, 2015). Une association significative entre NFE2L2 et KEAP1 et des mutations CTNNB1 ou AXIN1 a été décrite, suggérant que les réponses au stress oxydatif pourraient coopérer avec la voie Wnt/β-caténine pour favoriser la carcinogenèse hépatique ;
6. l'activation des voies RAS/RAF/MAP kinase et PI3K/AKT/MTOR. Les protéines RAF (*Rapidly Accelerated Fibrosarcoma*) / RAS (*Rat Sarcoma*) / MAP (*Mitogen-activated protein*) kinase et la voie PI3K (*phosphoinositide 3-kinase*) / AKT (*protein kinase B*) / MTOR (*mecanistic target of rapamycine*) sont activées en environ 5 à 10 % des CHC (Zucman-Rossi *et al*, 2015). L'activation de la voie RAF/RAS/MAP kinase favorise la prolifération cellulaire. Les mutations associées sont des mutations de RAS ou de

RPS6KA3 (*Ribosomal Protein S6 Kinase*) (2 à 10 %) (Nault *et al*, 2020). Les mutations activatrices de PIK3CA (*phosphatidylinositol-4,5-bisphosphate 3-kinase, catalytic subunit alpha*) (2 %), les mutations inactivatrices de TSC1 ou TSC2 (3–8 %) et la délétion homozygote de PTEN (2 –3 %) favorisent l'activation permanente de la voie AKT/MTOR (Nault & Zucman-Rossi, 2011). Les mutations TSC2 surviennent souvent en même temps que les mutations TP53 (Campani *et al*, 2023).

Enfin, le VHB peut entraîner la surexpression d'oncogènes, mais peut également déclencher des réarrangements chromosomiques entraînant des altérations génétiques à distance (Péneau *et al*, 2022).

Au total, sur la base des résultats de la génomique, de la transcriptomique et de l'épigénétique, les CHC sont classés en 2 grandes classes : la classe prolifération et la classe non-prolifération (Annexe 1). Les retombées cliniques des altérations génétiques, permettent également d'orienter certaines stratégies thérapeutiques comme pour les adénomes hépatocellulaires (Nault *et al*, 2017, 2022). Cependant, en plus des variations du type de CHC d'un patient à l'autre, il faut rajouter une hétérogénéité intratumorale, c'est-à-dire, qu'au sein de la même tumeur coexistent différentes populations cellulaires avec des caractéristiques biologiques différentes. Par conséquent, une simple biopsie peut ne pas permettre d'appréhender toute les facettes d'un processus tumoral et limiter ainsi la pertinence des choix thérapeutiques. L'intérêt de mesurer les marqueurs circulants, tels que les acides nucléiques tumoraux circulants, les cellules tumorales circulantes (CTC), l'ARNm, le microARN et les exosomes, permettrait d'avoir une approche globale des signatures tumorales et pourrait permettre de contourner ces hétérogénéités (Campani *et al*, 2023).

Diagnostic et traitements du CHC

Le CHC est l'une des rares tumeurs pour laquelle le diagnostic morphologique peut suffire à décider d'un traitement. Les critères d'imagerie ont été standardisés par le système LI-RADS (Liver Imaging Reporting and DataSystem)(Santillan *et al*, 2018) et doivent être validés en réunion de concertation pluri-disciplinaire spécialisée (Bruix *et al*, 2005). Le diagnostic de CHC est complété par un diagnostic d'extension de la maladie tumorale, par une évaluation de l'hépatopathie sous-jacente et par une évaluation globale du patient et de ses comorbidités. Au terme de cette évaluation, il est possible de classer les patients. Ces

classifications permettent d'élaborer des recommandations et des algorithmes de décision thérapeutiques (Blanc *et al*, 2021; Llovet *et al*, 2021; Reig *et al*, 2022) (Figure 4 et Figure 5).

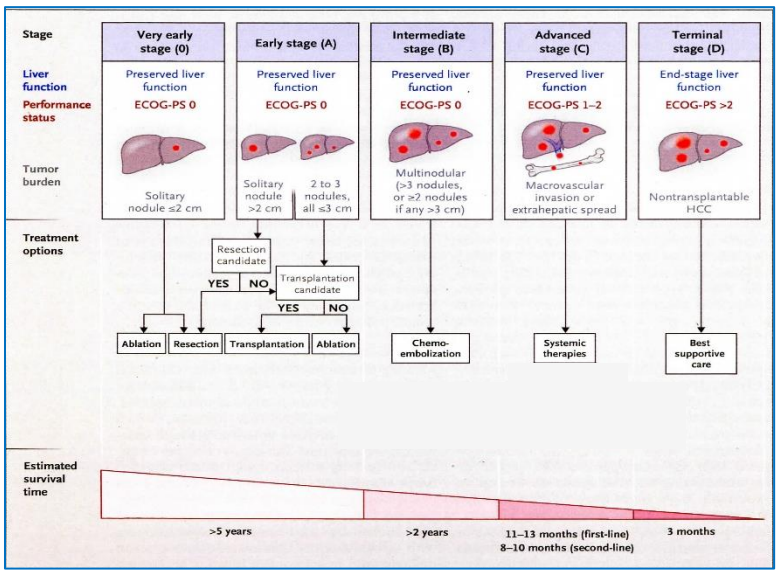

Figure 4: Schéma de prise en charge thérapeutique des carcinomes hépatocellulaires

Cet algorithme est basé sur celui du BCLC (Barcelona Clinic Liver Cancer) qui classe les patients en 5 stades et sur les recommandations de l'European Association for the Study of the Liver. La survie est estimée pour chacun des stades lorsque le traitement recommandé est appliqué. D'après Villanueva, 2019.

Le meilleur traitement est bien sûr la prévention, par la suppression de l'agression virale, l'arrêt de l'alcool, le contrôle des anomalies métaboliques. Cependant, au stade de cirrhose, le risque de CHC persiste et seul le dépistage de petits CHC (± 2cm) permet d'obtenir de bons résultats thérapeutiques avec un bon rapport coût/efficacité (Cadier *et al*, 2017). En cas d'hépatopathie non-cirrhotique les recommandations restent débattues (Costentin & Nahon, 2021; Poynard *et al*, 2019).

Les traitements non médicamenteux sont très efficaces mais ils s'adressent à un nombre limité de patients, parce qu'ils sont indiqués aux stades précoces ou intermédiaires de la maladie tumorale (Figure 4). Ainsi, les patients asymptomatiques avec une faible charge tumorale et une bonne fonction hépatique (BCLC 0 ou A) doivent être traités par des traitements curatifs locaux (résection ou destruction locale selon la présence d'une hypertension portale, le nombre de nodules et la fonction hépatique). Les indications de transplantation hépatique pour CHC sont avant tout guidées par l'extension tumorale et le taux d'α-foeto-protéine, résumés par le score alpha (Duvoux *et al*, 2012).

Les traitements médicamenteux non-systémiques sont destinés aux patients asymptomatiques présentant un CHC multinodulaire et une fonction hépatique adéquate (BCLC B). Il s'agit de la chimioembolisation ou de la radioembolisation.

Les patients ayant une thrombose portale tumorale ou une propagation extrahépatique (BCLC C) doivent être traités par des thérapies systémiques. Les traitements systémiques peuvent être classés en 3 groupes : les inhibiteurs de tyrosine kinase (TKI), les thérapies ciblées dirigées (anticorps dirigés contre le récepteur du VEGF) et les inhibiteurs des points de contrôle immunologique (ICI pour *immune-check point inhibitor*) (anticorps anti-CTA4, anti-PD1, anti-PDL1). Les mécanismes d'action et les schémas thérapeutiques récents sont illustrés en Annexe (Annexe 2).

L'avènement des ICI pour les CHC avancés a élargi les indications des traitements systémiques en raison de leur relative efficacité et de leur bonne tolérance par rapports aux TKI. Cependant, en monothérapie les taux d'événements indésirables liés aux traitements par ICI et de grade 3 à 4 variaient de 18% à 22 % (Finn *et al*, 2020b; Yau *et al*, 2019) et montaient à 37% en association (Finn *et al*, 2020a). Avec les ICI, une toxicité par activation du système immunitaire peut survenir dans n'importe quel système d'organes, allant d'événements légers et gérables comme les éruptions cutanées, les douleurs articulaires ou l'hypothyroïdie, à des événements graves et potentiellement mortels comme une pneumopathie, une entérocolite ou myocardite (Sangro *et al*, 2020). Un argument plus récent en faveur des ICI par rapport aux TKI est le rapport coût/bénéfice favorable (Gaugain *et al*, 2023). Actuellement, les traitements systémiques de première ligne sont donc de type atezolizumab/bevacizumab ou durvalumab/tremelimumab. Les traitements de seconde lignes ou les alternatives en cas de contre-indication sont les TKI et/ou des anti CTL4 (Figure 5).

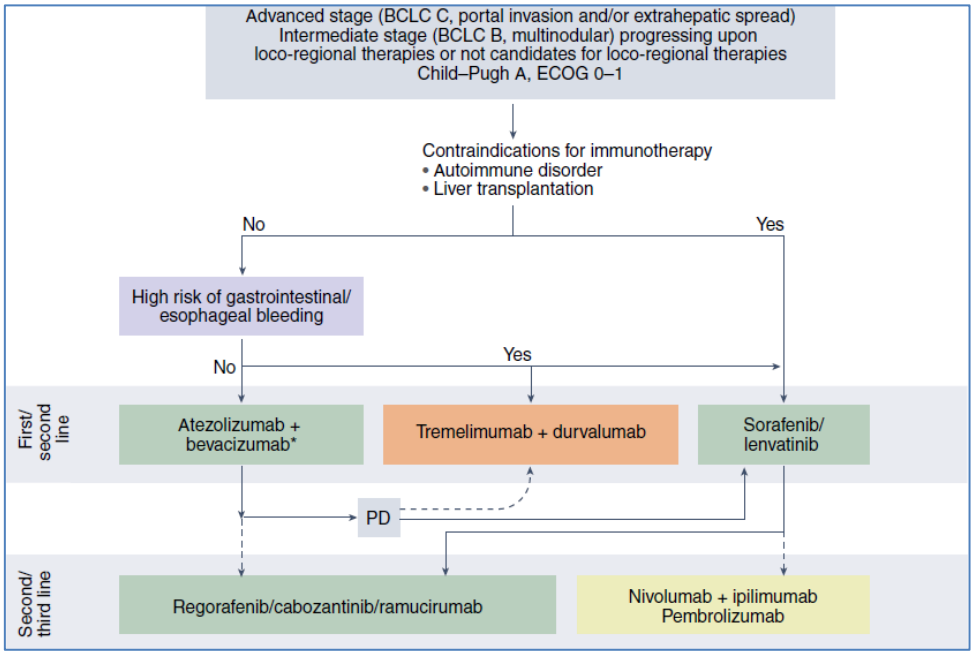

Figure 5: Stratégie de traitement du CHC avec des thérapies systémiques

En vert, traitements approuvés par les organismes de réglementation basés sur des études de phase III. En orange, combinaisons positives versus sorafenib. En jaune, les traitements qui ont reçu l'approbation accélérée de la FDA sur la base d'études de phase II. PD : progressive disease. D'après (Llovet et al*, 2022).*

Dans tous les cas, en dehors des coûts des traitements (anticorps monoclonaux), deux éléments limitent l'utilisation de ces molécules : leurs effets secondaires en particulier chez les patients ayant un désordre immunitaire (maladie ou traitement immunosuppresseur) et l'altération de la fonction hépatique (ictère, hypertension portale à haut risque de complication).

4.2 Les peptides thérapeutiques

Un peptide est une courte chaine d'acides aminés (< 50) (Annexe 3). Les protéines sont des macromolécules également constituées d'acides aminés qui assurent une multitude de fonctions au sein des cellules : protéines enzymatiques qui catalysent les réactions chimiques de synthèse et de dégradation nécessaires au métabolisme de la cellule, protéines structurelles au sein du cytosquelette (actine, collagène). Certaines sont des moteurs moléculaires qui permettent la mobilité (myosine), d'autres sont impliquées dans le conditionnement de l'ADN (histones), la régulation de l'expression génétique (facteurs de transcription), le métabolisme énergétique (ATP synthétase) ou encore la transmission de signaux cellulaires (récepteurs membranaires, hormones). Les peptides peuvent interagir avec les protéines et cette propriété débouche sur de nouvelles perspectives thérapeutiques

(Bidwell & Raucher, 2009; Hayashi *et al*, 2012). Ce sont les peptides interferants (IP pour *interering peptide*) (Figure 6).

Figure 6: Représentation schématique de l'effet d'un peptide interférant (IP) ciblant une interaction protéine-protéine (IPP).

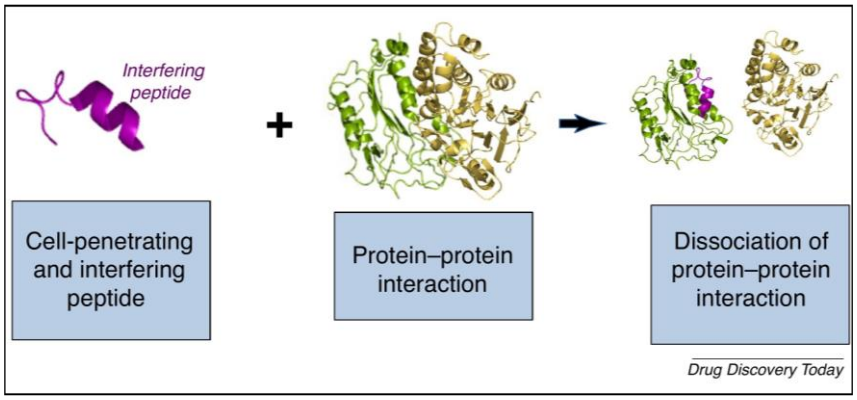

Un IP est un peptide qui peut affecter spécifiquement l'interaction normale entre deux protéines. Dans la plupart des cas, l'utilisation d'une IP entraîne la modulation d'une voie de signalisation. D'après Bruzzoni-Giovanelli et al*, 2018.*

Peptides anti tumoraux

Les peptides pénétrant dans les cellules (CPP pour *cell penetrating peptide*) sont apparus comme une nouvelle classe de vecteurs qui permettent la « délivrance » de biomolécules à travers les barrières biologiques. En fait, ils sont largement utilisés pour l'administration intracellulaire de diverses molécules, notamment des médicaments, des peptides, des protéines, des gènes et des nanoparticules. Cependant, l'un des freins à l'utilisation clinique des CPP est leur sensibilité à la dégradation par des protéases. Pour surmonter ce problème, différentes stratégies ont été élaborées, notamment la substitution des acides aminés lévogyres par des dextrogyres, la cyclisation et la stabilisation de l'hélice par agrafage peptidique (peptides agrafés ou *stappled peptides*).

Un second frein associé à l'administration systémique de médicaments par CPP est le manque de spécificité. Une méthode attrayante pour augmenter l'indice thérapeutique d'un médicament consiste à délivrer spécifiquement la molécule thérapeutique sous sa forme active non seulement dans le tissu ciblé, mais plus précisément dans la cellule ciblée et encore plus précisément dans l'organite cellulaire. Cette thérapeutique intracellulaire assurerait une efficacité «optimale ». Si l'on considère les chimiothérapies anticancéreuses, un défi majeur est de délivrer des médicaments exclusivement aux cellules tumorales tout en épargnant les cellules normales. Une sous-classe de peptides, les peptides pénétrant dans la tumeur (TPP pour *tumor penetrating peptide*) peut être utilisée pour augmenter

l'administration de médicaments, d'agents d'imagerie et de nanoparticules dans les tumeurs.

Pour cette thèse nous avons utilisé 2 types de peptides combinés, chacun ayant une fonction propre, d'où le titre de peptide bi-fonctionnel. Nous décrirons successivement 1) les TPP utilisés 2) les protéines cibles (PP2A et SET) du peptide interférant IP (IP pour *interfering peptide*) et 3) la méthode dite PEPscan utilisée pour isolée l'IP en question.

Peptides pénétrants les tumeurs (TPP)

Les peptides pénétrant dans la tumeur sont définis par la présence du motif C-end rule (CendR) avec le consensus R/KXXR/K (R-Arg ou K-Lys suivi de 2 acide aminés quelconques puis à nouveau de R-Arg ou K-Lys). Ce motif doit être démasqué en C-terminal pour permettre la liaison au récepteur de pénétration cellulaire neuropilin-1 (NRP-1) (Teesalu *et al*, 2009; Zanuy *et al*, 2013). NPR-1 est surexprimé dans le système vasculaire tumoral et dans diverses cellules tumorales, y compris les cellules tumorales péritonéales, *in vitro* et *in vivo* (Braun *et al*, 2016; Simon-Gracia *et al*, 2016; Sugahara *et al*, 2015b). La liaison du peptide CendR à NRP-1 active une voie de transport qui ressemble à de la macropinocytose mais qui en est différente mécanistiquement et qui entraîne la distribution des charges utiles profondément dans le parenchyme tumoral (Figure 7)(Pang *et al*, 2014).

Figure 7: Le peptide CendR déclenche un processus d'endocytose dépendant du NRP1 et qui ressemble à une macropinocytose.

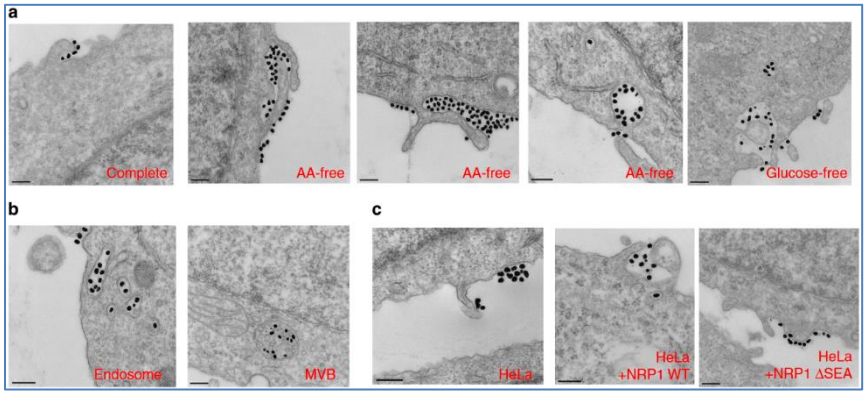

Microscopie électronique à transmission. (a) Culture pendant 16 h de cellules de la lignée de cancer de prostate PPC1 dans des milieux complets, sans acide-aminé (AA) ou sans glucose afin d'augmenter la captation, suivie par l'incubation avec des nanoparticules d'or recouvertes de peptide RPARPAR (R-Au) (points denses, 50 nm) pendant 30 min. (b) organites intracellulaires contenant du R-Au avec des caractéristiques d'endosome et de corps multivésiculaire (MVB). (c) Dépendance NRP1 de l'endocytose CendR. Des cellules HeLa, qui n'expriment pas naturellement NRP1, ont été transfectées avec des plasmides exprimant le type sauvage (WT) de NRP1, ou le mutant NRP1 DSEA (DSEA) où la séquence d'interaction GIPC1/synectine est absence, ce qui

bloque l'entrée de R-Au dans les cellules ont été incubées avec R-Au pendant 30 minutes avant la fixation. Barre d'échelle, 200 nm. D'après Pang et al*, 2014.*

Le premier peptide pénétrant dans la tumeur, iRGD (internalizing RGD, séquence: CRGDKGPDC), a été identifié par phage display *in vivo* sur des modèles de xénogreffes métastatiques de cancer de la prostate chez la souris (Sugahara *et al*, 2009). L'iRGD pénètre dans le tissu tumoral à l'aide d'un mécanisme en plusieurs étapes (Figure 8) :

(1) l'iRGD est recruté dans les vaisseaux tumoraux par l'interaction de son motif RGD avec les intégrines αvβ3 et αvβ5 sur les cellules tumorales et les cellules endothéliales tumorales ;

(2) Le peptide est ensuite scindé par une protéase liée à la tumeur ce qui expose en position C-terminale le motif CendR actif, CRGDK;

(3) le fragment CRGDK de iRGD se lie ensuite à NRP-1 pour déclencher une cascade de transcytose qui conduit à une pénétration profonde du peptide dans le tissu tumoral. Il est important de noter que pour la pénétration tumorale, la cargaison n'a pas besoin d'être conjuguée à l'iRGD : le peptide augmente l'accumulation et la pénétration des médicaments et des macromolécules co-administrés avec l'iRGD - un phénomène connu sous le nom d'effet de proximité (Sugahara *et al*, 2010).

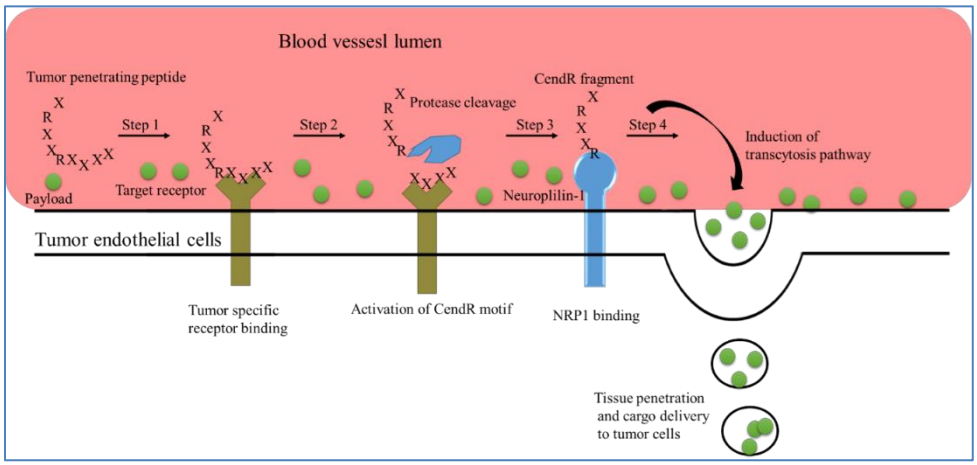

Figure 8: Transport trans-tissulaire par la voie CendR.

La voie de pénétration cellulaire et tissulaire du TPP est basée sur un processus en trois étapes. 1) le peptide se fixe sur les récepteurs cibles primaires spécifiques à la tumeur (par exemple, αvβ3/αvβ5 integrin dans le cas d'iRGD; p32/gC1qR dans le cas de LyP-1 et TT1). 2) le peptide est clivé par des protéases pour démasquer l'élément CendR cryptique (R/KXXR/K) en C-terminal. Enfin, le motif CendR interagit avec la neuropiline-1 (NRP-1) pour déclencher la pénétration des tissus vasculaires et tumoraux. D'après Lingasamy & Teesalu, 2021.

La surexpression des récepteurs iRGD (intégrines et NRP-1) dans les tissus malins et la capacité de l'iRGD à pénétrer directement dans les tumeurs par voie non vasculaire (Sugahara *et al*, 2009, 2010) rendent l'iRGD bien adapté à l'administration de précision. Dans le modèle de xénogreffe de cancer gastrique MKN-45P, l'iRGD administré par voie intrapéritonéale a potentialisé la pénétration tumorale et l'activité anticancéreuse de la doxorubicine libre co-administrée (Sugahara *et al*, 2015b). La co-administration d'iRGD a augmenté l'accumulation intra-tumorale de doxorubicine d'environ 2,5 fois, alors qu'elle n'a eu aucun effet sur les organes normaux. L'effet iRGD sur l'accumulation tumorale et la pénétration de la doxorubicine était indépendante de la circulation, suggérant que les tumeurs péritonéales petites et mal vascularisées sont directement ciblées (Sugahara *et al*, 2015a).

Une autre technologie très prometteuse pour l'administration ciblée de tumeurs, en particulier pour les charges utiles d'acide nucléique, est celle des nanoparticules de liposomes cationiques guidés par des peptides. Ainsi, chez des souris porteuses d'une carcinose péritonéale dérivée d'une tumeur gastrique humaine MKN-45P, des liposomes cationiques stabilisés par du polyéthylène glycol (PEG) avaient une certaine accumulation dans la tumeur. Cependant, si cRGD et iRGD était ajoutés au PEG, la localisation et la pénétration des nanoparticules était minimale dans les tissus sains et préférentielle dans les nodules tumoraux (Wonder *et al*, 2018).

Ces dernières années, plusieurs autres TPP ont été identifiés et validés pour une délivrance tumorale de précision (Teesalu *et al*, 2013). Le peptide cyclique TT1 (séquence : CKRGARSTC) a été identifié par biopanning de phage (Figure 9) sur la protéine purifiée p32 (Paasonen *et al*, 2016). La protéine p32, également connue sous le nom de gC1qR ou protéine de liaison à l'acide hyaluronique 1 (HABP1) est une protéine intracellulaire exprimée de manière aberrante à la surface des cellules tumorales activées, des cellules endothéliales vasculaires/lymphatiques et des macrophages/cellules myéloïdes dans les zones hypoxiques de la tumeur (Fogal *et al*, 2008). P32 a été validée comme ligand d'affinité de TT1 cyclique dans différents modèles tumoraux, y compris dans les modèles carcinose péritonéale avec administration intra-péritonéale (Hunt *et al*, 2017; Sharma *et al*, 2017). Une variante de TT1 cyclique est le TT1 linéaire (« LinTT1 », séquence : AKRGARSTA) qui se lit à la protéine p32. Un autre peptide, p32-ligand et identifié par phage display, est Lyp-1 (séquence:

CGNKRTRGC) (Fogal *et al*, 2008, 2010; Laakkonen *et al*, 2002). Il a été montré que Lyp-1 avait une activité antitumorale intrinsèque dans un modèle de tumeur mammaire chez la souris (Laakkonen *et al*, 2004) et une accumulation dans des plaques athéroscléroses exprimant p32 chez la souris (Laakkonen *et al*, 2004). Après la liaison à p32, le motif CendR (KRGAR) des peptides TT1 et LinTT1 est exposé par l'activateur de plasminogène de type urokinase associé à la tumeur (uPA), ce qui déclenche la liaison à NRP-1 et favorise la pénétration tumorale (Sharma *et al*, 2017) (Figure 8).

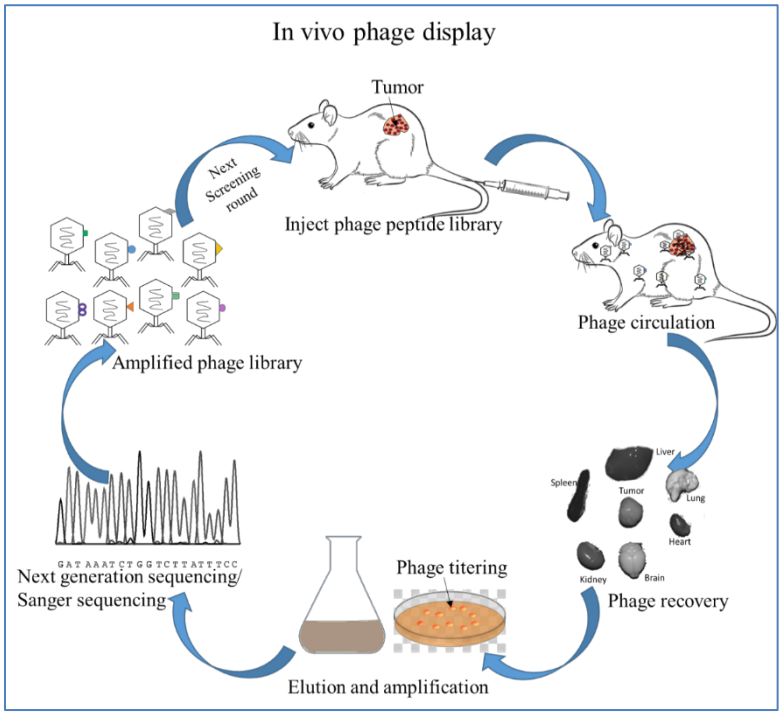

Figure 9: Biopanning de phages peptidiques ou phage display, in vivo

Le génome du bactériophage T7 est modifié pour exprimer les peptides étrangers sur la capside des particules de bactériophage comme fusions C-terminales de la protéine de couche 10A d'un bactériophage. Une bibliothèque de peptides est injectée par la veine de la queue de souris porteuses d'une tumeur. Dix minutes à 1 h après l'injection, les souris sont perfusées dans le cœur pour éliminer les phages non intégrés et des organes sont prélevés pour l'amplification des phages chez E. coli. Le phage récupéré de la tumeur est amplifié et réinjecté chez une souris pour un cycle supplémentaire de sélection, jusqu'à ce que l'enrichissement soit détectable. Les phages de chaque cycle sont soumis au séquençage de l'ADN pour identifier les peptides susceptibles de cibler les tumeurs. D'après Lingasamy & Teesalu, 2021.

4.3 Serine/thréonine phosphatase PP2A

La protéine phosphatase PP2A est un acteur important dans de nombreuses fonctions cellulaires (Figure 10). Elle contrôle le métabolisme cellulaire en régulant l'activité des enzymes impliquées dans la glycolyse, le métabolisme des lipides et la synthèse des catécholamines (Tung *et al*, 1985). Elle régule également divers processus biologiques tels que le cycle cellulaire (*via* l'activation de la cdc2 kinase), la réplication, la transcription et la traduction de l'ADN, la transduction du signal, la prolifération cellulaire, la dynamique du

cytosquelette, la mobilité cellulaire et l'apoptose. Il a également été démontré qu'elle joue un rôle dans la transformation cellulaire et le cancer (Alberts *et al*, 1993; Glenn & Eckhart, 1993; Ronne *et al*, 1991; Schonthal, 2001). Chez les eucaryotes, la séquence d'acides aminés prédite établit un degré élevé de conservation de la séquence (78 à 93 %) de PP2A entre la levure, la drosophile et les mammifères (Orgad *et al*, 1990). PP2A est exprimée de manière ubiquitaire et contribue à 1% des protéines cellulaires totales des cellules eucaryotes (Godet *et al*, 2011). La majorité de l'activité des phosphatases solubles à phosphosérine et phosphothréonine est catalysée par PP2A. PP2A est structurellement complexe et existe sous deux formes différentes : une forme dimérique (Cohen, 1997) et une forme trimérique (Mayer-Jaekel & Hemmings, 1994). La forme dimérique est connue sous le nom d'enzyme centrale et est composée de 2 sous-unités : catalytique et de structure (ou sous-unités d'aide à l'agencement spatial), tandis que la forme trimérique est un complexe holoenzyme actif qui se compose de trois sous-unités : catalytique (PP2Ac), structurelle (PP2Aa) et sous-unités régulatrices (PP2Ab) (Kamibayashi *et al*, 1994).

C est la sous-unité catalytique, A est la deuxième sous-unité réglementaire ou structurelle et B/B'/B''/B''' sont les troisièmes sous-unités variables, qui ne sont pas structurellement liées. Chez les mammifères, A et C sont encodés par deux gènes (α et β); les sous-unités B/PR55 sont codées par quatre gènes apparentés (α, β, γ et δ); la famille B'/PR61 est codée par cinq gènes apparentés (α, β, γ, δ et ε), de qui donnent lieu à d'autres produits par épissage; la famille B'' contient probablement trois gènes codant PR48, PR59 et les variantes d'épissage PR72 et PR130; SG2NA et striatin comprend la famille de sous-unités B''' (Janssens & Goris, 2001).

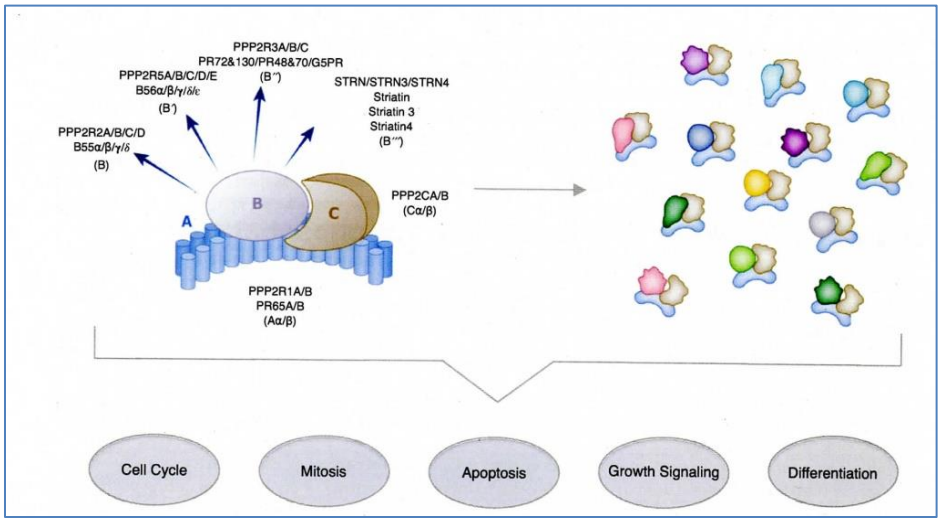

Figure 10: Famille des protéines phosphatases PP2A.

PP2A fait référence à un ensemble de serine/thréonine phosphatases distinctes. Chaque sous-unités A et C de PP2A a un isoforme alpha et beta, tandis

que la sous-unité B appartient à 4 familles de protéines, chacune contenant de multiples isoformes. Dans une cellule, il en résulte l'assemblage d'un pool hétérogène d'holoenzymes hétérotrimériques PP2A qui régulent collectivement les processus biologiques critiques souvent associés à la progression de la maladie. D'après Brautigan et al*, 2021.*

La sous-unité catalytique de PP2A (PP2Ac) est globulaire, exprimée de manière ubiquitaire dans presque tous les tissus et elle est plus abondante dans le cœur et le cerveau. Le niveau d'expression protéique de PP2Ac dans la cellule est régulé pour maintenir un niveau constant (Baharians & Schonthal, 1998). La séquence d'acides aminés de PP2Ac (37 kDa) est identique à 86 % chez l'homme et la levure et partage également 50 % de séquences d'acides aminés avec PP1 et 40 % de séquences identiques avec PP2B. PP2Ac existe sous deux isoformes Cα et Cβ. Ils sont codés par deux gènes distincts composés chacun de sept exons et de six introns. Les exons 2 à 6 participent à la liaison au substrat et à la catalyse, tandis que les exons 1 et 7 aident à la régulation. Les deux isoformes sont constituées de 309 acides aminés et partagent une similarité de séquence de 97 %. L'isoforme Cα est principalement exprimée dans la membrane plasmique et Cβ dans le cytoplasme et le noyau. Cα est exprimé en plus grande abondance que Cβ en raison de sa forte activité de promoteur ainsi qu'en raison de différences dans le taux de renouvellement de l'ARNm (Khew-Goodall & Hemmings, 1988).

L'extrémité C-terminale de PP2Ac est conservée de manière unique et se lie à la structure et aux sous-unités régulatrices (PR61γ). A l'extrémité N-terminale de PP2A, Cα et Cβ diffèrent de huit acides aminés et ces acides aminés ne sont pas non plus conservés dans PP1 et PP2B, suggérant que cette partie de la protéine pourrait ne pas jouer de rôle dans la catalyse (Janssens & Goris, 2001). Malgré le partage de 97% de similarité, les souris knock-out PP2Acα ne sont pas viables et meurent à 6,5 jour embryonnaire indiquant que PP2Acβ est incapable de se substituer à la perte de PP2Acα, soulignant la fonction non redondante de Cα dans le développement embryonnaire et la gastrulation (Gotz *et al*, 1998).

PP2A est considéré comme un suppresseur de tumeur et on pense qu'elle est fonctionnellement inactivée dans le cancer. Ainsi, l'inhibiteur de PP2A, l'acide okadaïque, lorsqu'il est injecté à des souris, provoque le développement de tumeurs (Nagao *et al*, 1995). Un autre antigène tumoral, l'antigène petit T du polyomavirus remplace la sous-unité B de

PP2A et altère l'activité phosphatase de PP2A, conduisant à la transformation (Campbell *et al*, 1995). Ces deux résultats ont établi le caractère suppresseur de tumeur de PP2A (Janssens *et al*, 2005). Il a été démontré que la structure PP2A et la sous-unité régulatrice étaient mutées ou exprimées de manière aberrantes dans de nombreux types de cancer. Une mutation dans PR65α/Aα a été trouvée dans le carcinome pulmonaire et le mélanome (Calin *et al*, 2000) et une mutation PR65β/Aβ a été observée dans le cancer du côlon et du poumon (Wang *et al*, 1998). Outre le cancer du poumon et du côlon, une perte de fonction des sous-unités de structure a également été observée dans les cancers du sein, de la peau, du col de l'utérus et de l'ovaire. La mutagenèse de Glu64 en Asp/Gly a perturbé la capacité de liaison de PR65α/Aα à PR56/B' (Ruediger *et al*, 2001). Une mutation faux-sens PR65β/Aβ a été détectée dans les cancers du poumon et du côlon (Wang *et al*, 1998). Récemment, des mutations du gène PPP2R1A de la sous-unité régulatrice du cancer de l'ovaire ont été identifiées. La mutation des sous-unités régulatrices a montré une capacité de liaison défectueuse des sous-unités B, B', indiquant une fonction de suppression tumorale réduite de PP2A dans le cancer de l'ovaire (Jones *et al*, 2010). Fait intéressant, dans 43% des tumeurs cérébrales (gliobastome, oligodendrogliome et oligodendroglime anaplasiques), le niveau de Aα était réduit d'au moins 10 fois. Par comparaison, les niveaux des sous-unités Bα et Cα étaient généralement normaux. Ces tumeurs avaient une diminution de l'expression de PP2A, enzyme centrale et holoenzyme, et des niveaux élevés de sous-unité C catalytique non régulée (Colella *et al*, 2001).

Dans les cellules HEK293, une réduction de 50% des niveaux de PP2A-Aα entraîne une réduction de l'holoenzyme PP2A-B'γ et une augmentation de la formation de tumeurs chez les souris immunodéficientes en raison de l'activation de la voie Akt (Chen *et al*, 2005). Comme Akt, la GTPase RalA participe à la transcription, à la migration, au transport à l'apoptose et à la prolifération cellulaire. Il a été découvert que PP2A-Aβ se lie et régule l'activité de RalA. La transformation associée au knockdown ou à la perte de PP2A-Aβ a montré une hyperphosphorylation de RalA (Sablina *et al*, 2007). Trois variantes d'épissage de PP2A-Aβ dues au saut de gène ont été observées dans la leucémie lymphoïde chronique à cellules B (B-CLL). Ces variants d'épissage étaient incapables d'assembler les sous-unités C et B et ont entraîné une perte d'activité PP2A (Kalla *et al*, 2007). Dans le cancer du sein, il y a une altération dans PP2A-Aβ. Plus récemment, Nagendra et coll. ont confirmé une

fréquence élevée de la mutation PP2A-Aα dans 32 % des carcinomes séreux utérins. À l'aide d'un séquençage à haut débit, des mutations ont été trouvés dans la lignée cellulaire de carcinome séreux ACI-158, une mutation dans un carcinome séreux primitif ainsi qu'une mutation dans le cancer de l'endomètre peu différencié (Nagendra *et al*, 2012).

Comme la sous-unité de structure, la sous-unité régulatrice de PP2A (principalement B55 et B56) a également été mutée dans de nombreux types de cancers. Chez les patients atteints de leucémie myéloïde aiguë (LAM), l'expression de PP2AB55α s'est avérée inférieure à la normale. Comme mentionné précédemment, B55α déphosphoryle Akt. Lorsque B55α est supprimé, cela conduit à une activation cohérente d'Akt et une prolifération accrue (Ruvolo *et al*, 2011).

PP2A et CHC

PP2A a été étudiée dans le CHC et il existe de nombreux arguments concordants qui étayent l'hypothèse du rôle délétère de l'inhibition de la PP2A dans l'apparition et le développement des CHC. Ainsi, Yang et coll. ont montré que l'expression de la sous-unité catalytique PPP2Cα était significativement plus élevée dans les CHC que dans les tissus non cancéreux et qu'elle était associée à une survie globale plus courte. Selon cette étude, PPP2Cα pourrait etre un marqueur diagnostique et pronostique du CHC (Yang *et al*, 2021).

La perte de la fructose 1-6 biphosphonate aldolase B (Aldob) conduit à une régulation paradoxale du métabolisme du glucose qui favorise la cancérogenèse du CHC (Figure 11), *via* des événements de signalisation en amont qui restent mal définis. La voie Akt est fortement activée dans le CHC. Or Aldob supprime l'activité d'Akt et la croissance tumorale grâce à un complexe protéique contenant Aldob, Akt et PP2A. Ce complexe conduit à une inhibition de la viabilité cellulaire, de la progression du cycle cellulaire, de l'absorption du glucose et du métabolisme. La perte d'Aldob ou la perturbation de l'interaction Aldob/Akt dans le mutant Aldob R304A restaurait l'activité Akt et ses effets pro-tumoraux. L'inhibition d'Akt ou l'utilisation d'un activateur de PP2A (SMAP pour *small-molecule activator of PP2A*) diminuait la tumorigénèse dans un modèle de souris xénogreffées. Au total, Aldob aurait un role non enzymatique dans la régulation négative de l'activation d'Akt et l'inhibition directe de l'activité d'Akt par la réactivation de PP2A pourrait etre une approche thérapeutique potentielle pour le traitement des CHC (He *et al*, 2020).

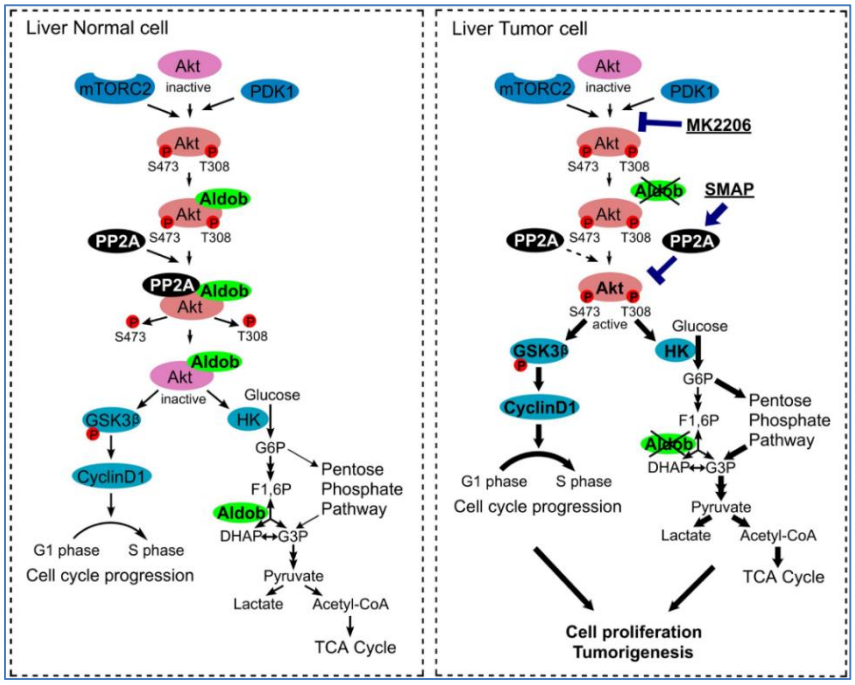

Figure 11: Schéma de de la régulation négative médiée par Aldob de l'activation d'Akt.

Dans les cellules normales, Aldob interagit avec Akt d'une manière dépendante de l'activité de la kinase Akt, ce qui favorise la liaison de la phosphatase PP2A à p-Akt et entraîne la déphosphorylation de p-Akt. Aldob est impliquée dans l'homéostasie intracellulaire de la phosphorylation d'Akt en modulant les interactions substrat/phosphatase. Dans les cellules cancéreuses déficientes en Aldob, la régulation à la baisse d'Aldob libère sa régulation négative de l'activité Akt, conduisant à l'activation constitutive de la signalisation oncogénique Akt, ce qui facilite la progression du cycle cellulaire et augmente la consommation de glucose et le flux métabolique vers la glycolyse et le cycle glycolysisand TCA pour la prolifération des cellules cancéreuses et la tumorigenèse. Cibler l'Akt hyperactif en inhibant directement l'activité de l'Akt ou en réactivant l'activité de la phosphatase PP2A peut être une approche thérapeutique pour traiter les cancers humains déficients en Aldob. Les flèches en gras représentent la régulation à la hausse des événements de signalisation indiqués en réponse à l'absence d'Aldob. Aldob : aldolase B; DHAP : dihydroxyacétone phosphate; GSK3ß : glycogène synthase kinase 3ß; HK : hexokinase; mTORC2 : cible mécanistique du complexe rapamycine 2 ; p-Akt : Akt phosphorylé; PDK1 : kinase 1 dépendante de l'ositide phosphoïne ; PP2A : protéine phosphatase 2A; SMAP : petit activateur de PP2A ; Cycle TCA : cycle acide tricarboxylique. D'après He et al*, 2020.*

Comme autre argument en faveur du rôle de PP2A dans l'apparition des CHC nous citerons les fait que les souris dépourvues de la sous-unité B56delta (Ppp2r5d) de PP2A développent spontanément des CHC (Lambrecht *et al*, 2020). Egalement, l'acide okadaïque est un inhibiteur de PP2A et un agent pro-tumoral (Nagao *et al*, 1995). L'administration de cet acide okadaïque à des cellules Hep3B et HepG2 favorisait l'expression de facteurs clefs de la transition épithélio-mésenchymateuse (EMT *epithelial-mesenchymal transition*). Ce résultat suggérait que l'inhibition de l'activité de PP2A favoriserait le potentiel métastatique des cellules de CHC (Kong *et al*, 2021).

Dans une étude clinico-biologique, Gong et coll. ont montré que l'expression élevée de PP2Ac était significativement associée à la positivité des antigènes de l'hépatite B (HBs et HBe), à la cirrhose du foie, au degré de différenciation, au stade avancé et à la récidive précoce de la maladie. L'analyse multivariée a révélé qu'une valeur élevée de PP2Ac dans le tissu tumoral était un facteur de mauvais pronostique indépendant pour la survie globale (Gong *et al*, 2016). L'inhibition de PP2Ac par un ARN interférant de petite taille a considérablement limité la prolifération cellulaire *in vitro*, la formation de colonies, la migration et l'invasion et a réduit la croissance tumorale dans un modèle de souris xénogreffe. En revanche, la surexpression de PP2Ac a favorisé la prolifération des cellules de CHC, la formation de colonies et la tumorigenèse. L'analyse du profil d'expression génétique a montré que la régulation descendante de PP2Ac modulait l'expression de nombreux gènes impliqués dans le cycle cellulaire et la régulation de l'apoptose. Inversement, la régulation ascendante de PP2Ac avait un impact défavorable sur la survie globale des patients atteints de CHC et contribuait à l'agressivité de CHC.

A l'hôpital Paul Brousse de Villejuif, Thièry et coll en 1999, avaient développé les lignées cellulaires de CHC du rat (HR-2, HR-3 et HR-4) et testé un inhibiteur spécifique et faible de PP2A, l'endothall. Ils avaient montré la plus grande sensibilité à l'endothall des lignées cellulaires de CHC par rapport à des cellules de cancer colique du rat (DHK/K12 et HT-29). Ils montraient également que l'endothall était responsable d'une cytostase en phase G2/M du cycle cellulaire, dépendante de la dose et du temps, avant mort cellulaire par apoptose (Thièry *et al*, 1999).

4.4 Oncoprotéine SET

SET est une oncoprotéine multifonctionnelle qui est impliquée dans de nombreux processus cellulaires (Figure 12). Elle est également connue sous le nom de facteur d'activation de matrice-I β (TAF-I β) ou inhibiteur 2 de la protéine phosphatase 2A (I2PP2A) ou putative histocompatibility leukocyte antigen class II-associated protein II (PHAPII). SET a été identifiée pour la première fois comme le gène de fusion set-can chez un patient atteint de leucémie aiguë indifférenciée en 1992 (von Lindern *et al*, 1992; Adachi *et al*, 1994). L'étude de ce gène de fusion a dévoilé le lien entre SET et le cancer et un sous-ensemble de ces études a démontré que SET joue un rôle important dans la tumorigenèse et les métastases.

SET est exprimée de manière ubiquitaire dans de nombreux types de tissus humains, notamment les reins, le foie, le cerveau, la rate, les poumons, le cœur et le système gonadique (Nagata *et al*, 1998). En raison de son rôle dans les fonctions cellulaires, sa dérégulation, en particulier sa surexpression, contribue au développement de diverses maladies dont la maladie d'Alzheimer, le syndrome des ovaires polykystiques et différents types de cancer (Arif *et al*, 2014; Madeira *et al*, 2005; Yu *et al*, 2013; Jiang *et al*, 2017; Switzer *et al*, 2011). Dans ce contexte nous nous focaliserons sur ses implications dans l'apparition des maladies cancéreuses.

De nombreuses preuves ont démontré une régulation à la hausse de l'oncoprotéine SET dans différents types de cancer et son association à de mauvais résultats cliniques. La surexpression de la protéine SET dans les cellules hématopoïétiques entraîne toujours des tumeurs malignes. Par exemple, dans la leucémie myéloïde chronique (LMC), la protéine SET est surexprimée et davantage dérégulée pendant la crise blastique (Neviani *et al*, 2005). Un phénomène similaire a été observé dans la leucémie lymphoïde chronique (LLC), le lymphome non hodgkinien et la leucémie myéloïde aiguë au niveau de l'ARNm et des protéines. Dans le même temps, l'augmentation des taux de protéines SET était corrélée à de moins bons résultats cliniques (Christensen *et al*, 2011a; Cristobal *et al*, 2012). Des études sur des échantillons de tumeurs de patients atteints de CHC, de cancer du pancréas et de cancer colorectal métastatique ont vérifié que la surexpression de SET était spécifique à la tumeur et contribuait à la progression tumorale (Farrell *et al*, 2014; Hung *et al*, 2016; Cristóbal *et al*, 2015). Janghorban et coll., ont découvert qu'environ 50 % des lignées cellulaires de cancer du sein présentaient une surexpression de SET (Janghorban *et al*, 2014). Inversement, le déficit en SET a significativement altéré le potentiel tumorigène des lignées cellulaires du cancer du sein. SET a également été signalée comme étant régulée positivement au niveau de l'ARNm et des protéines pour le carcinome épidermoïde de la tête et du cou, le choriocarcinome, la tumeur de Wilm, les tumeurs cérébrales malignes, le sarcome alvéolaire des parties molles, le carcinome gastrique, le carcinome testiculaire, le cancer du sein, du poumon, du foie, du côlon et de la prostate. Ces données indiquent que l'oncoprotéine SET joue un rôle fondamental dans la tumorigenèse (Janghorban *et al*, 2014; Saddoughi *et al*, 2013; Sobral *et al*, 2014; Carlson *et al*, 1998). SET joue également un role dans la résistance thérapeutique aux médicaments (Hung *et al*, 2016).

SET est donc une cible thérapeutique pour améliorer les traitements anticancéreux actuels. Plusieurs antagonistes de SET ont été développés et largement évalués pour le traitement du cancer. Le FTY720 (fingolimod) est un analogue de la sphingosine utilisé comme immunosuppresseur chez les patients atteints de sclérose en plaques (Cohen *et al*, 2010). Le FTY720 peut réactiver PP2A en perturbant les interactions SET-PP2Ac, entraînant une activité anticancéreuse significative. L'effet anticancéreux du FTY720 a été démontré dans de nombreuses tumeurs malignes hématologiques et solides (Saddoughi *et al*, 2013; Zhang *et al*, 2013; Li *et al*, 2018; Pippa *et al*, 2014; Ishitsuka *et al*, 2014; Neviani *et al*, 2007; Cristóbal *et al*, 2014; Yang *et al*, 2012; Arriazu *et al*, 2020). Le traitement FTY720 inhibe également la transition épithélio-mésenchymateuse (EMT) en affectant la signalisation SET/PP2A/c-Myc/NDRG1/Snail et restaure la sensibilité aux traitements standard tels que le cisplatine dans les cellules cancéreuses du poumon ou l'imatinib dans les cellules de LMC porteuses de mutations résistantes (Enjoji *et al*, 2015; Oaks & Ogretmen, 2014). Le COG112 est un peptide spécifique pénétrant dans les cellules. Il a été conçu en fusionnant un domaine de transduction protéique dérivé de la protéine antennapedia de Drosophila au peptide COG133 qui est un peptide mimétique créé à partir des résidus d'acides aminés 133-149 de l'holoprotéine Apolipoprotéine E (apoE) (Li *et al*, 2006). COG112 inhibe la réponse inflammatoire dans un modèle de colite inflammatoire par suppression de la signalisation NF-κB et de l'expression des cytokines pro-inflammatoires (Singh *et al*, 2011). Christensen et al ont découvert que COG112 était capable de se lier à SET exprimée dans les cellules immunitaires (Christensen *et al*, 2011b; Li *et al*, 2006). L'interaction Le COG112-SET inhibe la formation du complexe SET/PP2Ac, augmentant ainsi les niveaux d'activité cellulaire de PP2A et NM23H1. COG112 peut également empêcher la formation du complexe Rac1-SET entraînant l'inhibition de la migration et de l'invasion (Ghosal *et al*, 2013; Singh *et al*, 2008, 2011). OP449, dérivé du peptide COG112, interagit également avec SET et antagonise l'inhibition de PP2A par SET. OP449 non seulement réduit efficacement l'inhibition de PP2A par SET, mais possède également des propriétés cytotoxiques sélectives pour les cellules leucémiques (Farrell *et al*, 2014; Janghorban *et al*, 2014). D'autres études ont confirmé que l'antagonisme de SET en utilisant OP449 améliore de manière synergique l'efficacité des inhibiteurs de tyrosine kinase et surmonte la résistance aux médicaments dans les tumeurs malignes par un traitement combiné (Galiger *et al*, 2022; Richard *et al*, 2016).

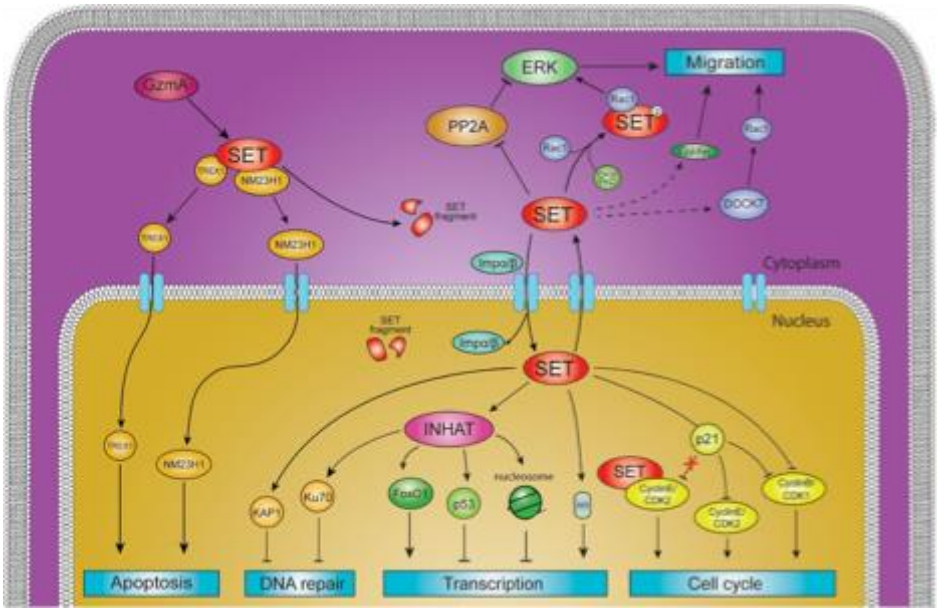

Figure 12: Fonctions physiologiques de SET et de ses interactions protéiques.

L'oncoprotéine SET participe à de multiples processus cellulaires, y compris la migration cellulaire, le cycle cellulaire, l'apoptose, la transcription des gènes et la réparation de l'ADN. La protéine SET régule les fonctions d'un sous-ensemble de protéines qui sont impliquées dans chaque processus. Les protéines interagissant avec SET sont indiquées. Les lignes noires représentent une interaction directe entre SET et les protéines, tandis que les lignes de points représentent une interaction inconnue ou indirecte. D'après Bayarkhangai et al*, 2018.*

4.5 PEPscan pour identification du site d'interaction entre deux protéines

Les puces à peptides sont constituées de différentes séquences peptidiques, immobilisées sur un support solide et qui sont analysées en termes de spots associés à un signal. Elles ont un large éventail d'applications en recherche fondamentale et appliquée. Leur utilisation diffère selon le choix de la méthode de synthèse peptidique, du support solide, de la méthode d'immobilisation, de la taille des peptides, de la densité de peptides sur le support solide et de la méthode de détection. La technique la plus largement utilisée pour générer des puces peptidiques est la synthèse SPOT. Cette technique est basée sur la chimie Fmoc en phase solide pour synthétiser des peptides sur un support membranaire, qui est généralement de la nitrocellulose (Frank, 2002; Gausepohl *et al*, 1992; Luu *et al*, 1996). Les matrices de peptides sont analysées pour révéler les spots positifs. Les méthodes de révélation les plus courantes sont la chimiluminescence, la colorimétrie et la fluorescence. Les puces à peptides offrent de nombreuses possibilités pour analyser différentes voies de signalisation entre des conditions normales et pathologiques (Katz *et al*, 2011). Elles ont été

utilisées pour la cartographie des épitopes d'anticorps (Frank & Overwin, 1996), l'identification du site de liaison entre l'IL-10 et son récepteur (Reineke *et al*, 1998), l'identification des épitopes des cellules T et B (Adler *et al*, 1994) ou la conception de peptides adhésifs cellulaires (Askoxylakis *et al*, 2005; Kato *et al*, 2006), etc...

Le PEPscan (Figure 13) est une classe particulière de puces peptidiques qui a été développée pour identifier, au sein de la séquence d'une protéine d'intérêt (Geysen *et al*, 1984), les régions qui interagissent avec un liant connu. Son principe est de découper une protéine ou un fragment de protéine, en une série de peptides de taille fixe. Chaque fragment est testé pour sa liaison à la protéine, peptide ou petite molécule partenaire. La taille la plus courante des peptides pour un PEPscan varie de 4 à 20 acides aminés, avec une plage de chevauchement de 1 à 10 acides aminés. L'une des premières applications du PEPscan a été l'identification d'épitopes reconnus par des anticorps monoclonaux (Scott & Smith, 1990). Plus récemment, le PEPscan a suscité un intérêt pour la modulation des interactions protéine-protéine, avec plusieurs résultats montrant son efficacité pour identifier des peptides capables d'interférer avec les interactions protéine-protéine (Bruzzoni-Giovanelli *et al*, 2018). Une approche similaire très récente concerne l'interférence entre LRRK2 et PP1 dans le cadre de la maladie de Parkinson (Dong *et al*, 2020). D'autres peptides interférants ont été identifiés en utilisant la technique du PEPscan (Andrini *et al*, 2020; Bergna *et al*, 2019; Rebollo *et al*, 2021, 2022; Simon-Gracia *et al*, 2022). Au-delà, on pourrait également se demander si l'utilisation du PEPscan pourrait être étendue pour cartographier les interactions des protéines avec d'autres types de partenaires que les protéines, y compris, par exemple, les petites molécules ou les peptides.

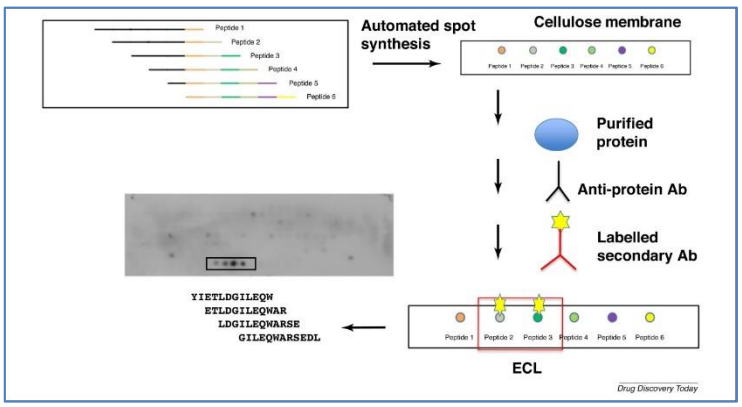

Figure 13: Schéma des étapes d'un PEPscan

Une protéine est scindée en séquences peptidiques de 4 à 20 acides aminés (AA). qui partagent entre eux un chevauchement de 1 à 10 acides aminés. Ces peptides une fois synthétisés sont immobilisés et alignés sur une membrane de nitrocellulose, afin de tester leur

capacité à se lier à la protéine d'interêt purifiée. Les points de fixation sont révélés par un anticorps (Ab) antiprotéine d'interêt lui-meme révélé par un Ab secondaire marqué. Les spots qui apparaissent correspondent aux candidats IP dont on connait la séquence en AA. D'après Bruzzoni-Giovanelli et al*, 2018.*

5 Résultats

5.1 Article 1: Bifunctional therapeutic peptides for targeting malignant B cells and hepatocytes: proof of concept in chronic Lymphocytic leukemia.

Simon-Gracia L*, Savier E*, Parizot C, Brossas JY, Loisel S, Teesalu T, Conti F, Charlotte F, Scatton O, Aoudjehane L and Rebollo A. *The two first authors equally contributed to this work.
Advanced Therapeutic. 2020. DOI:10.1002/adtp.202000131.

Introduction

Les interactions protéines-protéines peuvent être vues comme des cibles thérapeutiques. Par conséquent les peptides interférant (IP pour *interfering peptide*) qui bloquent ces interactions voient croitre leur intérêt dans le développement des traitements anticancéreux. Notre laboratoire a décrit un IP qui bloque l'interaction entre PP2A et SET (Tian *et al*, 2018a). PP2A est impliquée dans de nombreuses régulations cellulaires dont le contrôle de la prolifération (Janssens & Rebollo, 2012). Or PP2A est naturellement inhibée par SET et SET est surexprimée dans de nombreuses cellules tumorales. Dissocier l'interaction entre PP2A/SET peut aboutir à une restauration de l'activité de PP2A et rétablir une sensibilité à la chimiothérapie (Haesen *et al*, 2014). Pour faire pénétrer l'IP dans la cellule, le laboratoire a validé une combinaison de 2 peptides : un peptide de pénétration cellulaire (CPP pour *cell penetrating peptide*) couplé à l'IP (Zhang *et al*, 2018). Cette combinaison avait un effet antitumoral présent mais modeste (Tian *et al*, 2018a). En 2013, Teesalu et coll. ont décrit une sous-classe de peptide pénétrant les tumeurs (TPP pour *tumor penetrating peptide*) dont la particularité est de s'internaliser spécifiquement dans les cellules tumorales (Teesalu *et al*, 2013). Les TPP sont définis par la présence du motif suivant en C terminal : R/KxxR/K où x est un acide aminé quelconque. Ce motif appelé « CendR » autorise une fixation au récepteur neuropilin-1 (NRP-1) (Braun *et al*, 2016), qui est surexprimé à la surface des cellules tumorales (Sugahara *et al*, 2015a). Un IP a été associé à l'un des 4 TPP suivant : iRGD, RPARPAR, TT1 linéaire (LinTT1) et TT1 cyclique (TT1), créant ainsi 4 nouveaux peptides bi-fonctionnels capables de bloquer l'interaction intracellulaire PP2A/SET.

But du travail

Tester ces 4 peptides bi-fonctionnels TPP-IP et 1 peptide bi-fonctionnel CPP-IP *in vitro* sur des cellules malignes B et les hépatocytes tumoraux et *in vivo* sur un modèle murin de xénogreffe de leucémie lymphoïde chronique (LLC).

Matériel et méthode

Les cellules tumorales étaient obtenues à partir du sang de donneur sain ou atteint de LLC. Les hépatocytes normaux à partir de la plateforme ICAN et les hépatocytes tumoraux à partir d'échantillons de pièces opératoires, prélevés au laboratoire d'anatomie-pathologique.

Après culture cellulaire de 3 ou 4h avec des peptides fluorescents marqués au FITC, l'internalisation des peptides était mesurée par cytométrie en flux en simple (peptide-FITC) ou double marquage (anticorps anti-CD19 pour marquer les lymphocytes ou arginase pour marquer les hépatocytes). L'internalisation était visualisée par microscopie en fluorescence.

L'apoptose était mesurée par cytométrie en flux après culture cellulaire en présence des peptides et d'annexine V marquée au FITC pendant 12h.

La dégradation des peptides dans du sérum humain à 37°C était mesurée sur 24h par spectrométrie en masse.

Le modèle de xénogreffe comportait des souris immunodéficiences CB-17 SCID qui recevaient par voie intraveineuse 2,5 x 10^6 cellules de LLC Jok5.3. Le traitement par iRGD-IP ou Mut3DPT se faisait par injections intrapéritonéales de 20 mg/kg, à partir de j3 et durant 5 jours consécutifs pendant 4 semaines (n=7).

Les toxicités rénale, hépatique et métabolique ont été comparées chez des souris femelles BALB/c par dosage de la créatinine, de l'ALAT et du glucose 24h après injection d'une dose de 20 mg/kg de TT1-IP ou de NaCl 0.9%.

Résultats

Les TTP (iRGD, LinTT1, TT1 et RPARPAR) pouvaient pénétrer 10 à 60 fois plus dans les cellules B des patients souffrants d'une leucémie lymphoïde chronique (LLC) que dans les cellules B de donneurs sains et 40 à 80 fois plus dans les hépatocytes tumoraux que dans les

hépatocytes sains. L'internalisation du CPP (Mut3DPT) était comparable que les cellules (B ou hépatocyte) soient tumorales ou pas. L'association d'un IP n'affectait pas la pénétration des TTP-IP dans les cellules B de LLC. Les cellules B de LLC exprimaient fortement les récepteurs NRP-1, p32 et l'integrin v/β3. Après association d'un IP, l'internalisation de RPAPAR-IP et LinTT1-IP dans les hépatocytes tumoraux étaient satisfaisante mais faible pour iRGD-IP. Les hépatocytes tumoraux avaient une expression élevée en p32 et moindre pour NRP-1 et l'integrin v/β3. En microscopie à fluorescence, l'internalisation des peptides étaient uniquement cytoplasmique, similaires pour les cellules B malignes mais inhomogène pour les hépatocytes tumoraux (faible pour iRGD-IP). L'internalisation était minime dans les cellules B ou hépatocytes normaux. Tous les peptides bi-fonctionnels induisaient une apoptose dans les cellules B de LLC. Pour les hépatocytes tumoraux, l'effet apoptotique était présent pour RPARPAR-IP, LinTT1-IP, TT1-IP et faible pour iRDG-IP. Aucun TPP-IP n'induisait d'apoptose chez les cellules saines. Mut3DPT-S2 (CPP-IP) induisait également une apoptose, moindre que pour TPP-IP dans les cellules tumorales et faiblement présente dans les cellules saines. Les peptides bi-fonctionnels iRGD-IP, RPAR-IP, et TT1-IP étaient faiblement dégradées après 24 h d'incubation dans du sérum humain et le moins stables était RPARPAR-IP (-25% en 24h). L'iRGD-IP augmentait significativement la survie dans un modèle de xénogreffe de LLC. Aucun symptôme de toxicité n'a été détecté.

Conclusion

Ces résultats suggéraient que les peptides bi-fonctionnels peuvent avoir une application thérapeutique en ciblant l'interaction PP2A/SET spécifiquement dans les cellules tumorales.

FULL PAPER

ADVANCED THERAPEUTICS
www.advtherap.com

Bifunctional Therapeutic Peptides for Targeting Malignant B Cells and Hepatocytes: Proof of Concept in Chronic Lymphocytic Leukemia

*Lorena Simon-Gracia, Eric Savier, Christophe Parizot, Jean Yves Brossas, Severine Loisel, Tambet Teesalu, Filomena Conti, Frederic Charlotte, Olivier Scatton, Lynda Aoudjehane, and Angelita Rebollo**

Protein–protein interactions are well recognized as therapeutic targets and therefore interfering peptides (IP) that block these interactions are receiving increasing attention. Four different tumor-penetrating peptides (TPPs) (iRGD, RPARPAR, Linear TT1 (LinTT1), and cyclic TT1 (TT1)) are associated to an IP that blocks the interaction between the protein phosphatase PP2A and its binding protein SET, generating new bifunctional peptides able to intracellularly target the PP2A/SET interaction in malignant B cells and tumoral hepatocytes. The TPPs are able to penetrate into B cells of patients suffering chronic lymphocytic leukemia (CLL) and into tumoral hepatocytes but not into B cells from healthy donors and healthy hepatocytes. The association of cargo does not affect the penetration of the TPPs in CLL B cells. All the bifunctional peptides induce apoptosis in human CLL B cells and tumoral hepatocytes, and stability tests reveal that iRGD-IP, RPARPAR-IP, and TT1-IP are stable after 24 h incubation in human serum. The iRGD associated with the IP significantly increases the survival of mice bearing xenograft models of CLL without any symptom of toxicity, suggesting that the bifunctional peptides may have a therapeutic application for selective tumoral targeting of PP2A/SET interaction, which is deregulated in several cancers, including CLL.

1. Introduction

Tumor penetrating peptides (TPPs) are a subclass of tumor targeting peptides that specifically recognize, bind, and internalize into tumor cells.[1,2] TPP are defined by the presence of the C-end rule (CendR) motif with the consensus R/KXXR/K (X any amino acid).[3,4] This position-dependent motif must be C-terminally exposed to allow the binding to the receptor neuropilin-1 (NRP-1).[5] NRP-1 is overexpressed in the tumor vasculature and in a variety of malignant cells in vitro and in vivo.[6] Binding of the CendR peptide to NRP-1 activates intracellular transport pathway that is regulated by nutrient availability resulting in the tumor-specific extravasation and distribution of the payload into the tumor. It has been shown that NRP-1 is specifically expressed in B cells from chronic lymphocytic leukemia (CLL) patients.[7] The RPARPAR is a prototypic CendR peptide that binds to and internalizes into cells expressing NRP-1 and is able to cause vascular leakage and increase tumor extravasation.[8] iRGD

Dr. L. Simon-Gracia, Prof. T. Teesalu
Laboratory of Cancer Biology, Institute of Biomedicine and Translational Medicine
University of Tartu
Tartu 50411, Estonia

Dr. E. Savier, Dr. O. Scatton
Department of Hepatobiliary and Liver Transplantation Surgery, AP-HP
Pitié-Salpêtrière Hospital
Paris 75013 France

Dr. E. Savier, Dr. F. Conti, Dr. L. Aoudjehane
Sorbonne Université
INSERM, ICAN Paris 75006, France

C. Parizot
Department of Immunology, AP-HP
Pitié-Salpêtrière Hospital
Paris 75013, France

J. Y. Brossas
Department of Parasitology, AP-HP
Pitié-Salpêtrière Hospital
Paris 75013, France

Dr. S. Loisel
Service Général des plateformes, Animalerie Commune
Université de Brest
Brest 29238, France

Prof. T. Teesalu
Cancer Research Center
Sanford Burnham Prebys Medical Discovery Institute
La Jolla CA 92037, USA

The ORCID identification number(s) for the author(s) of this article can be found under https://doi.org/10.1002/adtp.202000131

DOI: 10.1002/adtp.202000131

(internalizing RGD, with sequence CRGDKGPDC) is a TPP that was identified by in vivo peptide phage display.[9] This TPP is recruited to the tumor vessels by interaction with integrins[10] ($\alpha v\beta 3$, $\alpha 5\beta 1$, and $\alpha IIb\beta 3$) through the RGD motif, and after that is cleaved by tumor-associated proteases to expose the CendR motif to allow interaction with NRP-1, triggering the extravasation and penetration of iRGD together with the cargo in the tumor tissue. iRGD has been widely used to increase the penetration of anticancer drugs and nanotherapeutics in several tumor models[11,12] and in 2018, iRGD entered a clinical trial on targeted drug delivery of coadministered Gemcitabine and Abraxane to metastatic pancreatic ductal carcinoma lesions (ClinicalTrials.gov identifier: NCT03517176).

Similar to iRGD, TT1 peptide (sequence CKRGARSTC) is a cyclic TPP that contains a cryptic CendR motif. TT1 was identified by phage display by cell-free biopanning on recombinant p32/gC1qR protein (p32). TT1 binds first to p32,[13] a mitochondrial chaperone expressed on the cell surface of malignant cells.[14,15] TT1 is cleaved by proteases expressed in tumor, exposing the CendR motif that can then bind to NRP-1. The linear version of TT1, LinTT1 (sequence AKRGARSTA) also binds to p32 protein and follows the same tumor internalization mechanism than TT1, but with the advantage of its easier synthesis and cargo coupling. LinTT1 has been used as a TPP for guiding therapeutic and imaging nanoparticles and has showed enhanced therapeutic efficacy in experimental treatments of glioblastoma, peritoneal carcinomatosis and breast tumors.[16] Finally, in recent years, other TPP have been described and validated for precision tumor delivery.[9,17,18]

Protein/proteins interactions (PPIs) are well recognized as promising therapeutic targets.[19] Given their physicochemical characteristics, interfering peptides (IPs) that modulate PPIs are better suited than small molecules to interfere with the large surface interactions in PPIs.[20] There is increasing evidence for the capacity of IPs to modify several cellular processes and support the notion that they would have a significant potential to become therapeutic tools. Progresses on peptide administration, stability, biodelivery, ADEM properties, and safety have encouraged the resurgence interest in peptide drug development.[21,22] IPs represents a new and exciting class of drug candidates for inhibition of intracellular PPIs. Using the PEP scan approach, we have identified the binding site among different PPIs involved in tumoral transformation.[23,24] In addition, we have preclinically validated a cell-penetrating and interfering peptide, which enters in clinical trials Phase I.[23]

SET is a multitask protein critically involved in the initiation and progression of cancer. Its overexpression is a recurrent and clinically relevant event in many malignant diseases and plays critical role in the development of therapeutic resistance.[25,26] SET affects the function of its interacting protein PP2A (protein phosphatase 2A), to induce tumor phenotype. The antitumoral PP2A is a crucial phosphatase involved in the control of cell proliferation and malignant transformation.[25] Targeting and disrupting PP2A/SET interaction would result in a recovered PP2A activity. Recent data showed that antagonizing SET restores sensitivity to chemotherapies in previously resistant models.[26] We have recently validated a cell-penetrating and interfering peptide targeting PP2A/SET interaction that induces apoptosis of tumoral cell lines and primary tumoral B cells in vitro and shows moderate antitumoral activity in mice bearing xenograft models of CLL.[27] This pathology offers the possibility to validate the tumor specificity of a given compound comparing primary B cells isolated from CLL patients and healthy donors. In addition, xenograft models of CLL are available and well characterized in the literature.[28]

Table 1. Sequence of the peptides used in this work. Ahx = aminohexanoic acid linker.

Peptide ID	Sequence
iRGD	FITC-Ahx-CRGDKGPDC-$CONH_2$ (C—C disulfide bond)
RPARPAR	FITC-Ahx-RPARPAR-OH
LinTT1	FITC-Ahx-AKRGARSTA-$CONH_2$
TT1	FITC-Ahx-CKRGARSTC-$CONH_2$ (C—C disulfide bond)
Mut3 DPT	FITC-Ahx-VKKKKIKAEIKI
	VKKKKIKAEIKI
IP (interfering peptide)	FITC-Ahx-ETVTLLVALKVRYRERIT
	ETVTLLVALKVRYRERIT
iRGD-IP	FITC-Ahx-ETVTLLVALKVRYRERIT-Ahx-CRGDKGPDC-$CONH_2$ (C—C disulfide bond)
	ETVTLLVALKVRYRERIT-Ahx-CRGDKGPDC-$CONH_2$ (C—C disulfide bond)
RPARPAR-IP	FITC-Ahx-ETVTLLVALKVRYRERIT-Ahx-RPARPAR-OH
	ETVTLLVALKVRYRERIT-Ahx-RPARPAR-OH
LinTT1-IP	FITC-Ahx-ETVTLLVALKVRYRERIT-Ahx-AKRGARSTA-$CONH_2$
	ETVTLLVALKVRYRERIT-Ahx-AKRGARSTA-$CONH_2$
TT1-IP	FITC-Ahx-ETVTLLVALKVRYRERIT-Ahx-CKRGARSTC-$CONH_2$ (C—C disulfide bond)
	ETVTLLVALKVRYRERIT-Ahx-CKRGARSTC-$CONH_2$ (C—C disulfide bond)
Mut3 DPT-S2	FITC-Ahx-ETVTLLVALKVRYRERIT-Ahx-VKKKKIKAEIKI
	ETVTLLVALKVRYRERIT-Ahx-VKKKKIKAEIKI

Prof. T. Teesalu
Center for Nanomedicine
University of California
Santa Barbara CA 93106, USA
Dr. F. Conti
Department of Medical Liver Transplantation
AP-HP
Pitié-Salpêtrière
Paris 75013, France
Dr. F. Charlotte
Department of Anatomophatoloty, AP-HP
Pitié-Salpêtrière Hospital
Paris 75013, France
Dr. A. Rebollo
Inserm U1267, CNRS-UMR 8258, Faculté de Pharmacie
Paris 75006, France
E-mail: angelita.rebollo@parisdescartes.fr

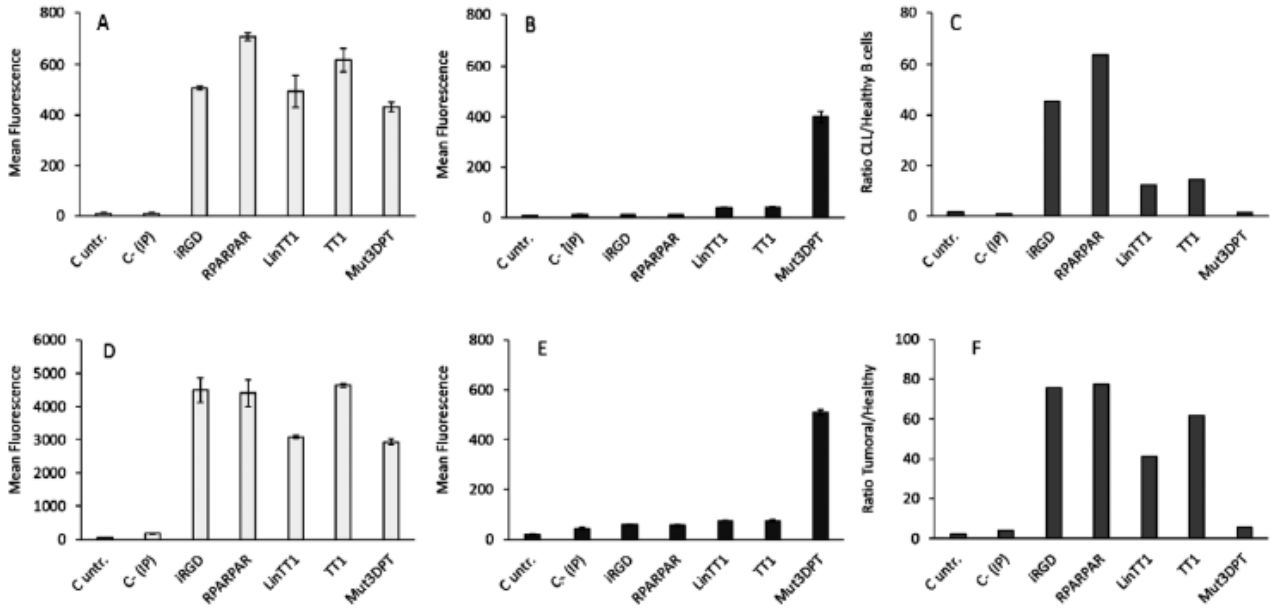

Figure 1. Selective internalization of TPPs in primary malignant and healthy B cells and hepatocytes. TPP internalization in A) B cells from CLL patients, B) B cells from healthy donors, D) tumoral hepatocytes, and E) healthy hepatocytes. Tumoral or healthy cells isolated from patients were incubated 4 h with 25×10^{-6} M of FITC-labeled TPPs. The mean fluorescence intensity was detected by flow cytometry and compared to untreated cells (C untr.) or cells treated with the IP without shuttle. The cell-penetrating peptide Mut3DPT was used as positive control. C) Ratio of TPP internalization between tumoral and healthy B cells. F) Ratio of TPP internalization between tumoral and healthy hepatocytes. The experiments were done in three to nine different patient samples. Error bars = ±SEM. The internalization of TPPs in malignant cells was significantly higher than in healthy cells ($P^{<}$ 0.001) except for the Mut3DPT in malignant and healthy B cells ($P = 0.3$). P values for the internalization of TPPs in malignant cells are shown in the table in the supporting information. For the statistical analysis, one-way analysis of variance ANOVA and Fisher's least significant difference (LSD) test was performed using the software StatSoft Statistica.

Here, we describe the design and in vitro validation in primary cells of new chimeric peptides composed of TPPs associated with an interfering peptide blocking PP2A/SET interaction. We also tested the stability in human serum of these peptides, their in vivo efficacy in experimental therapy of CLL, and their in vivo toxicity.

2. Results

2.1. Selective Internalization of TPPs into Malignant and Normal B Cells and Hepatocytes

We evaluated whether the TPPs iRGD, LinTT1, RPARPAR and TT1 (see peptide sequence in **Table 1**) internalized into malignant and healthy primary B cells and hepatocytes in vitro. Cells were incubated with 25×10^{-6} M of FITC-labeled peptides for 4 h and peptide internalization was analyzed by flow cytometry. As a positive control, we used the shuttle Mut3DPT (sequence in Table 1), a nontumor-specific cell-penetrating peptide (CPP). As a negative control, we used the interfering peptide (IP) without shuttle or untreated cells.

Figure 1A shows that all TPPs selectively penetrated into B cells from CLL patients and not in healthy B cells (Figure 1B). TPPs were internalized in B cells from CLL patients between 10- and 60-fold more than in healthy cells, being iRGD and RPARPAR the peptides with highest internalization into CLL B cells (more than 45-fold respect healthy B cells) (Figure 1C). The four TPPs also internalized preferentially in primary malignant hepatocytes (between 40 and 80 fold more in tumoral than healthy hepatocytes) (Figure 1D–F). These results demonstrate the selective penetration of TPPs into both primary malignant B cells and hepatocytes.

2.2. Impact of a Cargo on the Internalization of the TPPs into Primary B Cells

We analyzed the effect of a cargo, the IP, on the cell internalization properties of the TPPs. Taking advantage of the fact that we have mapped the binding site of the serine/threonine phosphatase PP2A to its physiological inhibitor, the oncoprotein SET, we have associated this IP to the four TPPs previously described to generate bifunctional peptides (TPP-IPs). The sequences of the TPP-IPs are shown in Table 1.

The cell internalization of the TPP-IPs was analyzed by flow cytometry. **Figure 2**A shows that the new generated TPPs-IP were internalized in malignant B cells (isolated from CLL patients) cultured for 4 h with 25×10^{-6} M of each peptide and were not internalized in healthy B cells (Figure 2B). As a positive control of internalization, we used Mut3DPT associated with the same IP (Mut3DPT-S2, sequence shown in Table 1). Figure 2C shows that the TPP-IPs penetrated between 20 and 60 fold more in malignant B cells than in healthy B cells. As TPPs recognize specific receptors on the cell surface (NRP-1 for RPARPAR,

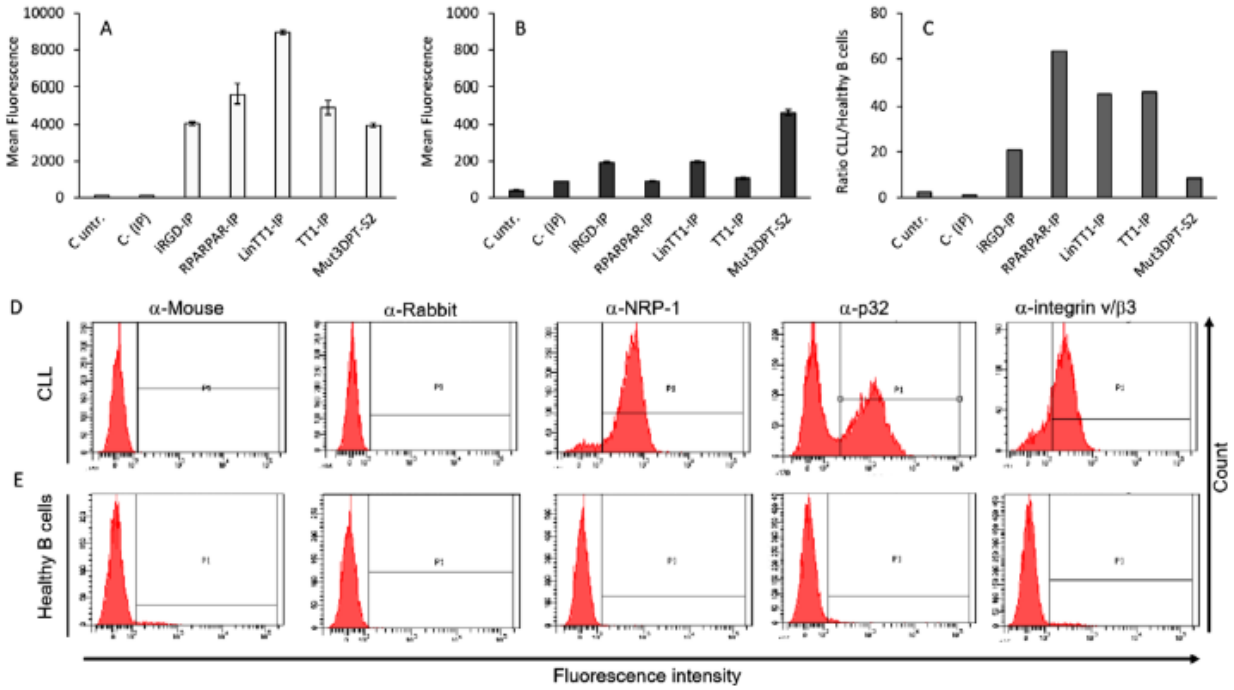

Figure 2. Impact of the association of a cargo on the internalization of TPPs into malignant and healthy B cells. Internalization of A) TPP-IPs in malignant or B) healthy B cells. B cells were treated with the FITC-labeled TPP-IPs for 4 h at a concentration of 25×10^{-6} M. Fluorescence intensity was detected by flow cytometry and compared to untreated cells (C untr.) or cells treated with an IP without shuttle. Mut3DPT-S2 was used as positive control of internalization. C) Ratio of TPP-IP internalization between tumoral and healthy B cells. Expression of TPP receptors in D) tumoral or E) healthy B cells. B cells were stained with antibodies against NRP-1, p32, and integrin v/β3, followed by an APC-labeled secondary antibody. Samples were analyzed by flow cytometry. Secondary antimouse or antirabbit antibodies were used as control. The experiments were done in three to seven different patient samples. Representative results from the different patients are shown. Error bars = ±SEM. The internalization of TPP-IPs in malignant B cells was significantly higher than in healthy B cells ($P < 0.001$). P values for the internalization of TPP-IPs in malignant cells are shown in the table in the Supporting Information. For the statistical analysis, one-way analysis of variance ANOVA and Fisher's LSD test was performed using the software StatSoft Statistica.

integrin v/β3 for iRGD and p32 for TT1 and LinTT1), we analyzed whether malignant B cells expressed these receptors. As shown in Figure 2D, tumoral B cells expressed integrin v/β3, p32, and NRP-1, whereas healthy B cells do not express these receptors (Figure 2E).

Next, we study the percentage of B cells that internalized the bifunctional TPP-IPs. We labeled malignant and healthy B cells with CD19 antibody, a marker for B cells, and analyzed by flow cytometry the percentage of CD19+ cells that internalized the peptide (FITC+) (**Figure** 3A,B). Figure 3C shows that almost all of the malignant B cells isolated from CLL patients internalized the TPP-IPs. In contrast, no CD19+/FITC+ double labeling was observed for healthy B cells (Figure 3D). As expected, the IP alone was not internalized by malignant nor healthy B cells.

2.3. Impact of a Cargo on the Internalization of the TPPs into Primary Hepatocytes

We analyzed the impact of the cargo on the internalization of the TPPs in primary healthy and malignant hepatocytes. As shown in **Figure** 4A, RPARPAR-IP and LinTT1-IP were well internalized into tumoral hepatocytes while the level of internalization of TT1-IP was lower, and iRGD-IP showed a very weak internalization. None of the TPP-IPs penetrated into healthy primary hepatocytes (Figure 4B). Untreated cells or cells incubated with the IP were used as negative controls. As a positive control, healthy hepatocytes were treated with Mut3DPT-S2. The ratio of penetration of the peptides in tumoral hepatocytes versus healthy hepatocytes is shown in Figure 4C, revealing that RPARPAR-IP internalized around 10 fold more in malignant hepatocytes. Figure 4D shows that malignant hepatocytes had high expression of p32 and moderate expression of integrin v/β3 and NRP-1 (Figure 4D).

We then analyzed the percentage of tumoral and healthy hepatocytes (arginase positive cells) that internalized the TPP-IPs (**Figure** 5A,B). We observed that more than 80% of tumoral hepatocytes internalized RPARPAR-IP, LinTT1-IP, and TT1-IP and less than 50% of tumoral hepatocytes internalize iRGD-IP (Figure 5C). Independently of the peptide treatment, only traces of arginase+/FITC+ cells were detected in healthy hepatocytes (Figure 5D).

2.4. Intracellular Localization of the TPP-IPs

To confirm the flow cytometry results and to visualize the intracellular distribution of the TPP-IPs, we treated malignant and healthy primary B cells and hepatocytes with FITC-labeled

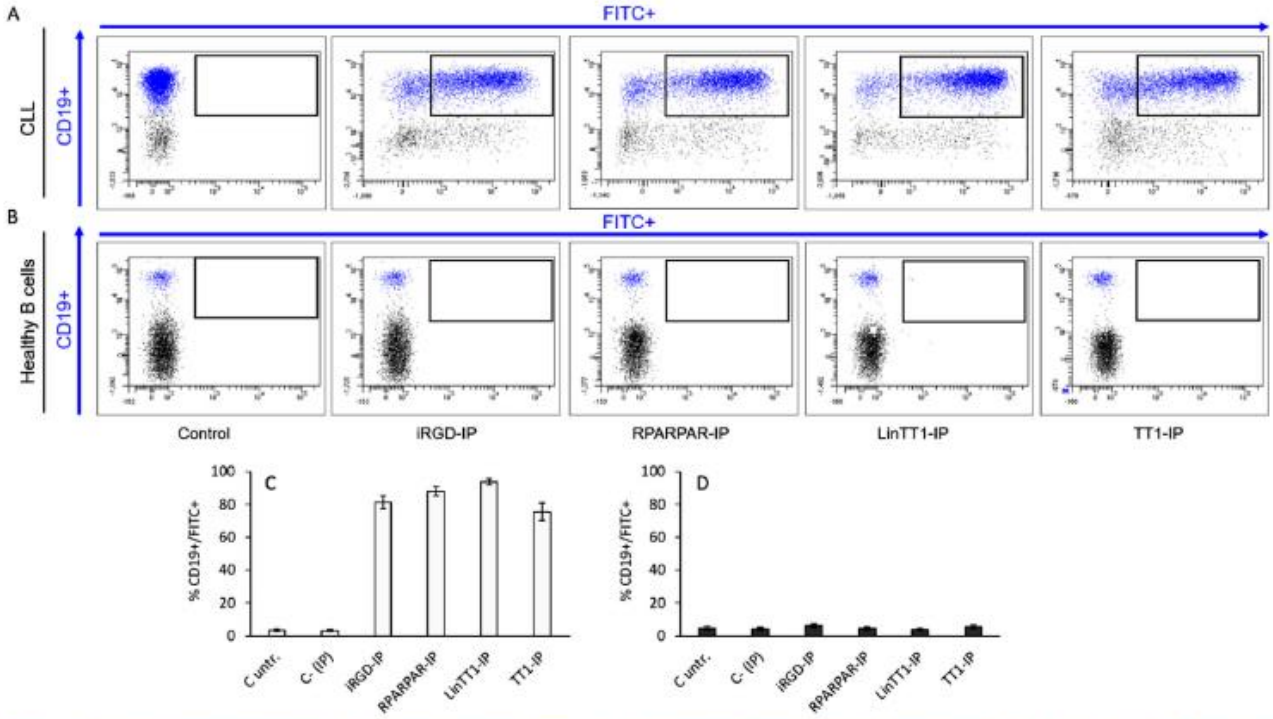

Figure 3. Analysis of the percentage of B cells internalizing the TPP-IPs. Flow cytometry analysis of A) the malignant or B) healthy B cells internalizing the TPP-IPs (FITC+) and expressing CD19 (CD19+, B cell marker). B cells were treated for 4 h with 25×10^{-6} M of FITC-labeled TPP-IPs. Representative results from the different patients are shown. Representation of the percentage of C) tumoral or D) healthy B cells (CD19+) positive for FITC analyzed by flow cytometry. Untreated cells (C untr.) or cells treated with the IP were used as negative control. The experiments were done in four different patient samples. Error bars = ±SEM. The %CD19+/FITC+ in malignant B cells was significantly higher than in healthy B cells ($P < 0.001$). *P* values for the %CD19+/FITC+ in malignant cells are shown in the table in the Supporting Information. For the statistical analysis, one-way analysis of variance ANOVA and Fisher's LSD test was performed using the software StatSoft Statistica.

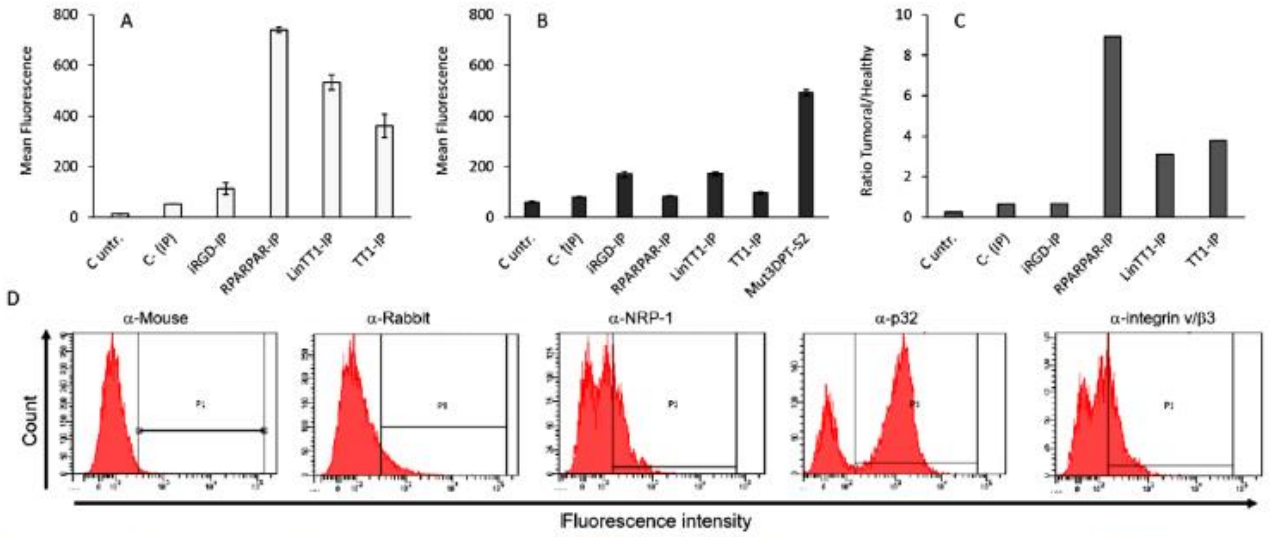

Figure 4. Impact of the association of a cargo on the internalization of TPPs into tumoral and healthy hepatocytes. Internalization of TPP-IPs in A) tumoral or B) healthy hepatocytes. Hepatocytes were treated with the FITC-labeled TPP-IPs for 4 h at a concentration of 25×10^{-6} M. Fluorescence intensity was detected by flow cytometry and compared to untreated cells (C untr.) or cells treated with an IP without shuttle. C) Ratio of TPP-IP internalization between tumoral and healthy hepatocytes. D) Expression of TPP receptors in tumoral hepatocytes. Hepatocytes were stained with antibodies against NRP-1, p32, and integrin v/β3, followed by an APC-secondary antibody. Samples were analyzed by flow cytometry. Secondary antimouse or antirabbit antibodies were used as control. The experiments were done in 3–7 different patient samples. Representative results from the different patients are shown. Error bars = ±SEM. The internalization of TPP-IPs in malignant hepatocytes was significantly higher than in healthy cells ($P < 0.001$). *P* values for the internalization of TPP-IPs in malignant cells are shown in the table in the Supporting Information. For the statistical analysis, one-way analysis of variance ANOVA and Fisher's LSD test was performed using the software StatSoft Statistica.

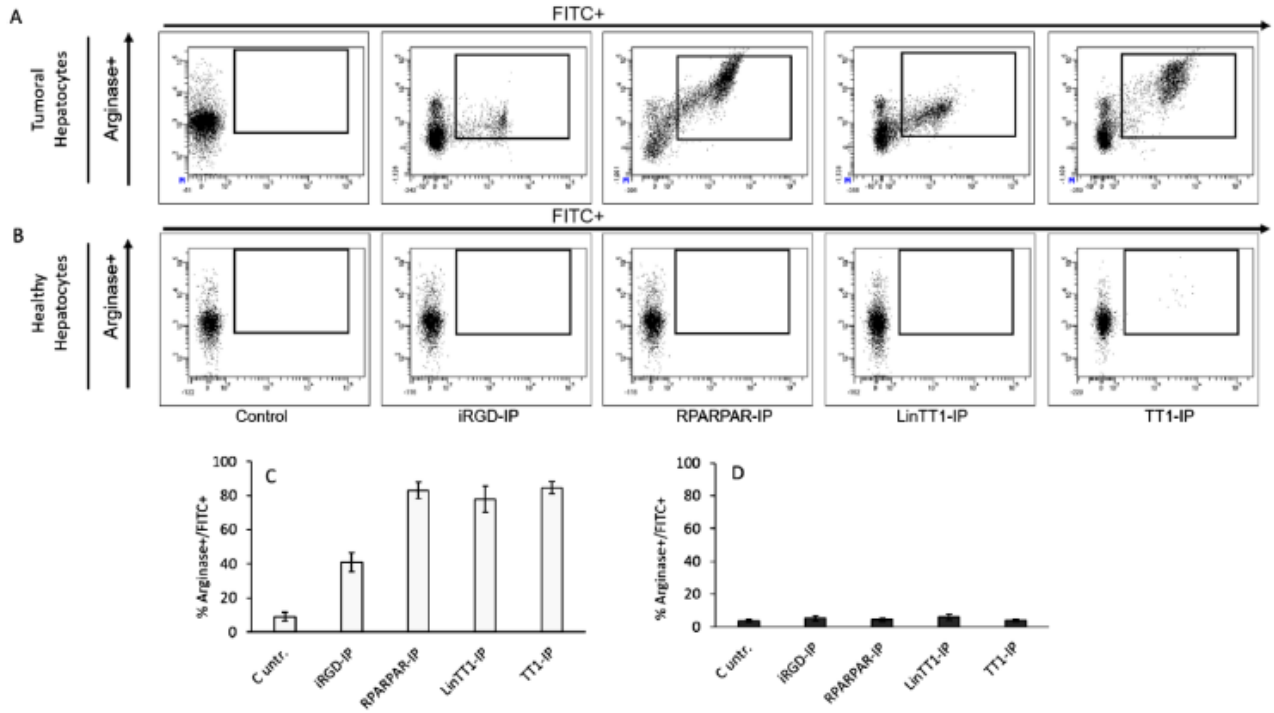

Figure 5. Analysis of percentage of hepatocytes internalizing the TPP-IPs. Flow cytometry analysis of the A) tumoral or B) healthy hepatocytes internalizing the TPP-IPs (FITC+) and expressing arginase (arginase+, hepatocyte marker). Hepatocytes were treated for 4 h with 25×10^{-6} M of FITC-labeled TPP-IPs. Representative results from the different patients are shown. Representation of the percentage of C) tumoral or D) healthy hepatocytes (arginase+) positive for FITC analyzed by flow cytometry. Untreated cells (C untr.) were used as negative control. The experiments were done in 3–5 different patient samples. Error bars = ±SEM. The %Arginase+/FITC+ in malignant hepatocytes was significantly higher than in healthy cells ($P < 0.001$). P values for the %Arginase+/FITC+ in malignant cells are shown in the table in the Supporting Information. For the statistical analysis, one-way analysis of variance ANOVA and Fisher's LSD test was performed using the software StatSoft Statistica.

peptides and analyzed the distribution by fluorescence microscopy upon 3 h of incubation with 25×10^{-6} M of each peptide. In malignant B cells, the staining pattern was similar among the different peptides, with the fluorescence located in the cytoplasm and excluded from the nucleus (**Figure 6**A). We did not detect or very low fluorescence in the healthy B cells. RPARPAR-IP, LinTT1-IP, and TT1-IP penetrated into tumoral hepatocytes and the internalization of iRGD-IP peptide was weak (Figure 6B), extending the result obtained by flow cytometry. Only traces of TPP-IPs were detected in healthy hepatocytes. Taken together, these results strongly suggest that we have selected tumor-specific penetrating peptides that are not affected by the addition of a cargo, an IP blocking the interaction PP2A/SET.

2.5. Apoptotic Effect of the Bifunctional Peptides on Malignant Primary Cells

We have previously shown that the IP blocking the interaction PP2A/SET, when associated with the CPP Mut3DPT, had an in vitro apoptotic effect as well as moderated antitumoral effect in vivo. We were interested in analyzing whether the specific tumoral-targeting would increase the apoptotic effect of the IP in primary cells. We observed that the TPP-IPs exerted an apoptotic effect on malignant B cells (**Figure 7**A) but not on healthy primary B cells (Figure 7B). It is interesting to notice that in our previous publication, to reach the same level of apoptosis when using the CPP Mut3DPT-S2, we incubated cells for 24 h with the peptide, compared to 12 h incubation used here.

We also analyzed the apoptotic effect of the TPP-IPs on healthy and malignant primary hepatocytes. RPARPAR-IP, LinTT1-IP, and TT1-IP induced strong level of apoptosis on tumoral hepatocytes after 12 h. However, in the case of iRGD-IP only a modest effect on apoptosis was observed, in accordance with the low level of penetration on tumoral hepatocytes (Figure 7C). Mut3DPT-S2 induced lower level of apoptosis than the TPP-IPs in both malignant B cells and hepatocytes. When tested in healthy primary hepatocytes, the TPP-IPs had not effect on apoptosis (Figure 7D). Our results showed that our TPP-IPs have tumor-specific apoptotic effect.

2.6. Resistance of the New Generated Peptides to Protease Degradation

We analyzed the stability of the peptides in human serum upon incubation at 37 °C for different periods of time. The resistance to proteases degradation was analyzed by mass spectrometry (MS).

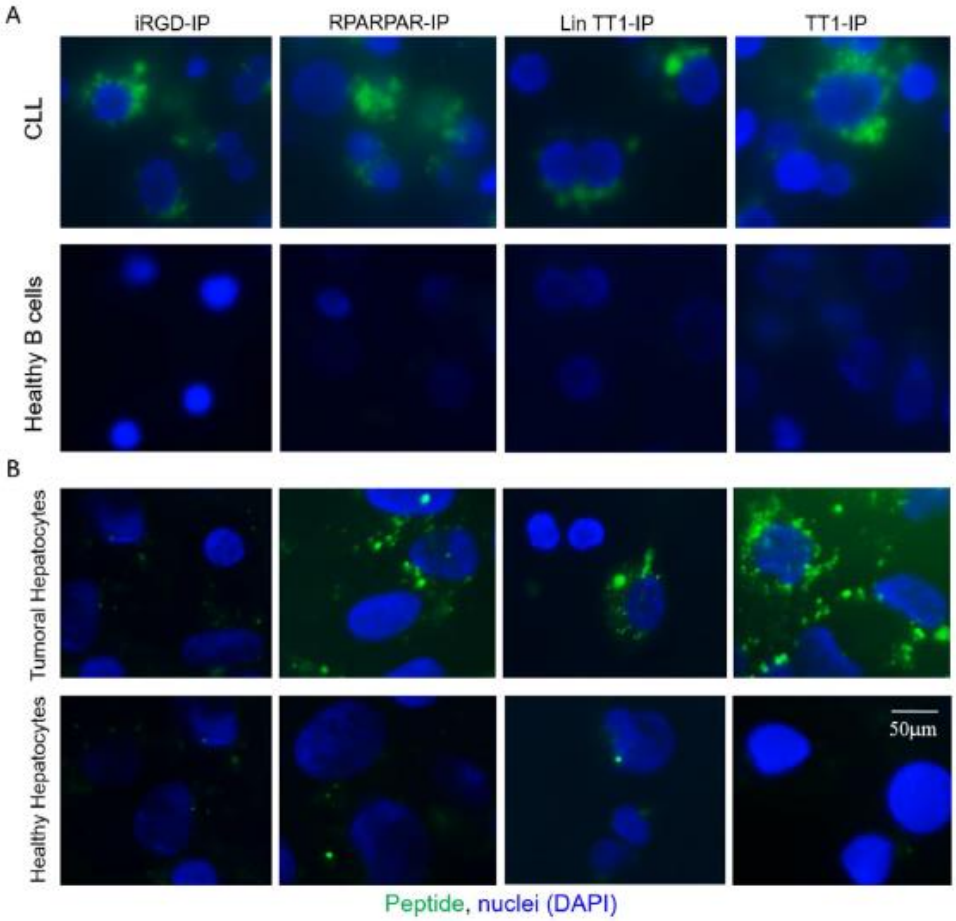

Figure 6. Intracellular localization of TPP-IPs. Fluorescence microscopy images of A) malignant or healthy B cells and B) tumoral or healthy hepatocytes. Cells were treated for 3 h with 25×10^{-6} M of the FITC-labeled TPP-IPs and attached by cytospin centrifugation to a coverslip and analyzed by fluorescence microscopy. Green = TTP-IPs (FITC), blue = nuclei (DAPI).

We did not detect significant degradation of iRGD-IP, TT1-IP and RPARPAR-IP (**Figure 8**) upon 24 h of incubation, contrarily to LinTT1-IP, that was less stable, recovering only around 25% of the total peptide after 24 h of incubation. Taken together, our results suggest that we have designed, developed, and in vitro validated new tumor-targeted therapeutic peptides compatible with clinical development.

2.7. Antitumoral Effect of the Chimeric Peptides on Human Xenograft Models of CLL

The in vivo efficacy of iRGD-IP was evaluated in a mouse model of CLL using the cell line Jok5.3. For the experimental treatment, we chose the iRGD-IP peptide for several reasons: i) iRGD showed high internalization in CLL B cells compared with healthy B cells, ii) iRGD-IP showed the highest stability in human serum, and iii) iRGD is in clinically development for the treatment of pancreatic cancer. In a previous work, we showed the anticancer efficacy of the CPP-IP (Mut3DPT-S2) in the CLL model.[27] Treatment of CLL-bearing mice with Mut3DPT-S2 using 20 mg kg^{-1} of peptide, 5 d per week yielded a moderate survival benefit, extending the survival to 20 d, while the survival of control group was 18 d (**Figure 9**A, panel constructed from previously published data).[27] To evaluate the tumor-targeting effect on the survival rate, we performed an experimental treatment with iRGD-IP using the previous dose. The mice treated with iRGD-IP showed a significant survival benefit ($p < 0.05$), compared with control mice treated with vehicle (NaCl) or the shuttle Mut3DPT. Nontreated control mice died after 20 d of disease manifested with CNS paralysis, a common symptom due to the infiltration of leukemic cells into CNS, while medium survival extended to 29 d in iRGD-IP treated mice (Figure 9B). No significant changes on body weight were observed in all treated groups compared to the control group (Figure 9C,D). The weight loss observed at day 14 in Figure 9C and day 18 in Figure 9D is due to the development of Jok5.3 symptoms of the disease. Therefore, no treatment-related effects on body weight were detected. Immunocompetent Balb/c mice were injected with 20 mg Kg^{-1} of iRGD-IP or Mut3DPT-S2 and after 24 h, the plasma was collected to evaluate the liver and renal toxicity. The peptides did not show any significant changes in the

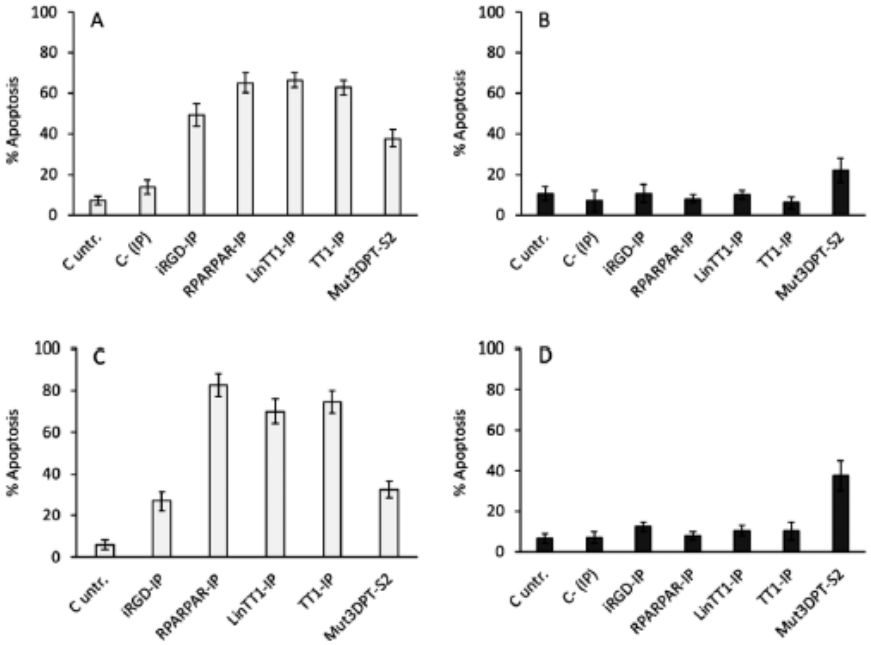

Figure 7. Cell apoptosis induced by the TPP-IPs. Apoptosis of A) malignant or B) healthy B cells and C) tumoral or D) healthy hepatocytes induced by TPP-IPs. Cells were treated for 12 h with 25×10^{-6} M of the TPP-IPs and apoptosis was tested by annexin-V-FITC staining. Untreated cells (C untr.) or cells treated with an IP were used as negative control, and Mut3DPT-S2 peptide was used as positive control. The experiments were done in two to three different patient samples. Error bars = ±SEM. The % of apoptosis of malignant cells was significantly higher than in healthy cells ($P < 0.001$) except for the Mut3DPT ($P > 0.05$). P values for the % of apoptosis in malignant cells are shown in the table in the Supporting Information. For the statistical analysis, one-way analysis of variance ANOVA and Fisher's LSD test was performed using the software StatSoft Statistica.

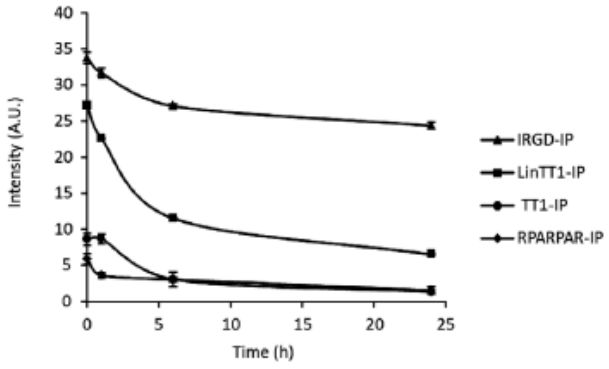

Figure 8. Stability of the TPP-IPs in human serum. Representation of the peptide intensity with time. Peptides were incubated at 37 °C in human serum for different periods of time and their integrity was analyzed by MS. Every measurement was performed in triplicate. A.U. = arbitrary units. Error bars = ±SEM.

level of glucose (Figure 9E), creatinine (Figure 9F), and alanine aminotransferase (ALAT) (Figure 9G), compared to control mice, suggesting that are not toxic at the dose used.

3. Discussion

During recent decades, a number of therapeutic approaches have been explored to specifically target tumoral cells, avoiding the side effects of chemotherapy. Consequently, IPs capable of interfering with PPIs are receiving increasing attention.[29] Several IPs have been validated in vivo, some are in clinical development, and some are already in the market.[30]

PP2A is known to be frequently altered in cancer.[26,31,32] Tumor suppressor function of PP2A makes it an interesting target for novel anticancer therapies.[25,26] The oncoprotein SET is a physiological inhibitor of PP2A and it acts by forming a complex with catalytic PP2A subunit.[33] Therefore, many efforts trying to restore PP2A activity have focused on interfering PP2A/SET interaction.[33,34] Elevated expression of SET has been linked to cell transformation, particularly in hematological malignancies.[31] Using PEP scan approach, we have previously identified the binding site between PP2A and SET. This sequence was associated with a CPP in order to generate a bi-functional peptide able to penetrate into cells and dissociate PP2A/SET interaction. This peptide has an apoptotic effect on tumor cell lines, as well as antitumoral effect on xenograft models of CLL.[27] We hypothesized that the addition of a tumor homing/penetrating module to the IP would increase its anticancer efficacy and therapeutic index. Compared to other tumoral targeting ligands, such as antibodies, peptides offer several advantages, including small size, low toxicity, low manufacturing cost and low immunogenicity. Here we generated chimeric TPP-IP peptides that possess anticancer activity in vitro and in vivo.

All four TPPs studied here, iRGD, RPARPAR, LinTT1, and TT1, showed high cell penetration due to their interaction with the primary and secondary TPP receptors overexpressed on the surface of primary malignant B cells and hepatocytes. The fusion in N-terminal of the cargo (the IP blocking PP2A/SET

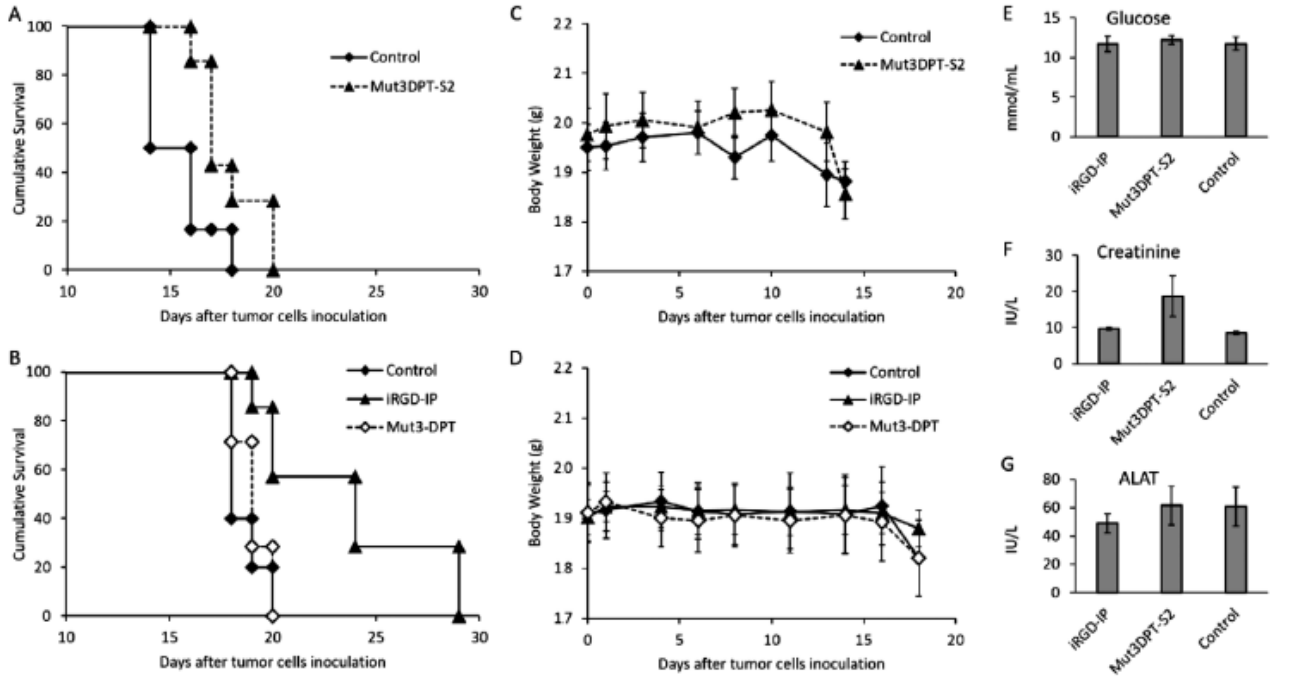

Figure 9. iRGD-IP has an in vivo antitumoral activity in human xenograft models of CLL. A) SCID mice were intravenously (IV) inoculated with 2.5×10^6 Jok5.3 cells in the tail and treated 3 days after injection with 20 mg kg^{-1} of Mut3DPT-S2 peptide 5 d per week. Control mice were injected with NaCl. Survival of the animals was monitored over time. $N = 7$. Cumulative survival of the group treated with Mut3DPT-S2 was significantly higher than control group ($P < 0.05$). (Constructed from published data[27]). B) SCID mice xenografts were generated as above and injected with the shuttle peptide Mut3DPT or the iRGD-IP at 20 mg Kg^{-1} 5 d per week. Control mice were injected with NaCl. Survival of the animals was followed as above. $N = 7$. Cumulative survival of the group treated with iRGD-IP was significantly higher than control group and group treated with Mut3-DPT ($P < 0.05$). Statistical comparisons between groups were performed using factorial analysis of variance ANOVA. Normality and homogeneity were evaluated by Shapiro-Wilk test. C) Average of the body weight with time in control mice or mice treated with Mut3DPT-S2. D) Average of the body weight with time in mice treated with iRGD-IP or Mut3DPT. $N = 7$. Error bars = ±SEM. E–G) Levels of E) glucose, F) creatinine and G) ALAT in the plasma of immunocompetent Balb/c mice treated with 20 mg Kg^{-1} of iRGD-IP, Mut2DPT-S2 or saline. $N = 3$. Error bars = ±SEM. The glucose and enzyme's values were not significantly different between the different treatment groups ($P > 0.05$). P values are shown in the table in the supporting information. For the statistical analysis, one-way analysis of variance ANOVA and Fisher's LSD test was performed using the software StatSoft Statistica.

interaction), to the TPPs did not affect the internalization of RPARPAR, LinTT1, and TT1 peptides in tumoral cells. However, the addition of IP decreased the cell penetration of iRGD, especially in tumoral hepatocytes. This result suggests a decrease in the ability of the iRGD to bind to its receptors on the cell surface, possibly due to a steric hindrance or different folding process by the addition of the cargo. However, this modification does not have a negative impact on the resistance to protease degradation of the iRGD-IP since it showed the highest stability in serum. In tumoral hepatocytes, the decrease of the iRGD-IP uptake was higher than in tumoral B cells, probably due to a lower expression of the iRGD receptors (integrin $v/\beta 3$ and NRP-1) in tumoral hepatocytes than in tumoral B cells.

The TPP-IPs showed high level of apoptosis when compared to the control shuttle, Mut3DPT, associated with the same IP. Compared with previous data, the TPP-IPs needed shorter time to produce the same apoptosis level than the IP associated with the Mut3DPT, which is not a tumor-specific peptide. The high penetration of TPP-IP is translated into high apoptotic effect mediated by the associated IP and to the specific tumoral penetration, avoiding loss of active product penetration in healthy cells. More importantly, the IP associated with iRGD showed an enhanced antitumoral effect in xenograft model of CLL, compared to the same IP associated with the Mut3DPT.

It has been shown that the in vivo tumor homing of iRGD-targeted nanoparticles was higher than RPARPAR-targeted nanoparticles in gastric tumor models in mice.[11] Tumor penetration of iRGD is the result of a multistep mechanism. First, it is recruited to αv-integrins on tumor endothelium, fibroblasts, and tumor cells and after proteolytic cleavage it binds to NRP-1, triggering the tumor penetration. This mechanism renders its high selectivity towards tumor cells expressing both αv-integrins and NRP-1 receptors.

LinTT1 and TT1 are not limited to vascular docking sites but have access to extended tumor extravascular space.[2] The receptor of LinTT1 and TT1, p32 protein, is expressed in the mitochondria of normal cells but it is aberrantly expressed on the surface of tumor cells.[13,15] Following similar multistep mechanism than iRGD, LinTT1 and TT1 bind to NRP-1 after proteolytic cleavage.[1,4,18] In our hands, LinTT1 and TT1 associated with the IP showed the same penetration properties while TT1 as a better profile of stability to proteases degradation, suggesting that TT1 is better candidate for further clinical development. It has been shown that to enhance the drug

penetration in tumor the drug does not need to be coupled to the TPP, being possible a coadministration of the TPP with the therapeutic agent. This has been shown for iRGD coadministrated with doxorubicin, and other reports have also shown that coadministration of unconjugated TPPs could improve the penetration of nanomedicines into tumor tissues.[35] The side effects of the doxorubicin were diminished by reduction of the drug's dose. Therefore, the TPP can be used to enhance the activity of the anticancer drugs and to reduce the side effects. Similar approach has been used by conjugating RPARPAR to liposomal doxorubicin to improve transport efficiency in tumor tissues.[36]

Taken together, we report a selective approach with potential use in cancer therapy. Our study has important implications for the design of clinically relevant therapeutic approach for selective inhibition of PP2A/SET interaction in tumor cells. Although in this work we have only tested the in vivo anticancer efficacy of the iRGD-IP, next studies will focus on testing the in vivo therapeutic effect of the other TPP-IPs.

4. Conclusion

In this study, we describe the design and in vitro and in vivo validation of new tumoral-addressed chimeric peptides for selective inhibition of PP2A/SET interaction in chronic lymphocytic leukemia and liver cancer. The peptides used in this study, as well as the approach, might have a clinical application in malignant transformations.

5. Experimental Section

Peptides: Peptides were synthesized in an automated multiple peptide synthesizer with solid phase procedure and standard Fmoc chemistry by GL Biopchem (Shanghai, China) or Smart Biosciences (Saint Egreve, France). The purity and composition of the peptides were confirmed by reverse phase high performance liquid chromatography (HPLC) and by mass spectrometry (MS). In some cases, the peptides were synthesized with the fluorochrome fluorescein isothiocyanate (FITC) at the N-terminus. For cell internalization studies, the FITC-labeled peptides were used. For the apoptosis assays and experimental treatments, the unlabeled peptides were used. The sequences of all peptides are shown in Table 1. The peptides Mut3DPT or Mut3DPT-S2 were used as positive control.

Isolation and Culture of Primary B Cells: Fresh blood from healthy donors (HD) was obtained from Etablissement Français du Sang. CLL patient samples were obtained from the Department of Hematology of the Hospital Saint Louis upon approval of the project by Ministry of Higher Education and Research (CODECOH DC-2018-3261) and signed informed consent of the patients according to the French law of using human samples. All the methods were performed in accordance with the guidelines and regulations of French law. Peripheral blood mononuclear cells (PBMC) from HD and CLL patients were prepared by Ficoll gradient centrifugation, as previously described.[22] Cells were maintained in RPMI 1640 supplemented with 10% of fetal calf serum (FCS, Eurobio, Courtaboeuf, France), 1% nonessential amino acids, 1% Hepes, 1% sodium pyruvate, and 1% glutamine. The selection of B cells was made using anti-CD19 antibody (Invitrogen).

Isolation and Culture of Primary Human Hepatocytes: Liver tissue samples were obtained from resected human liver of patients with primary or secondary liver tumors or benign local liver diseases. Primary human hepatocytes were isolated using the Human HepCell platform (IHU-ICAN, Paris, France, http://www.ican-institute.org/category/plateformes) as previously described.[37] Ethical approval for the isolation of human hepatocytes was granted by the Persons Protection Committee (CPP Ile de France III) and by the French Ministry of Health (N°: COL 2929 and COL 2930).

Hepatocytes were isolated using an established two-step-perfusion protocol with Collagenase.

First, the tissue was rinsed with prewarmed (37 °C) calcium-free buffer supplemented with 5 mmol L^{-1} ethylene glycol tetraacetic acid (Sigma, Saint-Quentin Fallavier, France). Then, the liver sample was perfused with recirculating perfusion solution containing 5 mg mL^{-1} collagenase (Sigma) at 37 °C. Afterwards, the tissue was transferred into a Petri dish containing Wash Medium (Lifetechnologies, Villebon sur Yvette, France). Tissue was disrupted mechanically by shaking and using tweezers to disrupt cells from the remaining extracellular matrix structures. Cellular suspension was filtered through a gauze-lined funnel. Cells were collected at low speed centrifugation. The supernatant was removed and pelleted hepatocytes were resuspended in Hepatocyte Wash Medium. Cell viability was determined by trypan blue exclusion test. Freshly isolated normal or steatotic hepatocytes were suspended in Williams' medium E (Life Technologies) containing 10% FCS (Eurobio, Courtaboeuf, France) 1% penicillin–streptomycin and insulin. Then, the cells were seeded in 12-well plates precoated with type I collagen and incubated at 37 °C in 5% CO_2 overnight. Medium was replaced with fresh complete hepatocyte medium supplemented with 1 μmol L^{-1} hydrocortisone hemisuccinate (SERB, Paris, France) and cells were left in this medium until incubation with peptides.

Tumoral human hepatocytes were isolated from tumoral liver samples collected from adult patients undergoing surgery. Samples were cut in small pieces and treated with 4 mL of dispase (10 mg mL^{-1} in PSA buffer: NaCl 8 g L^{-1}, KCl 0.2 g L^{-1}, glucose 1 g L^{-1}, $NaHCO_3$ 0.35 g L^{-1}, phenol red 1 mL L^{-1}) and 2 mL of collagenase type I (5 mg mL^{-1} in PSA buffer). Samples were incubated at 37 °C under agitation for a maximum of 1 h and then, the solution was filtered and passed through needles of different diameter size. The volume was completed up to 50 mL with culture medium and centrifuged at 900 rpm for 5 min. Supernatant was discarded and cells cultured in DMEM medium supplemented with FCS (10%) and antibiotics until treatment with peptides.

Quantification of Cellular Internalization: Primary human B cells or hepatocytes were seeded on 24-well plate and incubated for 4 h with FITC-labeled peptides. After treatment, cells were harvested and washed twice with PBS to remove the free peptides and resuspended in 200 μL of PBS. FITC fluorescence intensity of internalized peptides was measured by flow cytometry on a FACSCanto II as previously described[38] (Beckton Dickinson). Data were analyzed with FACSDiva 6.1.3 software (DB Biosciences). Untreated cells were used as control. For detection of the cell surface TPPs receptors, anti-p32 (ThermoFisher), anti-NRP-1 (in house generated antibody), and integrin v/β3 (Abcam) antibodies were used. For the hepatocyte labeling, anti-arginase (Invitrogen) antibody was used following cell permeabilization. Cells were immunostained following the manufacture's protocol.

Visualization of the Peptide Internalization by Fluorescence microscopy: For intracellular localization of FITC-labeled peptides, human primary B cells or hepatocytes were seeded in an eight-well plate Labtek (Thermo Fischer). Cells were treated with 25×10^{-6} M FITC-labeled peptides for 3 h, washed three times with PBS and fixed with 4% of formaldehyde for 15 min at room temperature. B cells were attached to a cover slip by cytospin centrifugation. Samples were washed twice with PBS and mounted in mounting buffer containing DAPI as described.[38] Images were captured with a fluorescence microscopy (Olympus Japan) using 40× magnification objective.

Detection of Apoptosis by Annexin-V Staining: The apoptosis induction of the different TPP-IPs was analyzed by flow cytometry on cells labeled with annexin V-FITC staining (Biosciences, Fisher Scientific). Primary cells were treated with 25×10^{-6} M of peptides for 12 h. After the treatment, cells were harvested, washed, and treated according to the manufacturer's protocol. The level of apoptosis was measured by flow cytometry (FACS Canto II, BD Biosciences, New Jersey, USA).

Analysis of Peptide Stability in Human Serum: Peptides were incubated at 37 °C in 250 μL of human serum for different periods of time. Samples were collected and peptide degradation stopped by freezing. Peptides

were extracted from samples using the Proteo Miner Protein Enrichment System (Bio-Rad). Percentage of intact peptide was estimated by matrix-assisted laser desorption/ionization-time of flight (MALDI-TOF) mass spectrometry using the protocol previously described[38] (Bruker Autoflex II) according to the manufacturer's instructions. Measurements were performed in triplicate. MS data were analyzed using the software Cliprot tools, Felx analysis, Bruker.

Animals and In Vivo Experimental Therapy Studies: The 6–8 weeks old SCID CB-17 mice (female, 20–23 g) were purchased from Charles River Laboratories (L'Arbresle, France). All mice were maintained under conditions and protocols in accordance with the Directive 2010/63/UE of the Council of Europe on Animal Welfare. The studies (number authorization 22312_2019100719342404 and 5220-2016042817212864) were approved by the French Ethics Committee for animal experimentation number 74 and all experiments were conducted following the guidelines of the aforementioned committee.

Balb/c mice (8–12 week old female) were breaded at the Institute of Biomedicine and Translational Medicine, University of Tartu. Animal experiment protocols were approved by the Estonian Ministry of Agriculture (project no. 48). All methods were performed in accordance with existing guidelines and regulations.

CLL Jok5.3 cells (2.5×10^6) were injected in 100 μL of NaCl 0.9% into the tail vein of SCID mice. Mice (7 mice per group) were injected with saline, Mut3 DPT, or iRGD-IP intraperitoneally (IP) after 3 d of cell transplantation and for five consecutive days during 4 weeks. The peptide dose used per injection was 20 mg Kg^{-1}. Mice were monitored daily for the presence of hindleg paralysis and in that case sacrificed.

Measurement of Toxicological Parameters: Healthy female Balb/c mice were injected intraperitoneally with 20 mg Kg^{-1} of peptides (200 μL) or saline (control) and after 24 h, mice were anesthetized and 500 μL of blood was collected by retro-orbital bleeding into lithium heparin tubes (BD Vacutainer, REF: 368 494). The samples were centrifuged for 10 min at 1800 g at 4 °C and the plasma was analyzed for the concentration of glucose, creatinine, and activity of alanine aminotransferase (ALAT), using a Cobas 6000 IT-MW (Roche Diagnostics Gmbh) machine and reagents for creatinine CREP2 (REF 03263991) and for ALAT ALTLP (REF 04467388).

Statistical Analysis: For in vitro data, *P* value was calculated performing one-way analysis of variance ANOVA and Fisher's least significant difference (LSD) test. The software StatSoft Statistica was used for the analysis. The obtained data were not processed before the statistical analysis. The bars in the graphs represents the standard error mean (±SEM). The sample size (N) was between 2 and 9 and it is described in the caption of the figures. For in vivo data, statistical comparisons between groups were performed using factorial analysis of variance ANOVA. Normality and homogeneity were evaluated by Shapiro-Wilk test and the data were found valid. The sample size for the in vivo experiments was $N = 7$.

Acknowledgements

L.S.-G. and E.S. contributed equally to this work. L.A. and A.R. contributed equally to this work. This work was supported by Inserm. T. Teesalu was supported by the European Union through the European Regional Development Fund (Project No. 2014-2020.4.01.15-0012), and Estonian Research Council (grants PRG230 and EAG79). The authors thank the animal facility platform of Brest for their technical assistance. L.S. thanks the French Institute of Estonia and the Campus France for the High Level Scientific Stays fellowship 2020. Thanks also to Karine Le Ster for JOK5.3 cell line.

Conflict of Interest

The authors declare no conflict of interest.

Keywords

cancer targeting, chronic lymphocytic leukemia, interfering peptides, liver cancer, tumor-penetrating peptides

Received: June 5, 2020
Revised: September 5, 2020
Published online:

[1] T. Teesalu, K. N. Sugahara, E. Ruoslahti, *Front. Oncol.* **2013**, *3*, 216.
[2] E. Ruoslahti, *Adv. Drug Delivery Rev.* **2017**, *110-111*, 3.
[3] D. Zanuy, R. Kotla, R. Nussinov, T. Teesalu, K. N. Sugahara, C. Aleman, N. Haspel, *J. Struct. Biol.* **2013**, *182*, 78.
[4] T. Teesalu, K. N. Sugahara, V. R. Kotamraju, E. Ruoslahti, *Proc. Natl. Acad. Sci. USA* **2009**, *106*, 16157.
[5] G. B. Braun, K. N. Sugahara, O. M. Yu, V. R. Kotamraju, T. Molder, A. M. Lowy, E. Ruoslahti, T. Teesalu, *J. Controlled Release* **2016**, *232*, 188.
[6] a) K. N. Sugahara, G. B. Braun, T. H. de Mendoza, V. R. Kotamraju, R. P. French, A. M. Lowy, T. Teesalu, E. Ruoslahti, *Mol. Cancer Ther.* **2015**, *14*, 120; b) K. N. Sugahara, P. Scodeller, G. B. Braun, T. H. de Mendoza, C. M. Yamazaki, M. D. Kluger, J. Kitayama, E. Alvarez, S. B. Howell, T. Teesalu, E. Ruoslahti, A. M. Lowy, *J. Controlled Release* **2015**, *212*, 59; c) S. Niland, J. A. Eble, *Int. J. Mol. Sci.* **2019**, *20*, 639.
[7] G. S. Nowakowski, D. Mukhopadhyay, X. Wu, N. E. Kay, *Leuk. Res.* **2008**, *32*, 1634.
[8] a) E. Wonder, L. Simon-Gracia, P. Scodeller, R. N. Majzoub, V. R. Kotamraju, K. K. Ewert, T. Teesalu, C. R. Safinya, *Biomaterials* **2018**, *166*, 52; b) A. M. Willmore, L. Simon-Gracia, K. Toome, P. Paiste, V. R. Kotamraju, T. Molder, K. N. Sugahara, E. Ruoslahti, G. B. Braun, T. Teesalu, *Nanoscale* **2016**, *8*, 9096; c) G. B. Braun, T. Friman, H. B. Pang, A. Pallaoro, T. Hurtado de Mendoza, A. M. Willmore, V. R. Kotamraju, A. P. Mann, Z. G. She, K. N. Sugahara, N. O. Reich, T. Teesalu, E. Ruoslahti, *Nat. Mater.* **2014**, *13*, 904.
[9] K. N. Sugahara, T. Teesalu, P. P. Karmali, V. R. Kotamraju, L. Agemy, O. M. Girard, D. Hanahan, R. F. Mattrey, E. Ruoslahti, *Cancer Cell* **2009**, *16*, 510.
[10] E. Ruoslahti, *Annu. Rev. Biochem.* **1988**, *57*, 375.
[11] L. Simon-Gracia, H. Hunt, P. Scodeller, J. Gaitzsch, V. R. Kotamraju, K. N. Sugahara, O. Tammik, E. Ruoslahti, G. Battaglia, T. Teesalu, *Biomaterials* **2016**, *104*, 247.
[12] H. Zuo, *J. Oncol.* **2019**, *20*, 936.
[13] L. Paasonen, S. Sharma, G. B. Braun, V. R. Kotamraju, T. D. Chung, Z. G. She, K. N. Sugahara, M. Yliperttula, B. Wu, M. Pellecchia, E. Ruoslahti, T. Teesalu, *ChemBioChem* **2016**, *17*, 570.
[14] a) V. Fogal, I. Babic, Y. Chao, S. Pastorino, R. Mukthavaram, P. Jiang, Y. J. Cho, S. C. Pingle, J. R. Crawford, D. E. Piccioni, S. Kesari, *Oncotarget* **2015**, *6*, 1157; b) V. Fogal, A. D. Richardson, P. P. Karmali, I. E. Scheffler, J. W. Smith, E. Ruoslahti, *Mol. Cell. Biol.* **2010**, *30*, 1303.
[15] V. Fogal, L. Zhang, S. Krajewski, E. Ruoslahti, *Cancer Res.* **2008**, *68*, 7210.
[16] a) P. Saalik, P. Lingasamy, K. Toome, I. Mastandrea, L. Rousso-Noori, A. Tobi, L. Simon-Gracia, H. Hunt, P. Paiste, V. R. Kotamraju, G. Bergers, T. Asser, T. Ratsep, E. Ruoslahti, R. Bjerkvig, D. Friedmann-Morvinski, T. Teesalu, *J. Controlled Release* **2019**, *308*, 109; b) H. Hunt, L. Simon-Gracia, A. Tobi, V. R. Kotamraju, S. Sharma, M. Nigul, K. N. Sugahara, E. Ruoslahti, T. Teesalu, *J. Controlled Release* **2017**, *260*, 142; c) S. Sharma, V. R. Kotamraju, T. Molder, A. Tobi, T. Teesalu, E. Ruoslahti, *Nano Lett.* **2017**, *17*, 1356; d) L. Simon-Gracia, P. Scodeller, S. S. Fuentes, V. G. Vallejo, X. Rios, E. San Sebastian, V. Sidorenko, D. Di Silvio, M. Suck, F. De Lorenzi, L. Y. Rizzo, S. von Stillfried, K. Kilk, T. Lammers, S. E. Moya, T. Teesalu, *Oncotarget* **2018**, *9*, 18682.
[17] P. Scodeller, E. K. Asciutto, *Molecules* **2020**, *25*, 808.
[18] L. Simon-Gracia, H. Hunt, T. Teesalu, *Molecules* **2018**, *23*, 1190.
[19] I. Petta, S. Lievens, C. Libert, J. Tavernier, K. De Bosscher, *Mol. Ther.* **2016**, *24*, 707.
[20] H. Bruzzoni-Giovanelli, V. Alezra, N. Wolff, C. Z. Dong, P. Tuffery, A. Rebollo, *Drug Discovery Today* **2018**, *23*, 272.

[21] a) X. D. Shi, K. Sun, R. Hu, X. Y. Liu, Q. M. Hu, X. Y. Sun, B. Yao, N. Sun, J. R. Hao, P. Wei, Y. Han, C. Gao, *J. Neurosci.* **2016**, *36*, 11959; b) Z. Qian, P. G. Dougherty, D. Pei, *Curr. Opin. Chem. Biol.* **2017**, *38*, 80.
[22] X. Zhang, J. Y. Brossas, C. Parizot, J. M. Zini, A. Rebollo, *Oncotarget* **2018**, *9*, 5944.
[23] I. Arrouss, F. Nemati, F. Roncal, M. Wislez, K. Dorgham, D. Vallerand, N. Rabbe, N. Karboul, F. Carlotti, J. Bravo, D. Mazier, D. Decaudin, A. Rebollo, *PLoS One* **2013**, *8*, e60816.
[24] I. Arrouss, D. Decaudin, S. Choquet, N. Azar, C. Parizot, J. M. Zini, F. Nemati, A. Rebollo, *Protein Pept. Lett.* **2015**, *22*, 539.
[25] V. Janssens, A. Rebollo, *Curr. Mol. Med.* **2012**, *12*, 268.
[26] D. Haesen, W. Sents, K. Lemaire, Y. Hoorne, V. Janssens, *Front. Oncol.* **2014**, *4*, 347.
[27] L. Tian, X. Zhang, D. Haesen, J. Bravo, J. Fominaya, S. Choquet, J. M. Zini, S. Loisel, E. Waelkens, V. Janssens, A. Rebollo, *Int. J. Pept. Res. Ther.* **2017**, *24*, 474.
[28] S. Loisel, K. L. Ster, I. Quintin-Roue, J. O. Pers, A. Bordron, P. Youinou, C. Berthou, *Leuk. Res.* **2005**, *29*, 1347.
[29] a) A. Gaida, U. B. Hagemann, D. Mattay, C. Rauber, K. M. Muller, K. M. Arndt, *Methods Mol. Biol.* **2009**, *535*, 263; b) J. M. Mason, K. M. Müller, K. M. Arndt, *Biochem. Soc. Trans.* **2008**, *36*, 1442; c) C. Recio, F. Maione, A. J. Iqbal, N. Mascolo, V. De Feo, *Front. Pharmacol.* **2016**, *7*, 526; d) B. O. Villoutreix, M. A. Kuenemann, J. L. Poyet, H. Bruzzoni-Giovanelli, C. Labbe, D. Lagorce, O. Sperandio, M. A. Miteva, *Mol. Inf.* **2014**, *33*, 414.
[30] a) K. Fosgerau, T. Hoffmann, *Drug Discovery Today* **2015**, *20*, 122; b) A. A. Kaspar, J. M. Reichert, *Drug Discovery Today* **2013**, *18*, 807; c) M. S. Kinch, *Drug Discovery Today* **2015**, *20*, 393.
[31] M. Ciccone, G. A. Calin, D. Perrotti, *Front. Oncol.* **2015**, *5*, 21.
[32] P. Kalev, A. A. Sablina, *Anti-Cancer Agents Med. Chem.* **2011**, *11*, 38.
[33] C. H. Switzer, R. Y. Cheng, T. M. Vitek, D. J. Christensen, D. A. Wink, M. P. Vitek, *Oncogene* **2011**, *30*, 2504.
[34] P. Neviani, J. G. Harb, J. J. Oaks, R. Santhanam, C. J. Walker, J. J. Ellis, G. Ferenchak, A. M. Dorrance, C. A. Paisie, A. M. Eiring, Y. Ma, H. C. Mao, B. Zhang, M. Wunderlich, P. C. May, C. Sun, S. A. Saddoughi, J. Bielawski, W. Blum, R. B. Klisovic, J. A. Solt, J. C. Byrd, S. Volinia, J. Cortes, C. S. Huettner, S. Koschmieder, T. L. Holyoake, S. Devine, M. A. Caligiuri, C. M. Croce, R. Garzon, B. Ogretmen, R. B. Arlinghaus, C. S. Chen, R. Bittman, P. Hokland, D. C. Roy, D. Milojkovic, J. Apperley, J. M. Goldman, A. Reid, J. C. Mulloy, R. Bhatia, G. Marcucci, D. Perrotti, *J. Clin. Invest.* **2013**, *123*, 4144.
[35] a) K. N. Sugahara, T. Teesalu, P. P. Karmali, V. R. Kotamraju, L. Agemy, D. R. Greenwald, E. Ruoslahti, *Science* **2010**, *328*, 1031; b) G. Gu, X. Gao, Q. Hu, T. Kang, Z. Liu, M. Jiang, D. Miao, Q. Song, L. Yao, Y. Tu, Z. Pang, H. Chen, X. Jiang, J. Chen, *Biomaterials* **2013**, *34*, 5138.
[36] Z. Yan, Y. Yang, X. Wei, J. Zhong, D. Wei, L. Liu, C. Xie, F. Wang, L. Zhang, W. Lu, D. He, *Mol. Pharmaceutics* **2014**, *11*, 218.
[37] a) L. Aoudjehane, P. Y. Boelle, G. Bisch, R. Delelo, F. Paye, O. Scatton, C. Housset, J. Becquart, Y. Calmus, F. Conti, *Lab. Invest.* **2016**, *96*, 672; b) L. Aoudjehane, P. Podevin, O. Scatton, P. Jaffray, I. Dusanter-Fourt, G. Feldmann, P. P. Massault, L. Grira, A. Bringuier, B. Dousset, S. Chouzenoux, O. Soubrane, Y. Calmus, F. Conti, *FASEB J.* **2007**, *21*, 1433.
[38] L. Dominguez-Berrocal, E. Cirri, X. Zhang, L. Andrini, G. H. Marin, S. Lebel-Binay, A. Rebollo, *Sci. Rep.* **2019**, *9*, 4771.

5.2 Article 2: Isolation of primary hepatocytes for testing tumor penetrating peptide in Tumor targeting as new therapeutic approach.

Savier E, Tuffery P, Bruzzoni-Giovanelli H and Rebollo A..
Cell penetrating peptides. Methods and protocols, Third Edition. Methods in Molecular Biology. 2021. doi: 10.1007/978-1-0716-1752-6_26.

Introduction

Les peptides ont de multiples applications en pharmacologie et en médecine (Wang *et al*, 2022) . L'intérêt des peptides bi-fonctionnel est de combiner 2 cibles spécifiques : d'une part un récepteur exprimé majoritairement sur les cellules tumorales et d'autre part l'administration d'un peptide interférant qui va bloquer l'interaction entre 2 protéines d'une voie métabolique dérégulée dans ces cellules tumorales. Nous avons testé ces peptides bi-fonctionnels sur un cancer solide fréquent et plutôt chimiorésistant : le carcinome hépatocellulaire (CHC). Le CHC représente 75%-80% des tumeurs primitive du foie et l'hépatocyte est considérée comme la cellule à l'origine de cette tumeur. Le CHC sur foie sain est rare. Au contraire, le CHC sur hépatopathie chronique représente le 6ème cancer dans le monde, est responsable de ±850 000 nouveaux cas / an et 810 000 morts / an (Sung *et al*, 2021). Sans rentrer dans les détails, déja exposés en introduction de cette thèse, nous rappellerons que la CHC est une tumeur hétérogène au sein d'un massif tumoral, que son traitement doit tenir compte de l'hépatopathie sous-jacente, qu'il est volontiers chimiorésistant et qu'il a une aptitude aux envahissements vasculaires (Llovet *et al*, 2021). L'utilisation de peptides thérapeutiques dans le CHC a déjà été testée et les résultats ont permis d'ouvrir des perspectives (Jin *et al*, 2018; Liu *et al*, 2016; Nambotin *et al*, 2011; Wang *et al*, 2016a, 2016b, 2018; Zan *et al*, 2019; Zhao *et al*, 2018). L'originalité de notre travail réside dans l'utilisation de peptide bi-fonctionnel, avec des TPP et sur les cellules hépatocytaires provenant de CHC humains.

Matériel et méthodes

Les peptides bi-fonctionnels comprenaient 4 TPP (RPARPAR, LinTT1, TT1, iRDG) et 1 IP dirigé contre l'interaction entre les protéines PP2A et SET (Tian *et al*, 2018b).

Les patients informés signaient un consentement et l'échantillon était prélevé au laboratoire d'anatomie-pathologie puis préparé à l'état frais pour isolation des cellules tumorales. Les hépatocytes normaux ont été obtenues à partir de la plateforme ICAN.

Les cellules mises en cultures en présence de peptides fluorescents pendant 4h étaient ensuite examinées par cytométrie en flux. Le marquage à l'arginase permettait d'identifier les cellules comme hépatocytaire.

L'analyse de la conformation des peptides a été faite par modélisation *in silico* et comparée à des séquences peptidiques connues et issues de bases de données de protéines. L'interaction entre les TPP et NRP-1 a également été explorée *in silico*.

Résultats

L'internalisation les peptides était spécifiques des hépatocytes de CHC. Aucun hépatocyte sain n'internalisait de peptide.

Chaque TPP avait une conformation propre, héliocoïdale pour LinTT1, sous forme de chaine beta pour iRGD, ou bien moins structurée pour TT1 et RPARPAR.

Le site d'interaction entre les TPP et le récepteur NRP-1 serait situé sur le domaine b1 du récepteur. Une séquence proche du CendR (K/RxxK/R) est le motif KETK, qui correspond à l'interaction entre NRP-1 et VEGF. Cependant, KETK est proche mais distinct du domaine b1.

Conclusion

Les résultats observés avec les 4 TPP-IP sur ces cellules de CHC étaient encourageants et incitaient à poursuivre dans cette direction.

Chapter 26

Isolation of Primary Hepatocytes for Testing Tumor Penetrating Peptides

Eric Savier, Pierre Tuffery, Heriberto Bruzzoni-Giovanelli, and Angelita Rebollo

Abstract

Methods for isolation of human primary cells is an important tool to be able to test the effect of several drugs for the treatment of diseases. Protocols have been described for the isolation of healthy and tumoral hepatocytes; however, the quality and the amount of the isolated cells is not satisfactory. We describe here protocols for the isolation of healthy and tumoral hepatocytes as well as the use of tumor penetrating and interfering peptides as new therapeutics. Peptides are showed to be safe drugs and taking into account recent improvements in peptide administration, biodelivery, and bioavailability. Tumor penetrating peptides fused to an interfering peptide have a great potential to become therapeutic agents.

Keywords Tumor penetrating peptides, Interfering peptides, Liver cancer

1 Introduction

1.1 Liver Cancer

Liver cancer includes heterogeneous malignant diseases, but 75–85% of primary liver cancer is the hepatocellular carcinoma (HCC) which derived from hepatocyte. Human HCC is classified into two major subgroups in terms of genomic stability. The histology-based definition of the morphological heterogeneity of liver cancer is modified in an effort to treat patients with personalized therapies. The morphological heterogeneity of liver cancer is demonstrated in tumor differentiation status, tumor growth patterns, and pathological features of paratumor tissues [1].

Other important primary liver cancer is the cholangiocarcinoma which derived from cholangiocyte or mixed histological type (hepatocholangiocarcinoma). Other histological types (angiosarcoma, etc.) have low incidence and will not be evocated in this chapter. In fact, HCC is the sixth most frequent cancer worldwide, and the fourth in terms of global cancer-related mortality with an

Ülo Langel (ed.), *Cell Penetrating Peptides: Methods and Protocols* , Methods in Molecular Biology, vol. 2383,
https://doi.org/10.1007/978-1-0716-1752-6_26,

increasing incidence responsible for 854,000 new cases/year and 810,000 dead (7% of all cancers) [2]. HCC is more frequent in East Asia and sub-Saharan Africa (85% of the cases) and in Europe its age-standardized incidence rate varies from <3.3 to >8.4/100,000 [3]. Therefore, incidence is influenced by the geography but also by the male sex, the viral infection (HBV, HDV, HIV), the alcohol abuse, the non-alcoholic fatty liver disease (NAFLD) [4, 5], some toxins (aflatoxin) or genetic disease (hemochromatosis, anti-alpha 1 antitrypsin deficiency). These factors of risk are responsible for a chronic liver inflammation and fibrosis (HCC with healthy liver exists but is rare) and may conduct to a cirrhosis. Cirrhosis, from any etiology, is a risk factor for HCC, but risk is higher in cirrhotic patients with chronic viral hepatitis [3]. The best treatment would be the prevention by suppression of the viral aggression, to stop alcohol, to control metabolic disorder [4, 5]. However, at the stage of cirrhosis, the risk of HCC persists and only surveillance and early diagnosis make possible to observe good therapeutic results. In any cases, the staging methodology will include the liver function to the tumor burden and performance status (for example BCLC staging system) [6] because liver function (stratification according to the Child–Pugh score or the MELD or portal hypertension) will prevent some therapeutic options. Many types of treatment are used against HCC, but surgical resection, liver transplantation, thermal ablation, transarterial chemoembolization, transarterial radioembolization, and stereotactic body radiation therapy are "local" treatment. Regarding systemic treatment, HCC is a chemoresistant tumor. Consequently, following a "curative" treatment, benefit of any adjuvant therapy has not been demonstrated. In the case of unresectable HCC or metastatic disease or macroscopic vascular invasion, drugs with some efficiency are tyrosine kinase inhibitors (TKI) (sorafenib, lenvatinib, regorafenib, cabozantinib) which are contraindicated in the case of altered liver function. Finally, immunotherapy treatments (PD-1 inhibitors such as nivolumab, pembrolizumab), combination of immune checkpoint inhibitors with TKI (atezolizumab + bevacizumab) are encouraging. Considering the current therapeutic challenge to treat this cancer, it is evident that new and more efficient targeted therapy to HCC is an imperative need. In function of evidence that we are going to detail below, we are convinced that the use of a dual peptide combining a tumor penetrating peptide (specific targeting tumor hepatic cells) and an interfering peptide (targeting PP2A-SET interaction) can be a well-adapted alternative to treat HCC.

We have fused four TPPs to the IP blocking PP2A/SET interaction generating bi-functional peptides able to specifically penetrate into tumoral hepatocytes (Fig. 1) via specific receptors expressed on the cells: NRP1, p32, and integrin v/β3. These peptides induce apoptosis on tumoral hepatocytes and without effect on healthy hepatocytes [7]. Nambotin and co-workers described an

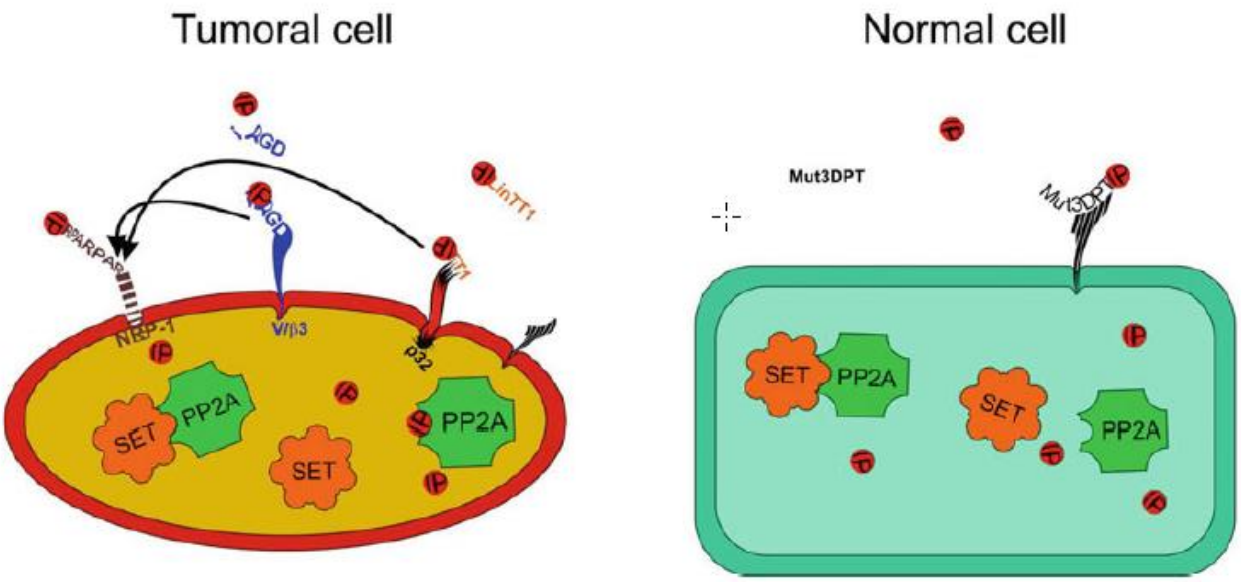

Fig. 1 Schematic representation of the internalization of TPP in normal and tumoral cells

interfering peptide able to internalize into the cells and to antagonize the binding of Frizzled-7 (FZD7) transmembrane receptor, which is overexpressed in HCC, to the PDZ domain of Disheveled adaptor protein (DVL). They demonstrate *in vitro* and *in vivo* that inhibition of FZD7-DVL interaction via an interfering peptide could be a pertinent strategy for HCC treatment [8]. Moreover, several reports have described the use of nanoparticles, cell penetrating peptides, or lipid-modified cell penetrating peptides to delivery of small molecules, inhibitors, chemotherapeutic agents or siRNA for HCC treatment [9–14]. Finally, iRGD-decorated nanoparticles are used for the efficient delivery of the kinase inhibitor vandetanib for HCC treatment, improving the potency and the targeted delivery of currently available agents [15].

1.2 Tumor Penetrating Peptides

Despite tremendous progress in the field of cancer research, little progress is made in the design of effective targeted anticancer therapy [16–18]. Two of most concerning issues of current cancer therapies are lack of addressing to cancer cell and poor molecular target selectivity. As consequence, they frequently induce off-target effects, adverse events and only a small proportion of administrated drug reach its target, the tumor cells. In this way, designing selective drug delivery for cancer drugs, that can bypass these problems and result in more effective and best tolerate treatments, is a priority goal.

In order to overcome these limitations, various approaches/strategies/delivery systems are developed. One of these approaches is the use of Tumor Penetrating Peptides (TPPs), which have gained recognition as specific drug delivery vehicles. TPPs are a subset of Cell Penetrating Peptides (CPPs), well known by their capacity to enter and drive conjugates inside the cell, that

specifically recognize, bind and internalize into tumor cells [19, 20]. They have strong affinity toward specific receptors often present in tumors cells and tumor vasculature. TPPs are defined by the presence of the C-end rule (CendR) motif with the consensus R/KXXR/K [21–23]. This position-dependent motif must be C-terminally exposed to allow the binding to the cell and tissue penetration receptor Neuropilin-1 (NRP-1) [24]. NRP-1 is over-expressed in the tumor vasculature and in a variety of malignant cells *in vitro* and *in vivo* [25]. Binding of the CendR peptide to NRP-1 activates intracellular transport pathway resulting in the tumor-specific extravasation and distribution of the payload into the tumor. The RPARPAR is a prototypic CendR peptide that binds to and internalizes into cells expressing NRP-1 [24, 26]. iRGD was identified by *in vivo* peptide phage display [27, 28]. This TPP is recruited to the tumor vessels by interaction with integrins, through the RGD motif, and after that, is cleaved by tumor-associated proteases to expose the CendR to allow interaction with NRP-1. iRGD has been widely used to increase the penetration of anticancer drugs and nanotherapeutics in several tumor models [29].

TT1 peptide is a cyclic TPP that contains a cryptic CendR motif. TT1 was identified by phage display and binds first to p32 [30], a mitochondrial chaperone aberrantly expressed on the cell surface of malignant cells [31]. TT1 is cleaved by proteases expressed in tumor, exposing the CendR motif that can then bind to NRP-1. The linear version of TT1, LinTT, also binds to p32 protein and follows the same tumor internalization mechanism than TT1. Finally, in recent years, other TPPs have been described and validated for precision tumor delivery [29].

One of the applications of TPP is their use in targeted therapy in which the properties of a TPP are combined with a toxin or drug molecule. Targeted therapy restricts the toxic effect of a drug to the malignant tissues, thereby increasing the efficacy and decreasing the undesired effects of the drug. A number of laboratories have used TPP associated to a cargo in tumor treatment studies using two approaches: either coupled or co-administration of the cargo (doxorubicin, gemcitabine, tyrosine kinase inhibitors, antibodies, nanoparticles).

1.3 Tumor Penetrating and Interfering Peptides

Protein–protein interactions (PPI) are now well recognized as promising therapeutic targets and as consequence molecules able to modulate these interactions have a drug potential [32]. In cancer cells, breaking these interactions could lead, for example, to liberate an antitumor protein (p53, Rb, phosphatases), to allow it to exert its physiological function, or to release an oncogenic protein to prevent its activity and facilitate its degradation. For this reason, peptides able to specifically disrupt PPIs, called interfering peptides (IPs), are receiving increasing attention. Apart from monoclonal

antibodies addressed to extracellular or membrane located targets, most of targeted therapeutic approaches in oncology have focused on the development of small molecules to inhibit intracellular enzymes. Small molecules are well suited to target proteins with particular structural characteristics (such as pockets, grooves, or slits), as is the case of enzymes. However, targeting the relatively large interaction surfaces of PPIs in order to modulate or disrupt them, is a real challenge using small molecules, frequently leading to off-target effects. Our hypothesis is that given their physico-chemical characteristics, medium-sized peptides are better suited than small molecules to interfere with the large surfaces involved in PPIs [32]. The concept of IPs has been validated for several membrane based and extracellular proteins interactions, generating great expectation for their use as therapeutic molecules. Thanks to the fusion of a penetrating sequence with an interfering peptide sequence, we obtain a bi-functional peptide able to target intracellular PPIs [33, 34].

The most targeted-oriented approach to identify IPs is PEP scan technology. The principle of PEP scan is to screening the sequence of one of the partners as a series of overlapping peptides that are associated to a solid support, which is hybridized with the other protein partner. The overlap between consecutive segments allows the identification of the binding site between the two proteins of interest [33, 35–38]. Taking advantage of this approach, we have recently validated a cell penetrating and interfering peptide targeting the PP2A/SET interaction [39, 40]. SET is a polyfunctional protein critically involved in the initiation and progression of cancer [41]. Its overexpression is a recurrent and clinically significant event in many hematologic and solid malignancies. SET also has a role in the development of therapeutic resistance and its functional antagonism allows restoring cancer sensitivity to chemotherapy [42]. The oncogenic activity of SET is mediated by the inhibition of the proteins with which it interacts, notably PP2A and P53. PP2A is a member of the serine-threonine phosphatase family and is responsible for the majority of this activity in eukaryotic cells. It maintains cellular homeostasis by neutralizing most of the intracellular signaling pathways induced by kinases [43].

PP2A is genetically modified or functionally inactivated in many solid cancers and numerous studies show that inhibition of expression and/or function of PP2A may contribute to leukemogenesis in several hematologic malignancies, characterized by an aberrant activity of oncogenic kinases [44–46]. Inhibition of PP2A activity is essential to promote cell transformation, tumor progression, and angiogenesis, indicating that PP2A has a tumor suppressor role [47]. Recent reports show that pharmacological restoration of PP2A tumor suppressor activity effectively antagonizes cancer development and progression [48, 49]. In consequence, the disruption of PP2A-SET interaction using interfering

peptides (PI) could lead to the recovery of antitumor activity of PP2A.

Previously, we have shown that peptides designed using this approach were able to induce apoptosis of tumoral cell lines and primary tumoral B cells *in vitro* and show moderate antitumoral activity in mice bearing xenograft models of chronic lymphocytic leukemia (CLL) [39, 40]. In the same way, we have also preclinically validated a cell penetrating and interfering peptide blocking the interaction between the protein caspase-9 and PP2A [33]. This peptide is entering Phase I clinical trials.

We fused four different TPPs (iRGD, RPARPAR, Linear TT1 (LinTT1) and cyclic TT1 (TT1)) to an IP targeting the SET/PP2A interaction, generating new bi-functional peptides able to target this intracellular interaction in tumoral hepatocytes (Fig. 2). We have shown that these peptides were able to penetrate into tumoral hepatocytes but not into healthy hepatocytes, and that this ability was not affected by the presence of the cargo (IP sequence). The iRGD associated to the IP significantly increases the survival of mice bearing xenograft models of CLL without any evident toxicity, suggesting that this targeted interfering and tumor penetrating peptide has an interesting therapeutic potential [7].

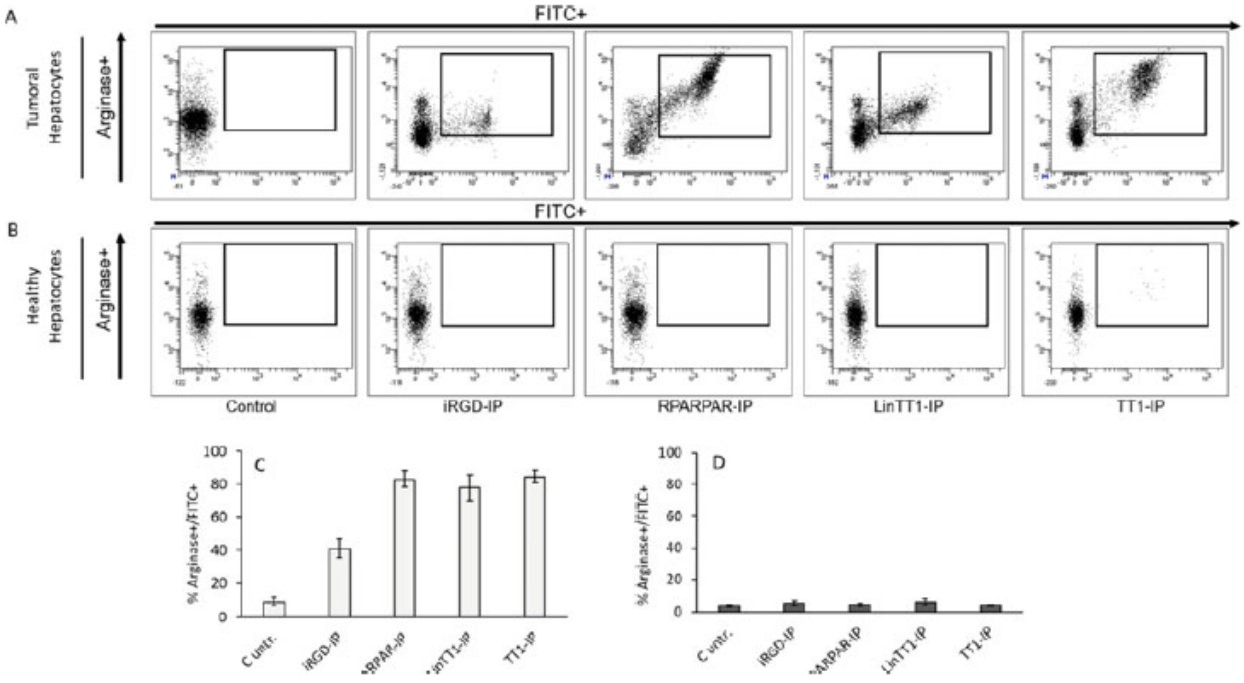

Fig. 2 Analysis of the percentage of hepatocytes internalizing the TPP-IPs. Flow cytometry analysis of the tumoral (**a**) or healthy hepatocytes (**b**) internalizing the TPP-IPs (FITC+) and expressing arginase (arginase+, hepatocyte marker). Hepatocytes are treated for 4 h with 25μM of FITC-labeled TPP-IPs. Representation of the percentage of tumoral (**c**) or healthy (**d**) hepatocytes (arginase+) positive for FITC analyzed by flow cytometry. Untreated cells (C untr.) are used as negative control

1.4 A Structural Perspective of TPPs

We have considered the possibility that the TPPs identified could be associated with some particular three-dimensional structure. To this end, we use a *de novo* approach to peptide structure prediction in the solvent [49], and we have also searched for occurrences of peptide with similar sequences in the structures available in the protein data-bank. Figure 3 shows the predicted structures for the four TPPs. For each, it depicts the conformation of the backbone (left) and a detail of the side chains (right). As can be seen, the structuration is peptide specific, and encompasses helical (AKRGAR STA), beta-turn like (CRGDKGPDC), and less structured conformations (CKRGARSTC, RPARPAR). All the peptides contain a large number of charged residues and the charge repartition in 3D appears also specific of each case, with positive and negative regions for AKRGARSTA and CRGDKGPDC, and a distribution more evenly positive for CKRGARSTC and RPARPAR. Finally, for the two peptides that have cysteines, one observes the possible formation of a disulfide bond between the first and last amino acids (C RGDKGPDC and CKRGARSTC) (Fig. 3).

Interestingly, although the TPPs discussed here have been discovered using random sequence sampling methods, some similar fragments could be identified using FASTA against the PDB sequences identified. The fragment corresponding to residues 195–203 of the PDB entry 3c07:A has a sequence of AERGARLTA , and adopts a helical conformation, similarly to AKRGARSTA. Three PDB entries 1wdy:A, 4g8k:A, and 4oav:B contain fragments of sequence CKRGASTDC, which is similar to CKRGARSTC. The

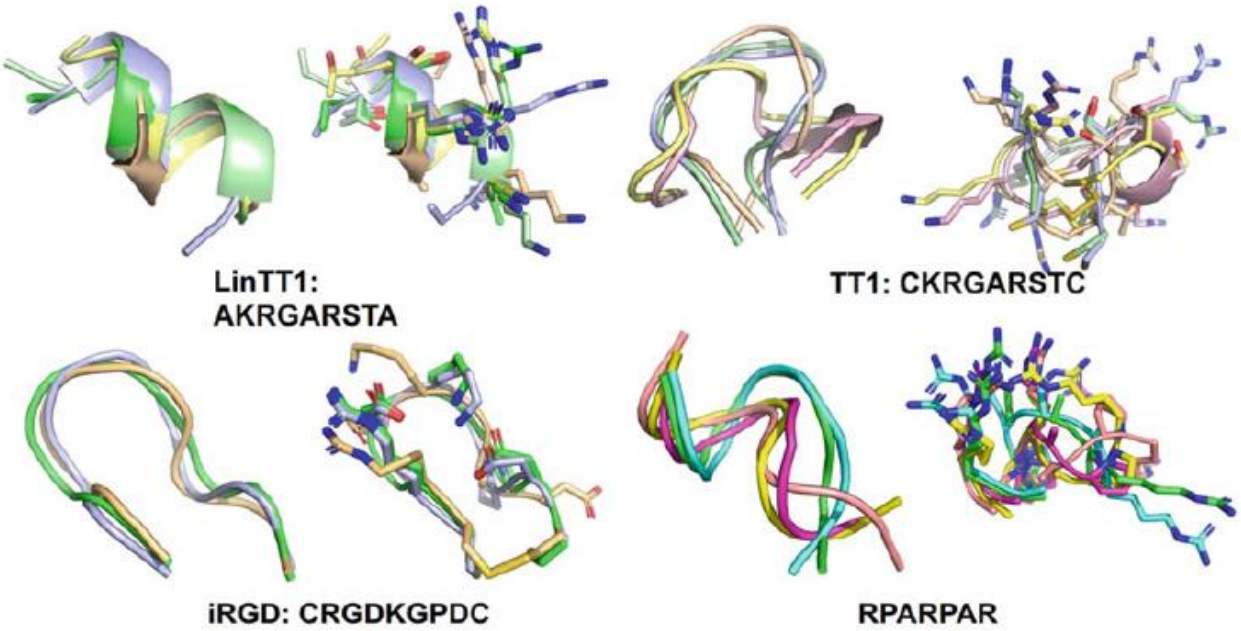

Fig. 3 Predicted TPP 3D-structures. For each TPP, we present the structures of the best models generated using PEP-FOLD. On the left, only a cartoon of the backbone is depicted, whereas side chains are represented on the right. Arrows point to closed disulfide-bonds that occur in some models

structure of one fragment displays a disulfide bond (1wdy:A) and the two others none. Several fragments similar to CRGDKGPDC are detected in PDB entries 1ajj:A, 1wes:A, and 5wlx:A. They adopt rather floppy conformations, and none displays a disulfide bond, despite two of them have at least two cysteines. Note that the significance of these similarities are weak, the E-values being on the order of only 1.

On the NRP1 side, several structures are solved experimentally, providing some insights about NRP1 peptide interactions. Figure 4 summarizes the information available so far, with a focus on domains b1 and b2 that have been reported as interacting with the TPPs. In brief, the residues of NRP1-b1b2 that interact most in the complex structures available are located in the b2 domain. Looking for the occurrence of K/RXXK/R motifs in the structures of the partners of NRP1-b1b2, only one such motif—KETK—could be identified at position 74 in PDB entry 4deq which describes the interaction between NRP1 and VEGF. The VEGF motif KETK is located close to but not in direct interaction with NRP1 b1 domain, which makes implications of this observation

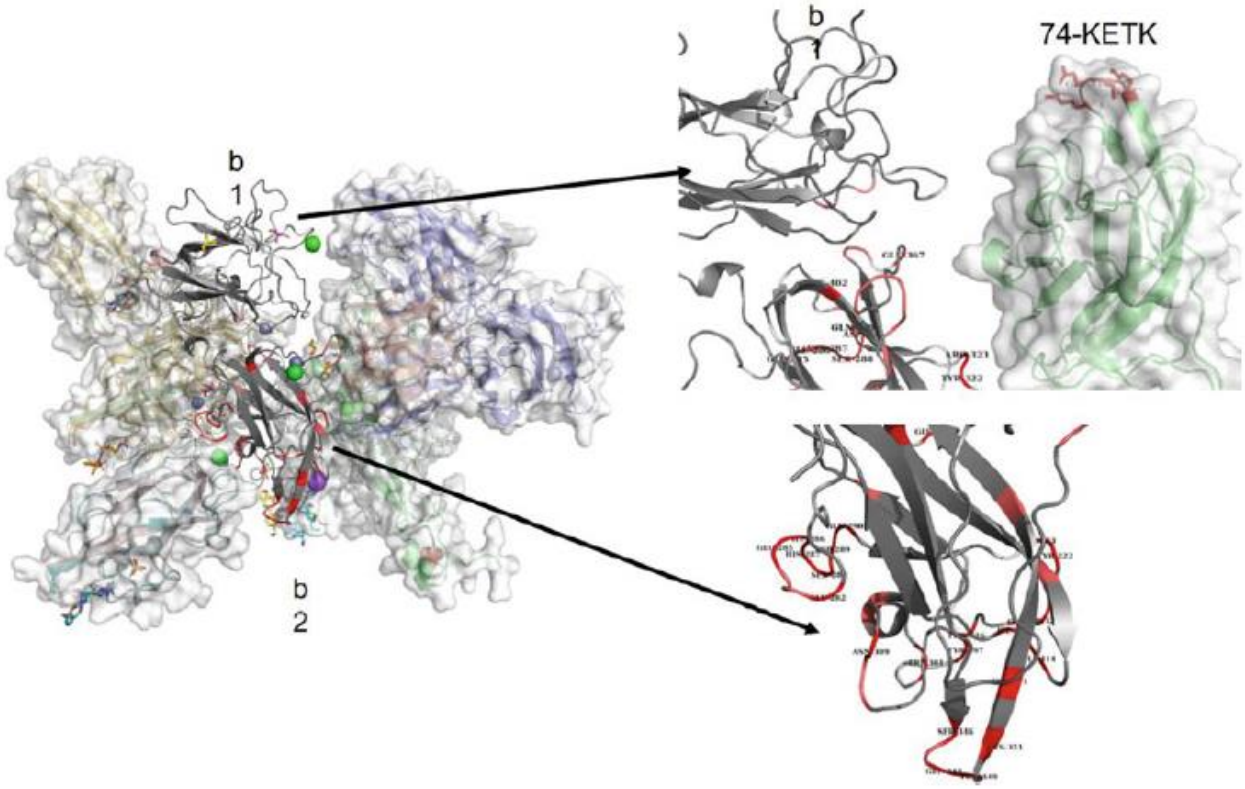

Fig. 4 Observed interactions of NRP1-b1b2 domains in experimentally solved structures. NRP1 domains b1 and b2 are represented as cartoon and surrounded by their interactants, as observed from the information available in the PDB. Most frequently interacting residues of NRP1 are colored using red shades, and occur more frequently in domain b2 (detailed bottom right). Looking at the occurrence of K/LXXK/R motifs in the interacting proteins, only one such motif (KETK) located close to NRP1 could be identified in PDB entry 4deq (right, top)

uncertain at this stage (Fig. 4). Nevertheless, peptide interaction with NRP1-b1 is consistent with the results of a former study, suggesting an interaction between the R/KXXR/X motif and NRP1 loop III, based on specific hydrogen bond pattern. However, despite implications of sequence variants on the interaction between R/KXXR/X motif containing peptides and NRP1 have been further studied [50], the exact mechanisms of peptide internalization after the interaction of TPP with NRP1 still remain to be identified.

2 Materials

2.1 FACS Analysis

1. PBS buffer: 8 g/L NaCl, 0.2 g/L KCl, 1.44 g/L $NaHPO_4$, 0.24 g/KH_2PO_4 L.
2. 24-well plates.
3. Anti-p32 antibody: 1:1000 dilution.
4. Anti-NRP-1 antibody: 1:1000 dilution.
5. Anti-integrin v/β3 antibody: 1:1000 dilution.
6. Anti-arginase antibody: 1:1000 dilution.
7. FITC-labeled secondary antibodies (*see* **Note 1**).
8. APC-labeled secondary antibodies (*see* **Note 1**).
9. FACScanto II for flow cytometry.
10. FITC-labeled peptides synthetized by solid phase procedure and standard Fmoc chemistry (*see* **Note 2**).

2.2 Microscopy

1. PBS buffer (NaCl 8 g/L, KCl 0.2 g/L, $NaHPO_4$ 1.44 g/L, KH_2PO_4 0.24 g/L).
2. DMEM culture medium.
3. 10% Fetal calf serum (FCS): 50 mL of FCS in 450 mL of culture medium DMEM.
4. 4% Formaldehyde diluted in PBS buffer.
5. Cytospin centrifuge.
6. DAPI nuclear labeling.
7. Fluorescence microscopy.
8. FITC-labeled peptides (*see* **Notes 3** and **4**).

2.3 Isolation of Primary Hepatocytes

1. PSA buffer: 8 g/L NaCl, 0.2 g/L KCl, 1 g/L glucose, 0.35 g/L $NaHCO_3$, 1 mL/L phenol red.
2. 5 mg/L Collagenase in PSA buffer.
3. 10 mg/mL Dispase in PSA buffer.

4. The liver sample is perfused with recirculating perfusion solution containing 5 mg/mL collagenase at 37 °C. Afterwards, the tissue is transferred into a Petri dish containing Wash Medium.
5. Tissue is disrupted mechanically by shaking and using tweezers to disrupt cells from the remaining extracellular matrix structures. Cellular suspension is filtered through a gauze-lined funnel. Cells are collected at low speed centrifugation. The supernatant is removed and pelleted hepatocytes are resuspended in Hepatocyte Wash Medium.
6. Cell viability is determined by trypan blue exclusion test. Freshly isolated normal or steatotic hepatocytes are suspended in Williams' medium E containing 10% FCS 1% penicillin–streptomycin and insulin.
7. The cells are seeded in 12-well plates pre-coated with type I collagen and incubated at 37 °C in 5% CO_2 overnight. Medium is replaced with fresh complete hepatocyte medium supplemented with 1μmol/L hydrocortisone hemisuccinate and cells are left in this medium until incubation with peptides.
8. Tumoral human hepatocytes are isolated from tumoral liver samples collected from adult patients undergoing surgery. Samples are cut in small pieces and treated with 4 mL of dispase and 2 mL of collagenase type I.
9. Samples are incubated at 37 °C under agitation for a maximum of 1 h and the solution is filtered and passed through needles of different diameter size. The volume is completed up to 50 mL with culture medium and centrifuged at 900 rpm for 5 min.
10. Supernatant is discarded and cells cultured in DMEM medium supplemented with 10% FCS and antibiotics until treatment with peptides.

3.3 Quantification of Cellular Internalization

1. Hepatocytes are seeded on 24-well plate and incubated for 4 h with FITC-labeled peptides. After treatment, cells are harvested and washed twice with PBS to remove the free peptides and resuspended in 200μL of PBS.
2. FITC fluorescence intensity of internalized peptides is measured by flow cytometry on a FACSCanto II [37].
3. Data are analyzed with FACSDiva 6.1.3 software.
4. Untreated cells are used as control.
5. We use antibodies for detection of the cell surface TPPs receptors, anti-p32, anti-NRP-1, and integrin v/β3.
6. For the hepatocyte labeling, anti-arginase antibody is used following cell permeabilization. Arginase is a marker for hepatocytes.

4. The liver sample is perfused with recirculating perfusion solution containing 5 mg/mL collagenase at 37 °C. Afterwards, the tissue is transferred into a Petri dish containing Wash Medium.
5. Tissue is disrupted mechanically by shaking and using tweezers to disrupt cells from the remaining extracellular matrix structures. Cellular suspension is filtered through a gauze-lined funnel. Cells are collected at low speed centrifugation. The supernatant is removed and pelleted hepatocytes are resuspended in Hepatocyte Wash Medium.
6. Cell viability is determined by trypan blue exclusion test. Freshly isolated normal or steatotic hepatocytes are suspended in Williams' medium E containing 10% FCS 1% penicillin–streptomycin and insulin.
7. The cells are seeded in 12-well plates pre-coated with type I collagen and incubated at 37 °C in 5% CO_2 overnight. Medium is replaced with fresh complete hepatocyte medium supplemented with 1μmol/L hydrocortisone hemisuccinate and cells are left in this medium until incubation with peptides.
8. Tumoral human hepatocytes are isolated from tumoral liver samples collected from adult patients undergoing surgery. Samples are cut in small pieces and treated with 4 mL of dispase and 2 mL of collagenase type I.
9. Samples are incubated at 37 °C under agitation for a maximum of 1 h and the solution is filtered and passed through needles of different diameter size. The volume is completed up to 50 mL with culture medium and centrifuged at 900 rpm for 5 min.
10. Supernatant is discarded and cells cultured in DMEM medium supplemented with 10% FCS and antibiotics until treatment with peptides.

3.3 Quantification of Cellular Internalization

1. Hepatocytes are seeded on 24-well plate and incubated for 4 h with FITC-labeled peptides. After treatment, cells are harvested and washed twice with PBS to remove the free peptides and resuspended in 200μL of PBS.
2. FITC fluorescence intensity of internalized peptides is measured by flow cytometry on a FACSCanto II [37].
3. Data are analyzed with FACSDiva 6.1.3 software.
4. Untreated cells are used as control.
5. We use antibodies for detection of the cell surface TPPs receptors, anti-p32, anti-NRP-1, and integrin v/β3.
6. For the hepatocyte labeling, anti-arginase antibody is used following cell permeabilization. Arginase is a marker for hepatocytes.

3.4 Visualization of the Peptide Internalization by Fluorescence Microscopy

1. For intracellular localization of FITC-labeled peptides, human primary hepatocytes are seeded in an 8-well plate Labtek.
2. Cells are treated with 25μM FITC-labeled peptides for 3 h, washed three times with PBS and fixed with 4% of formaldehyde for 15 min at room temperature.
3. Samples are washed twice with PBS and mounted in mounting buffer containing DAPI as described [37].
4. Images were captured with a fluorescence microscopy using 40× magnification objective.

3.5 Peptide Structure Prediction and PDB Mining

1. Peptide de novo structure prediction is performed using PEP-FOLD [53].
2. The collection of information from structures available in the PDB is performed using blastp [54] from the sequence of NRP1-b1b2 domains, using an *E*-value of 10^{-40}.
3. The structures associated with NRP1-b1b2 matching chains are collected and superimposed in a common reference piling-up all the PDB chains of the entries, based on the alignment returned by TM-align [55].
4. Pictures are generated using Pymol [56].

4 Notes

1. The fluorochrome-labeled antibodies are protected from light and kept at 4 °C.
2. The FITC-labeled peptides are also protected from light.
3. The solubilized peptides are kept at 4 °C for 3 weeks. For longer periods of time, peptides should be frozen at −20 °C in small aliquots.
4. All the peptides are solubilized in water.
5. The isolation of hepatocytes is made in sterile conditions.

Acknowledgments

This work was supported by Inserm.

References

1. Lu XY, Xi T, Lau WY, Dong H, Zhu Z, Shen F et al (2011) Hepatocellular carcinoma expressing cholangiocyte phenotype is a novel subtype with highly aggressive behavior. Ann Surg Oncol 18:2210–2217

2. Global Burden of Disease Liver Cancer C, Akinyemiju T, Abera S, Ahmed M, Alam N, Alemayohu MA et al (2017) The burden of primary liver cancer and underlying etiologies from 1990 to 2015 at the global, regional, and National Level: results from the global burden

of disease study 2015. JAMA Oncol 3:1683–1691

3. European Association for the Study of the Liver (2018) Electronic address eee, European Association for the Study of the L. EASL Clinical Practice Guidelines: Management of hepatocellular carcinoma. J Hepatol 69:182–236
4. Torre LA, Bray F, Siegel RL, Ferlay J, Lortet-Tieulent J, Jemal A (2015) Global cancer statistics, 2012. CA Cancer J Clin 65:87–108
5. Fattovich G, Stroffolini T, Zagni I, Donato F (2004) Hepatocellular carcinoma in cirrhosis: incidence and risk factors. Gastroenterology 127:S35–S50
6. Llovet JM, Bru C, Bruix J (1999) Prognosis of hepatocellular carcinoma: the BCLC staging classification. Semin Liver Dis 19:329–338
7. Simon-Gracia LSE, Parizot C, Brossas JY, Loisel S, Teesalu T, Conti F, Charllotte F, Scatton O, Aoudjehane L, Rebollo A (2020) Bi-functional therapeutic peptides for targeting malignant B cells and hepatocytes: proof of concept in chronic lymphocytic leukemia. Adv Ther 3:1–13
8. Nambotin SB, Lefrancois L, Sainsily X, Berthillon P, Kim M, Wands JR et al (2011) Pharmacological inhibition of Frizzled-7 displays anti-tumor properties in hepatocellular carcinoma. J Hepatol 54:288–299
9. Zan Y, Dai Z, Liang L, Deng Y, Dong L (2019) Co-delivery of plantamajoside and sorafenib by a multi-functional nanoparticle to combat the drug resistance of hepatocellular carcinoma through reprograming the tumor hypoxic microenvironment. Drug Deliv 26:1080–1091
10. Wang X, Wu F, Li G, Zhang N, Song X, Zheng Y et al (2018) Lipid-modified cell-penetrating peptide-based self-assembly micelles for co-delivery of narciclasine and siULK1 in hepatocellular carcinoma therapy. Acta Biomater 74:414–429
11. Zhao H, Wu M, Zhu L, Tian Y, Wu M, Li Y et al (2018) Cell-penetrating peptide-modified targeted drug-loaded phase-transformation lipid nanoparticles combined with low-intensity focused ultrasound for precision theranostics against hepatocellular carcinoma. Theranostics 8:1892–1910
12. Jin C, Bai L, Lin L, Wang S, Yin X (2018) Paclitaxel-loaded nanoparticles decorated with bivalent fragment HAb18 F(ab')2 and cell penetrating peptide for improved therapeutic effect on hepatocellular carcinoma. Artif Cells Nanomed Biotechnol 46:1076–1084
13. Liu Y, Wu X, Gao Y, Zhang J, Zhang D, Gu S et al (2016) Aptamer-functionalized peptide H3CR5C as a novel nanovehicle for codelivery of fasudil and miRNA-195 targeting hepatocellular carcinoma. Int J Nanomedicine 11:3891–3905
14. Wang G, Jia T, Xu X, Chang L, Zhang R, Fu Y et al (2016) Novel miR-122 delivery system based on MS2 virus like particle surface displaying cell-penetrating peptide TAT for hepatocellular carcinoma. Oncotarget 7:59402–59416
15. Wang J, Wang H, Li J, Liu Z, Xie H, Wei X et al (2016) iRGD-decorated polymeric nanoparticles for the efficient delivery of Vandetanib to hepatocellular carcinoma: preparation and in vitro and in vivo evaluation. ACS Appl Mater Interfaces 8:19228–19237
16. Xie HG, Frueh FW (2005) Pharmacogenomics steps toward personalized medicine. Per Med 2:325–337
17. Watters JW, McLeod HL (2003) Cancer pharmacogenomics: current and future applications. Biochim Biophys Acta 1603:99–111
18. Hanahan D, Weinberg RA (2011) Hallmarks of cancer: the next generation. Cell 144:646–674
19. Teesalu T, Sugahara KN, Ruoslahti E (2013) Tumor-penetrating peptides. Front Oncol 3:216–221
20. Ruoslahti E (2017) Tumor penetrating peptides for improved drug delivery. Adv Drug Deliv Rev 110–111:3–12
21. Zanuy D, Kotla R, Nussinov R, Teesalu T, Sugahara KN, Aleman C et al (2013) Sequence dependence of C-end rule peptides in binding and activation of neuropilin-1 receptor. J Struct Biol 182:78–86
22. Teesalu T, Sugahara KN, Kotamraju VR, Ruoslahti E (2009) C-end rule peptides mediate neuropilin-1-dependent cell, vascular, and tissue penetration. Proc Natl Acad Sci U S A 106:16157–16162
23. Simon-Gracia L, Hunt H, Teesalu T (2018) Peritoneal Carcinomatosis targeting with tumor homing peptides. Molecules 23:150–158
24. Braun GB, Sugahara KN, Yu OM, Kotamraju VR, Molder T, Lowy AM et al (2016) Urokinase-controlled tumor penetrating peptide. J Control Release 232:188–195
25. Sugahara KN, Scodeller P, Braun GB, de Mendoza TH, Yamazaki CM, Kluger MD et al (2015) A tumor-penetrating peptide enhances circulation-independent targeting of peritoneal carcinomatosis. J Control Release 212:59–69
26. Willmore AM, Simon-Gracia L, Toome K, Paiste P, Kotamraju VR, Molder T et al

(2016) Targeted silver nanoparticles for ratiometric cell phenotyping. Nanoscale 8:9096–9101

27. Sugahara KN, Teesalu T, Karmali PP, Kotamraju VR, Agemy L, Girard OM et al (2009) Tissue-penetrating delivery of compounds and nanoparticles into tumors. Cancer Cell 16:510–520
28. Sugahara KN, Braun GB, de Mendoza TH, Kotamraju VR, French RP, Lowy AM et al (2015) Tumor-penetrating iRGD peptide inhibits metastasis. Mol Cancer Ther 14:120–128
29. Simon-Gracia L, Scodeller P, Fuentes SS, Vallejo VG, Rios X, San Sebastian E et al (2018) Application of polymersomes engineered to target p32 protein for detection of small breast tumors in mice. Oncotarget 9:18682–18697
30. Paasonen L, Sharma S, Braun GB, Kotamraju VR, Chung TD, She ZG et al (2016) New p32/gC1qR ligands for targeted tumor drug delivery. Chembiochem 17:570–575
31. Fogal V, Zhang L, Krajewski S, Ruoslahti E (2008) Mitochondrial/cell-surface protein p32/gC1qR as a molecular target in tumor cells and tumor stroma. Cancer Res 68:7210–7218
32. Bruzzoni-Giovanelli H, Alezra V, Wolff N, Dong CZ, Tuffery P, Rebollo A (2018) Interfering peptides targeting protein-protein interactions: the next generation of drugs? Drug Discov Today 23:272–285
33. Arrouss I, Nemati F, Roncal F, Wislez M, Dorgham K, Vallerand D et al (2013) Specific targeting of caspase-9/PP2A interaction as potential new anti-cancer therapy. PLoS One 8:e60816
34. Arrouss I, Decaudin D, Choquet S, Azar N, Parizot C, Zini JM et al (2015) Cell penetrating peptides as a therapeutic strategy in chronic lymphocytic leukemia. Protein Pept Lett 22:539–546
35. Tian L, Zhang X, Nemati F, Vallerand D, Raimonide C, Decaudin D, Jy B, Jm Z, SylvainChoquet S, Mf S, Feillant M, Lester K, Loisel S, Rebollo A (2016) Identification of Ras/Raf binding site and design of interfering peptides with potential clinical application. Integrative Mol Med 36:1–9
36. Dong CZ, Bruzzoni-Giovanelli H, Yu Y, Dorgham K, Parizot C, Zini JM et al (2020) Identification of peptides interfering with the LRRK2/PP1 interaction. PLoS One 15: e0237110
37. Dominguez-Berrocal L, Cirri E, Zhang X, Andrini L, Marin GH, Lebel-Binay S et al (2019) New therapeutic approach for targeting hippo Signalling pathway. Sci Rep 9:4771–4783
38. Pierrot C, Zhang X, Zanghi G, Freville A, Rebollo A, Khalife J (2018) Peptides derived from Plasmodium falciparum leucine-rich repeat 1 bind to serine/threonine phosphatase type 1 and inhibit parasite growth in vitro. Drug Des Devel Ther 12:85–88
39. Tian L, Zhang X, Haesen D, Bravo J, Fominaya J, Choquet S, Zini J, Loisel S, Waelkens E, Janssens V, Rebollo A (2017) Identification of PP2A/SET binding sites and design of interfering peptides with potential clinical application. Int J Pept Res Ther 5:39–48
40. Andrini L, Marin GH, Inda AM, Bruzzoni-Giovanelli H, Garcia M, Errecalde J et al (2020) Anti-tumoral effect of a cell penetrating and interfering peptide targeting PP2A/SET interaction. Folia Med 62:31–36
41. Neviani P, Harb JG, Oaks JJ, Santhanam R, Walker CJ, Ellis JJ et al (2013) PP2A-activating drugs selectively eradicate TKI-resistant chronic myeloid leukemic stem cells. J Clin Invest 123:4144–4157
42. Hung MH, Chen KF (2017) Reprogramming the oncogenic response: SET protein as a potential therapeutic target in cancer. Expert Opin Ther Targets 21:685–694
43. Wlodarchak N, Xing Y (2016) PP2A as a master regulator of the cell cycle. Crit Rev Biochem Mol Biol 51:162–184
44. Seshacharyulu P, Pandey P, Datta K, Batra SK (2013) Phosphatase: PP2A structural importance, regulation and its aberrant expression in cancer. Cancer Lett 335:9–18
45. Janssens V, Goris J, Van Hoof C (2005) PP2A: the expected tumor suppressor. Curr Opin Genet Dev 15:34–41
46. Janssens V, Rebollo A (2012) The role and therapeutic potential of Ser/Thr phosphatase PP2A in apoptotic signalling networks in human cancer cells. Curr Mol Med 12:268–287
47. Ciccone M, Calin GA, Perrotti D (2015) From the biology of PP2A to the PADs for therapy of hematologic malignancies. Front Oncol 5:21–31
48. Chien W, Sun QY, Lee KL, Ding LW, Wuensche P, Torres-Fernandez LA et al (2015) Activation of protein phosphatase 2A tumor suppressor as potential treatment of pancreatic cancer. Mol Oncol 9:889–905
49. Oaks JJ, Santhanam R, Walker CJ, Roof S, Harb JG, Ferenchak G et al (2013) Antagonistic activities of the immunomodulator and PP2A-activating drug FTY720 (Fingolimod,

Gilenya) in Jak2-driven hematologic malignancies. Blood 122:1923–1934

50. Parker MW, Linkugel AD, Vander Kooi CW (2013) Effect of C-terminal sequence on competitive semaphorin binding to neuropilin-1. J Mol Biol 425:4405–4414
51. Aoudjehane L, Boelle PY, Bisch G, Delelo R, Paye F, Scatton O et al (2016) Development of an in vitro model to test antifibrotic drugs on primary human liver myofibroblasts. Lab Investig 96:672–679
52. Aoudjehane L, Podevin P, Scatton O, Jaffray P, Dusanter-Fourt I, Feldmann G et al (2007) Interleukin-4 induces human hepatocyte apoptosis through a Fas-independent pathway. FASEB J 21:1433–1444
53. Thevenet P, Shen Y, Maupetit J, Guyon F, Derreumaux P, Tuffery P (2012) PEP-FOLD: an updated de novo structure prediction server for both linear and disulfide bonded cyclic peptides. Nucleic Acids Res 40:W288–W293
54. Altschul SF, Gish W, Miller W, Myers EW, Lipman DJ (1990) Basic local alignment search tool. J Mol Biol 215:403–410
55. Zhang Y, Skolnick J (2005) TM-align: a protein structure alignment algorithm based on the TM-score. Nucleic Acids Res 33:2302–2309
56. DeLano WL (2002) Unraveling hot spots in binding interfaces: progress and challenges. Curr Opin Struct Biol 12:14–20

5.3 Article 3: PEPscan approach for the identification of protein-protein interfaces: lessons from experiment.

Rebollo A, Savier E and Tuffery P.
Biomolecules. 2021. 11, 772-780. doi.org/10.3390/biom11060772

Introduction

Le PEPscan est une technique ancienne qui a récemment connu un regain d'intérêt pour l'identification des peptides interférants (IP), c'est-à-dire des peptides capables d'interférer avec les interactions protéine-protéine (PPI pour *protein-protein interaction*). Son principe consiste à découper une séquence protéique en une série de peptides de 12 acides aminés (AA) qui partagent entre eux un chevauchement de 2 acides aminés. Ces peptides une fois synthétisés sont immobilisés et alignés sur une membrane de nitrocellulose, afin de tester leur capacité à se lier à la protéine dont on cherche à étudier l'interaction. Les points de fixation apparaissent en nombre limités et correspondent aux candidats IP.

But du travail

Décrire 14 PEPscans effectués pour des protéines d'intérêt en cancérologie et dont la structure tridimensionnelle était connue afin de confronter les résultats obtenus *in vitro* aux informations de structures *in silico*.

Matériel et méthodes

Les protéines et les PPI choisies concernaient : Bcl-2/K-Ras ; Bcl-X_L/K-Ras ; Caspase-9/PP2A ; Caspase-9/SET ; K-RAS/Raf ; PP2A/SET ; TEAD/YAP ; TEAD/TAZ.

Les protocoles PEPscan étaient tous identiques : peptides de 12 AA avec 2 AA de décalage.

La révélation de l'interaction peptide-protéine était faite par un anticorps anti-protéine lui-meme revelé par un anticorps secondaire conjugué à la peroxidase de raifort révélé par chemiluminescence.

Un site d'interaction était défini par la présence d'au moins 3 spots de fixation consécutifs et associés à un signal fort. La chaine d'acides aminés communs à ces spots consécutifs était appelée fragment maximal de chevauchement (MOF pour *maximally overlapping fragment*) et correspondait à une séquence candidate pour un possible IP.

A partir de bases de données sur la structure des protéines, des informations sur les sites d'interfaces considérées ou d'homologues protéiques ont été obtenues. Un z-score permettait d'estimer la position du MOF par rapport au site d'interface (z-score >0 : plutôt proche, z-score < 0 : plutôt éloigné).

Résultats

Nous avons montré que pour presque tous ces complexes, le PEPscan était capable d'identifier des candidats IP et en nombre relativement faible (moyenne = 2,21 et médiane = 2). La localisation des MOF sur la structure 3D des protéines pouvait correspondre ou non à un site proche de l'interface ou un site périphérique. Un z-score n'a été positif que 5 fois, parmi lesquels 1 seul avait une petite activité biologique. Inversement, parmi les 9 MOF qui présentaient une certaine activité biologique et pour lesquels les coordonnées 3D étaient disponibles, 8 avaient un z-score négatif.

Conclusions

PEPscan est une manière peu coûteuse et rapide d'identifier des IP susceptibles d'avoir des applications. Les informations structurelles disponibles doivent encore etre interprétées avec prudence.

biomolecules

MDPI

Article

Pepscan Approach for the Identification of Protein–Protein Interfaces: Lessons from Experiment

Angelita Rebollo [1], Eric Savier [2] and Pierre Tuffery [3,*]

[1] UTCBS, Inserm 1265, Faculté de Pharmacie, Université de Paris, 75013 Paris, France; angelita.rebollo@parisdescartes.fr
[2] Department of Hepatobiliary and Liver Transplantation Surgery, Pitié-Salpêtrière Hospital, AP-HP, Sorbonne Université, 75013 Paris, France; eric.savier@aphp.fr
[3] BFA, CNRS, UMR 8251, Inserm U1133, Université de Paris, F-75013 Paris, France
* Correspondence: pierre.tuffery@univ-paris-diderot.fr; Tel.: +331-5727-8374

Abstract: PEPscan is an old approach that has recently gained renewed interest for the identification of interfering peptides (IPs), i.e., peptides able to interfere with protein–protein interactions (PPIs). Its principle is to slice a protein sequence as a series of short overlapping peptides that are synthesized on a peptide array and tested for their ability to bind a partner, with positive spots corresponding to candidate IPs. PEPscan has been applied with a rather large success in various contexts, but the structural determinants underlying this success remain obscure. Here, we analyze the results of 14 PEPscan experiments, and confront the in vitro results with the available structural information. PEPscan identifies candidate IPs in limited numbers that in all cases correspond to solvent-accessible regions of the structures, their location at the protein–protein interface remaining to be further demonstrated. A strong point of PEPscan seems to be its ability to identify specific IPs. IPs identified from the same protein differ depending on the target PPI, and correspond to patches not frequently involved in the interactions seen in the 3D structures available. Overall, PEPscan seems to provide a cheap and rapid manner to identify candidate IPs, that also comes with room for improvement.

Keywords: PEP-scan; protein–protein interaction; interfering peptide; binding specificity

Citation: Rebollo, A.; Savier, E.; Tuffery , P. Pepscan Approach for the Identification of Protein–Protein Interfaces: Lessons from Experiment. *Biomolecules* **2021**, *11*, 772. https://doi.org/10.3390/biom11060772

Academic Editor: Mark S. Johnson

Received: 20 April 2021
Accepted: 18 May 2021
Published: 21 May 2021

1. Introduction

Peptide arrays are a technology with a wide range of applications in basic and applied research, which is now nearly 40 years old and has been commercially available for about ten years. An array comprises hundreds to thousands of different peptides sequences immobilized in a solid support that can be tested simultaneously, offering many possibilities to analyse different signalling pathways between normal and pathological conditions, drug discovery, sequence dependent reactivity etc. Among the applications, one of the most common has been epitope mapping for antibodies [1], including the identification of linear epitopes between the IL-10 and its receptor [2], viral antigen epitopes [3,4], T and B cell epitopes [5]. Other applications relate to the identification of binding sequences between protein/peptide or protein/protein, screen of enzyme substrate and identification of peptides implicated in cell adhesion. These include, to cite some, the identification of novel cell adhesion peptides using a SPOT array of fibronectin peptides [6], the identification of peptides adhering to tumoral breast cancer cell line MDAMB 435 and MCF7 [7], the screening of antimicrobial peptides [8], the identification of immunogenic epitopes in individuals exposed to malaria infection [9], the detection of HLA alloantibodies in organ transplantation [10], the identification and characterization of LIR motifs on ATG8 proteins, which are small ubiquitin-like proteins critically involved in autophagy [11].

The usage of peptide arrays differs depending on the choice of peptide synthesis, solid support, immobilization method, size of the peptides, overlapping size of the peptide, density of spots in the membrane and detection method. SPOT synthesis is the technique

the most widely used to generate peptide arrays [1,12–14]. It is based on solid-phase Fmoc chemistry to synthesize peptides on a membrane support. The membrane support used for arrays is usually cellulose, which is compatible with Fmoc-based peptide synthesis and the biological assay [1,15]. For other chemistries non-compatible with nitrocellulose, alternative material may be used, such as polytetrafluoroethylene (PTFE) membranes or polyethylene films [16–18], glass [19] or metal films. The choice of the support conditions the immobilization strategies, peptide density and detection method to analyze the array.

Although recent publications have reported labeling-free methods to analyze the arrays, such as surface plasmon resonance and mass spectrometry [20], the majority of the peptide arrays are analyzed using labeling-dependent assays. The most commonly used detection methods are based on radioactivity, chemiluminescence, colorimetry and fluorescence, the latter three being the preferred methods when using antibodies to analyze the experiment. These require an incubation with a primary antibody, that binds to the reacted peptides. The array is incubated with a secondary antibody that is usually conjugated to a reporter enzyme [21–25]. The membrane is then analyzed in terms of the spots associated with some signal. Of note, these assays are rapid but usually reported as giving rise to false positive results.

One method derived specifically to identify an active region of a sequence of interest is the PEPscan approach [3]. Its principle is to systematically slice a protein or a protein fragment as a series of overlapping fragments of fixed size, and to test each fragment for its binding with a partner protein using a peptide array. The most commonly used size of peptide for PEPscan ranges from 4 to 20 amino acids, with an overlap ranging from 1 to 10 peptides, while the density of the spot in a membrane ranges from a few to thousands of peptides. This to not to mention that each investigator may adapt this approach to its own needs. Although possible, the mapping of the discontinuous binding sites using PEPscan may sometimes turn more difficult due to the lower affinities of the individual fragments with the corresponding partner [26]. One of the first applications of PEPscan was the identification of epitopes recognized by monoclonal antibodies [27] as well as the recognition of T and B cells epitopes [5,28–30]. The epitopes recognized were mapped using a series of 15 mer peptides synthesized using the SPOT method and with a shift of five amino acids between two peptides. Finally, the PEPscan approach has recently re-gained interest due to the difficulties of designing small compounds targeting protein–protein interfaces (PPIs) [31]. According to its design, the goal of PEPscan is, in this context, to identify linear fragments corresponding to continuous sequences located at the protein–protein interface that are expected to interfere with the formation of the complex, thus affecting some biological pathway. However, although PEPscan has led to the successful identification of candidate interfering peptides (IP) showing effective biological activity, one should keep in mind that PEPscan is only an in vitro approach to identify fragments of a protein able to bind a partner it is known to bind to. The binding of a fragment in isolation might differ from the binding of the same fragment in the complete protein. The binding to the partner could trigger conformational changes, as observed for a few cases where the structure of the partner in isolation or in interaction with a peptide is known [32], biasing further interpretation. In terms of biological activity, effects upon binding could result from the binding to a region external to the PPI interface, as is the case for allosteric modulators [33], or simply come from the binding of the IP to other targets. So far, very few results have been reported about PEPscan's ability to truly identify peptides at the protein–protein interface or its ability to identify peptides specifically interfering with a target interaction. In this study, we re-analyze the results obtained for a series of eight protein/protein interactions for which IPs were identified by PEPscan, and we compare it to the structural data available.

2. Materials and Methods

2.1. Data

Given a target PPI between two proteins, two PEPscan experiments can be undertaken: either searching for partner 1 fragments able to bind partner 2, or scanning partner 2 fragments able to bind partner 1. In the former case, partner 1 is scanned as a series of peptides—on the membrane—whose ability to bind partner 2 is tested, while in the latter case, peptides on the membrane correspond to partner 2, and their ability to bind partner 1 one is tested. In the following, we note P1/P2 in an experiment where P1 is on the membrane that is hybridized using P2. In this study, we re-analyze the results of 14 PEPscan experiments targeting 8 PPIs for which structural data is available, at least for the two partners in isolation or in interaction. Table 1 reports the UniProt [34] and Protein Data Bank (PDB) [35] identifiers of the proteins involved in each PPI, whereas Table 2 summarizes the results of each PEPscan experiment related to the PPIs. These correspond to (1) the interaction between the kinase Raf and the pro-apoptotic proteins BLC2 and BCL-X_L (unpublished results), (2) the phosphatase PP2A and the cysteine protease caspase-9, which is deregulated in apoptosis and tumoral transformation [36,37], (3) the interaction between the oncoprotein Ras and the kinase Raf, also deregulated in many type of cancers [38,39], (4) the interaction between the transcription factors TEAD/YAP and TEAD/Taz, implicated in the Hippo signaling pathway, also deregulated in some type of cancers, such as breast cancer and uveal melanoma [40], (5) the interaction between the phosphatase PP2A and its physiological inhibitor, the oncoprotein SET, strongly deregulated in hematological malignancies [41,42] and (6) the interaction between the cysteine protease caspase-9 and the oncoprotein SET (patent WO2016156536). For BCL-2–K-Ras and TEAD-TAZ, the results for only one PEPscan experiment out of 2 were available. Apart from the interaction between kinase Raf and the pro-apoptotic proteins BLC2 and BCL-X_L, for which the membranes are presented in Figure 1, the raw data correspond to those of the corresponding references.

Table 1. UniProt and PDB identifiers of the proteins.

Protein	UniProt	Structure
BCL-2	P10415	2xa0
BCL-X_L	Q8SQ42	4qnq/1bxl
Caspase-9	P55211/Q8C3Q9	1jxq/2ar9
K-Ras	P32883-2	5uk9
PP2A	P67775	5w0w
Raf	P04049	3omv/4g0n
SET	Q01105-2	2e50
TEAD	Q15562	3kys/3l15
YAP	P46937	3kys
TAZ	Q9GZV5	5gn0

Other PEPscan experiments for which no experimental 3D structure could be identified were not included in this data set. This is the case of the experiment targeting the interaction between two proteins of the parasite *Plasmodium falciparum*, the phosphatase PP1 and the protein LRR1, involved in malaria parasite development [43], and of the recently published study targeting the phosphatase PP1 and the kinase LRRK2 involved in Parkinson disease [44] (Patent PCT 20141031).

2.2. PEPscan Protocol

All the PEPscan experiments were undertaken using a constant protocol.

2.2.1. Binding Assay on Cellulose-Bound Peptides

Overlapping dodecapeptides with two amino acid shifts, spanning the complete sequence of one protein, were prepared by automated spot synthesis (Abimed, Langerfeld, Germany) on an amino-derived cellulose membrane, as described [1,12]. The membrane

was saturated using 3% non-fat dry milk/3% bovine serum albumin (BSA) (2 h, room temperature) incubated with purified partner protein (overnight, 4 °C) and after several washing steps, incubated with an antibody against the protein partner (2 h, room temperature) followed by horse radish peroxidase (HRP)-conjugated secondary antibody (1 h, room temperature). Positive spots were visualized using the ECL system (Bio-Rad).

2.2.2. Peptide Synthesis and Sequence

Peptides were synthesized in an automated multiple peptide synthesis with a solid-phase procedure and standard Fmoc chemistry. The purity and composition of the peptides were confirmed by reverse-phase high-performance liquid chromatography (HPLC) and mass spectrometry.

2.3. Candidate Peptide Identification from Membranes

For the analysis of the PEPscan membranes, a specific question arises from the partial redundancy of the consecutive spots that share the overlapping residues. Commonly noticed is that there is no standard number of consecutive reacting spots revealing a positive interaction. In general, it is accepted that a positive binding site requires the presence of at least 3 consecutive positive spots with a strong enough signal, sometimes with a difference in the intensity signal between the medium spot and the end spots. However, this is not a general rule, as illustrated in Figure 1. Occasionally, a ringspot effect is observed. This corresponds to spots for which a stronger signal of hybridization is observed on the ring of the spot compared to the center of the spot. This irregular signal can make the choice between binding and non-binding [45]. One possible explanation for this effect is a possibly higher concentration of the peptide in the center of the spot, resulting in the exhaustion of the signal before detection. Another explanation is a concentration gradient of the amino acids from the center to the ring of the spot during synthesis, giving a lower concentration of peptide in the core of the spot. These spots are not considered in a particular manner in our study. Here, we have considered the IPs reported by the authors of the studies, but our re-analysis of the membrane sometimes led us to accept newcomers to better sense the significance of the positives in terms of 3D structure (see Table 1).

Since the sequences of the consecutive spots overlap here by all but two, i.e., by 10 amino acids, the spots of a series of consecutive positive spots usually share only a few amino acids. For instance, for a series of 3 consecutive positive spots, 16 amino acids are involved, but the common part of the 3 sequences correspond to the central 8 amino acids. The fragments in common in the largest number of spots, are here referred to as Maximally Overlapping Fragments (MOFs), and the sequences resulting from the union of all the spots are here referred to as candidate IPs.

2.4. Structurally Validated Patches of Interaction

To analyze the specificity of the binding patches, we have searched for structures containing several chains including the proteins of Table 1. For each sequence, we have used blast [46] against the sequences of the PDB with an e-value $< 10^{-10}$ to identify close homologs of the proteins. We have then analyzed which PDB entries encompass several chains (i.e., correspond to complex structures) and identified the chains in interaction with the query. Not to bias the results, we have discarded the interologs (complexes made of homologs) for which each chain has over 70% sequence identity with a previously identified complex. Doing so, we expect to obtain information about only the close homologs of the query, i.e., members of the same family or very close families, and obtain information on how specific the interaction of the associated peptide with a particular target could be, regarding the other structurally characterized interactions of this target, accepting close homologs should interact similarly. For instance, for PP2A, this procedure identifies complexes involving not only the PP2A catalytic chain, but also other phosphatases, such as PP1, PP5, etc. The propensity of a residue to be located at an interface was then simply set up as the number of times it was at an interface divided by the number of complexes

identified. Z-scores were calculated on a per protein basis, using as reference the mean and standard deviations of the propensities over the whole ensemble of residues of the protein, and as observation the propensities averaged over the residues of the IPs. Positive values indicate a tendency to be located more frequently at PPI interface, while negative values indicate a tendency to be located less frequently at PPI interface.

3. Results

3.1. A Note on PEPscan Experiment Reproducibility

It is important to note that the relationship between the signal intensity and the affinity of the peptide/ligand interaction is not straightforward. Several factors may influence the correlation between signal intensity and binding affinity; the synthesis can lead to different amounts of peptide in the spot and the type of detection assay used can also have an influence. In addition, the non-homogeneity of the cellulose membrane can influence the results [45,47]. In general, it is accepted that this type of approach is not well suited to quantify the interaction affinity. Importantly, however, peptide array experiments are fairly reproducible, as illustrated in Figure 1, which presents duplicates of one experiment. Some variations in the intensities of the spots can be observed, but strong signals appear for equivalent spots, meaning that usually, only one experiment is enough to obtain the information that is sought after.

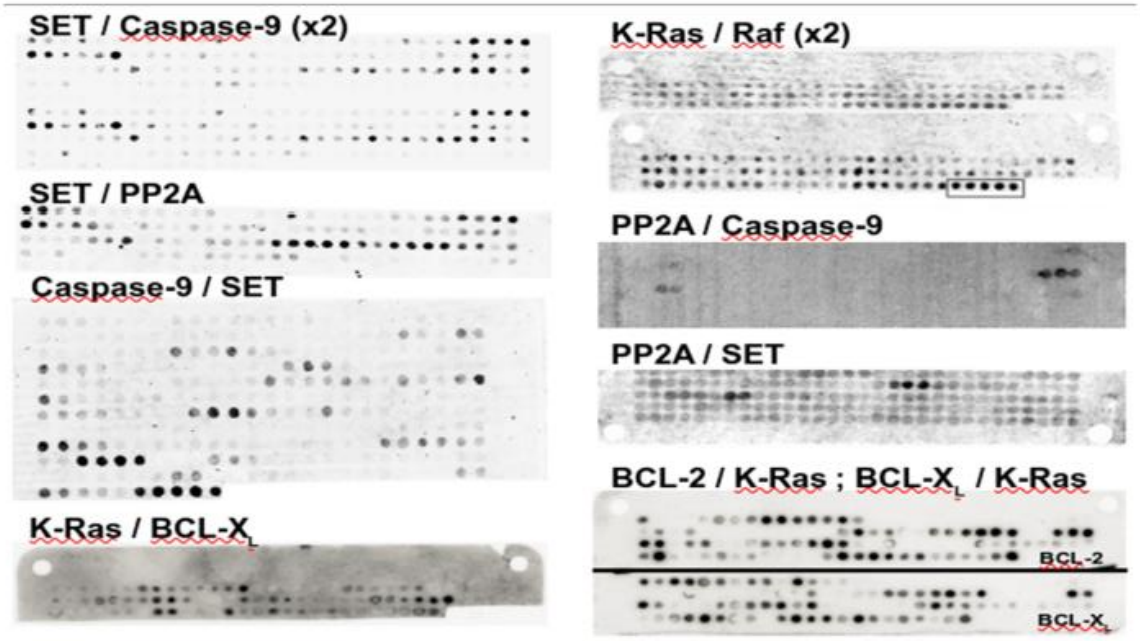

Figure 1. PEPscan membranes. For several cases, the images show the membranes resulting from the PEPscan experiment. Each spot in a raw image corresponds to a peptide of 12 amino acids, and consecutive spots share 10 amino acids in common. Black spots correspond to positive reacting spots. P1/P2 (e.g., SET/PP2A) indicates that P1 (resp. SET) is on the membrane that is hybridized using P2 (resp. PP2A).

3.2. Confronting PEPscan Positive Fragments with Structural Data

Successes achieved using PEPscan for the identification of protein fragments able to interfere with protein–protein interactions raise numerous questions in terms of structure. First, the conformation adopted by the peptides synthesized using SPOT technology is largely unknown and, particularly, the impact of the linker binding to the support (cellulose or other). Second, the impact of splitting proteins into fragments on their conformational balance is also unknown. Third, the strategy to systematically consider all possible fragments, which is necessary when not knowing/considering the structure, also comes with

numerous questions related to the behavior of the core hydrophobic fragments in terms of possibly non-specific binders. Finally, mechanisms for peptide interference with protein–protein interactions could also reveal greater complexity than the straight disruption of the 3D interaction patch. We now discuss these aspects from a series of results on interfering peptide identification.

Table 2 presents all the candidate IPs for 14 PEPscan experiments. The MOFs are in bold. Details on the secondary structure of the fragments corresponding to the IPs show a diversity of topologies. Figure 2 shows, when possible, the location in the 3D structure of the IPs and the MOFs.

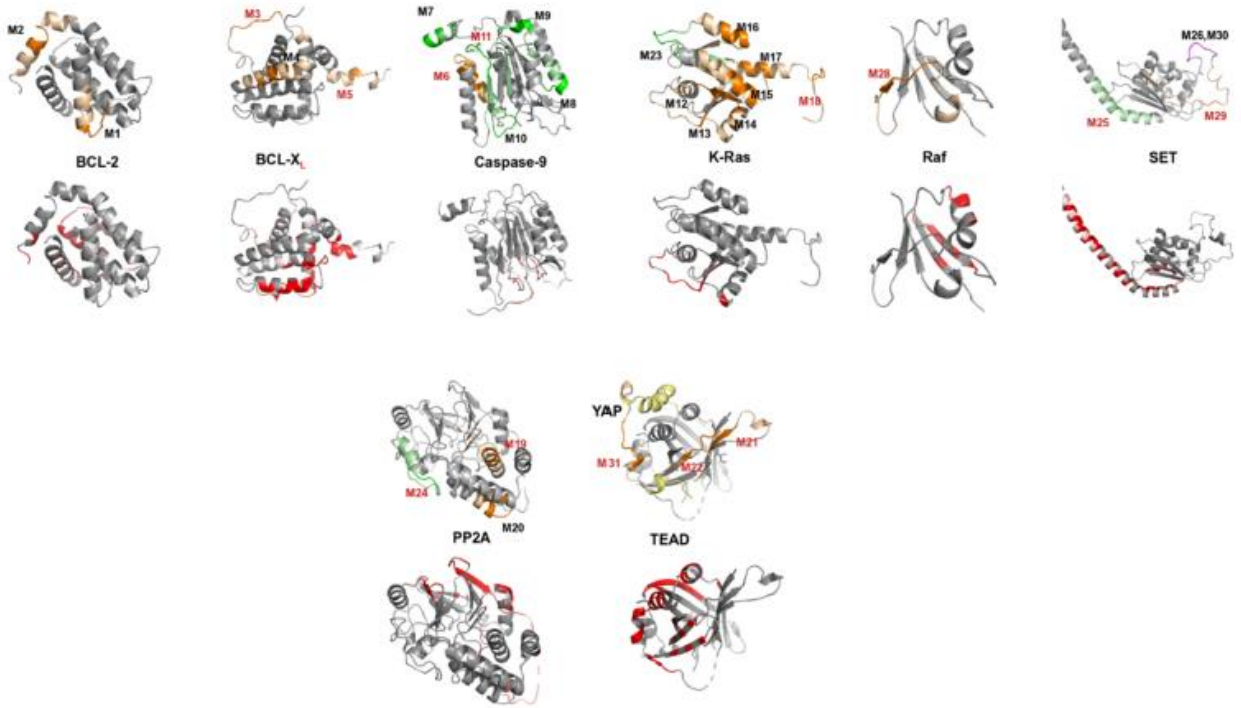

Figure 2. Top: For each of the 8 proteins having undergone a PEPscan, the location of the IPs in the structure is presented. For cases where the IPs of different PEPscans are presented, different colors are employed (green vs. orange). Darker shades correspond to the MOFs. MOFs are labeled as in Table 2. Red labels correspond to IPs showing some biological activity. Bottom: the residues most interacting in the complexes of structure available in the PDB are depicted using a red color gradient.

Table 2. IPs identified by PEPscan.

PEPscan	IPs									
	P1					P2				
	Lbl	Seq	s2	z-sc	Val.	Lbl	Seq	s2	z-sc	Val
BCL-2/K-Ras (×1)	M1	19-IHYKLSQRGYEWDAGDVG	αc	−0.33	-					-
	M2	187-TWIQDNGGWDAFVELYGP	αc	−0.14						
BCL-XL/K-Ras (×1)	M3	27-FSDVEENRTEAPEGTESE (*)	-	-	-	M23	111-MVLVGNKCDLPSRTVDTK	βc	−0.53	-
	M4	163-VSRIAAWMATYLNDHLEP	α	−0.44						
	M5	195-YGNNAAAESRKGQERFNRWFLTGM (*)	-	0.58						
Caspase-9/PP2A (×2)	M6	401-YIETLDGILEQWARSEDL (†+)	αc	−0.28	cpm, cell, aff	M24	175-DTLDHIRALDRLQEVPHEGP (†+)	αc	−0.36	cell
Caspase-9/SET (×2)	M7	133-SGGFGDVGALESLRGN (n)	α	−0.39	cell	M25	53-ILKVEQKYNKLRQPFFQKRSEL (†+)	α	0.94	cell
	M8	199-FMVEVKGDLTAKKMVLAL (n)	βα	−0.2						
	M9	267-FNGTSCPSLGGKPKLFFI (n)	cβ	−0.39						
	M10	348-FPGFVSWRDPKSGSWYVE (n)	cα	1.88		M26	169-RSSQTQNKASRKRQHEEP (†-)	cα	−0.22	
	M11	399-QMPGCFNFLRKKLFFKTS (†+)	βc	0						
K-Ras/Raf (×2)	M12	1-MTEYKLVVVGAGGVGK (n)	βc	−0.19	cpm, cell	M27	1-MEHIQGAWKTISNGFGLK (*†+)	-	-	cell
	M13	31-EYDPTIEDSYRKQVVIDG (3D site) (n)	cβ	1.74						
	M14	61-QEEYSAMRDQYMRTGEGFLCVF (n)	cαβ	0.19						
	M15	91-EDIHHYREQIKRVKDSED (n)	αc	−0.46		M28	103-HEHKGKKARLDWNTDAAS (†+)	cβc	−0.42	
	M16	127-TKQAQELARSYGIPFI (n)	αc	−0.34						
	M17	155-AFYTLVREIRKHKEKMSK (n)	α	−0.4						
	M18	169-KMSKDGKKKKKKSRTRCTVM (†+)	αc	−0.34						
PP2A / SET (×1)	M19	95-ETVTLLVALKVRYRERIT (†+)	αc	−0.28	cpm, cell	M29	151-PSSKSTEIKWKSGKDLTKRSSQ (†+)	Bcα	−0.59	cell
	M20	133-CLRKYGNANVWKYF (n)	α	−0.37		M30	165-DLTKRSSQTQNKASRKRQHEEP (n)	αcα	−0.28	
TEAD / YAP (×1)	M21	227-RLQLVEFSAFVEPPDAVD (†+)	βc	−0.52	cpm, cell	M31	76-KTANVPQTVPMRLRKLPD (†+, 3D site)	c	-	cell
TEAD / TAZ (×1)	M22	293-PPHAFFLVKFWADLNWGPSGEEAGAG (†+, 3D site)	ββ	−0.24	cell					cell

For each PEPscan experiment of identifier "protein1-protein2", P1 (resp. P2) corresponds to a PEPscan experiment in which the membrane containing the protein1 (resp. protein2) fragments is hybridized with protein2 (resp. protein1). The number of duplicates of the experiment is indicated as x1 or x2. Lbl: the unique label of each motif (see Figure 2). Seq: the sequence of the motifs in the UniProt sequence (see Table 1). s2: schematic organization in terms of secondary structure, as determined using dssp [48]. z-sc: specificity z-score (see methods). Val.: Experiment used to probe the motif's activity (cmp: in vitro competition, cell: physiological test, aff: binding affinity measurement, 3D site: the IP is located at PPI interface). Only the IPs labeled using (†) have been tested experimentally (see corresponding references). (†+): peptides showing some activity. (†-): peptides not showing any activity. *: IPs without coordinates in the 3D structures. (n) Peptides not previously reported, but considered during membrane re-analysis

3.3. PEPscan Identifies a Limited Number of IPs

A first observation is that overall, one denotes the existence of a specific answer depending on the PPI studied. Indeed, the IPs identified for the same protein with two different partners are all different, with the exception of SET, for which M26 and M30 have a large overlap. A second observation is that the number of candidate IPs is, as expected, fully unrelated to the size of the protein and, for most of the cases, it is rather low (2.2 on average). It is more than four for only two cases. One such example corresponds to the K-Ras/Raf interaction, for which many spots appear positive, and one region (C-terminus) shows a stronger signal in experiment 2 (Figure 1). The second one corresponds to the caspase-9/SET interaction for which several series of positive spots are lighter than others (Figure 1). For this case, one observes some heterogeneity in the intensities of the spots, and high-intensity spots are observed for only four series. Overall, the very low number of IPs per PEPscan experiment would support PEPscan IPs' suitability for systematic testing downstream. A final remark is that the only IP detected that corresponds to only two consecutive positive spots is M20, but it shows no activity, which is in agreement with the rule that IP detection should involve at least three consecutive spots.

3.4. Can MOFs Correspond to Fragments at the PPI Interface?

We now turn to considering whether the IPs can target PPI interfaces. As shown in Figure 2, the MOFs correspond to regions of the structures that are exposed to the solvent, which fulfils a requirement for the identification of motifs at the interface of protein complexes. Looking in more detail at if the MOFs could correspond to fragments at the interface of PPIs is limited by the number of cases for which the structure describing the PPI is available, which is often the rule in the context of PEPscan experiments. In our dataset, the structures of the proteins in interaction are only available for K-Ras/Raf, TEAD/YAP and TEAD/Taz, and the PDB identifiers are 4g0n, 3kys and 5gn0, respectively. The release dates of the 3kys and 5gn0 PDB entries are 2010 and 2017, i.e., synchronous or posterior to the publication of the PEPscan results for TEAD/YAP/Taz (2010).

For the K-Ras/Raf interaction, one MOF (M13) is clearly located at the complex interface. Interestingly, however, M13 does not correspond to the IP showing some activity. In fact, it was not originally considered as a candidate by the experimenters and was consequently not tested. M18, which is not close to the interface, was instead tested and shows some activity, including in terms of competition, meaning it is able to interfere with the formation of the K-Ras/Raf complex [39]. It is important to recall, however, that the structure of the complex does not encompass the totality of the sequences, suggesting alternative mechanisms underlying the interaction could occur. On the Raf side, none of the IPs are located at the interface of the K-Ras/Raf complex.

For the TEAD/YAP and TEAD/Taz interactions, two IPs, M22 and M3,1 are clearly located at PPI interaction sites in the 3D structures, which is not the case with M21, which is located at the opposite side of the structure (Figure 2). M22 is surprising, since it corresponds to a beta strand internal to a seven-stranded beta-sheet, but an interaction can clearly occur, particularly through TRP 303, which belongs to the associated MOF. For M31, the MOF is close to, but not in direct interaction with, that of M22. In terms of activity, it is again intriguing that the competition experiments [40] suggest that M21 is able to disrupt the TEAD/YAP complex. However, in this case again, the coordinates are only available for a linker part of the YAP and TAZ paralogous proteins, meaning other mechanisms of interaction not covered by the resolved part of the structure could be at stake. Moreover, the ELM repository [49] also suggests that some interactions would occur between TEAD and YAP through short linear motifs, suggesting the cellular effects observed could involve mechanisms not necessarily specific to the TEAD/YAP interaction.

Overall, despite that these results tend to suggest that PEPscan is able to identify, with some fuzziness, peptides at the PPI interface, the cellular tests highlight that the biological reality could be much less straightforward.

3.5. Can Candidate IPs Target Specific Patches on the Partner Protein?

A last aspect is the specificity of the putative interaction sites identified, and firstly the ability to identify IPs specific to a given interaction. In our dataset, IPs extracted from the same protein but targeting a different PPI are available in the cases of caspase-9 (caspase-9-SET, caspase-9-PP2A), PP2A (PP2A-caspase-9, PP2A-SET), SET (SET-PP2A, SET-caspase-9) and K-Ras (K-Ras-BCL-X_L and K-Ras-Raf), not considering the special case of TEAD. In Figure 2 (top), different color codes are used to depict the IPs identified on one protein, but targeting different PPIs. For all cases but one, the IPs identified involve different regions of the structures. This is particularly obvious for caspase-9, PP2A and K-Ras. SET is the only case where some IPs targeting PP2A or caspase-9 correspond to overlapping sequences. M26 and M29 can be considered as consecutive, and overlap by only four amino acids (169-RSSQ). M26 and M30 are almost fully overlapping. Here, we depict a full model where missing regions have been added by DaReUS-Loop [50,51], but these IPs correspond to parts of the structure predicted as disordered, and for which the coordinates are missing in PDB entry 2E50. It remains that all the IPs showing some biological activity (labeled in red in Figures 2 and 3) are fully distinct over all the cases analyzed.

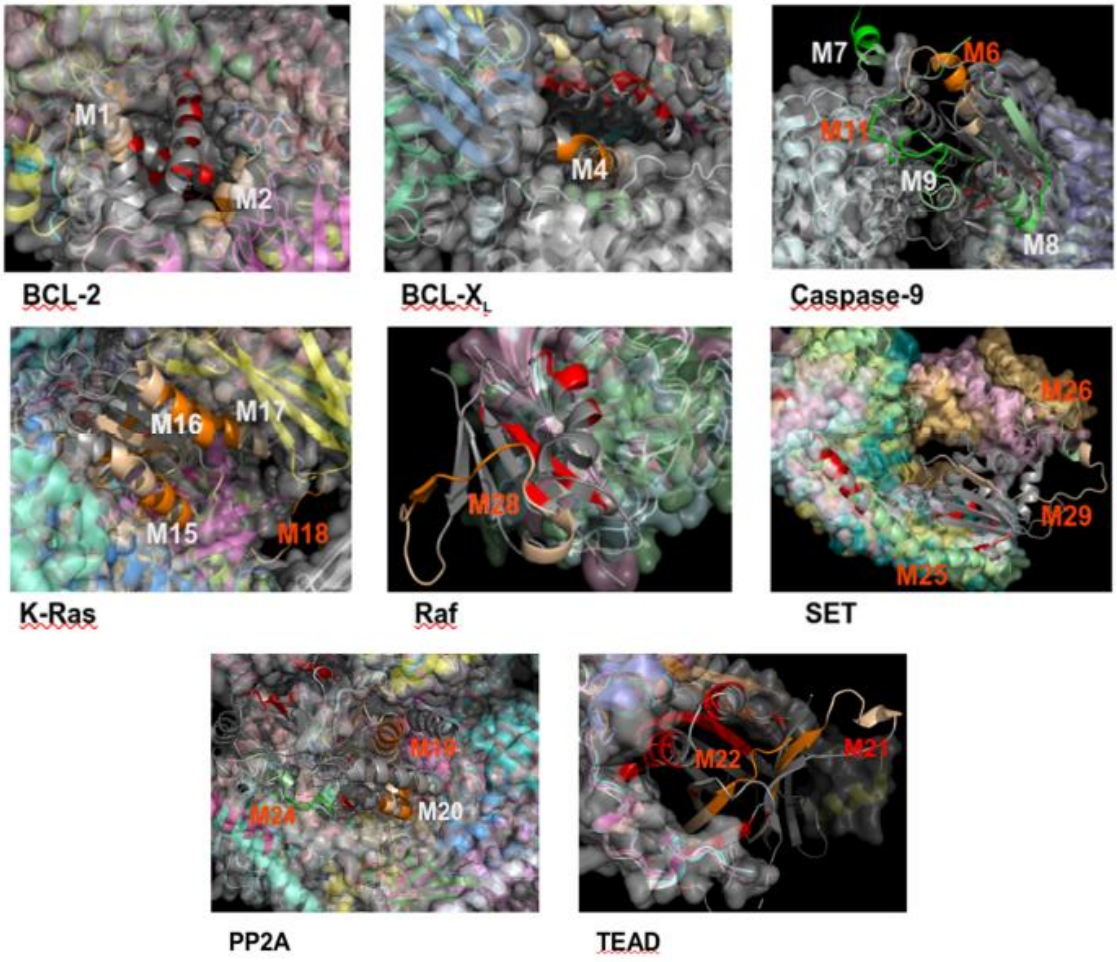

Figure 3. 3D illustration of the surroundings of the IPs when not frequently located at the protein–protein interface. Red labels correspond to IPs showing some biological activity.

Another aspect is the fact that the IPs could be non-specific in terms of interference, i.e., able to target different PPIs. To investigate this, we have analyzed the structural information available in the PDB about the interactions of each of the proteins of Table 1. Figure 2

(bottom) presents an overview of the regions contacted by the members of the complexes identified (the redder, the more amino acids are at the interface with other protein chains), using the same orientation as for the MOFs (top). Figure 3 provides details on the 3D environment of the less-contacted MOFs. MOFs that correspond to peptides showing some activity (Table 2) are labeled in red. Table 2 also reports z-scores as a quantification of the tendency of the IPs to be located more (positive values) or less (negative values) frequently at the PPI interface than the rest of the amino acids.

It is striking that the MOFs are not, in general, located in the structure regions frequently involved in complex interfaces, suggesting some specific mode of interaction could be grabbed. Positive z-score values are obtained only for M5 (BCL-X_L), M10 (caspase-9), M13-14 (K-Ras) and M25 (SET). Among these, only M25 shows some activity (see Table 2). It could correspond to a peptide that could interfere with the dimerization of SET (Figure 3). For M5, we identified 27 complexes of the PDB involving BCL-X_L or close homologs. Among these, 24 correspond to BCL-X_L in interaction with peptides designed to prevent the BCL-X_L heterodimerization that is involved in the regulation of programmed cell death. Those peptides are extracted from various partners (BAK, Bad, Puma, Beclin, BIM) or correspond to foldamers. It is thus legitimate to expect that M5 can be involved in the interaction with K-Ras, but the specificity of its interaction could probably be questioned. Overall, among the nine MOFs that exhibit some activity and for which 3D coordinates are available, all but one (i.e., eight IPs) have negative z-scores, i.e., correspond to regions less frequently contacted by partners (Figure 3), and thus could be considered as potentially specific to the interaction they target. Of course, this has to be tempered by the possible lack of structure in the PDB, and z-score values here are only indicative. A special case is that of M22 (TEAD), associated with a z-score of -0.24, for which very few complex structures of the PDB could be identified (only seven). Three of these correspond to TEAD in interaction with YAP, and another one to Taz. Others describe the interaction with VGLL. Hence, M22 can be expected to correspond to a true positive case, but clearly, the specificity cannot be assessed.

4. Discussion

PEPscan is an old approach that has recently raised new interest for the identification of IPs. PEPscan has been previously reported to sometimes generate false positives. The way it is employed here for IP identification, the number of hits per target appears rather limited. Indeed, only for one case (K-Ras) does the number of candidate IPs exceeds five. The average and median number of IP are respectively 2.21 and 2, which is fairly low.

Out of the 14 analyzed experiments, PEPscan was able to identify IPs showing some biological activity for all cases but two, i.e., a success rate in identifying IPs of close to 86%. The mechanisms underlying this activity are, however, less clear. If all the MOFs correspond to regions that are solvent-accessible, i.e., likely to be at the PPI interface, the analysis of the two examples for which structural information about the binding mode of the partners exists is limited in both cases by the lack of coordinates for large parts of the proteins. In some cases, IPs showing some activity are not located at the PPI interface of the regions of resolved structure. It is also noteworthy that for the K-Ras/Raf interaction, the fragment of Raf at the PPI interface did not show any signal in the PEPscan experiment. Reasons for this are unclear, and could come from the intrinsic properties of the associated sequence fragments. Looking at the aggregation propensities of the Raf sequence, various regions were predicted as aggregation-prone by the Walz server [52], but not in the region 66–71 located at the interface. It remains that PEPscan was able to identify a spot at an experimental 3D PPI interface in three cases out of five, further analysis being limited due to the absence of 3D coordinates.

A very promising aspect of this study is that our analyses suggest that when applied to IP identification, the PEPscan approach seems able to identify functional IPs that are specific to the target PPI. Indeed, functionally active IPs identified from one protein to address different PPIs correspond in all cases to different fragments of the protein. Of

note, the only case of protein SET, with one IP identified for the PP2A/SET interaction, was largely overlapping with that identified for the caspase-9/SET interaction, but was not active. Conversely, for eleven out of fifteen (73%) of the functional IPs identified, the fragment corresponds to a region of the protein not frequently involved in the assemblies of 3D structure determined, available in the PDB. This last observation must be, however, taken with care, since the structural data available in the PDB are far from covering the complete set of interactions expected in a cell [53,54].

Overall, it seems obvious that SPOT peptide arrays should continue playing a key role in the above-described applications, as well as for new purposes. From our analyses, this approach combines the advantages of being rather successful while being cheap and quick to enforce. In addition, we have here analyzed the results of experiments obtained using a constant protocol, proven effective over years, but there is room for evolution concerning the solid support, the array density and the size of the immobilized peptides, as well as the size of the overlapping sequence. The object of the interactions could also vary. Presently limited to proteins, the binding of different classes of molecules could be foreseen, such as nucleic acids, lipids and small compounds, to cite some. Continuing on PPIs, many perspectives are still open, particularly for therapeutic applications. PEPscan seems of particular interest when the structure of the partners in interaction is not known, and when in silico analyses cannot reliably be conducted. This is the case in numerous pathologies, such as various cancers, for which identifying a peptide can benefit from the coupling with cell-penetrating peptides [31], and more recently from tumor-addressing peptides [55].

Author Contributions: Conceptualization, A.R. and P.T.; Data curation, A.R. and E.S.; Investigation (3D analyses), P.T.; Writing—review and editing, A.R., E.S. and P.T. All authors have read and agreed to the published version of the manuscript.

Funding: This research was funded by ANR, ANR-18-IDEX-0001.

Institutional Review Board Statement: Not applicable.

Informed Consent Statement: Not applicable.

Data Availability Statement: Not applicable.

Acknowledgments: In this section, you can acknowledge any support given which is not covered by the author contribution or funding sections. This may include administrative and technical support, or donations in kind (e.g., materials used for experiments).

Conflicts of Interest: The authors declare no conflict of interest.

References

1. Frank, R.; Overwln, H. SPOT Synthesis: Epitope Analysis with Arrays of Synthetic Peptides Prepared on Cellulose Membranes. *Methods Mol. Biol.* **1996**, *66*, 149–169. [CrossRef] [PubMed]
2. Reineke, U.; Sabat, R.; Volk, H.-D.; Schneider-Mergener, J. Mapping of the interleukin-10/interleukin-10 receptor combining site. *Protein Sci.* **1998**, *7*, 951–960. [CrossRef] [PubMed]
3. Geysen, H.M.; Meloen, R.H.; Barteling, S.J. Use of peptide synthesis to probe viral antigens for epitopes to a resolution of a single amino acid. *Proc. Natl. Acad. Sci. USA* **1984**, *81*, 3998–4002. [CrossRef] [PubMed]
4. Bertoni, G.; Kostyal, D.A.; Reisert, P.S.; Humphreys, R.E.; Sairenji, T. Synthetic Peptides to Identify Antigenic Determinants on Epstein-Barr Virus Gp350/220. *Intervirology* **1990**, *31*, 290–294. [CrossRef]
5. Adler, S.; Frank, R.; Lanzavecchia, A.; Weiss, S. T Cell Epitope Analysis with Peptides Simultaneously Synthesized on Cellu-lose Membranes: Fine Mapping of Two DQ Dependent Epitopes. *FEBS Lett.* **1994**, *352*, 167–170. [CrossRef]
6. Kato, R.; Kaga, C.; Kunimatsu, M.; Kobayashi, T.; Honda, H. Peptide array-based interaction assay of solid-bound peptides and anchorage-dependant cells and its effectiveness in cell-adhesive peptide design. *J. Biosci. Bioeng.* **2006**, *101*, 485–495. [CrossRef]
7. Askoxylakis, V.; Zitzmann, S.; Mier, W.; Graham, K.; Krämer, S.; Von Wegner, F.; Fink, R.H.; Schwab, M.; Eisenhut, M.; Haberkorn, U. Preclinical Evaluation of the Breast Cancer Cell-Binding Peptide, p160. *Clin. Cancer Res.* **2005**, *11*, 6705–6712. [CrossRef]
8. López-Pérez, P.M.; Grimsey, E.; Bourne, L.; Mikut, R.; Hilpert, K. Screening and Optimizing Antimicrobial Peptides by Using SPOT-Synthesis. *Front. Chem.* **2017**, *5*, 25. [CrossRef]
9. Jaenisch, T.; Heiss, K.; Fischer, N.; Geiger, C.; Bischoff, F.R.; Moldenhauer, G.; Rychlewski, L.; Sié, A.; Coulibaly, B.; Seeberger, P.H.; et al. High-density Peptide Arrays Help to Identify Linear Immunogenic B-cell Epitopes in Individuals Naturally Exposed to Malaria Infection. *Mol. Cell. Proteom.* **2019**, *18*, 642–656. [CrossRef]

10. Liu, P.; Souma, T.; Wei, A.Z.-S.; Xie, X.; Luo, X.; Jin, J. Personalized Peptide Arrays for Detection of HLA Alloantibodies in Organ Transplantation. *J. Vis. Exp. JoVE* **2017**, 56278. [CrossRef]
11. Rasmussen, M.S.; Birgisdottir Å, B.; Johansen, T. Use of peptide arrays for identification and characterization of LIR motifs. In *Autophagy*; Methods in Molecular Biology, 1980; Humana Press: New York, NY, USA, 2019; pp. 149–161.
12. Gausepohl, H.; Boulin, C.; Kraft, M.; Frank, R.W. Automated multiple peptide synthesis. *Pept. Res.* **1992**, *5*, 315–320.
13. Luu, T.; Pham, S.; Deshpande, S. Automated multiple peptide synthesis: Improvements in obtaining quality peptides. *Int. J. Pept. Protein Res.* **1996**, *47*, 91–97. [CrossRef]
14. Frank, R. The SPOT-Synthesis Technique: Synthetic Peptide Arrays on Membrane Supports—Principles and Applications. *J. Immunol. Methods* **2002**, *267*, 13–26. [CrossRef]
15. Frank, R.; Heikens, W.; Heisterberg-Moutsis, G.; Blöcker, H. A New General Approach for the Simultaneous Chemical Syn-thesis of Large Numbers of Oligonucleotides: Segmental Solid Supports. *Nucleic Acids Res.* **1983**, *11*, 4365–4377. [CrossRef]
16. Saxinger, C.; Conrads, T.P.; Goldstein, D.J.; Veenstra, T.D. Fully Automated Synthesis of (Phospho) Peptide Arrays in Micro-titer Plate Wells Provides Efficient Access to Protein Tyrosine Kinase Characterization. *BMC Immunol.* **2005**, *6*, 1. [CrossRef]
17. Dikmans, A.J.; Morr, M.; Zander, N.; Adler, F.; Türk, G.; Frank, R. A new compact disc format of high density array synthesis applied to peptide nucleic acids and in situ MALDI analysis. *Mol. Divers.* **2004**, *8*, 197–207. [CrossRef]
18. Baleux, F.; Dubois, P. Novel Version of Multiple Antigenic Peptide Allowing Incorporation on a Cysteine Functionalized Ly-sine Tree. *Int. J. Pept. Protein Res.* **1992**, *40*, 7–12. [CrossRef]
19. Szymczak, L.C.; Kuo, H.-Y.; Mrksich, M. Peptide Arrays: Development and Application. *Anal. Chem.* **2018**, *90*, 266–282. [CrossRef]
20. Molony, R.D.; Rice, J.M.; Yuk, J.S.; Shetty, V.; Dey, D.; Lawrence, D.A.; Lynes, M.A. Mining the Salivary Proteome with Grating-Coupled Surface Plasmon Resonance Imaging and Surface Plasmon Coupled Emission Microarrays. *Curr. Protoc. Toxicol.* **2012**, *53*, 18.16.1–18.16.19. [CrossRef]
21. Hawkes, R.; Niday, E.; Gordon, J. A dot-immunobinding assay for monoclonal and other antibodies. *Anal. Biochem.* **1982**, *119*, 142–147. [CrossRef]
22. Blake, M.S.; Johnston, K.H.; Russell-Jones, G.J.; Gotschlich, E.C. A Rapid, Sensitive Method for Detection of Alkaline Phos-phatase-Conjugated Anti-Antibody on Western Blots. *Anal. Biochem.* **1984**, *136*, 175–179. [CrossRef]
23. Verastegui, M.; Moro, P.; Guevara, A.; Rodriguez, T.; Miranda, E.; Gilman, R.H. Enzyme-linked immunoelectrotransfer blot test for diagnosis of human hydatid disease. *J. Clin. Microbiol.* **1992**, *30*, 1557–1561. [CrossRef]
24. Landgraf, C.; Panni, S.; Montecchi-Palazzi, L.; Castagnoli, L.; Schneider-Mergener, J.; Volkmer-Engert, R.; Cesareni, G. Pro-tein Interaction Networks by Proteome Peptide Scanning. *PLoS Biol.* **2004**, *2*, e14. [CrossRef] [PubMed]
25. Dürauer, A.; Kopecky, E.; Berger, E.; Seifert, M.; Hahn, R.; Jungbauer, A. Evaluation of a sensitive detection method for peptide arrays prepared by SPOT synthesis. *J. Biochem. Biophys. Methods* **2006**, *66*, 45–57. [CrossRef] [PubMed]
26. Reineke, U.; Sabat, R.; Kramer, A.; Stigler, R.D.; Seifert, M.; Michel, T.; Volk, H.D.; Schneider-Mergener, J. Mapping Pro-tein-Protein Contact Sites Using Cellulose-Bound Peptide Scans. *Mol. Divers.* **1996**, *1*, 141–148. [CrossRef] [PubMed]
27. Scott, J.K.; Smith, G.P. Searching for peptide ligands with an epitope library. *Science* **1990**, *249*, 386–390. [CrossRef] [PubMed]
28. Wiertz, E.J.; Van Gaans-van den Brink, J.A.; Gausepohl, H.; Prochnicka-Chalufour, A.; Hoogerhout, P.; Poolman, J.T. Identi-fication of T Cell Epitopes Occurring in a Meningococcal Class 1 Outer Membrane Protein Using Overlapping Peptides As-sembled with Simultaneous Multiple Peptide Synthesis. *J. Exp. Med.* **1992**, *176*, 79–88. [CrossRef] [PubMed]
29. Schneider, F.S.; de Almeida Lima, S.; De Ávila, G.R.; Castro, K.L.; Guerra-Duarte, C.; Sanchez, E.F.; Nguyen, C.; Granier, C.; Molina, F.; Chávez-Olortegui, C. Identification of Protective B-Cell Epitopes of Atroxlysin-I: A Metalloproteinase from Both-rops Atrox Snake Venom. *Vaccine* **2016**, *34*, 1680–1687. [CrossRef]
30. Frieder, M.; Lewinsohn, D.M. T-Cell Epitope Mapping in Mycobacterium tuberculosis Using PepMixes Created by Mi-cro-Scale SPOTTM- Synthesis. In *Epitope Mapping Protocols*; Methods in Molecular Biology, 524; Humana Press: New York, NY, USA, 2009; pp. 369–382.
31. Bruzzoni-Giovanelli, H.; Alezra, V.; Wolff, N.; Dong, C.-Z.; Tuffery, P.; Rebollo, A. Interfering Peptides Targeting Protein–Protein Interactions: The next Generation of Drugs? *Drug Discov. Today* **2018**, *23*, 272–285. [CrossRef]
32. London, N.; Movshovitz-Attias, D.; Schueler-Furman, O. The Structural Basis of Peptide-Protein Binding Strategies. *Structure* **2010**, *18*, 188–199. [CrossRef]
33. Ni, D.; Liu, N.; Sheng, C. Allosteric Modulators of Protein–Protein Interactions (PPIs). *Adv. Exp. Med. Biol.* **2019**, *1163*, 313–334. [CrossRef]
34. The UniProt Consortium. UniProt: The universal protein knowledgebase. *Nucleic Acids Res.* **2018**, *46*, 2699. [CrossRef]
35. Berman, H.M.; Westbrook, J.; Feng, Z.; Gilliland, G.; Bhat, T.N.; Weissig, H.; Shindyalov, I.N.; Bourne, P.E. The Protein Data Bank. *Nucleic Acids Res.* **2000**, *28*, 235–242. [CrossRef]
36. Arrouss, I.; Nemati, F.; Roncal, F.; Wislez, M.; Dorgham, K.; Vallerand, D.; Rabbe, N.; Karboul, N.; Carlotti, F.; Bravo, J. Spe-cific Targeting of Caspase-9/PP2A Interaction as Potential New Anti-Cancer Therapy. *PLoS ONE* **2013**, *8*, e60816. [CrossRef]
37. Arrouss, I.; Decaudin, D.; Choquet, S.; Azar, N.; Parizot, C.; Zini, J.M.; Nemati, F.; Rebollo, A. Cell Penetrating Peptides as a Therapeutic Strategy in Chronic Lymphocytic Leukemia. *Protein Pept. Lett.* **2015**, *22*, 539–546. [CrossRef]
38. Marin, G.H.; Rebollo, A.; Bruzzoni-Giovanelli, H.; Schinella, G.; Piazzon, I.; Duarte, A.; Errecalde, J. T cell leukemia control via Ras-Raf pathway inhibition with peptides. *J. Med. Life* **2017**, *10*, 172–175.

39. Tian, L.; Zhang, X.; Nemati, F. Identification of Ras/Raf Binding Site and Design of Interfering Peptide with Potential Clinical Application. *Integr. Mol. Med.* **2016**, *3*, 1–9.
40. Dominguez-Berrocal, L.; Cirri, E.; Zhang, X.; Andrini, L.; Marin, G.H.; Lebel-Binay, S.; Rebollo, A. New Therapeutic Ap-proach for Targeting Hippo Signalling Pathway. *Sci. Rep.* **2019**, *9*, 1–11. [CrossRef]
41. Andrini, L.; Marin, G.H.; Inda, A.M.; Bruzzoni-Giovanelli, H.; Garcia, M.; Errecalde, J.; Rebollo, A. Anti-tumoral Effect of a Cell Penetrating and Interfering Peptide Targeting PP2A/SET Interaction. *Folia Med.* **2020**, *62*, 31–36. [CrossRef]
42. Tian, L.; Zhang, X.; Haesen, D.; Bravo, J.; Fominaya, J.; Choquet, S.; Zini, J.M.; Loisel, S.; Waelkens, E.; Janssens, V. Identifi-cation of PP2A/Set Binding Sites and Design of Interacting Peptides with Potential Clinical Applications. *Int. J. Pept. Res. Ther.* **2018**, *24*, 479–488. [CrossRef]
43. Pierrot, C.; Zhang, X.; Zhangi, G.; Fréville, A.; Rebollo, A.; Khalife, J. Peptides Derived from Plasmodium Falciparum Leu-cine-Rich Repeat 1 Bind to Serine/Threonine Phosphatase Type 1 and Inhibit Parasite Growth In Vitro. *Drug Des. Dev. Ther.* **2018**, *12*, 85. [CrossRef]
44. Dong, C.Z.; Bruzzoni-Giovanelli, H.; Yu, Y.; Dorgham, K.; Parizot, C.; Zini, J.M.; Brossas, J.Y.; Tuffery, P.; Rebollo, A. Identification of peptides interfering with the LRRK2/PP1 interaction. *PLoS ONE* **2020**, *15*, e0237110. [CrossRef]
45. Kramer, A.; Reineke, U.; Dong, L.; Hoffmann, B.; Hoffmüller, U.; Winkler, D.; Volkmer-Engert, R.; Schneider-Mergener, J. Spot synthesis: Observations and optimizations. *J. Pept. Res.* **1999**, *54*, 319–326. [CrossRef]
46. Altschul, S.F.; Gish, W.; Miller, W.; Myers, E.W.; Lipman, D.J. Basic local alignment search tool. *J. Mol. Biol.* **1990**, *215*, 403–410. [CrossRef]
47. Reineke, U.; Kramer, A.; Schneider-Mergener, J. Antigen sequence- and library-based mapping of linear and discontinuous protein-protein-interaction sites by spot synthesis. *Comb. Chem. Biol.* **1999**, *243*, 23–36. [CrossRef]
48. Kabsch, W.; Sander, C. Dictionary of protein secondary structure: Pattern recognition of hydrogen-bonded and geometrical features. *Biopolymers* **1983**, *22*, 2577–2637. [CrossRef]
49. Kumar, M.; Gouw, M.; Michael, S.; Sámano-Sánchez, H.; Pancsa, R.; Glavina, J.; Diakogianni, A.; Valverde, J.A.; Bukirova, D.; Čalyševa, J.; et al. ELM—the eukaryotic linear motif resource in 2020. *Nucleic Acids Res.* **2019**, *48*, D296–D306. [CrossRef]
50. Karami, Y.; Guyon, F.; De Vries, S.; Tufféry, P. DaReUS-Loop: Accurate loop modeling using fragments from remote or unrelated proteins. *Sci. Rep.* **2018**, *8*, 1–12. [CrossRef] [PubMed]
51. Karami, Y.; Rey, J.; Postic, G.; Murail, S.; Tufféry, P.; De Vries, S.J. DaReUS-Loop: A web server to model multiple loops in homology models. *Nucleic Acids Res.* **2019**, *47*, W423–W428. [CrossRef] [PubMed]
52. Maurer-Stroh, S.; Debulpaep, M.; Kuemmerer, N.; De La Paz, M.L.; Martins, I.C.; Reumers, J.; Morris, K.L.; Copland, A.; Serpell, L.; Serrano, L.; et al. Exploring the sequence determinants of amyloid structure using position-specific scoring matrices. *Nat. Methods* **2010**, *7*, 237–242. [CrossRef] [PubMed]
53. Mosca, R.; Céol, A.; Aloy, P. Interactome3D: Adding structural details to protein networks. *Nat. Methods* **2013**, *10*, 47–53. [CrossRef] [PubMed]
54. Murray, D.; Petrey, D.; Honig, B. Integrating 3D structural information into systems biology. *J. Biol. Chem.* **2021**, *296*, 100562. [CrossRef] [PubMed]
55. Simon-Gracia, L.; Savier, E.; Parizot, C.; Brossas, J.Y.; Loisel, S.; Teesalu, T.; Conti, F.; Charlotte, F.; Scatton, O.; Aoudjehane, L.; et al. Bifunctional Therapeutic Peptides for Targeting Malignant B Cells and Hepatocytes: Proof of Concept in Chronic Lymphocytic Leukemia. *Adv. Ther.* **2020**, *3*, 2000131. [CrossRef]

5.4 Article 4: Bi-functional therapeutic peptides against hepatocellular carcinoma.

Savier E, Simon-Gracia L, Charlotte F, Tuffery P, Scatton O and Rebollo A**.**
Pharmaceutics, 2021. **13**. Doi : 10.3390/pharmaceutics13101631

Introduction

Le carcinome hépato-cellulaire survient dans la plupart des cas sur un terrain particulier : foie d'hépatopathie chronique ou cirrhotique, cirrhose décompensée, comorbidités (HTA, diabète, obésité), patient âgé, immunodépression thérapeutique avec contre-indication aux drogues immunostimulantes …etc. De plus le CHC est considéré comme une tumeur chimiorésistante. Il est donc indispensable de disposer de traitements systémiques spécifiques des cellules tumorales afin de limiter au maximum les effets secondaires. Nous avons montré que les peptides bi-fonctionnels permettaient cette approche sélective.

But du travail

Mesurer l'internalisation et les effets biologiques de 4 peptides bi-fonctionnels (TPP-IP) sur des cellules tumorales isolées à partir de pièces opératoires de patients opérés pour CHC sans tenir compte de la conclusion du compte-rendu histologique définitif, ni du stade évolutif (tumeurs « tout venant », diagnostic préopératoire fait le plus souvent sur l'imagerie ou la biologie et non pas une biopsie).

Matériel et méthodes

Les patients informés signaient un consentement et l'échantillon était prélevé au laboratoire d'anatomie-pathologie puis préparé pour isolation des cellules hépatiques fraiches. Les cellules mises en cultures en présence de peptides fluorescents pendant 4h étaient ensuite examinées par cytométrie en flux.

Un score d'agressivité tumorale était calculé sur 6 critères : un critère biologie 1) l'alpha-foeto-protéine (Log_{10}(AFP)) préopératoire et 5 autres critères tirés de l'analyse histologique: 2) présence/absence d'une capsule incomplète, 3) présence/absence de nodules satellites, 4) présence/absence d'une invasion microvasculaire, 5) présence/absence du caractère macrotrabéculaire et 6) différentiation : bien différencié, moyennement indifférencié.

L'immunohistochimie était faite par application d'anticorps sur coupes fixées et déparaffinées.

L'apoptose était mesurée par cytométrie en flux après culture cellulaire en présence des peptides et d'annexine V marquée au FITC pendant 12h.

La spécificité du peptide a été vérifiée par compétition *in vitro* suivie d'un WesternBLot.

Résultats

Parmi 14 patients opérés pour carcinomes hépatocellulaires (CHC) ou tumeur compatible avec un CHC, il s'agissait en histologie définitive de 11 CHC et de trois tumeurs sans malignité (1 adénome hépatocellaire, 1 ganglion métastatique et nécrosé de CHC, 1 angiomyolipome).

Les 4 peptides bi-fonctionnels (iRGD-IP, RPARPAR-IP, LinTT1-IP, TT1-IP) étaient internalisés dans les hépatocytes malins mais pas dans les cellules non malignes. L'internalisation peptidique était corrélée de manière logarithmique à la quantité de récepteur exprimée à la surface des cellules. De même, l'internalisation était corrélée au score d'agressivité tumorale. L'internalisation des peptides iRGD-IP, LinTT1-IP, TT1-IP et RPARPAR-IP induisait une apoptose des hépatocytes malins et pas des cellules non-malignes. Il n'a pas été trouvé de relation entre les données de l'immunohistochimie et l'internalisation des TPP-IP.

Conclusion

Ce travail confirme la spécificité des peptides bi-fonctionnels TPP-IP pour atteindre des cellules de CHC « tout venant » Cette spécificité semble liée au niveau d'expression des récepteurs membranaires lui-meme corrélé à l'agressivité de la tumeur.

pharmaceutics

MDPI

Article

Bi-Functional Peptides as a New Therapeutic Tool for Hepatocellular Carcinoma

Eric Savier [1,2], Lorena Simon-Gracia [3], Frederic Charlotte [4], Pierre Tuffery [5], Tambet Teesalu [3,6], Olivier Scatton [1,2] and Angelita Rebollo [7,*]

1 Department of Hepatobiliary and Liver Transplantation Surgery, AP-HP, Pitié–Salpêtrière Hospital, Sorbonne Université, 75006 Paris, France; eric.savier@aphp.fr (E.S.); olivier.scatton@gmail.com (O.S.)
2 Sant Antoine Research Center (CRSA), Institut Nationale de la Santé et la Recherche Médicale (Inserm), Institute of Cardiometabolism and Nutrition (ICAN), Sorbonne Université, 75006 Paris, France
3 Laboratory of Precision and Nanomedicine, Institute of Biomedicine and Translational Medicine, University of Tartu, 50090 Tartu, Estonia; lorenasimongracia@gmail.com (L.S.-G.); tambet.teesalu@ut.ee (T.T.)
4 Department of Pathology, AP-HP, Pitié–Salpêtrière Hospital, 75006 Paris, France; frederic.charlotte@aphp.fr
5 Biologie Fontionelle Adaptative (BFA), Unité Mixte de Recherche (UMR) 8251, Centre National de la Recherche Scientifique (CNRS) ERL U1133, Inserm, Université de Paris, 75006 Paris, France; pierre.tuffery@univ-paris-diderot.fr
6 Center for Nanomedicine and Department of Cell, Molecular and Developmental Biology, University of California, Santa Barbara, CA 93106, USA
7 Faculté de Pharmacie, Unité des Technologies Chimiques et Biologiques pour la Santé (UTCBS), Inserm U1267, Centre National de la Recherche Scientifique CNRS UMR8258, Université de Paris, 75006 Paris, France
* Correspondence: angelita.rebollo@parisdescartes.fr

Citation: Savier, E.; Simon-Gracia, L.; Charlotte, F.; Tuffery, P.; Teesalu, T.; Scatton, O.; Rebollo, A. Bi-Functional Peptides as a New Therapeutic Tool for hepatocellular carcinoma. *Pharmaceutics* **2021**, *13*, 1631. https://doi.org/10.3390/pharmaceutics13101631

Academic Editors: Prisca Boisguérin, Sébastien Deshayes

Received: 6 September 2021
Accepted: 30 September 2021
Published: 6 October 2021

Abstract: Background: The interfering peptides that block protein–protein interactions have been receiving increasing attention as potential therapeutic tools. Methods: We measured the internalization and biological effect of four bi-functional tumor-penetrating and interfering peptides into primary hepatocytes isolated from three non-malignant and 11 hepatocellular carcinomas. Results: These peptides are internalized in malignant hepatocytes but not in non-malignant cells. Furthermore, the degree of peptide internalization correlated with receptor expression level and tumor aggressiveness levels. Importantly, penetration of the peptides iRGD-IP, LinTT1-IP, TT1-IP, and RPARPAR-IP induced apoptosis of the malignant hepatocytes without effect on non-malignant cells. Conclusion: Receptor expression levels correlated with the level of peptide internalization and aggressiveness of the tumor. This study highlights the potential to exploit the expression of tumor-penetrating peptide receptors as a predictive marker of liver tumor aggressiveness. These bi-functional peptides could be developed for personalized tumor treatment.

Keywords: hepatocellular carcinoma; tumor-penetrating peptides; interfering peptides

1. Introduction

Despite significant progress in translational cancer research, advances in the design of targeted anti-cancer therapies have remained disappointingly slow [1–6]. The two most important issues with current cancer therapies are the lack of tumoral specificity and the lack of selectivity. Treatments thus induce off-target effects and adverse side effects, and the amount of drug that actually reaches its target remains relatively low. Consequently, there is a real need for selective anti-cancer drugs.

Various targeted delivery strategies have been developed in an effort to overcome these limitations. One strategy is the use of Tumor-Penetrating Peptides (TPP), which are recognized as tumor-specific drug delivery vehicles that can penetrate into tumor cells to deliver cargo. TPPs are internalized via specific receptors expressed on tumor cells and

vasculature [7,8], and are characterized by the presence of the C-end Rule (CendR) motif with the consensus sequence R/KXXR/K [9,10]. This motif has to be C-terminally exposed to allow tumor-specific binding and penetration via the Neuropilin-1 (NRP-1) receptor.

RPARPAR is a prototypic CendR peptide that binds and internalizes via the NRP-1 receptor [11,12]. Another widely used TPP is iRGD (CRGDKGPDC), which is recruited to tumors via interaction with the integrins $\alpha v\beta 3/5$ through the RGD motif. On the cell surface, the tumor proteases cleave iRGD to C-terminally expose the CRGDK CendR motif that triggers internalization with the NRP-1 receptor [13]. The cyclic TT1 and its linear version, LinTT1, bind first to the p32 protein expressed on the tumor cell surface [14]. Both are also cleaved by tumoral proteases, thus exposing the CendR sequence that can then bind to NRP-1 [14–19].

TPPs are widely used as tumor-homing affinity ligands in targeted therapies, as they combine tumor specificity with cargo to reduce toxicity and increase efficacy [17,20–25]. In previous work, we paired TPPs with an Interfering Peptide (IP) that blocks the interaction between the phosphatase PP2A and its physiological inhibitor, the oncoprotein SET. This leads to bi-functional peptides that are able to specifically target tumoral cells where, once internalized, they dissociate the PP2A/SET interaction [26].

Hepatocellular Carcinoma (HCC) is a primary liver cancer that originates from hepatocytes [27]. HCC is the sixth most frequent cancer and the fourth leading cause of cancer-related mortality worldwide. Risk factors for HCC include viral infection, alcohol abuse, non-alcoholic fatty liver disease, certain toxins, and genetic diseases. These factors are responsible for chronic liver inflammation, fibrosis, and ultimately cellular transformation and liver function impairment [28]. Multimodal lines of therapy against HCC include surgical resection, chemotherapy, or radiotherapy. Tyrosine kinase inhibitors have some efficacy but are contraindicated in cases that involve altered liver function. Immunotherapy treatments hold promise for treating HCC [28], but more efficient targeted therapies are needed. An alternative way to treat HCC could be to use a dual-peptide strategy combining a TPP with an IP. Here, we show that the fused TPP-IPs can selectively internalize into primary tumoral hepatocytes isolated from HCC patients. Our results show that level of TPP-IP receptor expression by HCC tumor cells correlates with degree of peptide internalization and tumor aggressiveness, which raises prospects for a selective liver tumor-targeting approach.

2. Materials and Methods

2.1. Patients

Samples of benign and tumoral liver were collected from 14 patients. All patients gave informed consent. Samples 1 to 3 correspond to non-malignant tumors or necrotic HCC (following sorafenib treatment), and samples 4 to 14 correspond to HCC (Table 1). A tumor aggressiveness score was calculated based on histological or biological factors known to be associated with poor prognosis. This tumor aggressiveness score included tumor encapsulation [29], tumor differentiation [30], presence of satellite nodules, vascular invasion, macrotrabecular type [31], and $\log_{10}$ of the preoperative Alpha Feto Protein (AFP) value [32]. Tumors that scored 0 had zero aggressiveness, tumors that scored <6 were considered moderately aggressive, and tumors that scored >6 were considered highly aggressive.

Table 1. Clinical characteristics of the patients.

Patient	Sex	Age	Type Tumor	AFP	Log10AFP	Partially Encapsulated (0/1)	Satellite Nodule (0/1)	Vascular Invasion (0/1)	Differentiation (1/2/3) [1]	Macrotrabecular (0/1)	Aggressiveness [2]	Aggression Class
1	F	48.5	Hepatocellular adenoma	1.6	0	0	0	0	0	0	0	Null
2	M	65.3	Necrotic lymph node	2.6	0	0	0	0	0	0	0	Null
3	F	53.5	Angiomyolipoma	4.9	0	0	0	0	0	0	0	Null
4	M	56.5	Microtrabecular and pseudoglandular, Nuclear grade 2	7.7	0	1	0	0	2	0	3	Moderate
5	F	47.4	Microtrabecular	1010	3	1	1	0	2	0	7	High
6	F	59.9	Trabecular, Edmondson grade 2, nuclear grade 2	28,000	4	1	0	0	2	0	7	High
7	M	76.4	Microtrabecular and pseudoglandular	6662	3	1	0	0	2	1	7	High
8	M	47.1	Macro-trabecular, Edmonson grade 3, nuclear grade 3	6	0	1	1	1	2	1	6	High
9	M	73.4	Edmondson grade 3, nuclear grade 3	1.4	0	1	0	0	2	1	4	Moderate
10	M	67.3	Edmonson grade 2, nuclear grade 2	6.4	0	1	0	0	2	0	3	Moderate
11	M	57.5	Macrotrabecular	5.1	0	1	1	1	2	1	6	High
12	M	69.3	Trabecular, Edmonson grade 2, nuclear grade 2	343	2	1	0	2	2	0	6	High
13	M	68.7	Edmonson grade 2 HCC, nuclear grade 2	2.5	0	1	0	2	2	0	3	Moderate
14	M	78.8	Trabecular	341	2	0	0	2	2	0	5	Moderate

[1] Well differentiated HCC = 1, moderately differentiated HCC = 2, undifferentiated HCC = 3. [2] Sum of Log_{10} AFP, partially encapsulated, satellite nodule, vascular invasion, differentiation, macrotabecular HCC (min = 0, max: 7).

2.2. Peptide Synthesis and Sequences

The peptides were synthesized in an automated multiple peptide synthesizer with solid-phase and standard Fmoc chemistry (GL Biochem, Shanghai, China). The characterization was performed by High-Performance Liquid Chromatography (HPLC, Shimadzu France, Marne-la-Valle) and Mass Spectrometry (MS, Bruker, Wissembourg, France). For internalization experiments, the peptides were synthesized with a fluorochrome (FITC, Sigma-Aldrich, Saint Quentin, France). The peptides and sequences used are shown in Table 2.

Table 2. Sequence of the peptides used in this study.

Peptide ID	Sequence
iRGD-IP	FITC -Ahx-ETVTLLVALKVRYRERIT-Ahx-CRGDKGPDC-$CONH_2$ (C-C disulfide bond)
RPARPAR-IP	FITC -Ahx-ETVTLLVALKVRYRERIT-Ahx-RPARPAR-OH
LinTT1-IP	FITC -Ahx-ETVTLLVALKVRYRERIT-Ahx-AKRGARSTA-$CONH_2$
TT1-IP	FITC -Ahx-ETVTLLVALKVRYRERIT-Ahx-CKRGARSTC-$CONH_2$ (C-C disulfide bond)

Ahx: aminohexanoic acid.

2.3. Isolation and Culture of Primary Human Tumoral Hepatocytes

Healthy hepatocytes were isolated from patient samples following a protocol previously described [26]. Human tumoral hepatocytes were isolated from tumoral liver samples collected from adult patients undergoing surgery. Samples were cut into small pieces and treated with 4 mL of dispase (Gibco, Ref 17105-041, Thermo Fisher, France; 10 mg/mL in PSA buffer) (NaCl 8g/L, KCl 0.2 g/L, glucose 1g/L, $NaHCO_3$ 0.35g/L, phenol red 1mL/L; Thermo Fisher, France) and 2 mL of collagenase type I (Gibco Ref 17100-017; 5

mg/mL in PSA buffer). Samples were incubated at 37 °C under agitation for a maximum of 1 h, and then the solution was filtered and passed through needles of different diameters. The volume was filled up to 50 mL with culture medium and centrifuged at 177g for 5 min. Arginase expression confirmed that the isolated cells were hepatocytes. The supernatant was discarded, and the cells were cultured in DMEM medium (Thermo Fisher, France) supplemented with 10% Fetal Calf Serum (FCS, Gibco, Thermo Fisher, France) and antibiotics until treatment with peptides. The hepatocytes were maintained in culture for no more than 36 h to ensure that they did not enter differentiation.

2.4. Quantification of Cellular Internalization

Primary human hepatocytes were seeded overnight on 24-well plates and then incubated for 4 h with FITC-labeled peptides. After treatment, cells were detached, treated with trypsin (Gibco, Thermo Fisher, France) to remove non-internalized peptides, washed twice with PBS (Gibco, Thermo Fisher, France) to remove free peptides, and resuspended in 200 µL of PBS. FITC fluorescence intensity of internalized peptides was measured using a FACSCanto II flow cytometry system (Beckton Dickinson, Franklin Lakes, NJ, USA). Data were analyzed using FACSDiva 6.1.3 software (DB Biosciences, Franklin Lakes, NJ, USA). Healthy primary hepatocytes were used as control. For detection of TPP receptors on the cell surface, anti-p32 (Sigma Aldrich, St. Louis, MO, USA, AB2991), anti-NRP-1 (antibody generated in house, prepared by immunizing rabbits with human recombinant NRP1, followed by affinity purification) [24], and anti-integrin v/β3 (Abcam, Cambridge, UK, ab203123) antibodies were incubated with the cells for 30 min at room temperature. Cells were then washed and incubated with fluorophore-labeled secondary goat anti-mouse antibody (Alexa Fluor 647 goat anti-mouse, Thermo Fisher, Waltham, MA, USA, A-21238) or goat anti-rabbit antibody (Thermo Fisher, Waltham, MA, USA, A48285) for 10 min. Cells were then washed again, and receptor expression was analyzed by flow cytometry as described above.

2.5. Immunohistochemistry

The immunostaining procedure was performed on formalin-fixed, deparaffinized, 3µm-thick sections using a Ventana Benchmark Ultra platform (Roche Diagnostics, Basel, Switzerland) and the Ultraview visualization system (Roche Diagnostics, Basel, Switzerland) according to the manufacturer's instructions. The following primary antibodies were used: mouse monoclonal anti-CK19 antibody (dilution 1/100; clone RCK108; ref. M088801-2, Agilent, Santa Clara, CA, USA) followed by CC1 antigen retrieval buffer (36 min, 95 °C) and an antibody incubation time of 20 min at 20 °C; mouse monoclonal anti-human hepatocyte (HepPar) (dilution 3/100; clone OCH1E5; ref. M715801-2, Agilent, Santa Clara, CA, USA) followed by CC1 antigen retrieval buffer (64 min, 95 °C) and an antibody incubation time of 32 min at 20 °C; mouse monoclonal anti-human Glypican-3 (prediluted; clone 1G12; ref. F/261M-98, MM, Brignais, France) followed by CC1 antigen retrieval buffer (64 min, 95 °C) and an antibody incubation time of 32 min at 37 °C; mouse monoclonal anti-human b-catenin (prediluted; clone 14; ref. 05269016001, Roche Diagnostics, Basel, Switzerland) followed by CC1 antigen retrieval buffer (64 min, 95 °C) and an antibody incubation time of 32 min at 37 °C, and mouse monoclonal anti-human glutamine synthetase (prediluted; clone GS6; ref. 07107757001, Roche Diagnostics, Basel, Switzerland) followed by antigen retrieval protease (4 min, 20 °C) and an antibody incubation time of 40 min at 20 °C.

2.6. Detection of Apoptosis by Annexin-V Staining

The degree of apoptosis induced by the four TPP-IPs on primary benign and tumoral treated hepatocytes was measured by flow cytometry on cells stained with annexin-V FITC (Biosciences, Fischer Scientific, Hampton, NH, USA). The primary cells were incubated with the peptides for 12 h at 37 °C in DMEM supplemented with 10% FCS

(Gibco, Thermo Fisher, France), then washed and treated according to the manufacturer's protocol. Level of apoptosis was measured using FACSCanto II flow cytometry system (Becton Dickinson Biosciences, Franklin Lakes, NJ, USA).

2.7. Immunoprecipitation and Western Blotting

MDA-MB231 cells (ATCC, HTB-26) (5×10^6) were lysed for 20 min at 4 °C in lysis buffer (50 mM Tris pH8, 1% NP40, 137 mM NaCl, 1 mM $MgCl_2$, 1 mM $CaCl_2$, 10% glycerol and protease inhibitor mixture, Sigma Aldrich, St. Louis, MO, USA). Lysates (500 µg) were immunoprecipitated with the appropriate antibody overnight at 4 °C, and protein A/G Sepharose (Santa Cruz, Dallas, TX, USA) was added for 1 h at 4 °C. After washing with TBST (20 mM Tris-HCl pH7.5, 150 mM NaCl, 0.05% Tween 20; Gibco, Thermo Fisher, France), the PP2A/SET interaction was competed using 1 mM of PP2A/SET or Ras/Raf IP (GL Biochem, Shanghai, China) for 30 min at room temperature. After several washing steps, immunoprecipitates were separated by SDS-PAGE, transferred to nitrocellulose, and blotted with anti-PP2A antibody (Sigma Aldrich, St. Louis, MO, USA). The membrane was washed and incubated with HRP-conjugated secondary antibody (Dako, Hamburg, Germany, 1:1000 dilution). Protein detection was performed using the ECL system (Bio-Rad, Hercules, CA, USA). The blot was also hybridized with anti-SET antibody as internal control (Thermo Fischer, Waltham, MA, USA, MA5-34662).

2.8. Statistical Analysis

The data were analyzed using SigmaPlot version 12.0, Systat Software, Inc. (D-40699, Erkrath, Germany) and logarithmic regression with StatView version 5.0 for Windows SAS Institute Inc. Statistical tests used include *t*-tests and a Mann-Whitney rank sum test or Pearson correlations, as appropriate. Values of $p < 0.05$ were considered statistically significant.

3. Results

3.1. Clinical Characteristics of the Patients and Tumor Aggressiveness Classification

Samples from 14 patients were analyzed. Of these, three were from non-malignant tumors and 11 from HCC. The patient population had a median age of 62 years (range: 47–78 years) with a large predominance of males (71%). Clinical aggressiveness was calculated according to six parameters: AFP, non-encapsulation, satellite nodules, vascular embolization, differentiation, and macrotrabecular type (Table 1). Samples 1 to 3 corresponded to zero aggressiveness hepatocellular adenoma, necrotic tissue and angiomyolipoma, respectively. Samples 4 to 14 corresponded to HCC of moderate or high aggressiveness and were classified using the following parameters: for encapsulation, non-encapsulated = 0, partially encapsulated = 1; for differentiation, well-differentiated = 1, moderately differentiated = 2, undifferentiated = 3; for satellite nodes, positive = 1, negative = 0; for vascular invasion, positive = 1, negative = 0; for macrotrabecular type, positive = 1, negative = 0.

3.2. Immunohistochemical Characteristics of the Patients

The immunohistochemical markers that were analyzed in the patient samples were: CK19, to differentiate HCC from cholangiocarcinoma; HepPar, a marker that differentiates HCC from metastatic carcinoma [33]; GPC3, a member of the glypican family involved in progression of HCC [34]; β-catenin, a marker of development and progression of HCC [35]; and glutamine synthetase [36], which may enhance metastatic potential in HCC. Absence of CK19 expression confirmed that the patient samples corresponded to HCC but not to cholangiocarcinoma. Note that samples from patients #7, #8, #11 and #12, which were classified as highly aggressive HCC, showed the highest levels of HepPar marker expression. Similarly, samples from patients #6 and #7, which were also classified as highly aggressive HCCs, expressed the highest levels of glutamine synthase (Table 3).

Table 3. Immunohistochemical characteristics of the patients.

Patient	CK19	HepPar	GPC3	Nuclear β-Catenin	Glutamine Synthetase
1	-	+	-	+	-
2	necrosis	necrosis	necrosis	necrosis	necrosis
3	-	-	-	-	-
4	-	+	+	10–20%	+++
5	-	-	-	0	0
6	-	+	-	-	++
7	-	+++	-	+	+++
8	+	+++	-	-	-
9	-	+	+	-	-
10	-	+	-	-	+
11	-	+++	+	-	-
12	-	+++	+	-	-
13	-	+++	-	-	-
14	-	+	+++	+	-

0: no material was available.

3.3. In Vitro Competition against PP2A/SET Interaction

In vitro competition testing was performed to confirm that the IP targeted the PP2A/SET interaction. Lysates from MDA-MB231 cells were immunoprecipitated with anti-PP2A antibody, and the interaction with SET was competed using IP PP2A/SET (Figure 1). SET was detected in the control immunoprecipitates and in immunoprecipitates after competition with the IP disrupting the Ras/Raf interaction (peptide sequence: MEHIQGAWKTISGFGLK), whereas the levels detected were much lower after competition with 1 mM of the IP blocking the PP2A/SET interaction. PP2A was used as internal control of protein loading.

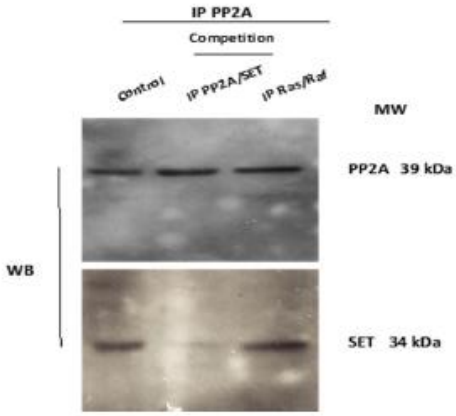

Figure 1. The IP disrupted PP2A/SET interaction in vitro. Lysates were immunoprecipitated with anti PP2A antibody. The PP2A/SET interaction was competed in vitro with 1 mM of the PP2A/SET IP and with an irrelevant Ras/Raf IP used as a negative control. The total amount of PP2A was used as internal control.

3.4. Internalization of Tumor-Penetrating and Interfering Peptides (TPP-IP) into Primary Tumoral Hepatocytes via Specific Receptors

We generated four bi-functional peptides composed of a TPP (iRGD, RPARPAR, LinTT1, or TT1) paired with the IP blocking the interaction between the phosphatase PP2A and its physiological inhibitor, the oncoprotein SET. These peptides penetrated specifically into tumoral B-cells [26]. We analyzed the intracellular penetration of these

TPP-IP in a group of 14 samples of non-malignant tumors (samples #1 to #3) or HCC (samples #4 to #14), graded according to histological tumor type.

Figure 2A shows that none of the four TPP-IPs penetrated non-malignant tumors. In HCC (samples #4 to #14), iRGD-IP showed the lowest level of internalization but with a significant difference between benign and aggressive tumors (p = 0.02). Bi-functional peptides RPARPAR-IP (p = 0.005), LinTT1-IP (p = 0.002), and TT1-IP (p = 0.005) showed higher levels of penetration in tumoral hepatocytes, again with a significant difference compared to non-malignant samples (Figure 2A). Interestingly, RPARPAR-IP showed the highest level of internalization in HCC samples, ahead of LinTT1-IP and TT1-IPs which showed very similar levels of internalization (Figure 2A). Crucially, none of the TPP-IPs internalized into healthy hepatocytes (control in Figure 2A).

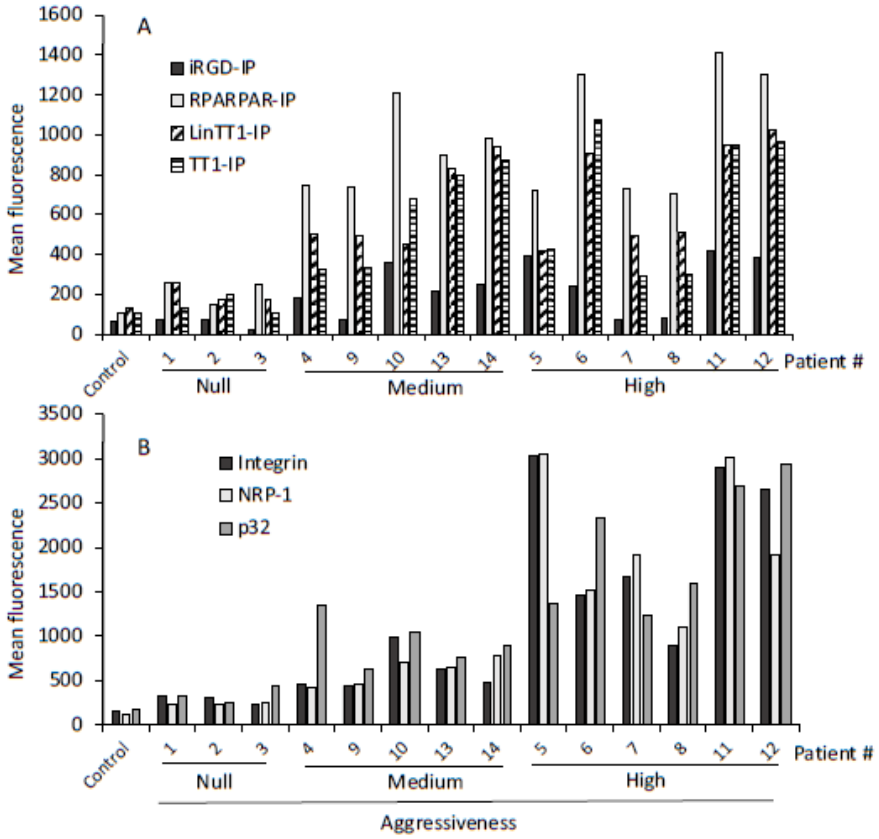

Figure 2. Selective internalization of TPP-IPs and receptor expression in malignant hepatocytes. (A) TPP-IP internalization. Hepatocytes isolated from benign or malignant liver patient samples were incubated for 4 h with 25 µM of FITC-labeled peptides. The mean fluorescence of internalized peptides was analyzed by flow cytometry and compared to control healthy hepatocytes. Internalization of the TPP-IPs was significantly higher in HCC compared to non-malignant tumors (HCC versus non-malignant tumors or normal hepatocytes respectively, n = 4 to 11 per group, mean ± standard error, iRGD-IP: 61 ± 12 vs. 244 ± 40, p = 0.022; RPARPAR-IP: 191 ± 38 vs. 977 ± 83, p = 0.005; LinTT1-IP: 184 ± 27 vs. 682 ± 73, p = 0.002; TT1-IP: 137 ± 23 vs. 637 ± 93, p = 0.005). (B) Receptor expression. Hepatocytes isolated from non-malignant or tumoral liver samples were incubated with antibodies against NRP-1, p32, and integrin v/b3, followed by an APC-labeled secondary antibody. Samples were analyzed by flow cytometry. Healthy hepatocytes were used as control. Receptor expression levels were significantly higher in tumoral hepatocytes than in non-malignant tumors (HCCs vs. non-malignant tumors or normal hepatocytes, respectively, n = 4 to 11 per group, Integrin v/b3: 254 ± 40 vs. 1416 ± 306, p = 0.005; NRP-1: 211 ± 31 vs. 1410 ± 290, p = 0.005; p32: 303 ± 58 vs. 1530 ± 238, p = 0.01).

Given that these peptides are internalized by tumoral hepatocytes via specific receptors on tumoral cells, we analyzed the expression of integrin v/β3, p32 and NRP-1.

Figure 2B shows that samples #1 to #3 (non-malignant tumors) and healthy control hepatocytes all showed very low levels of cell surface receptor expression, whereas samples #4 to #14 (HCC tumors) showed significantly higher receptor expression levels compared to non-malignant tumors ($p = 0.05$ for integrin v/β3; $p = 0.05$ for p32; $p = 0.05$ for NRP-1). We previously showed that the IP without TPP failed to internalize into malignant B cells and tumoral hepatocytes, whereas a non-tumoral-specific cell-penetrating peptide alone or combined with the IP effectively internalized in both malignant and healthy B cells and hepatocytes. The new results reported here confirm that the specific internalization of the TPP-IPs into tumor cells is due to internalization via specific receptors.

3.5. TPP Internalization and Receptor Expression Correlated with Tumor Aggressiveness

iRGD is recruited via interaction with integrins and then cleaved by tumoral proteases, thus allowing interaction with the NRP-1 receptor. Similarly, LinTT1 and TT1 first bind to p32, a mitochondrial protein aberrantly expressed on the cell surface of tumoral cells and are then cleaved by proteases expressed by the tumor cells, allowing them to interact with NRP-1. Finally, the RPARPAR peptide binds directly to tumoral cells expressing NRP-1.

We tested whether there was a correlation between the level of primary receptor expression on the tumoral cells and level of peptide internalization. Figure 3A shows a low level of iRGD-IP internalization (compared with RPARPAR-IP, LinTT1-IP, and TT1-IP) and variable expression of its receptor, integrin v/β3. The highest levels of integrin v/β3 expression were found in samples from patients #5, #6, #7, #11, and #12, which matched to the samples with the high tumor aggressiveness scores. Moreover, samples #5, #11, and #12 showed a higher degree of internalized iRGD-IP, which also matched with high tumor aggressiveness. A similar pattern was found for NRP-1 receptor expression and RPARPAR-IP internalization (Figure 3B), where the highest level of NRP-1 expression was found in samples from patients #5, #6, #7, #11, and #12, and the highest RPARPAR-IP internalization was found in samples #6, #11, and #12 that also corresponded to the most aggressive tumors. Finally, there was a different pattern of p32 receptor expression and LinTT1-IP/TT1-IP internalization, with the highest expression of the receptor in samples from patients #6, #11, and #12 that were classified as aggressive tumors, and these same samples also showed the highest peptide internalization (Figure 3C).

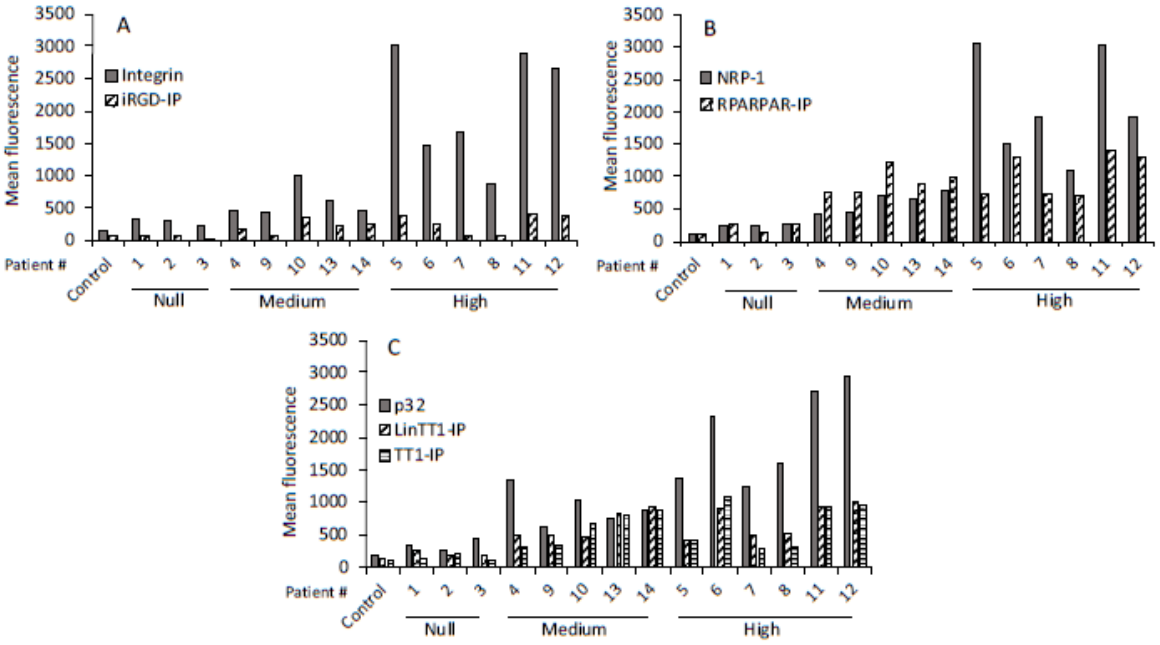

Figure 3. Primary receptor expression and internalization of TPP-IPs. (A) Expression of primary receptor integrin and iRGD-IP internalization. (B) Expression of NRP-1 receptor and RPARPAR-IP internalization. (C) Expression of the primary p32 receptor and LinTT-1-IP and TT1-IP internalization. Data are from Figure 2.

Analysis of NRP-1 expression levels in comparison to internalization of iRGD-IP (Figure 4A), LinTT1-IP and TT1-IP (Figure 4B), or RPARPAR-IP (Figure 3B) found that samples with the highest receptor expression also had high tumor aggressiveness scores and showed prominent TPP-IP internalization.

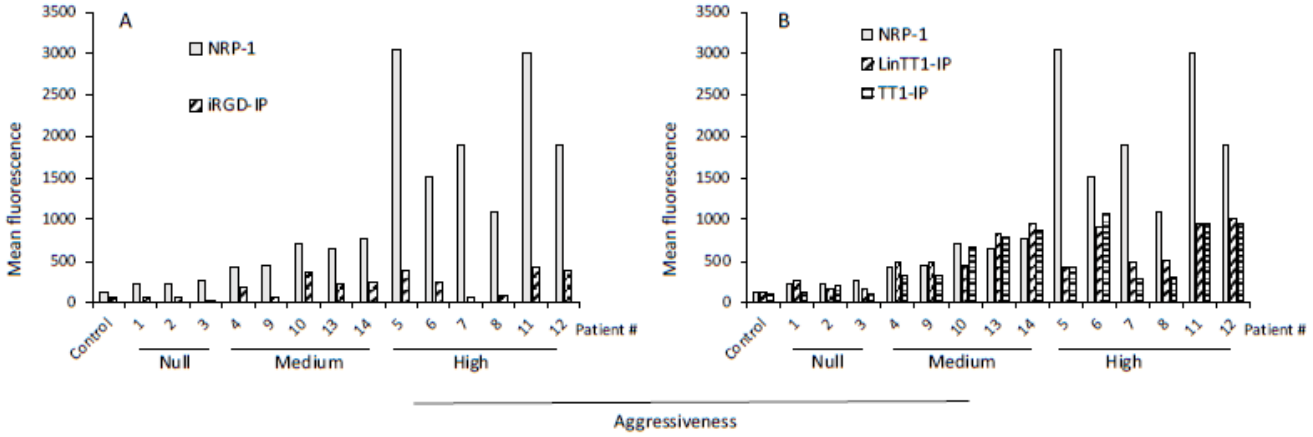

Figure 4. Secondary receptor expression and internalization of TPP-IPs. (A) Expression of secondary receptor (NRP-1) and iRGD-IP internalization. (B) Expression of secondary receptor (NRP-1) and internalization of LinTT1-IP and TT1-IP. Data are from Figure 2.

Figure 5A–C shows that there was a significant correlation between the levels of primary receptor expression (integrin vβ3, NRP-1 and p32) and peptide internalization ($p = 0.010$ for iRGD-IP; $p = 0.045$ for RPARPAR-IP; $p = 0.02$ for LinTT1-IP; $p = 0.03$ for TT1-IP). Figure 5C also shows that tumor aggressiveness score correlates with TPP-IP internalization ($p = 0.02$).

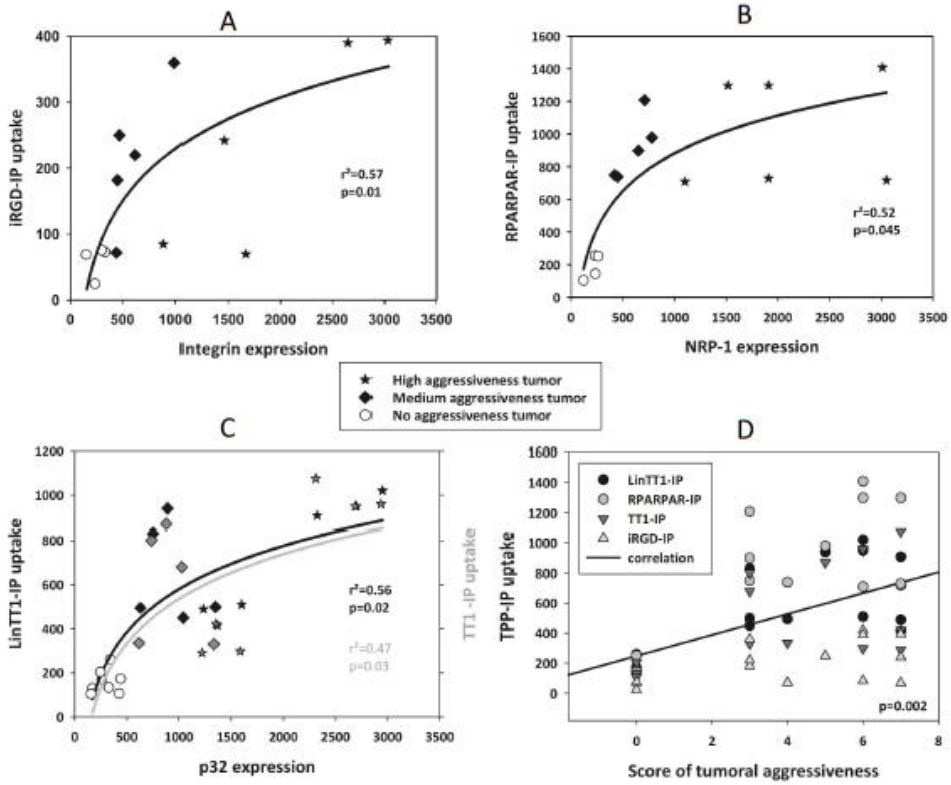

Figure 5. Correlation between receptor expression, peptide internalization, and aggressiveness of HCC. Correlation between integrin expression and internalization of iRGD-IP followed the equation: y = b0 +b1*log(x). White circle: non-malignant tumor or normal hepatocytes; black squares: samples from medium aggressiveness tumors; black stars: samples from high aggressiveness tumors. (A) Integrin expression and iRGD-IP internalization, (b0 = -610 ± 207, b1 = 121 ± 31) (B); NRP-1 expression and RPARPAR-IP internalization, (b0 = -1344 ± 600, b1 = 322 ± 89) (C), p32 expression and internalization of LinTT1-IP (b0 = -1456 ± 529, b1 = 294 ± 76) and TT1-IP (b0 = -1636 ± 665, b1 = 313 ± 96)(D) Correlation between score of aggressiveness and TTP-IP internalization (r = 0.479, standard error of estimate = 333.2, f = y0+a*x with y0 = 249 ± 83, a = 69.7 ± 17).

3.6. Apoptotic Effect of TPP-IPs on Tumoral Hepatocytes

We have previously demonstrated that TPP-IPs induced apoptosis in tumoral B-cells [26]. Figure 6 shows that iRGD-IP, RPARPAR-IP, LinTT1-IP, and TT1-IP induced apoptosis in HCC (sample #7 here) but not in non-malignant samples (sample #1). Apoptotic effect was stronger for LinTT1-IP and TT1-IP peptides, suggesting a tumor-specific induction of apoptosis.

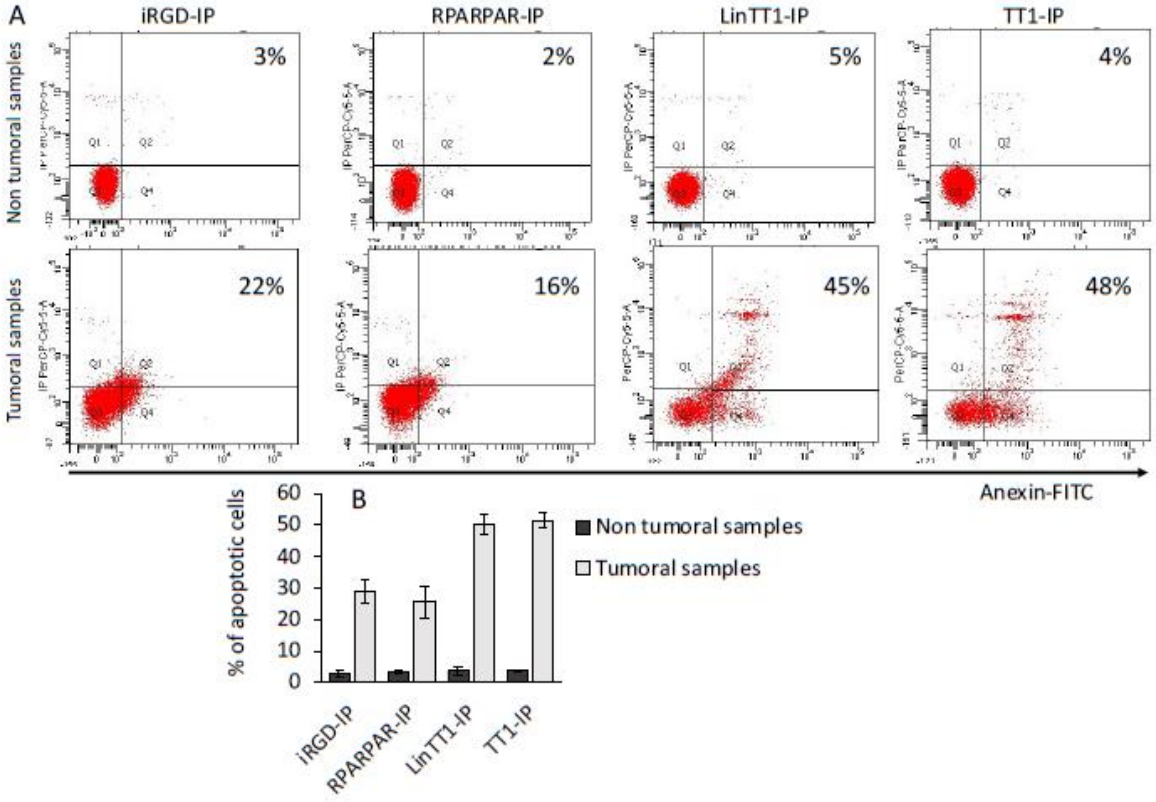

Figure 6. TPP-IPs induce apoptosis in HCC. Hepatocytes isolated from HCC (patient 7) or non-malignant tumors (patient 1) were cultured 12 h with 25 μM and the resulting apoptosis was estimated by annexin-V-FITC staining using flow cytometry. (A) Flow cytometry plots from one non-tumoral (patient 1) and one tumoral sample (patient 7). (B) Quantification of the percentage of apoptotic cells from three non-tumoral and three tumoral samples. Error bars = ± standard error.

4. Discussion

Liver cancer remains a global health challenge, and its incidence is growing worldwide. It is estimated that by 2025, liver cancer will affect one million people annually [37,38]. The most common form of liver cancer is hepatocellular carcinoma (HCC), which accounts for ~90% of cases. Approximately 25% of HCC tumors present mutations, but they remain undruggable [39,40]. The histology-based definition of the morphological heterogeneity of liver cancer has been modified in an effort to employ personalized therapies for patient treatment [27].

The type of HCC treatment depends on tumor stage, patient performance, and the hepatic functional reserve. The pathogenesis of HCC is a complex multistage process, where angiogenesis plays an important role. For patients with advanced disease, only a handful of kinase inhibitors are approved for therapy, such as cabozantinib, regorafenib, lenvatinib, or sorafenib [41–45]. Anti-angiogenic agents, as well as some monoclonal antibodies, are also approved for use in HCC treatment.

Several therapeutic approaches to specifically target tumoral cells have been investigated. Interfering peptides are emerging as promising therapeutic agents that block intracellular protein–protein interactions [46,47]. The serine/threonine phosphatase PP2A is frequently altered in cancer, either in terms of expression levels or activation [48–50]. The physiological inhibitor of PP2A, i.e., the oncoprotein SET, engages with the catalytic subunit of PP2A to block its activation. Competitive interfering peptides able to block the PP2A/SET interaction can therefore restore PP2A activity [51,52]. We have generated four TPP-IPs able to specifically penetrate tumoral hepatocytes and B-cells and induce apoptosis of malignant cells [26]. Here, the four peptides (iRGD-IP, RPARPAR-IP, LinTT1-IP, and TT1-IP) that block

the PP2A/SET interaction were able to penetrate tumoral hepatocytes isolated from HCC, but crucially, they were not internalized by non-malignant tumors.

Different parameters have been used to define an aggressiveness score. Recent publications define the aggressiveness score based on four clinical parameters, i.e., tumor size, multifocality, presence of portal vein thrombus, and blood alpha-fetoprotein levels [53,54]. Here we defined an aggressiveness score based on the six parameters indicated in Table 1. Given these criteria, we classified the patients into three groups: non-aggressive (non-malignant tumors), moderately aggressive (score up to five), and highly aggressive (score of six and higher). The results show that there was a correlation between the number of TPP receptors expressed by tumoral cells, level of TPP-IP internalization, and HCC aggressiveness.

Treatment of HCC cells with the bi-functional peptides tested here led to a higher level of apoptosis in HCC cells than in non-malignant samples. The penetration-induced apoptosis was mediated by the associated IP and the specific tumoral penetration. Internalization of the TPP-IPs is the result of a multistep mechanism. First, the bi-functional peptides are associated to their primary receptors ($\alpha v\beta 3/5$ integrins for iRGD, p32 for LinTT1, and TT1and NRP-1 for RPARPAR). After proteolytic cleavage by tumoral proteases, they bind to the NRP-1 receptor, triggering cellular internalization. One possible explanation for the lower internalization of iRGD-IP, TT1-IP, and LinTT1-IP compared to RPARPAR-IP could be that after the incubation times used here, only a fraction of these peptides gets cleaved to expose the CendR motif. The involvement of several tumor-dependent steps renders this mechanism highly selective toward tumor cells expressing integrin, p32, and NRP-1 receptors [7,10,14–16]. There are several lines of evidence showing that NRP-1 mediates angiogenesis and that increased NRP-1 expression correlates with a decrease in tumor progression, angiogenesis, and immune evasion [55,56]. Overexpression of NRP-1 in vitro and in vivo correlates with decreased tumor vascularization and apoptosis, suggesting a direct correlation between level of NRP-1 expression and aggressiveness of the tumor [55,56]. Similarly, the level of p32 expression by tumoral cells and tissues has been associated with cancer progression and metastasis in several cancers, such as thyroid, pancreatic, gastric, and lung cancer [57].

Uncontrolled tumor cell proliferation and escape from apoptosis play an important role in HCC growth, which makes inhibition of cancer proliferation and induction of apoptosis a crucial target for HCC treatment. Patients with late-stage HCC currently have to rely on systemic chemotherapy [58]. However, the prognosis of patients undergoing chemotherapy for HCC is severely compromised by the toxic side effects of the drugs and by the emergence of drug-resistant HCC tumors [59]. Consequently, there is a real need to search for new targets to treat liver tumors.

Protein phosphatase PP2A and its physiological inhibitor are implicated in HCC as well as other types of cancers. PP2A is a tumor suppressor that negatively regulates many signaling pathways associated with cancer progression by dephosphorylating crucial proteins in these pathways, such as Wnt/β-catenin, PI3K, MAPK, and so on [60,61].

PP2A phosphatase inhibitors have been shown to have therapeutic effects against HCC in clinical trials [62,63], suggesting that PP2A is a promising target for HCC treatment. Unfortunately, the extensive constitutive expression of PP2A in normal tissues, as well as the many PP2A partners and signaling pathways in which PP2A is involved, have bottlenecked the efforts to exploit PP2A as a target for therapeutic intervention. In addition, in clinical trials, phosphatase inhibitors exert a toxic effect against normal hepatic tissue [48–50,64], indicating that the therapeutic efficacy of PP2A inhibitors depends on precise cancer-targeted delivery systems. We have addressed this challenge by developing bi-specific peptides composed of a TPP and an IP module. Peptide drug conjugates are gaining importance in cancer therapy. For example, PEPAXTO® (melphalan flufenamide), a peptide drug conjugate that enters cells by passive diffusion and releases the drug via the action of intracellular aminopeptidases, has been recently approved for clinical use. The advantage of our TPP-IPs over other peptide drug conjugates like PEPAXTO is their high specificity for malignant cells. The TPPs target

receptors that are highly expressed in tumoral cells and, once inside the cell, they only dissociate the pool of PP2A associated to SET, without any effect on the free PP2A and SET partners.

Aberrant expression of SET has been reported in other cancers such as leukemia, breast cancer, and colon, liver, and lung carcinoma [65–69]. The oncogenic role of SET in HCC was first suggested by Fukukawa et al. [70] who demonstrated that SET expression is highly upregulated in progressive HCC, indicating that SET may be involved in HCC development. Furthermore, SET activity is associated with development of resistance to chemotherapies [71–73]. Results obtained with patient primary cells support the oncogenic role of SET in HCC, suggesting that SET may serve as a novel biomarker to guide treatment in patients with HCC [69].

In conclusion, we report a selective tumoral internalization and apoptotic effect of peptides with potential clinical applications in liver cancer. The correlation between TPP receptor expression levels, TPP-IP internalization levels, and tumor aggressiveness score suggests that TPP receptor expression could serve as a marker of HCC aggressiveness.

Author Contributions: E.S. and F.C. performed the experiment and provided samples; O.S. provided samples; L.S.-G., T.T. and A.R. wrote, reviewed, and edited the manuscript; P.T. analyzed the data. All authors have read and agreed to the published version of the manuscript.

Funding: This work was supported by Inserm. T.T. and L.S.G. were supported by the European Regional Development Fund (Project No. 2014-2020.4.01.15-0012) and the Estonian Research Council (grants PRG230 and EAG79).

Institutional Review Board Statement: The study was conducted according to the Declaration of Helsinki and approved by the Ethics Committee (CODECOH DC-2019-3261, Commission Nationale Informatique et Liberté, (CNIL) 1929196vO). Date of the approval: 10th January 2019. All the patients gave informed consent as per French law.

Informed Consent Statement: Informed consent was obtained from all subjects involved in this study.

Data Availability Statement: Data are available upon request.

Acknowledgements: We thank G. Langsley and G. Snounou for editing the manuscript.

Conflicts of Interest: The authors declare no conflict of interest.

References

1. Xie, H.G.; Frueh, F.W. Pharmacogenomics steps toward personalized medicine. *Per. Med.* **2005**, *2*, 325–337, doi:10.2217/17410541.2.4.325.
2. Watters, J.W.; McLeod, H.L. Cancer pharmacogenomics: Current and future applications. *Biochim. Biophys. Acta* **2003**, *1603*, 99–111, doi:10.1016/s0304-419x(03)00003-9.
3. Hanahan, D.; Weinberg, R.A. Hallmarks of cancer: The next generation. *Cell* **2011**, *144*, 646–674, doi:10.1016/j.cell.2011.02.013.
4. Seebacher, N.A.; Stacy, A.E.; Porter, G.M.; Merlot, A.M. Clinical development of targeted and immune based anti-cancer therapies. *J. Exp. Clin. Cancer Res.* **2019**, *38*, 156, doi:10.1186/s13046-019-1094-2.
5. Man, S.; Luo, C.; Yan, M.; Zhao, G.; Ma, L.; Gao, W. Treatment for liver cancer: From sorafenib to natural products. *Eur. J. Med. Chem.* **2021**, *224*, 113690, doi:10.1016/j.ejmech.2021.113690.
6. Wildner, G. Tumors, tumor therapies, autoimmunity and the eye. *Autoimmun. Rev.* **2021**, *20*, 102892, doi:10.1016/j.autrev.2021.102892.
7. Teesalu, T.; Sugahara, K.N.; Ruoslahti, E. Tumor-penetrating peptides. *Front. Oncol.* **2013**, *3*, 216, doi:10.3389/fonc.2013.00216.
8. Ruoslahti, E. Tumor penetrating peptides for improved drug delivery. *Adv. Drug Deliv. Rev.* **2017**, *110*, 3–12, doi:10.1016/j.addr.2016.03.008.
9. Zanuy, D.; Kotla, R.; Nussinov, R.; Teesalu, T.; Sugahara, K.N.; Aleman, C.; Haspel, N. Sequence dependence of C-end rule peptides in binding and activation of neuropilin-1 receptor. *J. Struct. Biol.* **2013**, *182*, 78–86, doi:10.1016/j.jsb.2013.02.006.
10. Teesalu, T.; Sugahara, K.N.; Kotamraju, V.R.; Ruoslahti, E. C-end rule peptides mediate neuropilin-1-dependent cell, vascular, and tissue penetration. *Proc. Natl. Acad. Sci. USA* **2009**, *106*, 16157–16162, doi:10.1073/pnas.0908201106.
11. Willmore, A.M.; Simon-Gracia, L.; Toome, K.; Paiste, P.; Kotamraju, V.R.; Molder, T.; Sugahara, K.N.; Ruoslahti, E.; Braun, G.B.; Teesalu, T. Targeted silver nanoparticles for ratiometric cell phenotyping. *Nanoscale* **2016**, *8*, 9096–9101, doi:10.1039/c5nr07928d.

12. Wonder, E.; Simon-Gracia, L.; Scodeller, P.; Majzoub, R.N.; Kotamraju, V.R.; Ewert, K.K.; Teesalu, T.; Safinya, C.R. Competition of charge-mediated and specific binding by peptide-tagged cationic liposome-DNA nanoparticles in vitro and in vivo. *Biomaterials* **2018**, *166*, 52–63, doi:10.1016/j.biomaterials.2018.02.052.
13. Sugahara, K.N.; Teesalu, T.; Karmali, P.P.; Kotamraju, V.R.; Agemy, L.; Girard, O.M.; Hanahan, D.; Mattrey, R.F.; Ruoslahti, E. Tissue-penetrating delivery of compounds and nanoparticles into tumors. *Cancer Cell* **2009**, *16*, 510–520, doi:10.1016/j.ccr.2009.10.013.
14. Fogal, V.; Zhang, L.; Krajewski, S.; Ruoslahti, E. Mitochondrial/cell-surface protein p32/gC1qR as a molecular target in tumor cells and tumor stroma. *Cancer Res.* **2008**, *68*, 7210–7218, doi:10.1158/0008-5472.CAN-07-6752.
15. Simon-Gracia, L.; Scodeller, P.; Fuentes, S.S.; Vallejo, V.G.; Rios, X.; San Sebastian, E.; Sidorenko, V.; Di Silvio, D.; Suck, M.; De Lorenzi, F.; et al. Application of polymersomes engineered to target p32 protein for detection of small breast tumors in mice. *Oncotarget* **2018**, *9*, 18682–18697, doi:10.18632/oncotarget.24588.
16. Paasonen, L.; Sharma, S.; Braun, G.B.; Kotamraju, V.R.; Chung, T.D.; She, Z.G.; Sugahara, K.N.; Yliperttula, M.; Wu, B.; Pellecchia, M.; et al. New p32/gC1qR Ligands for Targeted Tumor Drug Delivery. *Chembiochem* **2016**, *17*, 570–575, doi:10.1002/cbic.201500564.
17. Sugahara, K.N.; Scodeller, P.; Braun, G.B.; de Mendoza, T.H.; Yamazaki, C.M.; Kluger, M.D.; Kitayama, J.; Alvarez, E.; Howell, S.B.; Teesalu, T.; et al. A tumor-penetrating peptide enhances circulation-independent targeting of peritoneal carcinomatosis. *J. Control. Release* **2015**, *212*, 59–69, doi:10.1016/j.jconrel.2015.06.009.
18. Saalik, P.; Lingasamy, P.; Toome, K.; Mastandrea, I.; Rousso-Noori, L.; Tobi, A.; Simon-Gracia, L.; Hunt, H.; Paiste, P.; Kotamraju, V.R.; et al. Peptide-guided nanoparticles for glioblastoma targeting. *J. Control. Release* **2019**, *308*, 109–118, doi:10.1016/j.jconrel.2019.06.018.
19. Hunt, H.; Simon-Gracia, L.; Tobi, A.; Kotamraju, V.R.; Sharma, S.; Nigul, M.; Sugahara, K.N.; Ruoslahti, E.; Teesalu, T. Targeting of p32 in peritoneal carcinomatosis with intraperitoneal linTT1 peptide-guided pro-apoptotic nanoparticles. *J. Control. Release* **2017**, *260*, 142–153, doi:10.1016/j.jconrel.2017.06.005.
20. Simon-Gracia, L.; Hunt, H.; Teesalu, T. Peritoneal Carcinomatosis Targeting with Tumor Homing Peptides. *Molecules* **2018**, *23*, 1190, doi:10.3390/molecules23051190.
21. Simon-Gracia, L.; Hunt, H.; Scodeller, P.; Gaitzsch, J.; Kotamraju, V.R.; Sugahara, K.N.; Tammik, O.; Ruoslahti, E.; Battaglia, G.; Teesalu, T. iRGD peptide conjugation potentiates intraperitoneal tumor delivery of paclitaxel with polymersomes. *Biomaterials* **2016**, *104*, 247–257, doi:10.1016/j.biomaterials.2016.07.023.
22. Diaz Bessone, M.I.; Simon-Gracia, L.; Scodeller, P.; Ramirez, M.L.A.; Lago Huvelle, M.A.; Soler-Illia, G.; Simian, M. iRGD-guided tamoxifen polymersomes inhibit estrogen receptor transcriptional activity and decrease the number of breast cancer cells with self-renewing capacity. *J. Nanobiotechnol.* **2019**, *17*, 120, doi:10.1186/s12951-019-0553-4.
23. Scodeller, P.; Asciutto, E.K. Targeting Tumors Using Peptides. *Molecules* **2020**, *25*, 808, doi:10.3390/molecules25040808.
24. Simon-Gracia, L.; Sidorenko, V.; Uustare, A.; Ogibalov, I.; Tasa, A.; Tshubrik, O.; Teesalu, T. Novel Anthracycline Utorubicin for Cancer Therapy. *Angew. Chem. Int. Ed. Engl.* **2021**, *60*, 17018-17027, doi:10.1002/anie.202016421.
25. Ikemoto, H.; Lingasamy, P.; Anton Willmore, A.M.; Hunt, H.; Kurm, K.; Tammik, O.; Scodeller, P.; Simon-Gracia, L.; Kotamraju, V.R.; Lowy, A.M.; et al. Hyaluronan-binding peptide for targeting peritoneal carcinomatosis. *Tumor Biol.* **2017**, *39*, 1010428317701628, doi:10.1177/1010428317701628.
26. Simon-Gracia, L.; Savier, E.; Parizot, C.; Brossas, J.Y.; Loisel, S.; Teesalu, T.; Conti, F.; Charlotte, F.; Scatton, O.; Aoudjehane, L.; et al. Bifunctional Therapeutic Peptides for Targeting Malignant B Cells and Hepatocytes: Proof of Concept in Chronic Lymphocytic Leukemia. *Adv. Ther.* **2020**, *3*, 2000131, doi:ARTN 200013110.1002/adtp.202000131.
27. Lu, X.Y.; Xi, T.; Lau, W.Y.; Dong, H.; Zhu, Z.; Shen, F.; Wu, M.C.; Cong, W.M. Hepatocellular carcinoma expressing cholangiocyte phenotype is a novel subtype with highly aggressive behavior. *Ann. Surg. Oncol.* **2011**, *18*, 2210–2217, doi:10.1245/s10434-011-1585-7.
28. Llovet, J.M.; Kelley, R.K.; Villanueva, A.; Singal, A.G.; Pikarsky, E.; Roayaie, S.; Lencioni, R.; Koike, K.; Zucman-Rossi, J.; Finn, R.S. Hepatocellular carcinoma. *Nat. Rev. Dis. Primers* **2021**, *7*, 6, doi:10.1038/s41572-020-00240-3.
29. Iguchi, T.; Aishima, S.; Sanefuji, K.; Fujita, N.; Sugimachi, K.; Gion, T.; Taketomi, A.; Shirabe, K.; Maehara, Y.; Tsuneyoshi, M. Both fibrous capsule formation and extracapsular penetration are powerful predictors of poor survival in human hepatocellular carcinoma: A histological assessment of 365 patients in Japan. *Ann. Surg. Oncol.* **2009**, *16*, 2539–2546, doi:10.1245/s10434-009-0453-1.
30. Decaens, T.; Roudot-Thoraval, F.; Badran, H.; Wolf, P.; Durand, F.; Adam, R.; Boillot, O.; Vanlemmens, C.; Gugenheim, J.; Dharancy, S.; et al. Impact of tumour differentiation to select patients before liver transplantation for hepatocellular carcinoma. *Liver. Int.* **2011**, *31*, 792–801, doi:10.1111/j.1478-3231.2010.02425.x.
31. Ziol, M.; Pote, N.; Amaddeo, G.; Laurent, A.; Nault, J.C.; Oberti, F.; Costentin, C.; Michalak, S.; Bouattour, M.; Francoz, C.; et al. Macrotrabecular-massive hepatocellular carcinoma: A distinctive histological subtype with clinical relevance. *Hepatology* **2018**, *68*, 103–112, doi:10.1002/hep.29762.
32. Duvoux, C.; Roudot-Thoraval, F.; Decaens, T.; Pessione, F.; Badran, H.; Piardi, T.; Francoz, C.; Compagnon, P.; Vanlemmens, C.; Dumortier, J.; et al. Liver transplantation for hepatocellular carcinoma: A model including alpha-fetoprotein improves the performance of Milan criteria. *Gastroenterology* **2012**, *143*, 986–994, doi:10.1053/j.gastro.2012.05.052.

33. Akiba, J.; Nakashima, O.; Hattori, S.; Naito, Y.; Kusano, H.; Kondo, R.; Nakayama, M.; Tanikawa, K.; Todoroki, K.; Umeno, Y.; et al. The expression of arginase-1, keratin (K) 8 and K18 in combined hepatocellular-cholangiocarcinoma, subtypes with stem-cell features, intermediate-cell type. *J. Clin. Pathol.* **2016**, *69*, 846–851, doi:10.1136/jclinpath-2015-203491.
34. Nishida, T.; Kataoka, H. Glypican 3-Targeted Therapy in Hepatocellular Carcinoma. *Cancers* **2019**, *11*, 1339, doi:10.3390/cancers11091339.
35. Sempoux, C.; Chang, C.; Gouw, A.; Chiche, L.; Zucman-Rossi, J.; Balabaud, C.; Bioulac-Sage, P. Benign hepatocellular nodules: What have we learned using the patho-molecular classification. *Clin. Res. Hepatol. Gastroenterol.* **2013**, *37*, 322–327, doi:10.1016/j.clinre.2013.04.008.
36. Moudi, B.; Heidari, Z.; Mahmoudzadeh-Sagheb, H. Study of liver in HBV-related hepatocellular carcinoma: Stereology shows quantitative differences in liver structure. *Eur. J. Histochem.* **2018**, *62*, 2950, doi:10.4081/ejh.2018.2950.
37. Llovet, J.M.; Zucman-Rossi, J.; Pikarsky, E.; Sangro, B.; Schwartz, M.; Sherman, M.; Gores, G. Hepatocellular carcinoma. *Nat. Rev. Dis. Primers* **2016**, *2*, 16018, doi:10.1038/nrdp.2016.18.
38. Villanueva, A. Hepatocellular Carcinoma. *N. Engl. J. Med.* **2019**, *380*, 1450–1462, doi:10.1056/NEJMra1713263.
39. Schulze, K.; Imbeaud, S.; Letouze, E.; Alexandrov, L.B.; Calderaro, J.; Rebouissou, S.; Couchy, G.; Meiller, C.; Shinde, J.; Soysouvanh, F.; et al. Exome sequencing of hepatocellular carcinomas identifies new mutational signatures and potential therapeutic targets. *Nat. Genet.* **2015**, *47*, 505–511, doi:10.1038/ng.3252.
40. Llovet, J.M.; Montal, R.; Sia, D.; Finn, R.S. Molecular therapies and precision medicine for hepatocellular carcinoma. *Nat. Rev. Clin. Oncol.* **2018**, *15*, 599–616, doi:10.1038/s41571-018-0073-4.
41. Abou-Alfa, G.K.; Meyer, T.; Cheng, A.L.; El-Khoueiry, A.B.; Rimassa, L.; Ryoo, B.Y.; Cicin, I.; Merle, P.; Chen, Y.; Park, J.W.; et al. Cabozantinib in Patients with Advanced and Progressing Hepatocellular Carcinoma. *N. Engl. J. Med.* **2018**, *379*, 54–63, doi:10.1056/NEJMoa1717002.
42. Haber, P.K.; Puigvehi, M.; Castet, F.; Lourdusamy, V.; Montal, R.; Tabrizian, P.; Buckstein, M.; Kim, E.; Villanueva, A.; Schwartz, M.; et al. Evidence-based management of HCC: Systematic review and meta-analysis of randomized controlled trials (2002–2020). *Gastroenterology* **2021**, *161*, 879-898, doi:10.1053/j.gastro.2021.06.008.
43. Bruix, J.; Qin, S.; Merle, P.; Granito, A.; Huang, Y.H.; Bodoky, G.; Pracht, M.; Yokosuka, O.; Rosmorduc, O.; Breder, V.; et al. Regorafenib for patients with hepatocellular carcinoma who progressed on sorafenib treatment (RESORCE): A randomised, double-blind, placebo-controlled, phase 3 trial. *Lancet* **2017**, *389*, 56–66, doi:10.1016/S0140-6736(16)32453-9.
44. Kim, J.J.; McFarlane, T.; Tully, S.; Wong, W.W.L. Lenvatinib Versus Sorafenib as First-Line Treatment of Unresectable Hepatocellular Carcinoma: A Cost-Utility Analysis. *Oncologist* **2019**, *25*, 512-519, doi:10.1634/theoncologist.2019-0501.
45. Llovet, J.M.; Ricci, S.; Mazzaferro, V.; Hilgard, P.; Gane, E.; Blanc, J.F.; de Oliveira, A.C.; Santoro, A.; Raoul, J.L.; Forner, A.; et al. Sorafenib in advanced hepatocellular carcinoma. *N. Engl. J. Med.* **2008**, *359*, 378–390, doi:10.1056/NEJMoa0708857.
46. Ahmad, A.; Ahmad, E.; Rabbani, G.; Haque, S.; Arshad, M.; Khan, R.H. Identification and design of antimicrobial peptides for therapeutic applications. *Curr. Protein Pept. Sci.* **2012**, *13*, 211–223, doi:10.2174/138920312800785076.
47. Rabbani, G.; Baig, M.H.; Ahmad, K.; Choi, I. Protein-protein Interactions and their Role in Various Diseases and their Prediction Techniques. *Curr. Protein Pept. Sci.* **2018**, *19*, 948–957, doi:10.2174/1389203718666170828122927.
48. Haesen, D.; Sents, W.; Lemaire, K.; Hoorne, Y.; Janssens, V. The Basic Biology of PP2A in Hematologic Cells and Malignancies. *Front. Oncol.* **2014**, *4*, 347, doi:10.3389/fonc.2014.00347.
49. Ciccone, M.; Calin, G.A.; Perrotti, D. From the Biology of PP2A to the PADs for Therapy of Hematologic Malignancies. *Front. Oncol.* **2015**, *5*, 21, doi:10.3389/fonc.2015.00021.
50. Kalev, P.; Sablina, A.A. Protein phosphatase 2A as a potential target for anticancer therapy. *Anticancer Agents Med. Chem.* **2011**, *11*, 38–46, doi:10.2174/187152011794941172.
51. Switzer, C.H.; Cheng, R.Y.; Vitek, T.M.; Christensen, D.J.; Wink, D.A.; Vitek, M.P. Targeting SET/I(2)PP2A oncoprotein functions as a multi-pathway strategy for cancer therapy. *Oncogene* **2011**, *30*, 2504–2513, doi:10.1038/onc.2010.622.
52. Neviani, P.; Harb, J.G.; Oaks, J.J.; Santhanam, R.; Walker, C.J.; Ellis, J.J.; Ferenchak, G.; Dorrance, A.M.; Paisie, C.A.; Eiring, A.M.; et al. PP2A-activating drugs selectively eradicate TKI-resistant chronic myeloid leukemic stem cells. *J. Clin. Invest.* **2013**, *123*, 4144–4157, doi:10.1172/JCI68951.
53. Carr, B.I.; Guerra, V. A Hepatocellular Carcinoma Aggressiveness Index and Its Relationship to Liver Enzyme Levels. *Oncology* **2016**, *90*, 215–220, doi:10.1159/000444394.
54. Carr, B.I.; Guerra, V.; Giannini, E.G.; Farinati, F.; Ciccarese, F.; Rapaccini, G.L.; Di Marco, M.; Benvegnu, L.; Zoli, M.; Borzio, F.; et al. A Liver Index and its Relationship to Indices of HCC Aggressiveness. *J. Integr. Oncol.* **2016**, *5*, 178, doi:10.4172/2329–6771.1000178.
55. Miao, H.Q.; Lee, P.; Lin, H.; Soker, S.; Klagsbrun, M. Neuropilin-1 expression by tumor cells promotes tumor angiogenesis and progression. *FASEB J.* **2000**, *14*, 2532–2539, doi:10.1096/fj.00-0250com.
56. Jubb, A.M.; Strickland, L.A.; Liu, S.D.; Mak, J.; Schmidt, M.; Koeppen, H. Neuropilin-1 expression in cancer and development. *J. Pathol.* **2012**, *226*, 50–60, doi:10.1002/path.2989.
57. Saha, P.; Datta, K. Multi-functional, multicompartmental hyaluronan-binding protein 1 (HABP1/p32/gC1qR): Implication in cancer progression and metastasis. *Oncotarget* **2018**, *9*, 10784–10807, doi:10.18632/oncotarget.24082.
58. El-Serag, H.B. Hepatocellular carcinoma. *N. Engl. J. Med.* **2011**, *365*, 1118–1127, doi:10.1056/NEJMra1001683.
59. Asghar, U.; Meyer, T. Are there opportunities for chemotherapy in the treatment of hepatocellular cancer? *J. Hepatol.* **2012**, *56*, 686–695, doi:10.1016/j.jhep.2011.07.031.

60. Bos, C.L.; Kodach, L.L.; van den Brink, G.R.; Diks, S.H.; van Santen, M.M.; Richel, D.J.; Peppelenbosch, M.P.; Hardwick, J.C. Effect of aspirin on the Wnt/beta-catenin pathway is mediated via protein phosphatase 2A. *Oncogene* **2006**, *25*, 6447–6456, doi:10.1038/sj.onc.1209658.
61. Meng, G.; Wang, W.; Chai, K.; Yang, S.; Li, F.; Jiang, K. Combination treatment with triptolide and hydroxycamptothecin synergistically enhances apoptosis in A549 lung adenocarcinoma cells through PP2A-regulated ERK, p38 MAPKs and Akt signaling pathways. *Int. J. Oncol.* **2015**, *46*, 1007–1017, doi:10.3892/ijo.2015.2814.
62. Wang, G.S. Medical uses of mylabris in ancient China and recent studies. *J. Ethnopharmacol.* **1989**, *26*, 147–162, doi:10.1016/0378-8741(89)90062-7.
63. Li, W.; Xie, L.; Chen, Z.; Zhu, Y.; Sun, Y.; Miao, Y.; Xu, Z.; Han, X. Cantharidin, a potent and selective PP2A inhibitor, induces an oxidative stress-independent growth inhibition of pancreatic cancer cells through G2/M cell-cycle arrest and apoptosis. *Cancer Sci.* **2010**, *101*, 1226–1233, doi:10.1111/j.1349-7006.2010.01523.x.
64. Kinch, M.S. An overview of FDA-approved biologics medicines. *Drug Discov. Today* **2015**, *20*, 393–398, doi:10.1016/j.drudis.2014.09.003.
65. Carlson, S.G.; Eng, E.; Kim, E.G.; Perlman, E.J.; Copeland, T.D.; Ballermann, B.J. Expression of SET, an inhibitor of protein phosphatase 2A, in renal development and Wilms' tumor. *J. Am. Soc. Nephrol.* **1998**, *9*, 1873–1880.
66. Chae, H.; Lim, J.; Kim, M.; Park, J.; Kim, Y.; Han, K.; Lee, S.; Min, W.S. Phenotypic and genetic characterization of adult T-cell acute lymphoblastic leukemia with del(9)(q34);SET-NUP214 rearrangement. *Ann. Hematol.* **2012**, *91*, 193–201, doi:10.1007/s00277-011-1289-x.
67. Cristobal, I.; Garcia-Orti, L.; Cirauqui, C.; Cortes-Lavaud, X.; Garcia-Sanchez, M.A.; Calasanz, M.J.; Odero, M.D. Overexpression of SET is a recurrent event associated with poor outcome and contributes to protein phosphatase 2A inhibition in acute myeloid leukemia. *Haematologica* **2012**, *97*, 543–550, doi:10.3324/haematol.2011.050542.
68. Cristobal, I.; Rincon, R.; Manso, R.; Carames, C.; Zazo, S.; Madoz-Gurpide, J.; Rojo, F.; Garcia-Foncillas, J. Deregulation of the PP2A inhibitor SET shows promising therapeutic implications and determines poor clinical outcome in patients with metastatic colorectal cancer. *Clin. Cancer Res.* **2015**, *21*, 347–356, doi:10.1158/1078-0432.CCR-14-0724.
69. Hung, M.H.; Chen, Y.L.; Chu, P.Y.; Shih, C.T.; Yu, H.C.; Tai, W.T.; Shiau, C.W.; Chen, K.F. Upregulation of the oncoprotein SET determines poor clinical outcomes in hepatocellular carcinoma and shows therapeutic potential. *Oncogene* **2016**, *35*, 4891–4902, doi:10.1038/onc.2016.21.
70. Fukukawa, C.; Shima, H.; Tanuma, N.; Ogawa, K.; Kikuchi, K. Up-regulation of I-2(PP2A)/SET gene expression in rat primary hepatomas and regenerating livers. *Cancer Lett.* **2000**, *161*, 89–95, doi:10.1016/s0304-3835(00)00598-x.
71. Agarwal, A.; MacKenzie, R.J.; Pippa, R.; Eide, C.A.; Oddo, J.; Tyner, J.W.; Sears, R.; Vitek, M.P.; Odero, M.D.; Christensen, D.J.; et al. Antagonism of SET using OP449 enhances the efficacy of tyrosine kinase inhibitors and overcomes drug resistance in myeloid leukemia. *Clin. Cancer Res.* **2014**, *20*, 2092–2103, doi:10.1158/1078-0432.CCR-13-2575.
72. Hung, M.H.; Wang, C.Y.; Chen, Y.L.; Chu, P.Y.; Hsiao, Y.J.; Tai, W.T.; Chao, T.T.; Yu, H.C.; Shiau, C.W.; Chen, K.F. SET antagonist enhances the chemosensitivity of non-small cell lung cancer cells by reactivating protein phosphatase 2A. *Oncotarget* **2016**, *7*, 638–655, doi:10.18632/oncotarget.6313.
73. Huang, C.Y.; Hung, M.H.; Shih, C.T.; Hsieh, F.S.; Kuo, C.W.; Tsai, M.H.; Chang, S.S.; Hsiao, Y.J.; Chen, L.J.; Chao, T.I.; et al. Antagonizing SET Augments the Effects of Radiation Therapy in Hepatocellular Carcinoma through Reactivation of PP2A-Mediated Akt Downregulation. *J. Pharmacol. Exp. Ther.* **2018**, *366*, 410–421, doi:10.1124/jpet.118.249102.

5.5 Article 5: Targeted delivery of a therapeutic peptide for the treatment of chronic lymphocytic leukemia.

Simon-Gracia L, Loisel S, Sidorenko V, Scodeller P, Parizot C, **Savier E**, Teesalu T and Rebollo A.
Mol. Pharmaceutics. 2022. doi.org/10.1021/acs.molpharmaceut.1c00837

Introduction

La leucémie lymhoïde chronique (LLC) est la plus fréquente des leucémies chez l'adulte. Elle se définit par une prolifération monoclonale de lymphocytes B qui ont subi des altérations génomiques conduisant à la perte du signal d'apoptose ou mort cellulaire programmée. Le pronostic de la maladie dépend non seulement des dérégulations cellulaires mais aussi du terrain. Ainsi, le score pronostic international de la LLC (International CLL-IPI working group, 2016) tient compte de 5 facteurs pronostic indépendants: status TP53, mutation du gène des chaines lourdes des immunoglobulines, concentration en β2-microglobuline, état clinique [selon Binet (Binet *et al*, 1981) ou selon Rai (Rai *et al*, 1975)] et l'âge. L'apparition de mutations successives conduit à la résistance des cellules tumorales aux immuno-chimiothérapies et à une progression rapide de la maladie. Meme si le sujet sort du cadre de cette thèse, il est important de voir que la LLC finit par échapper aux traitements, que les combinaisons de drogues deviennent de plus en plus complexes et les effets secondaires sévères demeurent incontournables. Le fait que le pronostic soit lié à l'âge et par conséquent à ses comorbidités est un argument majeur pour développer des stratégies thérapeutiques spécifiques des cellules tumorales. Nous avons montré que les peptides bi-fonctionnels (TPP-IP) s'internalisaient dans les cellules tumorales B et les hépatocytes de manière spécifique grâce au peptide pénétrant les tumeurs (TPP) (Simon-Gracia *et al*, 2020) et induisaient une apoptose. *In vitro*, le peptide interférant (IP) permettait de bloquer l'interaction entre la phosphatase PP2A et son inhibiteur naturel, la protéine SET. Cette interaction permettait de supposer que l'apoptose observée était secondaire au rétablissement de l'activité de PP2A. Parmi les 4 peptides bi-fonctionnels que nous avons utilisés, nous avons montré qu'iRGD-IP augmentait la survie des souris dans un modèle murin de xénogreffe (Simon-Gracia *et al*, 2020).

But du travail

Tester l'efficacité *in vivo* de 3 peptides bi-fonctionnels (RPARPAR-IP, TT1-IP et LinTT1-IP) dans un modèle murin de xénogreffe puis compléter par une analyse de la biodistribution et de la pharmacocinétique du plus performant.

Matériel et méthodes

Le modèle de xénogreffe comportait des souris immunodéficiences CB-17 SCID qui recevaient par voie intraveineuse des cellules de LLC Jok 1.3. Le traitement se faisait par injections intrapéritonéales de 5 mg/kg de TTP-IP à partir de j3 et 5 consécutifs jours par semaine.

La diffusion du peptide TT1-IP a été mesurée après injection intra-veineuse de peptides marqués par un fluorochrome (Cy7), puis acquisition d'image *in vivo*, sous anesthésie générale dans une chambre d'acquisition équipée d'une caméra haute définition.

Les toxicités rénale, hépatique et métabolique ont été comparées chez des souris femelle BALB/c par dosage de la créatinine, de l'ALAT et du glucose 24h après injection d'une dose de 5 mg/kg de TT1-IP ou de NaCl 0.9%.

L'apoptose a été mesurée par cytométrie en flux après marquage par de l'annexine V sur des cellules tumorales ou non et traitées 12h par TT1-IP ou TT1 seul ou IP seul ou un témoin.

La dégradation sur 24h de TT1-IP dans du sérum humain à 37°C et la pharmacocinétique de TT1-IP chez la souris BALB/c ont été mesurées par spectrométrie de masse.

Résultats

TT1-IP et LinTT1-IP prolongeaient la survie des souris greffés avec une lignée tumorale humaine de LLC, mais seul TT1-IP avait un effet significatif. En revanche RPARPAR-IP n'avait pas d'effet. Pourtant, l'apoptose induite sur les cellules tumorales par TT1-IP, LinTT1-IP et RPARPAR-IP était comparables et aucun effet apoptotique n'était observé avec IP seul ou TT1 seul ou sur des cellules saines. Ces derniers résultats démontraient les rôles complémentaires du TPP et de l'IP pour obtenir une apoptose spécifique des cellules tumorales.

Les résultats suivants ont été observés avec TT1-IP : L'intensité de captation de Cy7-TT1-IP fluorescent était plus importante chez une souris porteuse de cellules de LLC. Sur les souris immunocompétentes nous n'avons pas observé de toxicité de TT1-IP et montré que la concentration plasmatique maximale était atteinte en 10 minutes, suivie d'une clairance plasmatique avec un temps de ½ vie de 28 minutes. Enfin, 40% de TT1-IP était détectable après 6h d'incubation dans du sérum humain montrant ainsi sa lente dégradation par protéolyse.

Conclusion

Les résultats obtenus laissent à penser que l'utilisation de peptides thérapeutiques dans le traitement des cancers est une possibilité réelle.

molecular pharmaceutics

pubs.acs.org/molecularpharmaceutics

Article

Preclinical Validation of Tumor-Penetrating and Interfering Peptides against Chronic Lymphocytic Leukemia

Lorena Simón-Gracia,◆ Severine Loisel,◆ Valeria Sidorenko, Pablo Scodeller, Christophe Parizot, Eric Savier, Tanguy Haute, Tambet Teesalu,◆ and Angelita Rebollo*,◆

Cite This: *Mol. Pharmaceutics* 2022, 19, 895−903

Read Online

ACCESS | Metrics & More | Article Recommendations

ABSTRACT: Chronic lymphocytic leukemia (CLL) is the most common form of leukemia in adults. The disease is characterized by the accumulation of tumoral B cells resulting from a defect of apoptosis. We have *in vitro* and *in vivo* preclinically validated a tumor-penetrating peptide (named TT1) coupled to an interfering peptide (IP) that dissociates the interaction between the serine/threonine protein phosphatase 2A (PP2A) from its physiological inhibitor, the oncoprotein SET. This TT1-IP peptide has an antitumoral effect on CLL, as shown by the increased survival of mice bearing xenograft models of CLL, compared to control mice. The peptide did not show toxicity, as indicated by the mouse body weight and the biochemical parameters, such as renal and hepatic enzymes. In addition, the peptide-induced apoptosis *in vitro* of primary tumoral B cells isolated from CLL patients but not of those isolated from healthy patients. Finally, the peptide had approximately 5 h half-life in human serum and showed pharmacokinetic parameters compatible with clinical development as a therapeutic peptide against CLL.

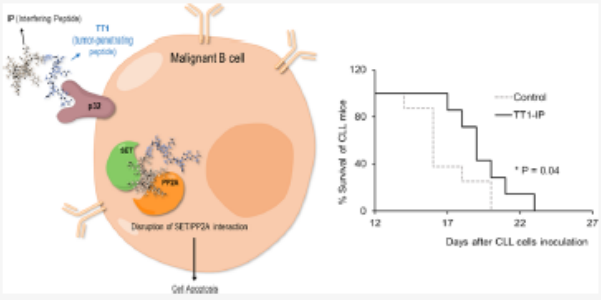

KEYWORDS: *chronic lymphocytic leukemia, xenograft models, tumor-penetrating and interfering peptides*

INTRODUCTION

Chronic lymphocytic leukemia (CLL), the most common form of leukemia in adults,[1] is defined by an accumulation of monoclonal neoplastic B cells in hematopoietic organs resulting from a defect in programmed cell death. Clinical outcomes and the prognosis of CLL patients depend on factors such as cellular and genetic markers, as well as the age and health profile of the patients. For young CLL patients, the standard chemo-immunotherapy combining chemotherapy (cytostatic agents such as fludarabine and cyclophosphamide) and immunotherapy (anti-CD20 antibodies, Rituximab) is well tolerated and effective in controlling the disease.[2] In contrast, with underlying health conditions, this frontline treatment can cause severe adverse effects.[3] Moreover, the patient cohort with a deletion in chromosome 17 (del17), or mutation in the p53 protein, shows resistance to chemotherapy that cannot be overcome by treatment with anti-CD20 antibodies. These patients, as well as patients with IGHC unmutated status,[4] have rapid disease progression and lower survival. In these cases, the use of specific inhibitors interrupting pathways for CLL cell survival (such as inhibitors of the Bruton kinase and antiapoptotic Bcl-2) has shown promising results.[3] However, some patients relapse due to acquired mutations (e.g., in the gene encoding for Bruton tyrosine kinase), rendering the disease resistant to the proliferation inhibitors. Therefore, it is important to develop new CLL therapies for patients in which the current treatments are not effective or have severe side effects.

We have recently developed bifunctional peptides composed of a tumor-penetrating peptide (TPP), which selectively internalizes in malignant B cells and tumoral hepatocytes,[5] in tandem with an interfering peptide (IP), which blocks the interaction between two cytoplasmic proteins, PP2A and SET.[6,7] SET is an oncoprotein overexpressed in several cancers including CLL. In CLL, SET is involved in the disease initiation and progression as well as in the development of therapeutic resistance.[7−9] The IP blocks the interaction of SET and PPA2, resulting in cancer cell death.[7] PP2A is a serine/threonine phosphatase that regulates pathways involved in apoptosis, proliferation, and DNA damage reparation, and its inhibition leads to malignant transformation.[10] The dissociation of PP2A from SET allows the reactivation of PP2A. To guide and deliver the IP peptide to the tumoral CLL cells, we previously tested four different TPPs: RPARPAR, iRGD, TT1, and LinTT1. TPPs

Received: November 3, 2021
Revised: January 25, 2022
Accepted: January 25, 2022
Published: February 3, 2022

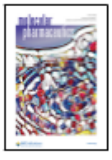

bind to and internalize into tumor cells and are used to deliver therapeutic and imaging cargoes into tumors. The TPPs containing the sequence R/KXXR/K at the C-terminal (CendR peptides) bind to neuropilin-1 (NRP-1), a receptor overexpressed in different types of tumors and malignant cells, including B cells from CLL patients.[11] The CendR peptide RPARPAR binds NRP-1[12] and has been used to deliver nanoparticles into cancer cells.[13,14] iRGD peptide (internalizing RGD) binds to $\alpha\beta 3/5$ integrin in the tumor vasculature and after being processed by tumor-related proteases engages NRP-1 to activate penetration into the tumor tissue.[15−18] The receptor of the cyclic TT1 peptide (CKRGARSTC) and its linear version LinTT1 (AKRGARSTA) is the p32/gC1qR/C1QBP/HABP1 protein (p32) that is aberrantly expressed on the surface of malignant and tumor-environment cells (tumor-associated lymphatic vessels and tumor-associated macrophages).[19] TT1 and LinTT1 are first recruited to p32, followed by proteolytic cleavage to allow NRP-1 engagement.[20] LinTT1 has been used for precision therapy and imaging of different solid tumor models.[21−25] We previously found that the B cells from CLL patients express receptors (integrin $\alpha v\beta 3$, NRP-1, and p32) of the four TPPs mentioned here and that the TPPs in tandem with the IP (TPP-IP) specifically internalize in and kill malignant B cells from CLL patients *in vitro*.[6] Importantly, we have shown that the treatment with iRGD-IP significantly increased the survival of CLL mice.[6] In the current report, we describe the *in vitro* and *in vivo* validation in a xenograft model of CLL of the three bifunctional tumor-penetrating and interfering peptides (RPARPAR-IP, TT1-IP, and LinTT1-IP) as well as the biodistribution and pharmacokinetic (PK) parameters of TT1-IP, the peptide that showed the highest increase in the survival of CLL mice.

MATERIALS AND METHODS

Peptide Synthesis and Sequence. Peptides were synthesized in an automated multiple peptide synthesizer with a solid-phase procedure and standard Fmoc chemistry by GL Biochem with a purity of 98% (Shanghai, China). The purity and composition of the peptides were confirmed by reverse-phase high-performance liquid chromatography (HPLC) using an increasing CH_3CN gradient and by mass spectrometry (MS). Unlabeled peptides were used for the apoptosis assays and experimental treatments. For live imaging experiments, TT1-IP was synthesized with the fluorochrome Cy7 at the N-terminus. The sequences of all peptides are shown in Table 1.

CLL Xenograft Models and Experimental Treatments. The 6−8-week-old female CB-17 SCID mice were purchased from Envigo (Gannat, France). All mice were maintained under conditions and protocols in accordance with the directives of the Council of European Animal Welfare. The animal experiments were done following the protocols approved by the Estonian Ministry of Agriculture, Committee of Animal Experimentation (project #196), and all of the experiments were conducted following the guidelines of the mentioned committee.

Table 1. Sequence of the Peptides Used in the Study[a]

peptide ID	sequences
TT1	CKRGARSTC-$CONH_2$ (C−C disulfide bond)
iRGD-IP	ETVTLLVALKVRYRERIT-Ahx-CRGDKGPDC-$CONH_2$ (C−C disulfide bond)
RPARPAR-IP	ETVTLLVALKVRYRERIT-Ahx-RPARPAR-OH
LinTT1-IP	ETVTLLVALKVRYRERIT-Ahx-AKRGARSTA-$CONH_2$
TT1-IP	Cy7-Ahx-ETVTLLVALKVRYRERIT-Ahx-CKRGARSTC-$CONH_2$ (C−C disulfide bond)
	ETVTLLVALKVRYRERIT-Ahx-CKRGARSTC-$CONH_2$ (C−C disulfide bond)

[a]Ahx = aminohexanoic acid.

CLL Jok1.3 cells (2×10^6) in 100 μL of phosphate saline buffer were injected into the tail vein. We have previously used the same CLL xenograft model[6] and observed that 100% of the tumor-induced mice developed CLL; therefore, no evaluation of the transplantation was performed before starting the treatment. Mice were intraperitoneally (IP) injected with saline (control group) or with the peptides three days after the inoculation. One experimental treatment was performed with four different groups (control, TT1-IP, LinTT1-IP, and RPARPAR-IP) and another treatment was performed with the control and TT1 groups. In both treatments, seven mice per group were used. The peptide dose was 2.6 μmol/kg (corresponding to 5 mg/kg of the TT1-IP peptide). Mice were monitored daily for the presence of hind leg paralysis, which is indicative of infiltration of leukemic cells in the central nervous system; in the case of infiltration, the mice were sacrificed.

Fluorescence Live Imaging. The 6−8-week-old female CB-17 SCID mice were purchased from Charles River Laboratories (L'Arbresle, France). All mice were maintained under conditions and protocols in accordance with the Directive 2010/63/UE of the Council of Europe on Animal Welfare. The study (number authorization 27656) was approved by the French Ethics Committee for animal experimentation number 74 and all experiments were conducted following the guidelines of the aforementioned committee.

Animals were sedated with 2% isoflurane in air. CLL Jok5.3 cells (2×10^6) in 100 μL of NaCl 0.9% were injected into the retro-orbital vein of the SCID mice. Three days after cell transplantation, the mice were intravenously (IV) injected with saline or 2.6 μmol/kg (5 mg/kg) of Cy7-TT1-IP peptide, followed by fluorescence imaging. Acquisitions were performed 15 min after IV injection, then regularly, up to 6 h postadministration. Before the acquisition, the animal was anesthetized by isoflurane inhalation (2% air−isoflurane blend). Then, the mouse was placed inside the acquisition chamber of an *in vivo* imaging system equipped with a cooled slow-scan CCD camera and driven with Indigo software (Berthold Technologies, Bad Wildbad, Germany). Images were captured at 1×1 binning with exposure times ranging from 0.1 to 1.0 s, depending on the fluorescence intensity.

Measurement of Toxicity of TT1-IP Peptide. Eight week-old-female BALB/c mice bred at the Institute of Biomedicine and Translational Medicine (Tartu, Estonia) were IP injected with 2.6 μmol/kg (5 mg/kg) of TT1-IP or saline (control); after 24 h, the mice were anesthetized and 500 μL of blood were collected by retro-orbital bleeding into lithium heparin tubes (BD Vacutainer, BD-Plymouth, UK). The samples were centrifuged for 10 min at 1800*g* at 4 °C and the plasma was analyzed for the concentration of glucose, creatinine, and activity of alanine aminotransferase (ALAT), using a Cobas 6000 IT-MW (Roche Diagnostics GmbH, Mannheim, Germany) machine and reagents for creatinine CREP2 and for alanine aminotransferase (ALAT) ALTLP.

Detection of Apoptosis by Annexin V Staining. The apoptosis induction of the peptides was analyzed by flow cytometry in cells labeled with annexin V-FITC staining (Biosciences, Fisher Scientific, France). Primary cells were

https://doi.org/10.1021/acs.molpharmaceut.1c00837
Mol. Pharmaceutics 2022, 19, 895−903

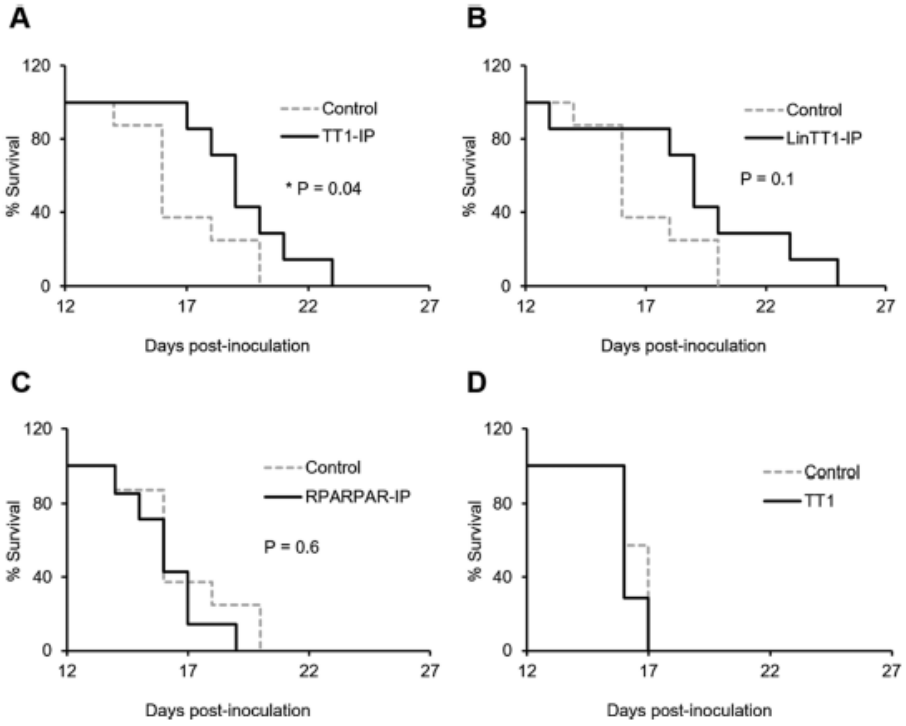

Figure 1. TPP-IP peptide increased the survival of the CLL mice. Survival curves of mice treated with TT1-IP (A), LinTT1-IP (B), RPARPAR-IP (C), or TT1 (D). Panels A–C represent the graphs from the same treatment. SCID mice were IV inoculated with Jok1.3 cells and treated 3 days after injection with 2.6 μmol/kg of peptides or saline (control), 5 days per week. The survival was monitored over time. Gray dashed line: control group; black line: group treated with the corresponding peptide. Statistical comparisons were performed using the Gehan–Breslow–Wilcoxon test ($N = 7$ per group).

treated with 25 μM of peptides for 12 h. After the treatment, cells were harvested, washed, and treated according to the manufacturer's protocol. The level of apoptosis was measured by flow cytometry (FACS Canto II, BD Biosciences, New Jersey).

Analysis of Peptide Stability in Human Serum. The peptide TT1-IP was incubated at 37 °C in 250 μL of human serum (Gibco, Villebon-sur-Yvette, France) for different periods of time (0, 1, 6, and 24 h). The samples were collected and peptide degradation stopped by freezing at −20 °C. The peptide was extracted from samples using a Proteo Miner protein enrichment system (Bio-Rad, France). The percentage of the intact peptide was estimated by MS using Matrix-Assisted Laser Desorption/Ionization–Time of Flight (MALDI-TOFF) according to the protocol previously described[26] (Bruker Autoflex II, France) as per the manufacturer's instructions. Measurements were performed in triplicate. MS data were analyzed using the software Cliprot tools, Flex analysis, Bruker (Palaiseau, France).

Liquid Chromatography/Mass Spectrometry (LC/MS)-based Analysis of Pharmacokinetic of TT1-IP Peptide. BALB/c mice (Janvier, France) were injected with 2.6 μmol/kg (5 mg/kg) of TT1-IP peptide and plasma collected at 10, 20, 30, 45, 60, 120, and 360 min.

Plasma samples (0.05 mL) of injected mice were transferred to 1.5 mL polypropylene tubes. A total of 0.08 mL of acetonitrile/water (10/90 volume/volume, v/v) containing 2.5% of ammonia was added. The samples were mixed and then transferred to Oasis HLB elution plates (Waters Corporation, Guyancourt, France) preconditioned with 0.2 mL of methanol and 0.2 mL of water. The plates were washed with 0.2 mL of acetonitrile/water (10/90, v/v). Plates were dried and the analytes were eluted three times with 0.1 mL of acetonitrile/water (75/20, v/v) containing 1% of formic acid. The elution fractions were dried under nitrogen at 40 °C. The residue was reconstituted by 30 μL of a mixture of acetonitrile/water (75/25 v/v) containing 1% formic acid. The plate was vortexed for 2 min and then 0.12 mL of water was added to each well. The plate was gently shaken for 30 s. Aliquots of 20 μL were injected onto the HPLC system. The specifications of the LC-MS/MS instrumentation were: Autosampler SIL-20AC XR maintained at approximately 10 °C, Shimadzu (Noisiel, France), LC-20AD XR pumps UFLC, Shimadzu (Noisiel, France), flow rate of 0.3 mL/min, DGU-20A5 degasser, Shimadzu (Noisiel, France), and CTO-20AC column oven set at 60 °C, Shimadzu (Noisiel, France). The mobile phase was a linear gradient consisting of acetonitrile containing 0.25% formic acid and an aqueous solution of 0.25% formic acid.

Statistical Analysis. For *in vivo* data, statistical comparisons between groups were performed using Gehan–Breslow–Wilcoxon test. For the *in vitro* apoptosis assay, one-way analysis of variance (ANOVA) and Fisher's least significant difference (LSD) tests were used.

RESULTS

Antitumoral Effect of TPP-IPs on CLL Xenograft Models. The antitumoral effect of TT1-IP, LinTT1-IP, and RPARPAR-IP was evaluated in a mouse model of CLL generated using the cell line Jok1.3. The mice were treated with the peptides using a dose of 2.6 μmol/kg (corresponding to

https://doi.org/10.1021/acs.molpharmaceut.1c00837
Mol. Pharmaceutics 2022, 19, 895−903

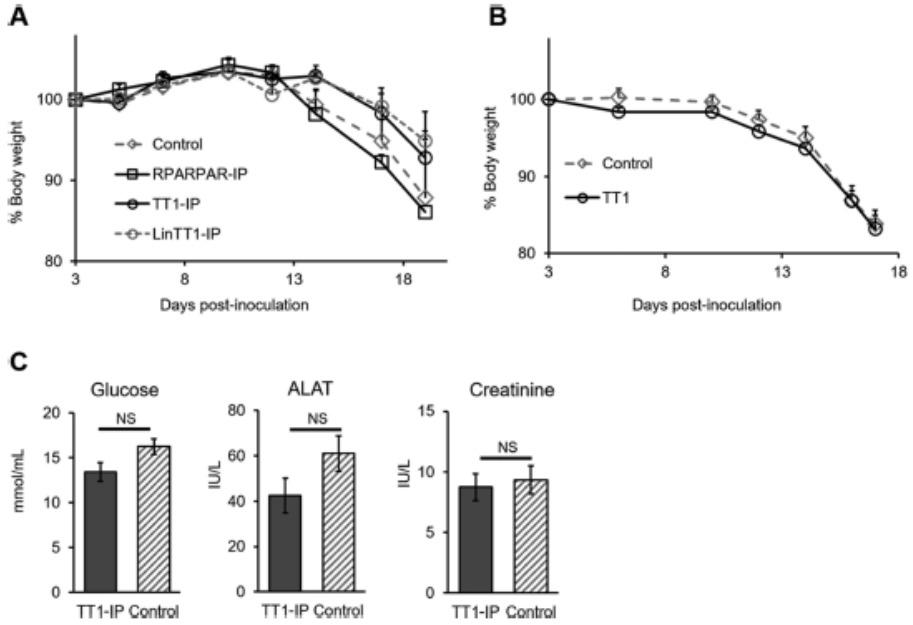

Figure 2. Effect of TPP-IPs on the body weight and plasma biochemical parameters. (A) Percent of the initial body weight of CLL-bearing mice treated with RPARPAR-IP, TT1-IP, LinTT1-IP, or saline (control). (B) Percent of the initial body weight of CLL-bearing mice treated with TT1 or saline (control). The weight of the mice was monitored every three days. Gray dashed line with square markers: control group; gray dashed line with round markers: LinTT1-IP; black line with square markers: RPARPAR-IP; black line with round markers: TT1-IP or TT1. $N = 7$; bars = ±SEM (standard error of the mean). (C) Effect of the TT1-IP peptide on the level of glucose and hepatic and renal enzymes. Immunocompetent BALB/c mice were injected with the TT1-IP peptide (2.6 μmol/kg, equivalent to 5 mg/kg) and glucose, creatinine, and ALAT in plasma were quantified after 24 h of injection. Bars with solid gray fill: TT1-IP; bars with gray pattern fill: control. $N = 3$; bars = ±SEM. NS means "non-significant difference".

5 mg/kg of TT1-IP), 5 days per week, or with saline (control group) until paralysis of the hind legs was observed. As shown in Figure 1A,B, treatment of CLL-bearing mice with TT1-IP and LinTT1-IP had a therapeutic effect, reflected by an increase in the median survival. The average survival for TT1-IP- and LinTT1-IP-treated groups was 19 days (the survival range for the TT1-IP group was 17−23 days and that for the LinTT1-IP group was 13−25 days) and that for the control group was 16 days (range of 14−20 days). In contrast, treatment with RPARPAR-IP did not increase the median survival (16 days, range of 14−19 days; Figure 1C). When compared with the control group, TT1-IP showed a significantly higher survival rate; therefore, TT1-IP was chosen to further study its *in vivo* toxicity, biodistribution, stability in serum, and PK parameters.

To confirm that the therapeutic effect of TT1-IP was due to the cargo (IP) associated with TPP, the CLL xenografted mice were treated with the shuttle TT1 alone. Figure 1D shows that TT1 did not increase the median survival compared with the control group, confirming that the anticancer effect resulted from the activity of the therapeutic interfering peptide.

Systemic TPP-IP Treatment Does Not Cause Toxicity in Mice. To assess the potential toxicity of TPP-IPs, we first compared the dynamics of body weight of the mice in different treatment groups. As shown in Figure 2A,B, the mice started to lose weight between days 10 and 14. However, no significant reduction in body weight was observed in the treated mice compared with the control group, suggesting that the weight loss was due to the disease development but not to the peptide toxicity. Although the mice treated with TT1-IP and LinTT1-IP showed a higher survival rate, the mice in these groups also showed a weight loss due to the progression of the disease. To confirm the absence of toxicity of TT1-IP, immunocompetent BALB/c mice were injected with 2.6 μmol/kg (5 mg/kg) of the peptide and after 24 h, the blood was collected to evaluate the liver and renal toxicity by quantification of the hepatic and renal enzymes ALAT and creatinine. The level of glucose was also quantified as indicative of the correct metabolic and endocrine functions. Figure 2C shows that the peptide did not produce any significant change in the levels of glucose, creatinine, and ALAT when compared to control mice, suggesting that the peptide did not produce hepatic and renal toxicity or glucose-related metabolic dysfunction at the used dose.

TT1-IP Peptide Treatment Causes Apoptosis on Primary B Cells from CLL. Disrupting the SET/PP2A interaction reactivates PP2A activity and produces cancer cell apoptosis.[27] We tested the apoptotic effect of TT1-IP, RPARPAR-IP, and LinTT1-IP and studied whether the TT1 and IP alone have any apoptotic effect. B cells from healthy donors and CLL patients were treated with the peptides, and the apoptotic effect was estimated by annexin staining. Figure 3 shows that TT1-IP, RPARPAR-IP, and LinTT1-IP strongly induced apoptosis of primary CLL cells but not of healthy B cells, while TT1 alone and IP alone did not have an apoptotic effect on any of the primary B cells. These results confirm that the apoptotic effect of TT1-IP, RPARPAR-IP, and LinTT1-IP is specific for malignant B cells and is mediated by the PP2A/SET-interfering peptide.

Stability of TT1-IP Peptide in Serum. Proteolytic degradation of peptide-based drugs is considered a major drawback, often limiting systemic therapeutic applications.[28] We analyzed the stability of TT1-IP peptide upon incubation at 37 °C in human serum by MS. Figure 4 shows that approximately 40% of the peptide was recovered after 6 h incubation and approximately 20% after 24 h.

https://doi.org/10.1021/acs.molpharmaceut.1c00837
Mol. Pharmaceutics 2022, 19, 895−903

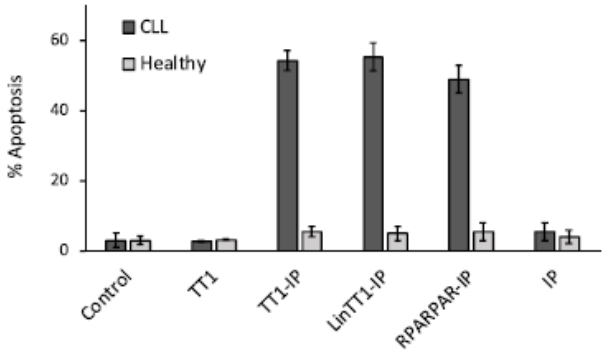

Figure 3. TPP-IPs and not TT1 induced apoptosis of B cells from CLL patients. Healthy B cells from donors or B cells from CLL patients were isolated, treated with 25 μM of TT1, TT1-IP, LinTT1-IP, RPARPAR-IP, or IP peptides for 12 h, and apoptosis measured by annexin-FITC staining. Untreated cells were used as control. Dark gray bars: B cells from CLL patients; light gray bars: B cells from healthy donors. $N = 2-3$. Bars = ±SEM.

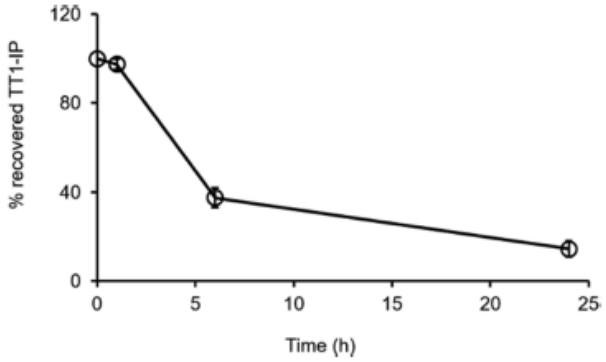

Figure 4. Stability of the TT1-IP peptide in human serum. The TT1-IP peptide was incubated in human serum at 37 °C for different periods of time. The integrity of the peptide was analyzed by MS. The percentage of the recovered peptide with time is represented. Every measurement was performed in triplicate. Bars represent ± SEM.

Fluorophore-Labeled TT1-IP Peptide Accumulates in CLL Xenograft. We evaluated by intravital imaging whether the targeting of TT1-IP to malignant B cells translated to a higher accumulation of the peptide in CLL mice than in nongrafted mice. Mice were IV injected with 2.6 μmol/kg (5 mg/kg) of Cy7-labeled TT1-IP (Cy7-TT1-IP) and imaged at different time points postinjection. The fluorescence in CLL xenografted and healthy mice was observed after 15 min postinjection (Figure 5A) and the intensity increased to reach a plateau at 1 h postinjection. A decrease in fluorescence intensity was observed after 3 h, showing only traces of fluorescence after 6 h of injection. Interestingly, the intensity of fluorescence observed in CLL mice was higher than that in healthy mice and the intensity ratio between CLL and healthy mice increased with time, reaching a value of 4 after three hours of peptide injection (Figure 5B). This is consistent with the fact that Cy7-TT1-IP is specifically internalized by circulating malignant B cells of CLL in the xenograft model.

PK Parameters of the TT1-IP Peptide. We then analyzed the PK parameters of TT1-IP to study whether this peptide could be developed as a drug candidate for the treatment against CLL. PK parameters were assessed by monitoring variations in the concentration of the peptide in plasma after IV injection, thus giving an overall indication of the behavior of the peptide in the body. The analyzed parameters, shown in Table 2, were T_{max} (time to reach maximum concentration), C_{max} (maximum concentration), T_{last} (time of the last observed concentration), C_{last} (concentration of the time point with measurable concentration), AUC_{Total} (total area under the curve), AUC_{last} (area under the curve in the last point), $T_{1/2}$ (terminal half-life), CL (total clearance), V_{ss} (volume of distribution at steady state), and C_0 (initial concentration). The detected C_0 was 2976 ng/mL and the V_{ss} 2700 mL/kg, indicating a good distribution capacity. The time to reach maximum concentration was 10 min. The $T_{1/2}$ was 28 min. The concentration of TT1-IP in plasma decreased with time, indicating the peptide clearance from the body. The clearance was 96 mL/min/kg and the exposure (AUC_{Total}) was 1003 ng/mL/min.

Taken together, our results describe the antitumor effect of a new tumor-penetrating and interfering peptide in a chronic lymphocytic leukemia xenograft model (Figure 6).

DISCUSSION

Despite improvement in the overall survival of CLL patients, in some clinical situations (e.g., in the case of relapsed or refractory CLL) new therapeutic approaches are needed.[29] The most recent approaches for transforming a combination therapy into a targeted chemotherapy (antibody–drug conjugated, ADC)[30] are unfortunately not applicable to CLL. For the ADC strategy to be effective, the receptor targeted by the antibody needs to be internalized after binding to transport the drug inside the cells, but monoclonal antibodies evaluated for CLL treatment bind to noninternalizing targets (CD20). Alternative targeted therapies for CLL are the use of B-cell receptors inhibitors, as well as the use of PI3K and Bcl-2 inhibitors. However, these treatments can cause adverse effects, such as neutropenia, thrombocytopenia, or diarrhea, among others.[31,32]

The use of peptides as targeting ligands in cancer has been widely explored,[33,34] as they offer several advantages over antibodies, such as superior penetration in solid tumors due to their lower molecular weight and lower affinity[34] and lower production cost. We show here that the use of tumor-penetrating peptides targeting p32 can be an alternative strategy to selectively deliver a bioactive IP into malignant B cells.

We previously showed that malignant B cells from CLL patients but not healthy B cells expressed the p32 and NRP-1 receptors.[6] CendR or cryptic CendR peptides in tandem with the IP disrupting the PP2A/SET interaction[7] were internalized by the tumoral B cells, producing apoptosis. Herein, we showed that TT1-IP significantly increased the survival of mice in a CLL xenograft model and that caused apoptosis of the malignant B cells from CLL patients. Importantly, as we previously showed with the iRGD-IP bifunctional peptide,[6] TT1-IP did not cause body weight loss in the treated mice and did not modify the levels of glucose, ALAT, and creatinine, suggesting the absence of liver and kidney toxicity. These findings suggest a potential advantage of TPP-IPs over current CLL therapies based on chemotherapy, which is not tolerated by patients due to the severe side effects.[3]

The cell surface-expressed form of p32 is a marker of tumor cells and tumor-associated macrophages/myeloid cells, being a good target in tumor diagnosis and therapy.[19] TT1 and LinTT1 are proteolytically cleaved by tumor-related enzymes after binding to p32.[20] The cleavage activates the CendR motif to become able to interact with NRP-1 to trigger internalization of the peptide along with cargo in tumor cells. This multistep

https://doi.org/10.1021/acs.molpharmaceut.1c00837
Mol. Pharmaceutics 2022, 19, 895−903

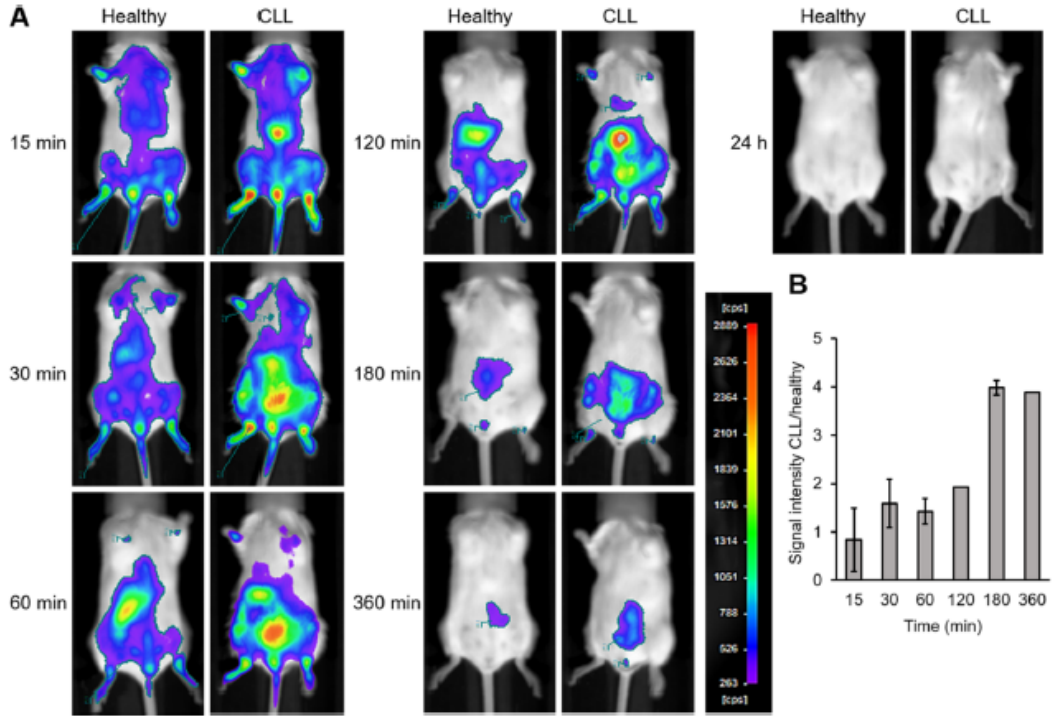

Figure 5. (A) Biodistribution of the Cy7-TT1-IP peptide in CLL and control mice. The SCID mice were grafted with Jok5.3 cell line and 3 days after being injected with 2.6 μmol/kg of Cy7-labeled TT1-IP peptide (Cy7-TT1-IP). Healthy mice injected with the same dose of peptide were used as control. The mice were imaged at different times after injection. Representative images from $N = 2$. The scale bar on the right shows the intensity of the fluorescence. Red represents higher intensity and purple lower intensity. (B) Ratio of the peptide intensity signal in CLL mice/healthy mice. The intensity was quantified as overall counts per second (cps) using the Indigo software (Berthold Technologies, Bad Wildbad, Germany). $N = 2$. Bars = ±SEM. The signal could not be detected in one of the healthy mice at 120 and 360 min.

Table 2. PK Parameters of TT1-IP[a]

T_{max} (min)	C_{max} (ng/mL)	T_{last} (min)	C_{last} (ng/mL)	AUC_{total} (ng/mL × h)	AUC_{last} (ng/mL × h)	$T_{1/2}$ (min)	CL (mL/min/Kg)	V_{ss} (mL/Kg)	C_0 (ng/mL)
10	1173	120	49	1003	963	28	96	2700	2976

[a]TT1-IP was IV administered in a single dose of 2.6 μmol/kg (5 mg/kg). The peptide was extracted from the serum, quantified by HPLC/MS and the PK parameters were calculated, T_{max} = time to reach maximum concentration; C_{max} = maximum concentration; T_{last} = time of the last observed concentration; C_{last} = concentration of the time point with measurable concentration; AUC_{Total} = total area under the curve; AUC_{last} = area under the curve in the last point; $T_{1/2}$ = half-life; CL = total clearance; V_{ss} = volume of distribution; C_0 = initial concentration.

mechanism makes TT1 highly tumor-specific, as opposed to RPARPAR peptide, which directly binds to NRP-1.

Functionalization of nanocarriers with LinTT1 peptide increased the nanocarrier homing to different solid tumors.[21−25] When analyzing the biodistribution of Cy7-labeled TT1-IP, the higher fluorescence intensity in xenograft models of CLL was observed compared to healthy mice, suggesting a preferential targeting to malignant B cells and expanding its applicability in the treatment of leukemia.

The serine/threonine phosphatase PP2A is known to be frequently deregulated in hematological cancers,[35−37] being an interesting target for novel anticancer therapies. The oncoprotein SET, the physiological inhibitor of PP2A, associates with the catalytic subunit of PP2A. The disruption of the PP2A/SET interaction restores the PP2A function inducing cell death; therefore, many efforts have been made to restore PP2A activity by dissociating the PP2A/SET interaction.[8,38−41]

We previously identified the binding site between PP2A and SET and designed a peptide that blocks this interaction.[7] We showed that the IP alone did not internalize in either B cells from CLL patients or in healthy B cells and that the IP coupled to a cell-penetrating peptide internalized in both cancer and healthy B cells.[6,7] Here, we show that TT1 promotes the specific internalization of the IP in malignant B cells but not healthy cells, causing cell apoptosis.

Poor PK parameters are the major reason for the lack of therapeutic activity of some drug candidates. PK parameters are assessed by monitoring variations on the concentration of the drug and/or its metabolites in physiological fluids that are easy to access, such as plasma and urine. PK parameters give an overall indication of the behavior of the drug in the body. The $T_{1/2}$ of the intravenously administered TT1-IP peptide was 28 min, similar to the half-life found for other peptides in preclinical or clinical stages.[42] For example, $T_{1/2}$ of some Bombesin analogue was around 30 min, and that for the peptide in clinical development Ep-100 (LHRH coupled to a cationic peptide) was 16 min.[42] Similarly, the half-life of aspirin is around 20 min and that of antibiotics ampicillin and clavulanic acid is in the range of 40−60 min.

https://doi.org/10.1021/acs.molpharmaceut.1c00837
Mol. Pharmaceutics 2022, 19, 895−903

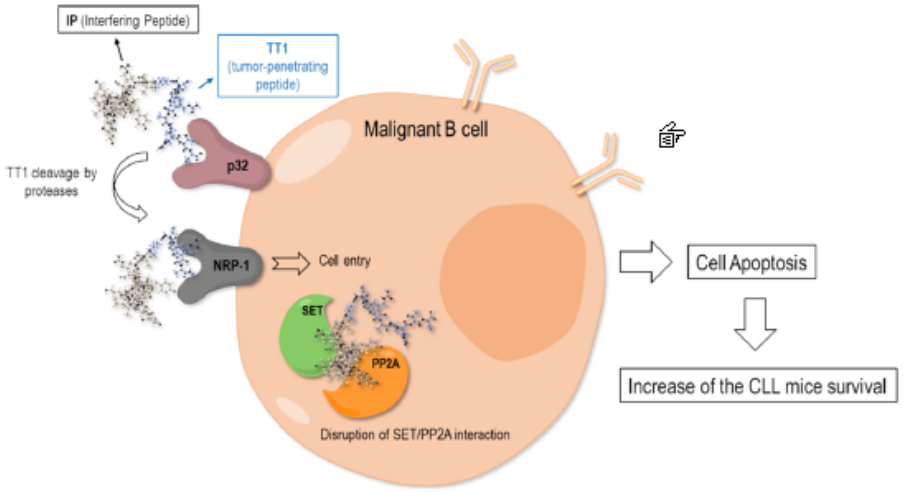

Figure 6. Cartoon summarizing the mechanism of action of the TT1-IP peptide. The TT1-IP internalizes in the tumoral B cells via specific receptors. First, the TT1 peptide binds to the p32 receptor overexpressed on the surface of malignant B cells. TT1 can then be cleaved by proteases exposing the CendR motif that binds to NRP-1, triggering the peptide cell internalization. Once inside the cell, the IP dissociates the interaction PP2A/SET and, consequently, there is induction of apoptosis and death of the tumoral cell.

Immune dysfunction in CLL contributes to tumor immune escape promoting cancer development. Recent findings showed that the expression of programmed death 1 ligand (PDL-1) is higher in CLL patients than that in control[43] and that disrupting the PD-1/PDL-1 interaction prevents immune dysfunction and leukemia development in a mouse model of CLL.[44] Therefore, the combination of our TPP-IPs with immune check inhibitors (such as PD-1) could be an interesting strategy to develop a more potent CLL therapy with lower side effects. Our results show that the bifunctional peptide targeting the p32 receptor in malignant cells and disrupting the SET/PP2A interaction has potential clinical translation as a new CLL treatment strategy.

■ CONCLUSIONS

The tumor-penetrating and interfering peptide TT1-IP increased the survival of mice with CLL and had an apoptotic effect in malignant B cells from CLL patients. Moreover, the PK parameters of TT1-IP suggest that it could be a potential candidate for the clinical treatment of this disease.

■ AUTHOR INFORMATION

Corresponding Author

Angelita Rebollo – *Université de Paris, Inserm U1267, CNRS, Faculté de Pharmacie, 75006 Paris, France;* orcid.org/0000-0002-1293-9686; Email: angelita.rebollo@parisdescartes.fr

Authors

Lorena Simón-Gracia – *Laboratory of Precision and Nanomedicine, Institute of Biomedicine and Translational Medicine, University of Tartu, 50411 Tartu, Estonia*

Severine Loisel – *Université de Brest, Service Général des plateformes, Animalerie Commune, 29238 Brest, France*

Valeria Sidorenko – *Laboratory of Precision and Nanomedicine, Institute of Biomedicine and Translational Medicine, University of Tartu, 50411 Tartu, Estonia*

Pablo Scodeller – *Laboratory of Precision and Nanomedicine, Institute of Biomedicine and Translational Medicine, University of Tartu, 50411 Tartu, Estonia*

Christophe Parizot – *Sorbonne Université, Inserm, CIMI-Paris, Paris, France; AP-HP, Hôpital Pitié-Salpêtrière, Département d'Immunologie, 75013 Paris, France*

Eric Savier – *Department of Hepato-Biliary and Pancreatic Surgery and Liver Transplantation, Pitie-Salpetriere Hospital, Assistance Publique-Hôpitaux de Paris (AP-HP), Sorbonne University, 75013 Paris, France; St Antoine Research Center (CRSA), Institute of Cardiometabolism and Nutrition (ICAN), Sorbonne University, INSERM, 75012 Paris, France*

Tanguy Haute – *Université de Brest, Plateforme SyNanoVect, 29238 Brest, France*

Tambet Teesalu – *Laboratory of Precision and Nanomedicine, Institute of Biomedicine and Translational Medicine, University of Tartu, 50411 Tartu, Estonia; Center for Nanomedicine, University of California Santa Barbara, 92037 Santa Barbara, California, United States*

Complete contact information is available at: https://pubs.acs.org/10.1021/acs.molpharmaceut.1c00837

Author Contributions

◆L.S.-G., S.L., T.T., and A.R. contributed equally to this article. The manuscript was written through contribution of all authors. All authors have given approval to the final version of the manuscript.

Notes

The authors declare no competing financial interest.

■ ACKNOWLEDGMENTS

Thanks to Dr. Fariba Nemati for helping with plasma collection for PK experiments. The authors thank the animal facility platform of Brest for their technical assistance and the SyNanoVect platform. Thanks also to Karine Le Ster for the Jok5.3 cell line. T.T. was supported by the European Regional Development Fund (Project No. 2014-2020.4.01.15-0012) and by the Estonian Research Council (grants PRG230 and EAG79).

REFERENCES

(1) Siegel, R. L.; Miller, K. D.; Jemal, A. Cancer statistics, 2019. *CA-Cancer J. Clin.* **2019**, *69*, 7−34.

(2) Woyach, J. A.; Johnson, A. J. Targeted therapies in CLL: mechanisms of resistance and strategies for management. *Blood* **2015**, *126*, 471−477.

(3) Hallek, M. Chronic lymphocytic leukemia: 2020 update on diagnosis, risk stratification and treatment. *Am. J. Hematol.* **2019**, *94*, 1266−1287.

(4) Rotbain, E. C.; Frederiksen, H.; Hjalgrim, H.; Rostgaard, K.; Egholm, G. J.; Zahedi, B.; Poulsen, C. B.; Enggard, L.; da Cunha-Bang, C.; Niemann, C. U. IGHV mutational status and outcome for patients with chronic lymphocytic leukemia upon treatment: a Danish nationwide population-based study. *Haematologica* **2020**, *105*, 1621−1629.

(5) Savier, E.; Simon-Gracia, L.; Charlotte, F.; Tuffery, P.; Teesalu, T.; Scatton, O.; Rebollo, A. Bi-Functional Peptides as a New Therapeutic Tool for Hepatocellular Carcinoma. *Pharmaceutics* **2021**, *13*, No. 1631.

(6) Simon-Gracia, L.; Savier, E.; Parizot, C.; Brossas, J. Y.; Loisel, S.; Teesalu, T.; Conti, F.; Charlotte, F.; Scatton, O.; Aoudjehane, L.; Rebollo, A. Bifunctional Therapeutic Peptides for Targeting Malignant B Cells and Hepatocytes: Proof of Concept in Chronic Lymphocytic Leukemia. *Adv. Ther.* **2020**, *3*, No. 2000131.

(7) Tian, L.; Z, X.; Haeesen, D.; Bravo, J.; Fominaya, J.; Choauet, S.; Zini, J. M.; Loisel, S.; Waelkens, E.; Janssens, V.; Rebollo, A. Identification of PP2A/SET binding sites and design of interacting peptides with potential clinical application. *Int. J. Pept. Res. Ther.* **2017**, *24*, 479−488.

(8) Christensen, D. J.; Chen, Y.; Oddo, J.; Matta, K. M.; Neil, J.; Davis, E. D.; Volkheimer, A. D.; Lanasa, M. C.; Friedman, D. R.; Goodman, B. K.; Gockerman, J. P.; Diehl, L. F.; de Castro, C. M.; Moore, J. O.; Vitek, M. P.; Weinberg, J. B. SET oncoprotein overexpression in B-cell chronic lymphocytic leukemia and non-Hodgkin lymphoma: a predictor of aggressive disease and a new treatment target. *Blood* **2011**, *118*, 4150−4158.

(9) Cristobal, I.; Garcia-Orti, L.; Cirauqui, C.; Cortes-Lavaud, X.; Garcia-Sanchez, M. A.; Calasanz, M. J.; Odero, M. D. Overexpression of SET is a recurrent event associated with poor outcome and contributes to protein phosphatase 2A inhibition in acute myeloid leukemia. *Haematologica* **2012**, *97*, 543−550.

(10) Mazhar, S.; Taylor, S. E.; Sangodkar, J.; Narla, G. Targeting PP2A in cancer: Combination therapies. *Biochim. Biophys. Acta, Mol. Cell Res.* **2019**, *1866*, 51−63.

(11) Nowakowski, G. S.; Mukhopadhyay, D.; Wu, X.; Kay, N. E. Neuropilin-1 is expressed by chronic lymphocytic leukemia B cells. *Leuk. Res.* **2008**, *32*, 1634−1636.

(12) Teesalu, T.; Sugahara, K. N.; Kotamraju, V. R.; Ruoslahti, E. C-end rule peptides mediate neuropilin-1-dependent cell, vascular, and tissue penetration. *Proc. Natl. Acad. Sci. U.S.A.* **2009**, *106*, 16157−16162.

(13) Wonder, E.; Simon-Gracia, L.; Scodeller, P.; Majzoub, R. N.; Kotamraju, V. R.; Ewert, K. K.; Teesalu, T.; Safinya, C. R. Competition of charge-mediated and specific binding by peptide-tagged cationic liposome-DNA nanoparticles in vitro and in vivo. *Biomaterials* **2018**, *166*, 52−63.

(14) Willmore, A.-M.; Simon-Gracia, L.; Toome, K.; Paiste, P.; Kotamraju, V. R.; Molder, T.; Sugahara, K. N.; Ruoslahti, E.; Braun, G. B.; Teesalu, T. Targeted silver nanoparticles for ratiometric cell phenotyping. *Nanoscale* **2016**, *8*, 9096−9101.

(15) Sugahara, K. N.; Teesalu, T.; Karmali, P. P.; Kotamraju, V. R.; Agemy, L.; Girard, O. M.; Hanahan, D.; Mattrey, R. F.; Ruoslahti, E. Tissue-penetrating delivery of compounds and nanoparticles into tumors. *Cancer Cell* **2009**, *16*, 510−520.

(16) Sugahara, K. N.; Teesalu, T.; Karmali, P. P.; Kotamraju, V. R.; Agemy, L.; Greenwald, D. R.; Ruoslahti, E. Coadministration of a tumor-penetrating peptide enhances the efficacy of cancer drugs. *Science* **2010**, *328*, 1031−1035.

(17) Simón-Gracia, L.; Hunt, H.; Scodeller, P.; Gaitzsch, J.; Kotamraju, V. R.; Sugahara, K. N.; Tammik, O.; Ruoslahti, E.; Battaglia, G.; Teesalu, T. iRGD peptide conjugation potentiates intraperitoneal tumor delivery of paclitaxel with polymersomes. *Biomaterials* **2016**, *104*, 247−257.

(18) Diaz Bessone, M. I.; Simon-Gracia, L.; Scodeller, P.; Ramirez, M. L. A.; Lago Huvelle, M. A.; Soler-Illia, G.; Simian, M. iRGD-guided tamoxifen polymersomes inhibit estrogen receptor transcriptional activity and decrease the number of breast cancer cells with self-renewing capacity. *J. Nanobiotechnology* **2019**, *17*, No. 120.

(19) Fogal, V.; Zhang, L.; Krajewski, S.; Ruoslahti, E. Mitochondrial/cell-surface protein p32/gC1qR as a molecular target in tumor cells and tumor stroma. *Cancer Res* **2008**, *68*, 7210−7218.

(20) Paasonen, L.; Sharma, S.; Braun, G. B.; Kotamraju, V. R.; Chung, T. D.; She, Z. G.; Sugahara, K. N.; Yliperttula, M.; Wu, B.; Pellecchia, M.; Ruoslahti, E.; Teesalu, T. New p32/gC1qR Ligands for Targeted Tumor Drug Delivery. *Chembiochem* **2016**, *17*, 570−575.

(21) Säälik, P.; Lingasamy, P.; Toome, K.; Mastandrea, I.; Rousso-Noori, L.; Tobi, A.; Simon-Gracia, L.; Hunt, H.; Paiste, P.; Kotamraju, V. R.; Bergers, G.; Asser, T.; Ratsep, T.; Ruoslahti, E.; Bjerkvig, R.; Friedmann-Morvinski, D.; Teesalu, T. Peptide-guided nanoparticles for glioblastoma targeting. *J. Controlled Release* **2019**, *308*, 109−118.

(22) Simón-Gracia, L.; Scodeller, P.; Fuentes, S. S.; Vallejo, V. G.; Rios, X.; San Sebastian, E.; Sidorenko, V.; Di Silvio, D.; Suck, M.; De Lorenzi, F.; Rizzo, L. Y.; von Stillfried, S.; Kilk, K.; Lammers, T.; Moya, S. E.; Teesalu, T. Application of polymersomes engineered to target p32 protein for detection of small breast tumors in mice. *Oncotarget* **2018**, *9*, 18682−18697.

(23) Hunt, H.; Simon-Gracia, L.; Tobi, A.; Kotamraju, V. R.; Sharma, S.; Nigul, M.; Sugahara, K. N.; Ruoslahti, E.; Teesalu, T. Targeting of p32 in peritoneal carcinomatosis with intraperitoneal linTT1 peptide-guided pro-apoptotic nanoparticles. *J. Controlled Release* **2017**, *260*, 142−153.

(24) Simón-Gracia, L.; Hunt, H.; Teesalu, T. Peritoneal Carcinomatosis Targeting with Tumor Homing Peptides. *Molecules* **2018**, *23*, No. 1190.

(25) Simon-Gracia, L.; Sidorenko, V.; Uustare, A.; Ogibalov, I.; Tasa, A.; Tshubrik, O.; Teesalu, T. Novel Anthracycline Utorubicin for Cancer Therapy. *Angew. Chem., Int. Ed.* **2021**, *60*, 17018−17027.

(26) Fominaya, J.; Bravo, J.; Decaudin, D.; Brossa, J. Y.; Nemati, F.; Rebollo, A. Enhanced serum proteolysis resistance of cell-penetrating peptides. *Ther. Delivery* **2015**, *6*, 139−147.

(27) Hung, M. H.; Chen, Y. L.; Chu, P. Y.; Shih, C. T.; Yu, H. C.; Tai, W. T.; Shiau, C. W.; Chen, K. F. Upregulation of the oncoprotein SET determines poor clinical outcomes in hepatocellular carcinoma and shows therapeutic potential. *Oncogene* **2016**, *35*, 4891−4902.

(28) Fominaya, J.; Bravo, J.; Rebollo, A. Strategies to stabilize cell penetrating peptides for in vivo applications. *Ther. Delivery* **2015**, *6*, 1171−1194.

(29) Fischer, K.; Al-Sawaf, O.; Bahlo, J.; Fink, A. M.; Tandon, M.; Dixon, M.; Robrecht, S.; Warburton, S.; Humphrey, K.; Samoylova, O.; Liberati, A. M.; Pinilla-Ibarz, J.; Opat, S.; Sivcheva, L.; Le Du, K.; Fogliatto, L. M.; Niemann, C. U.; Weinkove, R.; Robinson, S.; Kipps, T. J.; Boettcher, S.; Tausch, E.; Humerickhouse, R.; Eichhorst, B.; Wendtner, C. M.; Langerak, A. W.; Kreuzer, K. A.; Ritgen, M.; Goede, V.; Stilgenbauer, S.; Mobasher, M.; Hallek, M. Venetoclax and Obinutuzumab in Patients with CLL and Coexisting Conditions. *N. Engl. J. Med.* **2019**, *380*, 2225−2236.

(30) Dreger, P.; Schetelig, J.; Andersen, N.; Corradini, P.; van Gelder, M.; Gribben, J.; Kimby, E.; Michallet, M.; Moreno, C.; Stilgenbauer, S.; Montserrat, E.; European Research Initiative on C. L. L.; the European Society for Blood and Marrow Transplantation (EBMT).. Managing high-risk CLL during transition to a new treatment era: stem cell transplantation or novel agents? *Blood* **2014**, *124*, 3841−3849.

(31) Patel, K.; Pagel, J. M. Exploring a Future for PI3K Inhibitors in Chronic Lymphocytic Leukemia. *Curr. Hematol. Malig. Rep.* **2019**, *14*, 292−301.

(32) Perini, G. F.; Ribeiro, G. N.; Pinto Neto, J. V.; Campos, L. T.; Hamerschlak, N. BCL-2 as therapeutic target for hematological malignancies. *J. Hematol. Oncol.* **2018**, *11*, No. 65.

https://doi.org/10.1021/acs.molpharmaceut.1c00837
Mol. Pharmaceutics 2022, 19, 895−903

(33) Ikemoto, H.; Lingasamy, P.; Anton Willmore, A. M.; Hunt, H.; Kurm, K.; Tammik, O.; Scodeller, P.; Simon-Gracia, L.; Kotamraju, V. R.; Lowy, A. M.; Sugahara, K. N.; Teesalu, T. Hyaluronan-binding peptide for targeting peritoneal carcinomatosis. *Tumour Biol.* **2017**, *39*, No. 1010428317701628.
(34) Scodeller, P.; Asciutto, E. K. Targeting Tumors Using Peptides. *Molecules* **2020**, *25*, No. 808.
(35) Haesen, D.; Sents, W.; Lemaire, K.; Hoorne, Y.; Janssens, V. The Basic Biology of PP2A in Hematologic Cells and Malignancies. *Front. Oncol.* **2014**, *4*, No. 347.
(36) Ciccone, M.; Calin, G. A.; Perrotti, D. From the Biology of PP2A to the PADs for Therapy of Hematologic Malignancies. *Front. Oncol.* **2015**, *5*, No. 21.
(37) Neviani, P.; Harb, J. G.; Oaks, J. J.; Santhanam, R.; Walker, C. J.; Ellis, J. J.; Ferenchak, G.; Dorrance, A. M.; Paisie, C. A.; Eiring, A. M.; Ma, Y.; Mao, H. C.; Zhang, B.; Wunderlich, M.; May, P. C.; Sun, C.; Saddoughi, S. A.; Bielawski, J.; Blum, W.; Klisovic, R. B.; Solt, J. A.; Byrd, J. C.; Volinia, S.; Cortes, J.; Huettner, C. S.; Koschmieder, S.; Holyoake, T. L.; Devine, S.; Caligiuri, M. A.; Croce, C. M.; Garzon, R.; Ogretmen, B.; Arlinghaus, R. B.; Chen, C. S.; Bittman, R.; Hokland, P.; Roy, D. C.; Milojkovic, D.; Apperley, J.; Goldman, J. M.; Reid, A.; Mulloy, J. C.; Bhatia, R.; Marcucci, G.; Perrotti, D. PP2A-activating drugs selectively eradicate TKI-resistant chronic myeloid leukemic stem cells. *J. Clin. Invest.* **2013**, *123*, 4144−4157.
(38) Janssens, V.; Rebollo, A. The role and therapeutic potential of Ser/Thr phosphatase PP2A in apoptotic signalling networks in human cancer cells. *Curr. Mol. Med.* **2012**, *12*, 268−287.
(39) Lambrecht, C.; Haesen, D.; Sents, W.; Ivanova, E.; Janssens, V. Structure, regulation, and pharmacological modulation of PP2A phosphatases. *Methods Mol. Biol.* **2013**, *1053*, 283−305.
(40) Pippa, R.; Dominguez, A.; Christensen, D. J.; Moreno-Miralles, I.; Blanco-Prieto, M. J.; Vitek, M. P.; Odero, M. D. Effect of FTY720 on the SET-PP2A complex in acute myeloid leukemia; SET binding drugs have antagonistic activity. *Leukemia* **2014**, *28*, 1915−1918.
(41) Sangodkar, J.; Farrington, C. C.; McClinch, K.; Galsky, M. D.; Kastrinsky, D. B.; Narla, G. All roads lead to PP2A: exploiting the therapeutic potential of this phosphatase. *FEBS J.* **2016**, *283*, 1004−1024.
(42) Bumbaca, B.; Li, Z.; Shah, D. K. Pharmacokinetics of protein and peptide conjugates. *Drug Metab. Pharmacokinet.* **2019**, *34*, 42−54.
(43) Grzywnowicz, M.; Karczmarczyk, A.; Skorka, K.; Zajac, M.; Zaleska, J.; Chocholska, S.; Tomczak, W.; Giannopoulos, K. Expression of Programmed Death 1 Ligand in Different Compartments of Chronic Lymphocytic Leukemia. *Acta Haematol.* **2015**, *134*, 255−262.
(44) McClanahan, F.; Hanna, B.; Miller, S.; Clear, A. J.; Lichter, P.; Gribben, J. G.; Seiffert, M. PD-L1 checkpoint blockade prevents immune dysfunction and leukemia development in a mouse model of chronic lymphocytic leukemia. *Blood* **2015**, *126*, 203−211.

https://doi.org/10.1021/acs.molpharmaceut.1c00837
Mol. Pharmaceutics 2022, 19, 895−903

5.6 Article 6: Binding and kinetic analysis of human protein phosphatase PP2A interactions with Caspase 9 protein and the interfering peptide C9h

Dorgham K, Murail S, Tuffery P, **Savier E**, Bravo J and Rebollo A.
Pharmaceutics. 2022. DOI : 10.3390/pharmaceutics14102055

Introduction

Interférer dans les interactions entre les protéines est un moyen thérapeutique innovant, précis et applicable à de nombreuses pathologies. Un certain nombre de peptides sont en cours de développement et certains en phase clinique (Rafferty *et al*, 2016; Wang *et al*, 2022) (Annexe 5). Notre laboratoire a initié une étude de phase II, avec le peptide interférant PEP 010 (clinical trial, NCT04733027). PEP 010 (Mut3DPT-C9h) qui a été développé par notre laboratoire et interfère entre la PP2A et la protéine Caspase 9.

PP2A est une phosphatase sérine/thréonine, dont il a été montré qu'elle avait une fonction pro-apoptotique et dans certains cas, une fonction anti-apoptotique (Ayllón *et al*, 2000; Kang & Choi, 2001). PP2A est dérégulée dans de nombreux types de cancers et ainsi que d'autres maladies comme la maladie d'Alzheimer ou les maladies cardiovasculaires (Brautigan *et al*, 2021). L'inhibition de l'activité de PP2A est essentielle pour favoriser la transformation cellulaire, la progression tumorale et l'angiogenèse. PP2A a donc un rôle suppresseur de tumeur (Brautigan *et al*, 2021; Chen *et al*, 2004; Janssens *et al*, 2005). Des résultats récents montrent que la restauration pharmacologique de l'activité de PP2A antagonise efficacement le développement des cancers (Arrouss *et al*, 2013).

La Caspase 9 est une cystéine protéase, initiatrice de l'apoptose en étant la Caspase initiatrice et qui interfère avec PP2A. Notre équipe a identifié un IP (C9h) capable de bloquer l'interaction entre PP2A et Caspase 9 (Arrouss *et al*, 2013). C9h dérive de la séquence de Caspase 9 et a montré un effet anti-tumoral *in-vitro* et *in-vivo* dans un modèle de xénogreffe de cancer du sein (Arrouss *et al*, 2013).

But du travail

Mesurer l'affinité entre PP2A et Caspase 9 d'une part, entre PP2A et C9h, d'autre part, *in vitro* et *in silico.*

Materiel et methods

La présence d'une hélice α dans le peptide C9h a été analysée par dichroïsme circulaire, en faisant varier la concentration en trifluoroethanol dans le mileu et à l'aide d'un spectropolarimètre.

Des simulations moléculaires dynamiques étaient faites *in silico* (par ordinateur) à partir de banques de données de protéines.

Le C9h était marqué par de la biotine en N-terminal (C9h-Nter) ou en C-terminal (C9h-Cter) puis, selon une technique ELISA, fixé sur plaque enduite de streptavidine avant addition de PP2A, dont la révélation était faite par un anticorps (AC) anti-PP2A lui-meme lui-meme revelé par un AC secondaire conjugué à la peroxidase de raifort révélé par chemiluminescence.

Les cinétiques d'interaction protéine/protéine (Caspase 9/PP2A ou vice versa) ou protéine/peptide (PP2A/C9h) ont été mesurés par interférométrie de biocouche (BLI pour *biolayer interferometry*). BLI est une méthode de caractérisation optique utilisée pour surveiller en temps réel les interactions entre les molécules. Elle est basée sur le décalage de longueur d'onde reflétant le changement d'épaisseur de la couche biologique provoqué par la liaison des molécules à la sonde. Des anti-corps anti-Caspase 9 de souris ou d'anti-PP2A de lapin ont été immobilisés sur le capteur pendant 150 s puis Caspase 9 ou PP2A ont été chargés sur l'immunocapteur pendant 150 s. L'étape de dissociation a ensuite été surveillée pendant 120 s. Les mesures cinétiques de PP2A contre le peptide biotinylés C9h-Cter ont été effectuées avec des biocapteurs à la streptavidine enrobés par le peptide.

Résultats

En présence de quantités croissantes de trifluoroéthanol, la structure du C9h adoptait progressivement un pourcentage plus élevé de structure en hélice alpha. Par simulation moléculaire dynamique, des courbes similaires de structures ont été obtenues. Ces résultats suggéraient que, bien qu'il soit isolé de son environnement naturel, c'est à dire au sein de de la protéine Caspase 9, C9h avait toujours la capacité de conserver son caractère hélicoïdal, ce qui peut être important pour exercer des actions biologiques ou biochimiques.

La comparaison entre les peptides biotinylés en C9h-Cter ou en C9h-Nter de la fixation sur PP2A montrait un signal plus fort pour C9h-Cter qui a donc été utilisé pour les expériences de dissociation.

Des mesures d'affinité entre PP2A et Caspase 9 immobilisée ont été effectuées à différentes concentrations de PP2A et a permis de déterminer la constante de liaison à l'équilibre (KD = 8,94 × 10^{-8} M). Dans une procédure inverse, PP2A a été immobilisé sur la sonde et différentes concentrations de protéine Caspase 9 ont été utilisées pour déterminer la constante à l'équilibre (KD = 2,28 × 10^{-7} M). Dans l'ensemble, dans les deux modèles, il a été observé que les protéines PP2A et Caspase 9 se lient avec une affinité relativement bonne (proche de 10^{-7} M).

Des mesures d'affinité entre C9h-Cter immobilisé et PP2A ont permis de déterminer la constante à l'équilibre (KD = 7,8 × 10^{-7} M). Les taux de dissociation avec PP2A étaient d'environ un log supérieur à ceux observés avec Caspase 9 et témoignaient d'une affinité légèrement inférieure.

Conclusion

En conclusion, ces résultats démontrent une bonne affinité entre PP2A et le peptide interférant C9h. Par conséquent, le peptide C9h peut être utilisé comme outil pour manipuler cette interaction.

pharmaceutics

MDPI

Article

Binding and Kinetic Analysis of Human Protein Phosphatase PP2A Interactions with Caspase 9 Protein and the Interfering Peptide C9h

Karim Dorgham [1,†], Samuel Murail [2,†], Pierre Tuffery [2], Eric Savier [3], Jeronimo Bravo [4] and Angelita Rebollo [5,*]

1 Faculty of Medicine, Sorbonne Université, Inserm, CIMI Paris, 91, bd de l'hôpital, 75013 Paris, France
2 BFA, Université Paris Cité, Inserm 1133, 75013 Paris, France
3 AP-HP, Sorbonne Université, CRSA, 75013 Paris, France
4 Instituto de Biomedicina de Valencia IBV-CSIC, Jaime Roig, 11, 46010 Valencia, Spain
5 Faculty of Pharmacy, UTCBS, Université Paris Cité, Inserm 1267, 75006 Paris, France
* Correspondence: angelita.rebollo@parisdescartes.fr
† These authors contributed equally to this work.

Abstract: The serine/threonine phosphatase PP2A and the cysteine protease Caspase 9 are two proteins involved in physiological and pathological processes, including cancer and apoptosis. We previously demonstrated the interaction between Caspase 9 and PP2A and identified the C9h peptide, corresponding to the binding site of Caspase 9 to PP2A. This interfering peptide can modulate Caspase 9/PP2A interaction leading to a strong therapeutic effect in vitro and in vivo in mouse models of tumor progression. In this manuscript, we investigate (I) the peptide binding to PP2A combining docking with molecular dynamics and (II) the secondary structure of the peptide using CD spectroscopy. Additionally, we compare the binding affinity, using biolayer interferometry, of the wild-type protein PP2A with Caspase 9 and vice versa to that observed between the PP2A protein and the interfering peptide C9h. This result strongly encourages the use of peptides as new therapeutics against cancer, as shown for the C9h peptide already in clinical trial.

Keywords: biolayer interferometry; PP2A; Caspase 9; circular dichroism; binding affinity; C9h interfering peptide

Citation: Dorgham, K.; Murail, S.; Tuffery, P.; Savier, E.; Bravo, J.; Rebollo, A. Binding and Kinetic Analysis of Human Protein Phosphatase PP2A Interactions with Caspase 9 Protein and the Interfering Peptide C9h. *Pharmaceutics* **2022**, *14*, 2055. https://doi.org/10.3390/pharmaceutics14102055

Academic Editor: Toni Todorovski

Received: 19 July 2022
Accepted: 23 September 2022
Published: 27 September 2022

1. Introduction

Targeting protein/protein interactions are considered a good therapeutic strategy in several pathologies. Indeed, interfering peptides blocking a specific protein/protein interaction are considered important tools to manipulate a given interaction. Moreover, administration routes, stability, pharmacokinetic parameters, and safety of the peptides have made these molecules an attractive new generation of drugs [1]. Several interfering peptides have been identified and validated in vitro and in vivo [2–5] as new potential medicaments, and some of them are in clinical development or already in the market (PEP 010, clinical trial, NCT04733027, [6,7]).

Protein phosphatase 2A (PP2A), a serine/threonine phosphatase, has been shown to have a pro-apoptotic, and also in some cases, an anti-apoptotic function [8,9]. PP2A is deregulated in many types of cancers and a number of other human diseases, including Alzheimer and cardiovascular diseases [10]. PP2A has been shown to be genetically altered and functionally inactivated in many solid cancers and leukemias. Inhibition of PP2A activity is critical to promote cell transformation, tumor progression, and angiogenesis, which indicates that PP2A has a tumor suppressive role [11–13]. Recent reports show that pharmacological restoration of PP2A tumor-suppressor activity effectively antagonizes cancer development and progression.

Several partners of the PP2A have been identified, including the cysteine protease Caspase 9 [14]. Caspase 9 is the initiator of intrinsic apoptosis regulating physiological cell death and pathological tissue degeneration. Clinical reports suggest that alterations in Caspase 9 expression or activation can be involved in several diseases, including cancer [15].

We previously described the interaction between the Caspase 9 and PP2A and identified the binding peptide, also called interfering peptide, able to block this interaction [14]. This peptide (C9h) derived from Caspase 9 sequence, which includes residues involved in binding to PP2A, has been validated in vitro and shows an anti-tumoral effect in vivo on xenograft models of breast cancer [14].

In this manuscript, we analyze and compare the affinity of PP2A to its protein partner, Caspase 9 and to C9h, the interfering peptide from Caspase 9 sequence, as well as the molecular dynamics and peptide structure.

2. Materials and Methods

2.1. Peptide Synthesis and Sequence

The C9h peptide was synthesized in an automated multiple peptide synthesizer with solid-phase procedure and standard Fmoc chemistry by GL Biochem (Shanghai, China). The purity and composition of the peptide were confirmed by reverse phase high-performance liquid chromatography (HPLC) and by mass spectrometry (MS). The sequence of the peptide, isolated from Caspase 9 protein, is:

Y V E T L D D I F E Q W A H S E D L

2.2. Docking

To generate initial poses, we have used PEP-FOLD using the sOPEP2 force-field [16], taking as constraints positions generated from the amino acids of PP2A identified by PEPscan as being at the interface between catalytic subunits alpha of the PP2A (PP2Acα and Caspase 9) similarly to the protocol previously described [17]. One hundred models were generated and clustered using ligand RMSD as criterion. After the initial peptide generation, a Monte-Carlo refinement was performed using 30,000 steps at 350 K. Since previous studies have shown that PEPscan most overlapping fragments [18,19] usually better correspond to the binding interface, and to accelerate calculations as well as conformational sampling during simulations, only the central part of the peptide, corresponding to sequence LDDIFEQWAH, has been considered.

2.3. Molecular Dynamics (MD) Simulation

Structure preparation and protonation were conducted using the pdbfixer module of OpenMM package. The complexes were solvated in truncated octahedron boxes with a padding of 1.0 nm and the TIP3P water model, as the Amber14SB [20] forcefield was used to model the protein atoms; 6 and 11 sodium ions were added to counter the charge of the C9h in aqueous solvent and C9h-PP2A complex systems, respectively. Simulations were computed using the OpenMM 7.6 package [21]. Systems were minimized up to 1000 steps and equilibrated for 10 ns in NPT ensemble, and temperature and pressure were equilibrated using a Monte Carlo barostat at a temperature of 300 K and a 1 atmosphere pressure. We used a 4 fs integration time step using heavy hydrogen assigned a mass of 3 atomic mass units.

Simulations were performed using the OpenMM library, with the original OpenMM script for simulated tempering (ST) simulations [22] written by Peter Eastman, modified to implement the weight calculation of Park and Pande [23] and an on-the-fly weight calculation developed by Nguyen et al. [24]. During simulated tempering (ST) simulations, 21 and 32 temperature ladders were chosen spaced exponentially between 300 and 400 K, for C9h in aqueous solvent and C9h-PP2A complex systems, respectively. Temperature exchanges were attempted every 2 ps. During C9h-PP2A complex ST simulation, and to avoid high deformation of the protein during ST, position restraints were applied on the PP2A Cα atoms of 10.0 KJ/mol/nm^2, while the Caspase 9 fragment was free. However,

to prevent the peptide from moving too far away from the initial position, some weak distance restraints were applied on the peptide backbone atoms of 100.0 KJ/mol/nm^2, if the peptide backbone centroid moves more than 15 Å away from its initial position. Two PEPFOLD poses were simulated with ST during 4.4 and 4.6 µs. MD simulations analysis were conducted using the MDAnalysis python library [25]. For simulation in isolation, the complete C9h peptide was considered.

2.4. Circular Dichroism Analysis

Wild-type Caspase-9-derived synthetic peptide covering PP2Acα binding site (corresponding to residues 363–380) was synthesized. Circular dichroism was performed on a Jasco J-010 spectropolarimeter to study the presence of α-helix.

The peptide was dissolved in 10mM sodium phosphate pH 7.5 prepared from 10 mL solution A + 84 mL solution B in a final volume of 200 mL.

Solution A: 2.76 g NaH2PO4·3H2O. (0.0552 g/20 mL) (AppliChem, Darmstadt, Germany).

Solution B: 5.365 g Na2HPO4·7H2O. (0.5365 g/100 mL) (Sigma, Darmstardt, Germany).

Final pH of the mix was adjusted to 7.65.

To induce α-helix formation, a titration with trifluoroethanol (TFE) (Sigma) was performed. Samples were prepared with 50 µM of peptide dissolved in a final volume of 300 µL with increasing concentrations of TFE (20%, 40%, 60%, and 80% *v*/*v*). Samples were introduced in the spectropolarimeter in a Quartz Suprasil Precision cell 0.1 cm cuvette (Hellma), using 300 µL of buffer solution as blank. Measurements were repeated 10 times at 20 °C for each sample and 5 times for each blank. Data were processed with spectropolarimeter software to subtract blank from sample spectra and millidegrees units were further converted to molar ellipticity.

CD spectrum predictions from the MD simulations were performed using the PDBMD2CD [26] web server. Conversion from delta ellipticity (DE) to molar ellipticity (ME) was performed using the rule: ME = 3298 × DE.

2.5. Characterization of PP2A and C9h Peptide Interaction by ELISA

A total of 100 µL of biotinylated peptides diluted at 100 µM in PBS was incubated for 2 h at room temperature in a 96-well Streptavidine-coated plate (Pierce, Illkirch, Strasbourg, France). Wells were washed five times with PBS/0.05% Tween-20 (PBST) and filled with 100 µL of PP2A (Sigma) diluted in PBS/2.5% BSA (Sigma) at the indicated dilutions. The plate was incubated over night at 4 °C and washed five times with PBST. A total of 100 µL of rabbit polyclonal IgG anti-human PP2Aα (Santa Cruz Biotechnology, Heidelberg, Germany) was added at 5 µg/mL in PBS/BSA for 1 h at room temperature. Wells were washed 5 times with PBST and filled with 100 µL of HRP conjugated anti-rabbit IgG (Sigma) diluted at 1:20,000 in PBS/BSA for 1 h at room temperature. Wells were washed 5 times with PBST, and 100 µL of TMB substrate (Pierce) were added and incubated for 15–45 min. The reaction was stopped with 50 µL of 2 N sulphuric acid, and the absorbance was measured at 450 nm on a Multiskan EX plate reader (Thermo Scientific, Illkirch, Strasbourg, France). The Caspase 9 peptide C9h was labelled with biotin at the N-terminal and C-terminal end of the peptide.

2.6. Biolayer Interferometry and Kinetic Analysis

Kinetic analysis was performed based on biolayer interferometry (BLI) by using a BLItz instrument (ForteBio, Bayonne, France) at room temperature. Prior to use, each biosensor was hydrated in sample diluent (SD: PBS1X, pH 7.0, 0.02% Tween 20, 0.1% BSA) for at least 10 min. Kinetic measurements of PP2A/Caspase 9 interactions were run with Protein A biosensors (Fortebio) and consisted of seven steps, all performed in reaction buffer, as follows: (i) initial baseline in 300 µL SD for 30 s was measured; (ii) 4 µL of mouse anti-Caspase 9 or rabbit anti-PP2A were immobilized on the sensor for 150 s at

133 nM; (iii) the immunosensor was washed with 300 µL SD for 120 s; (iv) 4 µL of purified ligand Caspase 9 at 566 nM (Origen) or PP2A at 694 nM (LSBio) were loaded on the immunosensor for 150 s; (v) the ligand-coated immunosensor was washed with 300 µL SD for 120 s; (vi) association of purified analytes diluted in SD at the mentioned concentrations was studied for 150 s in 4 µL; and (vii) dissociation step was then monitored in 300 µL SD for 120 s.

Kinetic measurements of PP2A against biotinylated C9h-Cter peptide were run with Streptavidin biosensors (Fortebio, #18-5019). The initial step consisted of coating the biosensor with the peptide diluted in SD at 100 µM for 180 s in 4 µL (not shown) and was followed by three steps for the kinetic study: (i) initial baseline in 300 µL SD for 30 s was measured; (ii) association of PP2A at the indicated concentrations for 180 s in 4 µL was used; and (iii) dissociation step was then monitored in 300 µL SD for 150 s.

Experiments using empty immunosensors (no ligand loaded) were run as control. Sensorgrams were fit globally to a 1:1 binding model by BLItz Pro software, from which the association (kon) and dissociation (koff) rate constants and apparent affinities (KD) were calculated. X2 is the sum of squared deviations between the actual data point and the fitted curve. Values close to zero indicate a good curve fit. The R2 coefficient of determination is a statistical measure of how well the fitted curve approximate the real data points. Values of R2 near 1 indicate a near-perfect fit.

3. Results

3.1. Dynamic Behavior of C9h Using ST Simulations

We first present the results of ST simulations of C9h in aqueous solvent for a 9.5 microseconds simulation. As can be seen from Figure 1A, the energy landscape at 300 K is rather flat, the barriers between the different conformations being on the order of less than 3 to 4 kJ/mol. One also observes a large variability in the conformations of the representative conformations (depicted for each of the 11 clusters identified using k-mean clustering algorithm). Over all 300 K frames, the average helical content is of 36%. The most populated one (cluster 5–13%) shows propensity for helical conformations at the N- and C-terminus, whereas less populated ones (cluster 8–8% or cluster 6–7%) adopt alpha-helical conformations in the middle of C9h. Other ones (such as cluster 4–9%) adopt a largely unstructured conformation. Over all 300 K MD frames, as shown Figure 1B, the central part of the peptide shows the largest propensity to adopt helical conformations but for no more than 60% of the frames, meaning that coiled conformations occur at frequencies of more than 40% over all positions—no beta conformation being observed. It has to be noted that the force field used for the simulations (Amber14SB [20]) is not designed to simulate disordered peptides and may favor helical structures. Overall, our simulation suggests that C9h is rather flexible with a strong tendency toward helix.

3.2. Peptide Secondary Structure Evaluation by Circular Dichroism (CD)

The circular dichroism (CD) has been exploited for protein and peptide folding, conformational changes, intramolecular interactions, and ligand binding studies. We were interested in analyzing whether the interfering peptide (IP) C9h, a fragment of the human Caspase 9 involved in binding to the phosphatase PP2A, can maintain the secondary structure shown in the context of Caspase 9 protein. To this end, a CD analysis of the peptide was performed. Figure 2 shows that a concentration of 50 µM C9h peptide behaves as a random coil in 10 mM of sodium phosphate pH 7.5. In the presence of increasing amounts of trifluoroethanol (TFE), the structure pattern was progressively adopting a higher percentage of alpha helical structure as indicated by circular dichroism spectroscopy. The percentage of helix deduced from the CD spectra are of 2.62, 7.72, 21.58, 24.34, and 31.01% for TFE concentrations of 0, 20, 40, 60, and 80% *v*/*v*, respectively.

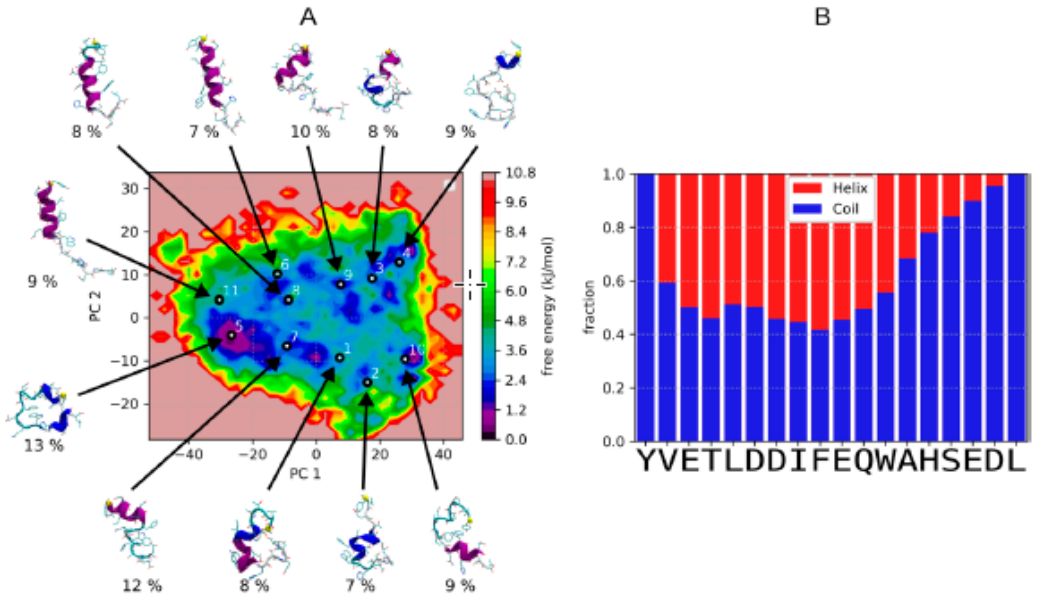

Figure 1. Structural landscape explored during ST simulations of C9h in aqueous solvent: (**A**) Free energy landscape at 300 K frames projected on principal component 1 (36% of variance) and 2 (10% of variance). Principal component analysis (PCA) applied to the 300 K frames ST simulation dataset of Caspase 9 peptide. Conformations representative of the clusters identified using k-means algorithm with k = 11 clusters (k has been chosen using the minimum silhouette score value for k values between 2 and 20) are depicted for each cluster together with the population of each cluster (%). (**B**) Analysis of the fraction of secondary structure adopted at each position of the peptide over all 300 K frames. Assignment of secondary structures was computed using DSSP [27].

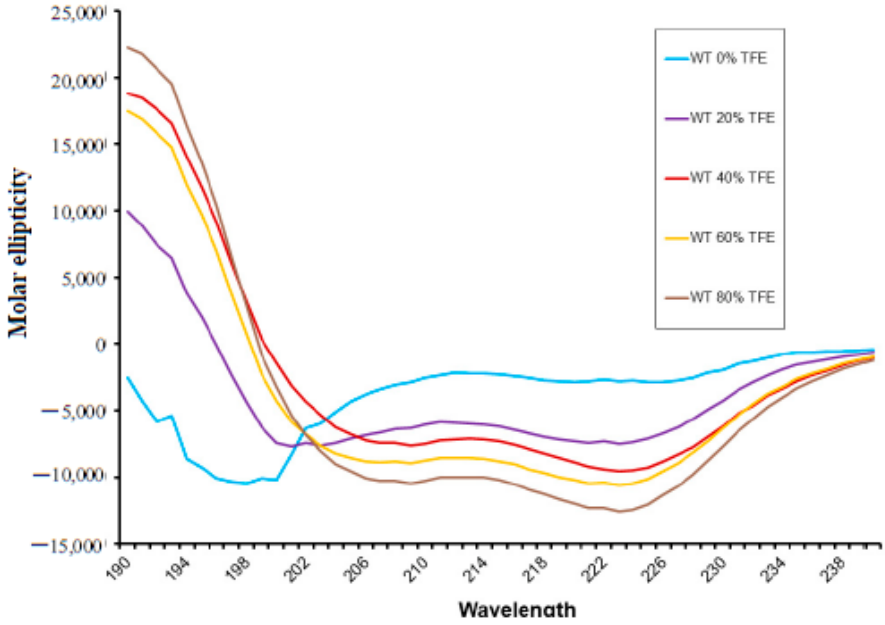

Figure 2. CD of C9h peptide. Data of molar ellipticity versus wavelength in circular dichroism (CD). Data obtained with peptide C9h in 10mM sodium phosphate pH 7.5 (Sky blue curve) are shown together with CD data using 20% (purple), 40% (red), 60% (orange), and 80% (brown) *v/v* of trifluoroethanol (TFE) in the same buffer. C9h shows a double CD signal at 208 and 222 nm proportional to increasing amounts of TFE indicating a-helix secondary structure content.

It is possible to compare the experimental spectrum with that inferred from the MD simulations (Figure 3A), although the correspondence between the experimental and predicted CD spectra must be taken with caution. For 208 nm, the average molar ellipticity

of the predicted CD spectrum value is to −15028, i.e., clearly showing a propensity toward helix.

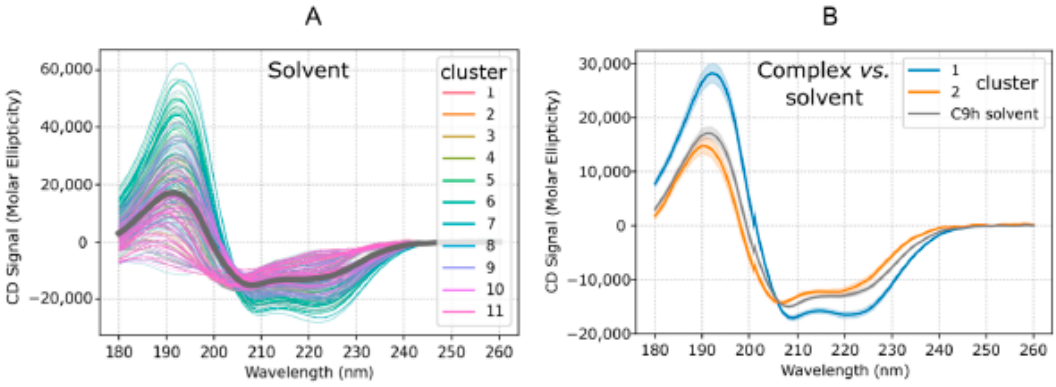

Figure 3. Predicted CD of C9h peptide. Data of molar ellipticity versus wavelength predicted from the MD simulation: (**A**) Spectra predicted for 702 frames periodically taken from the MD trajectory at 300 K (1 step out of 20). Color shades are attributed to the clusters as assigned in Figure 1A. The dark curve corresponds to the average over all conformations. (**B**) Average CD spectrum for C9h in solvent and simulations of C9h in interaction with PP2A starting from different positions. Clusters 1 and 2 correspond to the clusters described in Section 3.3.

3.3. Molecular Modeling of Peptide Interaction with PP2A

PEP-FOLD poses best target (i) the active site, (ii) a position between two helices at positions 26–40 and 141–151 of PP2Aca, and (iii) a position on top of the loop encompassing residues 175–193. The two latter positions in contact with the loop 175–193 have been simulated using simulated tempering for 4.39 and 4.58 µs, respectively.

To obtain a better sampling of peptide position during MD simulations, we used the simulated tempering method [22] starting from two different PEP-FOLD poses. During ST simulation, starting on top of the loop encompassing residues 175–193, the peptide structure moves rapidly after 300 ns and finds a stable position until the end of the simulation (for 4.2 µs). This position will be referred to as cluster 1 (Figure 4A). The RMSD of peptide backbone atoms at 300 K frames, relative to the central structure of the cluster 1 after 300 ns, was 3.3 ± 1.2 Å. The low RMSD denotes a stable position of the peptide. To be noted, the peptide was mainly structured in alpha helix, with the exception of the three last residues. Concerning ST simulation starting from a position between two helices at positions 26–40, the peptide position deviates slightly more, and a stable position could be identified between 1.4 and 3.8 µs (for 2.4 µs). This position will be referred as cluster 2 (Figure 4A). The RMSD of peptide backbone atoms at 300 K frames, relative to the central structure of the cluster 2 between 1.4 and 3.8 µs, was 4.3 ± 2.1 Å. The peptide was also mainly structured as an alpha helix, with the exception of the three first residues. The two ST simulations were aggregated and submitted to a PCA analysis (Figure 4B), and frames from both simulations were then clustered using the HDBSCAN algorithm. HDBSCAN identifies 11 clusters with 7.9% of frames not part of any cluster. The two main clusters were cluster 1 (35.46% of all frames) and cluster 2 (26.93%), as the third biggest cluster concerned only 8.4% of frames. For all clusters, the average structure of the peptide was computed, the closest frame to this average structure was considered as the cluster reference structure. Reference structures of clusters 1 and 2 are represented in Figure 4A. In summary, the simulations strongly suggest the existence of stable poses of the peptide, compatible with rather low affinity values. Both best poses are in the vicinity of the PP2A loop identified by PEPscan as interacting with Caspase 9. However, even using advanced sampling techniques, a unique binding site does not seem to emerge.

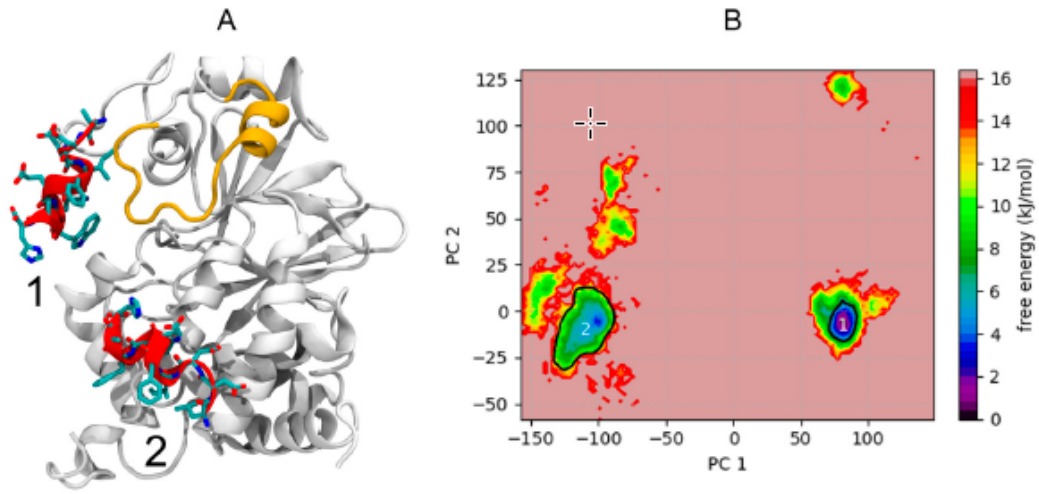

Figure 4. Structural landscape explored during ST simulations: (**A**) Central poses of clusters 1 and 2 are represented for the peptide as red cartoon and colored licorice, while the structure of PP2A is represented as white cartoon (only the structure of cluster 1 is represented for clarity), and the loop D172 to G190 is represented as an orange cartoon. (**B**) Free energy landscape projected on principal components 1 and 2. Principal component analysis (PCA) applied to the whole 300 K frames of ST MD simulation dataset of Caspase 9 peptide, after structural alignment on PP2A backbone atoms. Projection of first (88% of variance, *y*-axis) and second (6% of variance, *x*-axis) PCA modes computed on peptide backbone atoms. The white outline represents the contour of positions of clusters 1 and 2 frames.

Finally, it is also interesting to compare the behavior of the peptide in isolation and in interaction with PP2A. As shown Figure 3B, the CD spectra predicted for clusters 1 and 2 clearly show that for cluster 2 the spectrum is similar to that of C9h in the solvent whereas the helical signal is strengthened for cluster 1. This suggests that the cluster 1 pose might have a higher entropic cost upon binding to PP2A than the cluster 2 pose, despite it being the pose that contacts directly the PP2A loop identified by PEPscan. The possible impact on the binding affinities of the two poses remains, however, largely speculative at this point.

3.4. Qualitative Interaction between PP2A and the Biotinylated C9h Peptide

Biotinylation of peptides is an efficient method to specifically bind peptides to streptavidin-coated surfaces. Nevertheless, the positioning of the biotin tag in a peptide sequence can markedly influence binding interaction. In this regard, we tested whether the biotin label should be added on the N- or C-terminus of the C9h peptide. To this end, we tested by ELISA the binding of PP2A protein to the biotinylated C9h-Nter and C9h-Cter peptides, immobilized on streptavidin-coated plate. Figure 5 shows that the biotinylated peptides C9h-Cter and C9h-Nter peptides bind to the PP2A protein in a specific manner. However, the biotinylated C9h-Cter peptide shows stronger signal recognition than that of C9h-Nter. An irrelevant biotinylated peptide was used as a negative control. According to this result, we used for further experiments the biotinylated C9h-Cter peptide.

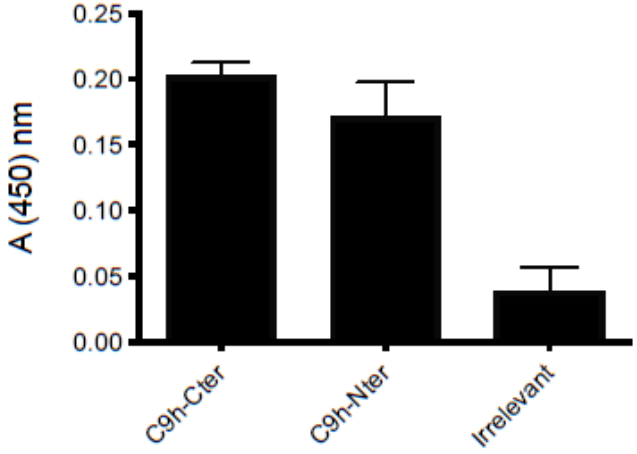

Figure 5. Detection of PP2A binding to C9h peptide by ELISA. Biotinylated C9h-Cter and C9h-Nter biotinylated peptides were immobilized on a Streptavidin-coated plate and incubated overnight with PP2A catalytic subunit at 0.6 µg/mL. After washing, rabbit anti-PP2A was added in each well and incubated 1 h at room temperature. Wells were washed and filled with a dilution of HRP-conjugated anti-Rabbit secondary antibody. Binding activity of PP2A is expressed as mean OD at 450 nm of duplicate wells, and bars indicate SD. These data are representative of two independent experiments.

3.5. Affinity of PP2A Protein to Caspase 9 Protein and C9h Peptide

Kinetic parameters of protein/protein (Caspase 9/PP2A or vice versa) or protein/peptide (PP2A/C9h) interaction were measured by biolayer interferometry (BLI). BLI is an optical characterization method used to monitor interactions between label-free molecules in real time. It is based on the wavelength shift reflecting the change in thickness of the biological layer caused by the binding of molecules to the probe. After ensuring the absence of unspecific binding of Caspase 9 and PP2A to the protein-A biosensor, specific antibodies for Caspase 9 and PP2A were immobilized onto the probes. After a washing step, Caspase 9 and PP2A were respectively loaded onto the probes to constitute the working biosensors of interest. First, the relative PP2A interaction to the immobilized Caspase 9 molecule was studied (Figure 6A). Affinity measurements were conducted with varying concentrations of PP2A to determine the range of equilibrium binding constant values ($KD = 8.94 \times 10^{-8}$ M). In a vice versa procedure, PP2A was immobilized onto the probe (Figure 6B) and different concentrations of Caspase 9 protein were used to determine the constant at equilibrium ($KD = 2.28 \times 10^{-7}$ M). Overall, in both models, PP2A and Caspase 9 proteins were observed to bind with relatively good affinity (close to 10^{-7} M). Figure 6C summarize the results of constants of association, dissociation, and affinity.

Kinetic measurements of PP2A against biotinylated C9h-Cter peptide were run by using streptavidin biosensors (Figure 6D). Different concentrations of PP2A protein were loaded onto the immobilized C9h-Cter peptide to determine the constant at equilibrium ($KD = 7.8 \times 10^{-7}$ M). Unspecific binding of PP2A to the sensor tip in absence of peptide was checked using PP2A at the same working concentrations. It is of note that the abrupt increase in signal looks like a bump artifact occurring when the streptavidin biosensor moves during the transition from the association to the dissociation step. In this conformation, the dissociation rate of PP2A was approximatively one log higher than those observed with the immobilized Caspase 9 protein resulting to a slightly lower affinity. Figure 6E summarize the values of constants of association, dissociation, and affinity.

In conclusion, these results demonstrate an effective interaction between PP2A and Caspase 9 proteins, as well as a good affinity between PP2A and the interfering peptide corresponding to the sequence of Caspase 9 involved in binding to PP2A. Therefore, C9h peptide can be used as a tool to manipulate this interaction.

A

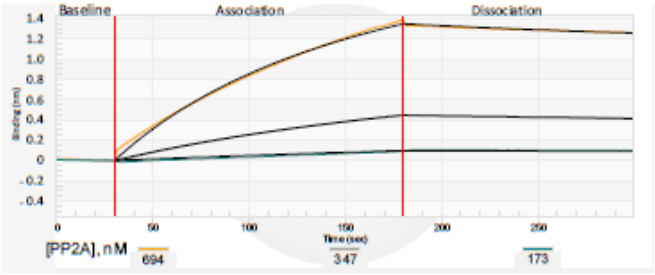

B

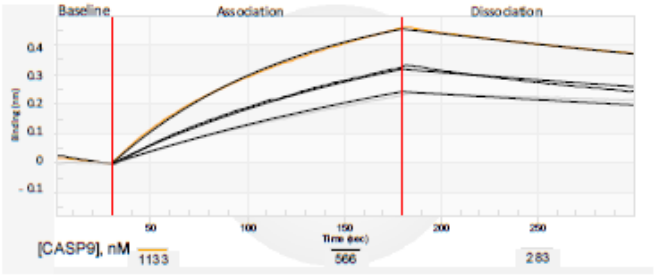

C

Ligand	Analyte	k_{on} (1/Ms)	k_{off} (1/s)	KD (M)	X^2	R^2
CASP9	PP2A	8.13×10^{3}	7.27×10^{-4}	8.94×10^{-8}	0.367	0.999
PP2A	CASP9	7.53×10^{3}	1.72×10^{-3}	2.28×10^{-7}	0.0934	0.997

D

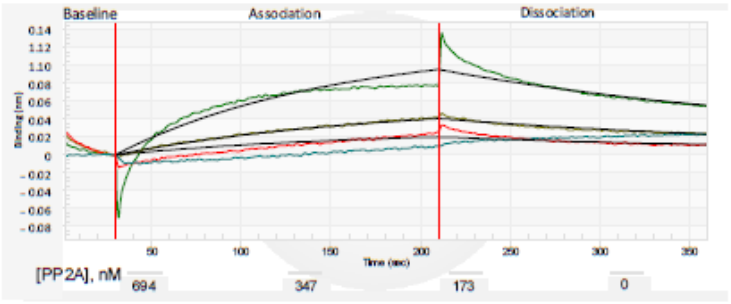

E

Ligand	Analyte	k_{on} (1/Ms)	k_{off} (1/s)	KD (M)	X^2	R^2
C9h- Cter	PP2A	1.13×10^{3}	8.7×10^{-3}	7.8×10^{-7}	0.1656	0.9091

Figure 6. Blitz sensorgrams of PP2A/Caspase 9 interaction. The biolayer interferometry (BLI) signal is given in relative intensity units (nm): (**A**) Caspase 9 ligand was immobilized at 566 nM onto a Protein A biosensor previously coated with a mouse anti-Caspase 9 monoclonal antibody. The association and dissociation steps of the PP2A analyte injected at concentrations of 649, 347, and 173 nM were shown. (**B**) PP2A ligand was immobilized at 694 nM onto a Protein A biosensor previously coated with a rabbit anti-PP2A polyclonal antibody. Association and dissociation of the Caspase 9 analyte loaded at 694, 347, and 173 nM were shown. (**C**) Binding rate constants and apparent affinities of PP2A/Caspase 9 interactions in BLI were calculated with BLItz Pro Software. (**D**) PP2A was used at 463, 556, and 694 nM as indicated, and sample diluent (PP2A, 0 nM) was designed as sample for reference subtraction. Unspecific binding of PP2A to the sensor tip in absence of peptide was checked using PP2A at the same concentrations. (**E**) Binding rate constants and affinities of C9h-Cter peptide and PP2A were calculated with BLItz Pro Software.

4. Discussion

In this study, we have first investigated the behavior of C9h in isolation, using both in silico and in vitro techniques. Circular dichroism (CD) spectroscopy is a widely used technique for the study of protein/peptide structure [28]. In the past decade, several algorithms based on quantitative analysis of CD spectroscopy have been proposed to

predict the secondary structure content [29,30]. In the absence of high-resolution structures, CD is regarded. The isolated C9h peptide does not seem to show its natural helical structure, which was, however, achieved easily in the presence of an alpha helical inductor, such as TFE. This result suggests that, despite being isolated from its natural environment within Caspase, C9h still has the ability to maintain its helical character, which may be important to exerting biological and biochemical actions. MD simulations suggest for their part a much stronger helical content although associated with a large conformational diversity. The direct comparison between the two approaches is, however, complex, because the impact of the force field used for simulations is not well quantified, and CD prediction from structure also comes with uncertainty. These predictions have, however, interest as a means to compare the conformation ensembles of the peptide in isolation or interacting with PP2A.

In a second part, we have turned to the interaction of the peptide with PP2A. Two poses compatible with low affinity values were identified. Compared to classical MD, the ST approach we have used has improved sampling ability, but no convergence of the two MD simulations starting from two different poses could be observed. Longer simulations might be needed to conclude more strongly on the putative peptide affinities, and in parallel, using higher maximum temperature during the ST simulations could also allow a better sampling of the peptide structure. It is also possible that the peptide might interact with different patches on PP2A surface. However, the conversion of the time they bind to a patch in terms of affinity remains presently out of reach. Of note, however, both poses identified are close to the PP2A loop identified, and none really explored the region of the catalytic site of PP2A. Interestingly, also in the two proposed poses, a helical conformation is observed in different regions of the sequence suggesting that the peptide could be rather flexible. Indeed, additional clusters identified during ST simulations show intermediary non-structured forms of the peptide, which is consistent with the results of the CD experiment and suggest that the peptide could adopt a helical conformation only when binding to PP2A.

Finally, we have measured the affinity of two interacting proteins, Caspase 9 and PP2A, as well as the interaction between PP2A and the interfering peptide C9h, which has been previously identified as Caspase 9 binding site to PP2A using PEPscan approach [14], This interfering peptide was used to measure the affinity for its partner, the PP2A protein, showing a similar affinity to that obtained using the whole protein Caspase 9. To our knowledge, this is the first affinity binding constant reported between PP2A and Caspase 9.

Biolayer interferometry approach has proven effective in measuring the binding affinity of different partners, such as protein/protein or protein/peptide molecules [31–33]. Studying the interaction between proteins and their ligand partners using conventional methods often requires large amounts of substrates and multistep experimental methods. These concerns prevent the easy and accurate quantification of the strength of an interaction [34,35]. BLI is an optical technique for real-time measurement of macromolecular interactions. The objective is achieved through the analysis of interference with the white light, reflected by the biosensor surface. In a typical BLI experiment, the ligand is immobilized on the biosensor tip and then allowed to interact with the analyte [36]. Using BLI, a quantitative set of equilibrium binding affinities (KD) and rate of association and dissociation (Kon, Koff) can be measured in minutes using nanomolar quantities of sample. Thereby, in this work, PP2A/Caspase 9 interaction studies were conducted in the range of 173 to 694 nM and 283 to 1133 nM for PP2A and Caspase 9 proteins, respectively. The results showed that the binding affinity of PP2A to Caspase 9 is in the range of 150 nM, which can be considered as a good affinity between two protein partners. Moreover, PP2A binds to the C9h peptide with a slightly lower affinity, around 800 nM, i.e., slightly worse, which might possibly be related to C9h helical structuration upon binding.

5. Conclusions

In conclusion, our work suggests that the interfering peptide C9h, isolated from its molecular environment into the Caspase 9 protein, remains able to associate with PP2A in a manner relatively comparable to that observed when using the whole Caspase 9 protein. This is the first time that the interaction affinity between two proteins involved in tumoral transformation, PP2A and Caspase 9, has been measured. Overall, these results may explain the efficacy observed in vitro and in vivo of the use of C9h peptide to block PP2A/Caspase 9 interaction. Finally, our result opens the possibility to the use of peptides as tools to manipulate protein/protein interaction and its use of therapeutic peptides, as it is the case for C9h peptide.

Author Contributions: K.D., S.M., J.B. and E.S. performed the experiments and provided samples. P.T. analyzed the data. A.R., P.T. and S.M. wrote, reviewed, and edited the manuscript. All authors have read and agreed to the published version of the manuscript.

Funding: This work was supported by Inserm. JB work was funded by the Spanish Ministry of Science and Innovation PID 2020-120243RB-100.

Institutional Review Board Statement: Not applicable.

Informed Consent Statement: Not applicable.

Conflicts of Interest: The authors declare no conflict of interest.

References

1. Bruzzoni-Giovanelli, H.; Alezra, V.; Wolff, N.; Dong, C.Z.; Tuffery, P.; Rebollo, A. Interfering peptides targeting protein-protein interactions: The next generation of drugs? *Drug Discov. Today* **2018**, *23*, 272–285. [CrossRef] [PubMed]
2. Dong, C.Z.; Bruzzoni-Giovanelli, H.; Yu, Y.; Dorgham, K.; Parizot, C.; Zini, J.M.; Brossas, J.Y.; Tuffery, P.; Rebollo, A. Identification of peptides interfering with the LRRK2/PP1 interaction. *PLoS ONE* **2020**, *15*, e0237110. [CrossRef] [PubMed]
3. Savier, E.; Simon-Gracia, L.; Charlotte, F.; Tuffery, P.; Teesalu, T.; Scatton, O.; Rebollo, A. Bi-Functional Peptides as a New Therapeutic Tool for Hepatocellular Carcinoma. *Pharmaceutics* **2021**, *13*, 1631. [CrossRef] [PubMed]
4. Savier, E.; Tuffery, P.; Bruzzoni-Giovanelli, H.; Rebollo, A. Isolation of Primary Hepatocytes for Testing Tumor Penetrating Peptides. *Methods Mol. Biol.* **2022**, *2383*, 413–427. [CrossRef]
5. Simon-Gracia, L.; Loisel, S.; Sidorenko, V.; Scodeller, P.; Parizot, C.; Savier, E.; Haute, T.; Teesalu, T.; Rebollo, A. Preclinical Validation of Tumor-Penetrating and Interfering Peptides against Chronic Lymphocytic Leukemia. *Mol. Pharm.* **2022**, *19*, 895–903. [CrossRef] [PubMed]
6. Wang, L.; Wang, N.; Zhang, W.; Cheng, X.; Yan, Z.; Shao, G.; Wang, X.; Wang, R.; Fu, C. Therapeutic peptides: Current applications and future directions. *Signal Transduct. Target. Ther.* **2022**, *7*, 48. [CrossRef]
7. Rafferty, J.; Nagaraj, H.; McCloskey, A.P.; Huwaitat, R.; Porter, S.; Albadr, A.; Laverty, G. Peptide Therapeutics and the Pharmaceutical Industry: Barriers Encountered Translating from the Laboratory to Patients. *Curr. Med. Chem.* **2016**, *23*, 4231–4259. [CrossRef]
8. Ayllon, V.; Martinez, A.C.; Garcia, A.; Cayla, X.; Rebollo, A. Protein phosphatase 1alpha is a Ras-activated Bad phosphatase that regulates interleukin-2 deprivation-induced apoptosis. *EMBO J.* **2000**, *19*, 2237–2246. [CrossRef]
9. Kang, H.S.; Choi, I. Protein phosphatase 2A modulates the proliferation of human multiple myeloma cells via regulation of the production of reactive oxygen intermediates and anti-apoptotic factors. *Cell Immunol.* **2001**, *213*, 34–44. [CrossRef]
10. Brautigan, D.L.; Farrington, C.; Narla, G. Targeting protein phosphatase PP2A for cancer therapy: Development of allosteric pharmaceutical agents. *Clin. Sci.* **2021**, *135*, 1545–1556. [CrossRef]
11. Chen, W.; Possemato, R.; Campbell, K.T.; Plattner, C.A.; Pallas, D.C.; Hahn, W.C. Identification of specific PP2A complexes involved in human cell transformation. *Cancer Cell* **2004**, *5*, 127–136. [CrossRef]
12. Janssens, V.; Goris, J.; Van Hoof, C. PP2A: The expected tumor suppressor. *Curr. Opin. Genet. Dev.* **2005**, *15*, 34–41. [CrossRef]
13. Perrotti, D.; Neviani, P. Protein phosphatase 2A: A target for anticancer therapy. *Lancet Oncol.* **2013**, *14*, e229–e238. [CrossRef]
14. Arrouss, I.; Nemati, F.; Roncal, F.; Wislez, M.; Dorgham, K.; Vallerand, D.; Rabbe, N.; Karboul, N.; Carlotti, F.; Bravo, J.; et al. Specific targeting of caspase-9/PP2A interaction as potential new anti-cancer therapy. *PLoS ONE* **2013**, *8*, e60816. [CrossRef]
15. Avrutsky, M.I.; Troy, C.M. Caspase-9: A Multimodal Therapeutic Target with Diverse Cellular Expression in Human Disease. *Front. Pharmacol.* **2021**, *12*, 701301. [CrossRef]
16. Binette, V.; Mousseau, N.; Tuffery, P. A Generalized Attraction-Repulsion Potential and Revisited Fragment Library Improves PEP-FOLD Peptide Structure Prediction. *J. Chem. Theory Comput.* **2022**, *18*, 2720–2736. [CrossRef]
17. Lamiable, A.; Thevenet, P.; Rey, J.; Vavrusa, M.; Derreumaux, P.; Tuffery, P. PEP-FOLD3: Faster de novo structure prediction for linear peptides in solution and in complex. *Nucleic Acids Res.* **2016**, *44*, W449–W454. [CrossRef]

18. Rebollo, A.; Fliedel, L.; Tuffery, P. PEPscan: A Broad Spectrum Approach for the Characterization of Protein-Binder Interactions? *Biomolecules* **2022**, *12*, 178. [CrossRef]
19. Rebollo, A.; Savier, E.; Tuffery, P. Pepscan Approach for the Identification of Protein-Protein Interfaces: Lessons from Experiment. *Biomolecules* **2021**, *11*, 772. [CrossRef]
20. Maier, J.A.; Martinez, C.; Kasavajhala, K.; Wickstrom, L.; Hauser, K.E.; Simmerling, C. ff14SB: Improving the Accuracy of Protein Side Chain and Backbone Parameters from ff99SB. *J. Chem. Theory Comput.* **2015**, *11*, 3696–3713. [CrossRef]
21. Eastman, P.; Swails, J.; Chodera, J.D.; McGibbon, R.T.; Zhao, Y.; Beauchamp, K.A.; Wang, L.P.; Simmonett, A.C.; Harrigan, M.P.; Stern, C.D.; et al. OpenMM 7: Rapid development of high performance algorithms for molecular dynamics. *PLoS Comput. Biol.* **2017**, *13*, e1005659. [CrossRef] [PubMed]
22. Marinari, E.; Parisi, G. Simulated tempering: A new Monte Carlo scheme. *Europhys. Lett.* **1992**, *19*, 451. [CrossRef]
23. Park, S.; Pande, V.S. Choosing weights for simulated tempering. *Phys. Rev. E Stat. Nonlin. Soft Matter Phys.* **2007**, *76*, 016703. [CrossRef] [PubMed]
24. Nguyen, P.H.; Okamoto, Y.; Derreumaux, P. Communication: Simulated tempering with fast on-the-fly weight determination. *J. Chem. Phys.* **2013**, *138*, 061102. [CrossRef]
25. Michaud-Agrawal, N.; Denning, E.J.; Woolf, T.B.; Beckstein, O. MDAnalysis: A toolkit for the analysis of molecular dynamics simulations. *J. Comput. Chem.* **2011**, *32*, 2319–2327. [CrossRef]
26. Drew, E.D.; Janes, R.W. PDBMD2CD: Providing predicted protein circular dichroism spectra from multiple molecular dynamics-generated protein structures. *Nucleic Acids Res.* **2020**, *48*, W17–W24. [CrossRef]
27. Kabsch, W.; Sander, C. Dictionary of protein secondary structure: Pattern recognition of hydrogen-bonded and geometrical features. *Biopolymers* **1983**, *22*, 2577–2637. [CrossRef]
28. Micsonai, A.; Wien, F.; Kernya, L.; Lee, Y.H.; Goto, Y.; Refregiers, M.; Kardos, J. Accurate secondary structure prediction and fold recognition for circular dichroism spectroscopy. *Proc. Natl. Acad. Sci. USA* **2015**, *112*, E3095–E3103. [CrossRef]
29. Greenfield, N.J. Using circular dichroism collected as a function of temperature to determine the thermodynamics of protein unfolding and binding interactions. *Nat. Protoc.* **2006**, *1*, 2527–2535. [CrossRef]
30. Woollett, B.; Whitmore, L.; Janes, R.W.; Wallace, B.A. ValiDichro: A website for validating and quality control of protein circular dichroism spectra. *Nucleic Acids Res.* **2013**, *41*, W417–W421. [CrossRef]
31. Ren, B.; Sayed, A.M.M.; Tan, H.L.; Mok, Y.K.; Chen, E.S. Identifying Protein Interactions with Histone Peptides Using Bio-layer Interferometry. *Bio. Protoc.* **2018**, *8*, e3012. [CrossRef] [PubMed]
32. Groner, M.; Ng, T.; Wang, W.; Udit, A.K. Bio-layer interferometry of a multivalent sulfated virus nanoparticle with heparin-like anticoagulant activity. *Anal. Bioanal. Chem.* **2015**, *407*, 5843–5847. [CrossRef]
33. Sieker, F.; May, A.; Zacharias, M. Predicting affinity and specificity of antigenic peptide binding to major histocompatibility class I molecules. *Curr. Protein Pept. Sci.* **2009**, *10*, 286–296. [CrossRef] [PubMed]
34. Berggard, T.; Linse, S.; James, P. Methods for the detection and analysis of protein-protein interactions. *Proteomics* **2007**, *7*, 2833–2842. [CrossRef] [PubMed]
35. Wierer, M.; Mann, M. Proteomics to study DNA-bound and chromatin-associated gene regulatory complexes. *Hum. Mol. Genet.* **2016**, *25*, R106–R114. [CrossRef]
36. Sultana, A.; Lee, J.E. Measuring protein-protein and protein-nucleic Acid interactions by biolayer interferometry. *Curr. Protoc. Protein Sci.* **2015**, *79*, 19.25.1–19.25.26. [CrossRef]

6 Discussion

Au terme de l'exposé de nos résultats, nous pouvons conclure :

1. Que les peptides bi-fonctionnels, c'est-à-dire un TTP et un IP, permettent d'administrer spécifiquement au sein de cellules tumorales (rôle du TPP) un agent interférant (rôle de l'IP) entre 2 protéines cibles et ce, pour des cellules humaines de LLC mais également de CHC,
2. Qu'il est possible de trouver simplement par PEPscan des candidats IP et donc de cibler une interaction protéique,
3. Que l'administration d'un IP spécifique de l'interaction PP2A/SET s'accompagne d'effets observables sur la survie dans un modèle de xénogreffe murin et que cet effet est en cohérence avec les nombreux travaux qui ont étudié la dérégulation de PP2A par SET dans les cellules cancéreuses,
4. Que l'effet biologique des peptides bi-fonctionnels est proportionnelle au nombre de récepteurs présents sur les cellules cibles. Ces récepteurs (integrin, p32, NRP-1) semblent anormalement exprimés d'autant plus que la cellule tumorale est dédifférenciée. Or les tumeurs dédifférenciées sont de moins bons pronostic en raison de leurs aptitudes métastatiques. Elles nécessitent non pas des traitements « locaux », comme les traitements chirurgicaux, mais des traitements systémiques. Cette observation est à mettre en parallèle avec le fait que les CHC sont associés à une hépathopathie qui limite la tolérance aux effets secondaires et donc les traitements systémiques.

Nous développerons dans les chapitres suivants, les perspectives des peptides en thérapeutique, les applications de leur spécificité, les perspectives expérimentales puis cliniques dans le CHC.

6.1 Perspectives des peptides en thérapeutique

Les perspectives que les peptides thérapeutiques ouvrent progressivement sont proprement fascinante. Historiquement, le premier peptide thérapeutique utilisé est l'insuline (1922) (Muttenthaler *et al*, 2021). Depuis des hormones peptidiques ont enrichi l'arsenal

thérapeutique ainsi que l'illustre la Figure 14. Deux éléments sont à souligner dans le développement des peptides thérapeutiques et qui sont premièrement l'apparition des techniques de recombinaison, ce qui a permis de synthétiser la somatostatine en 1982, premier peptide humain produit avec cette technologie (Muttenthaler *et al*, 2021) et deuxièmement les techniques de screening : phages display (Smith, 1985), levures displays, ribosome display et mRNA display.

Figure 14: Chronologie historique et étapes clés dans le développement des peptides thérapeutiques

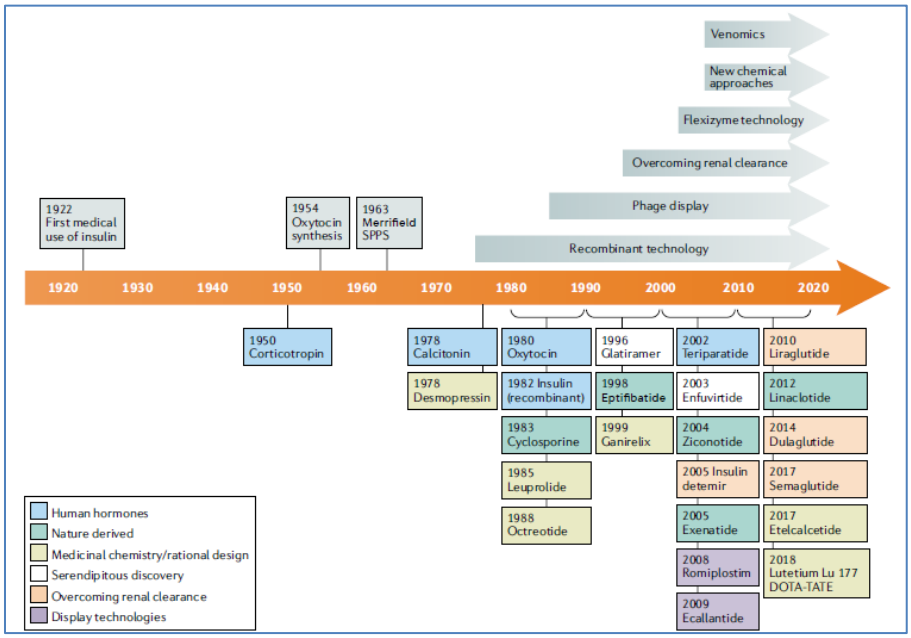

Le premier médicament peptidique était l'insuline, extraite du pancréas bovin et porcin. Les polypeptides ont été synthétisés chimiquement pour la première fois en 1954, lorsque le groupe de Vincent du Vigneaud a publié la synthèse totale de l'ocytocine et de la vasopressine. Un autre bond en avant a été l'idée visionnaire de Bruce Merrifield d'automatiser la synthèse peptidique en assemblant des acides aminés sur une phase solide, conduisant à l'invention en 1963 de la synthèse peptidique en phase solide (SPPS). L'avènement de la technologie recombinante dans les années 1980 a permis une production propre de peptides plus gros. Par la suite, des stratégies visant à augmenter le poids moléculaire des peptides par conjugaison à des lipides, des protéines plus grosses et du polyéthylène glycol ont permis de surmonter le problème de la clairance rénale et d'augmenter les temps de circulation plasmatique. Les technologies d'affichage par bactériophages (phage display) permettent désormais la découverte ciblée de peptides avec des propriétés plus similaires à celles des médicaments à partir de vastes bibliothèques. La technologie Flexizyme permet l'incorporation d'acides aminés non protéinogènes dans des bibliothèques d'affichage (display libraries). La découverte de peptides naturels, en particulier de peptides de venins et de nouvelles approches chimiques font également progresser le domaine. D'après Muttenthaler et al*, 2021.*

Dans les pays développés, les cancers sont la première cause de mortalité (Sung *et al*, 2021). L'incidence dans ces pays devrait encore augmenter en raison de l'âge des populations qui progresse et de l'importance des facteurs de risque (Vogelstein *et al*, 2013). L'exploration

des peptides pour lutter contre les cancers a-t-elle un intérêt ? Nous pouvons tirer de notre expérience que les peptides ont des applications dans tous les domaines de la cancérologie : thérapeutiques (Résultats: 5.1, 5.5), mais également diagnostique (Résultat : 5.5), pronostique (Résultats: 5.4), pharmacologique (Résultats: 5.3, 5.6).

Certains pourraient faire remarquer que les recherches dans le domaine des peptides thérapeutiques, depuis 20 ans, se limitent pour l'essentiel à des résultats *in vitro* voire *in silico*, à des modèles cellulaires ou murins. Il existe de nombreux peptides thérapeutiques approuvés ou en cours de développement, dont des listes indicatives sont reportée en annexe (Annexe 4, Annexe 5). Cependant, parmi 36 peptides approuvés depuis 2000, 5 (14%) s'appliquent aux cancers en général (Annexe 4) (Wang *et al*, 2022). Parmi ceux en cours de développement clinique, 7 (20%) se rapportent à la cancérologie (Annexe 5) (Wang *et al*, 2022). Il est donc possible que des effets complexes ou inattendus rendent les progrès plus difficiles en cancérologie par rapport à l'endocrinologie.

A titre d'illustration nous avons vu que les TPP utilisaient le récepteur NRP-1 pour s'internaliser dans les cellules tumorales (Résultats : 5.1 à 5.5). Or, NRP est une famille de récepteurs trans-membranaires qui interviennent dans de très nombreuses régulations (Figure 15). L'importance des NRP dans l'angiogenèse et le guidage axonal est fermement établie. NRP1 joue un rôle majeur dans les migrations cellulaires tandis que NRP2, joue un rôle important pour les vaisseaux lymphatiques. NRP1 est surexprimé dans beaucoup de lignées cellulaires cancéreuses et est impliqué dans la migration, la prolifération et la survie. NRP1 est surexprimé sur les cellules tumorales mais également sur les cellules stromales (Bagri *et al*, 2009; Pellet-Many *et al*, 2008). NRP1 est une cible des thérapies anti-cancéreuses avec des anticorps et des peptides thérapeutiques (Hong *et al*, 2007; Jia *et al*, 2006; Karjalainen *et al*, 2011; Liang *et al*, 2007; Nasarre *et al*, 2010).

NRP1 agit comme co-recepteur avec de nombreux ligands extracellulaires comme les isoformes du vascular endothelial growth factor (VEGF), les semaphorins de class 3, l'hepatic growth factor (HGF), fibroblast growth factor (FGF) et transforming growth factor-β (TGF-β). L'interaction la plus étudiée est celle qui se fait avec le VEGFR 1/2 et la VEGF165. Ce complexe stimule l'angiogénèse tumorale, les invasions cellulaires et les métastases. Le complexe VEGF165-VEGFR2-NRP1 joue également un rôle dans le développement des

vaisseaux lymphatiques. De plus la voie d'activation médiée par le VEGF, les facteurs de croissance tels que FGF, HGF, TGF-β et leur récepteur peuvent interagir avec le NRP1 sur les cellules tumorales et péritumorales (cellules immunitaires, cellules endothéliales et fibroblastes) pour augmenter l'agressivité tumorale (Banerjee *et al*, 2006; Elahouel *et al*, 2015; Glinka & Prud'homme, 2008; West *et al*, 2005). Nous avons observé que site d'interaction entre NRP-1 et les TPP était proche de celui du VEGF (Résultats: 5.2) (Figure 15). On peut donc se demander si les TPP en activant le récepteur NRP1 ne favoriseraient pas le mécanisme métastatique. C'est l'inverse qui a été observé dans un modèle de métastases spontanée, où les souris traitées par les TPP iRGD ou cNGR avaient une réduction significative de leur métastases (Sugahara *et al*, 2015a).

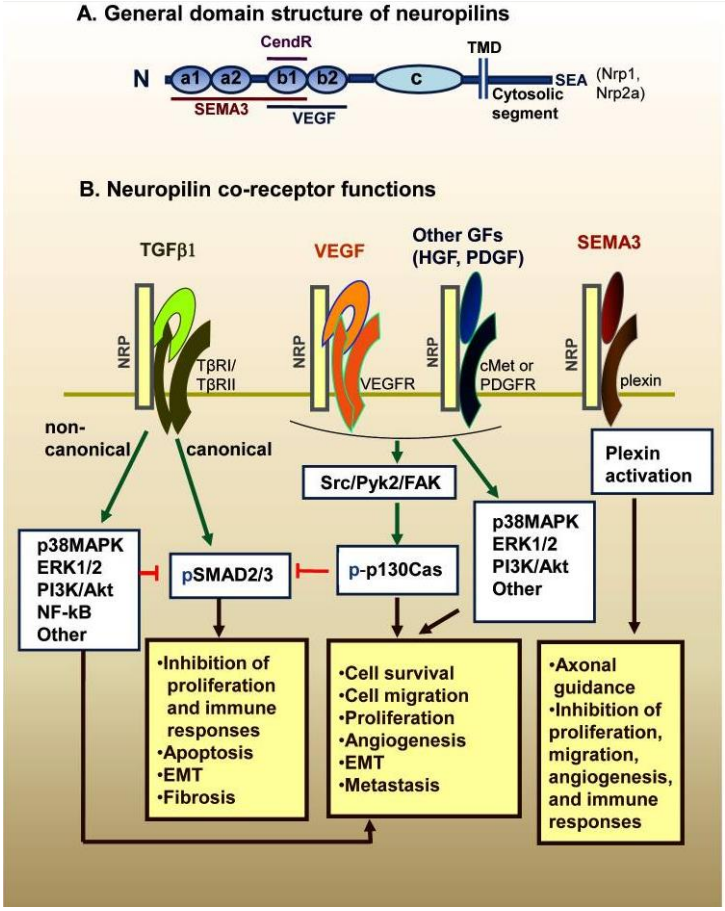

Figure 15: Structure de la neuropiline (NRP) et modèle hypothétique d'interaction avec de multiples facteurs de croissance.

De nombreuses combinaisons récepteur/corécepteur sont possibles, ce qui peut déclencher un grand nombre de réponses cellulaires dans le système vasculaire tumoral et le microenvironnement tumoral D'après Prud'homme & Glinka, 2012 et Niland & Eble, 2019.

Au total, agir sur des tumeurs solides avec des peptides thérapeutiques est probablement une voie d'avenir. Agir sur des récepteurs complexes comme le NRP peut déclencher des interactions imprévues. Les tumeurs malignes solides sont des ensembles cellulaires non moins complexes fait de cellules tumorales et de cellules péritumorales qui participent au développement tumoral et réduisent sa reconnaissance par le système immunitaire. Des modèles *in-vivo* qui reproduisent ces conditions sont donc indispensable pour avancer. Ce point sera développé dans le paragraphe suivant.

6.2 Spécificité en thérapeutique

Nous avons observé qu'un IP pouvait induire une apoptose chez des cellules saines, certes faible mais surtout observable lorsque l'IP était porté par un CPP (non-spécifique) (Résultats: 5.1). D'un autre côté, les TPP s'internalisent dans les cellules *via* le récepteur NRP-1. Les récepteurs NRP sont largement exprimés sur les tissus normaux, mais surexprimés sur les tissus tumoraux. Cette surexpression offre donc un moyen d'être plus spécifique sur les cellules tumorales (Résultats: 5.4).

Sur un plan pharmacologique, la spécificité anti-tumorale permet de réduire les doses administrées et de réduire les effets secondaires. Sur un plan clinique la spécificité améliore l'efficacité et diminue les effets indésirables. A ce jour, nous n'avons pas connaissance de résultats cliniques qui démontrent cette spécificité thérapeutique en terme d'effets indésirables. En revanche, la spécificité des TPP pour les cellules tumorales peut s'appliquer à la détection tumorale à un stade très précoce : détection de tumeurs oesophagienne (Fang *et al*, 2022) ou urinaire (Zhang *et al*, 2020). C'est le domaine d'application clinique qui semble le plus développé, actuellement.

En ce qui concerne le CHC, la possibilité d'une spécificité du traitement permettrait d'éviter la cardiotoxicité cumulative de la doxorubicine (Alberici *et al*, 2013) et pourrait permettre d'améliorer l'accès aux TKI des patients cirrhotiques (Rosmorduc *et al*, 2010). La récidive d'un CHC chez un patient transplanté pour CHC pose des difficultés thérapeutiques certaines : d'une part, les TKI sont mal tolérées et les effets secondaires sont difficilement gérables, d'autre part, les immunothérapies comme les ICI peuvent déclencher des rejets persistants et incontrôlables qui aboutissent à la perte du greffon (Jin *et al*, 2022; Larrey *et al*, 2022; Yin *et al*, 2022).

6.3 Développement expérimental

De ce qui précède, il ressort qu'une utilisation des peptides bi-fonctionnels pour traiter des CHC est une perspective intéressante mais qu'il persiste trop d'inconnues pour l'envisager sans une phase préclinique. Pour ce faire nous prévoyons d'utiliser un modèle de xénotransplantation (Figure 16) de CHC sur des souris immunodéprimées. L'avantage de ce modèle est de pouvoir utiliser les lignées cellulaires humaines (HepG2). L'inconvénient est de méconnaitre le rôle de l'environnement péri-tumoral et immunitaire. Une fois le modèle validé avec des lignées cellulaires connues (Scatton *et al*, 2006, 2008), l'implantation de cellules de CHC de patients pourrait être réalisée afin de tester différent protocole de traitement systémique. Cet aspect sera développé dans le paragraphe suivant.

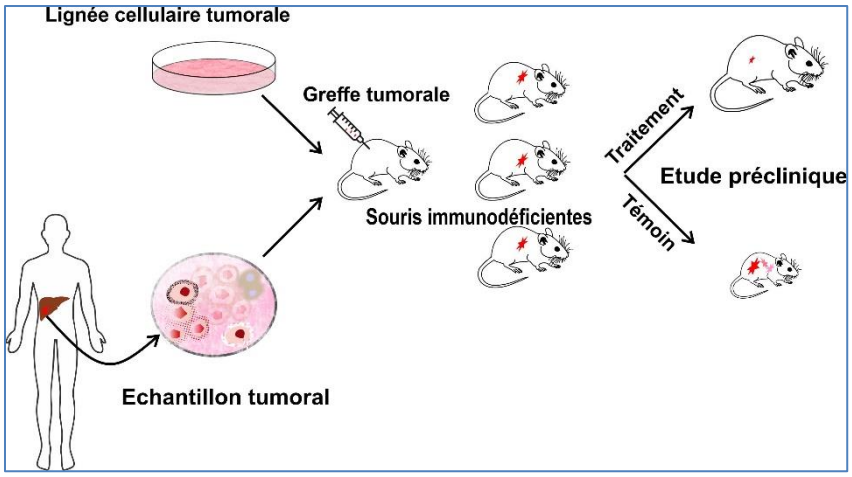

Figure 16: représentation schématique d'un modèle de xénotransplantation (PDX).

Des souris immunodéficientes sont greffées avec une lignée cellulaire tumorale ou du tissu tumoral humain. Ce modèle permet de tester différents protocoles thérapeutiques dans un but préclinique.

6.4 Perspectives Clinique

Dosages PP2A et SET dans des CHC réséqués

Nous avons vu que les TPP-IP pouvaient bloquer l'interaction PP2A/SET et cet effet permettait de supposer que l'apoptose observée était secondaire au rétablissement de l'activité de PP2A. Cibler cette voie métabolique est-elle pertinente dans le CHC ? Nous n'avons trouvé qu'une seule publication qui rapportait à partir d'échantillons de 147 CHC, une surexpression de SET dans 31 % et était un facteur pronostique défavorable (Hung *et al*, 2016). Une application pratique de notre travail serait de doser PP2A et SET dans les CHC réséqués afin de vérifier s'il s'agit d'un facteur pronostic, et, de manière plus ambitieuse, si

cette information pourrait aider à instituer un traitement préventif de récidive par des peptides bi-fonctionnels.

Combinaison de traitement

Dans les cellules cancéreuses, les cascades de signalisation sont souvent activées par un oncogène. Sur cette base une thérapie qui inhibe ces voies de signalisations peut être établie (Torti & Trusolino, 2011). Malheureusement, ces thérapies ciblées perdent généralement leur efficacité par des mécanismes adaptatifs des cellules cancéreuses, par exemple par une régulation positive des cascades de signaux parallèles qui favorisent la survie et la prolifération des cellules tumorales (Fallahi-Sichani *et al*, 2017). Par exemple, les cellules tumorales augmentent l'expression et l'activité des récepteurs de tyrosine kinase, tels que l'EGFR, le MET et le FGFR, par des cytokines et des facteurs de croissance dans le microenvironnement tumoral pour échapper à la thérapie tumorale (Wilson *et al*, 2012).

Pour s'opposer à ces mécanismes de résistance, une stratégie est d'utiliser des traitements combinés, par exemple un inhibiteur des kinase et un activateur des phosphatases (Chen *et al*, 2010; Galiger *et al*, 2022; Richard *et al*, 2016). Le mécanisme d'action est représenté dans la Figure 17. Enfin, pour aller encore un peu plus loin dans le CHC, une trithérapie associant TKI, ICI et peptides bi-fonctionnels pourrait etre envisagée.

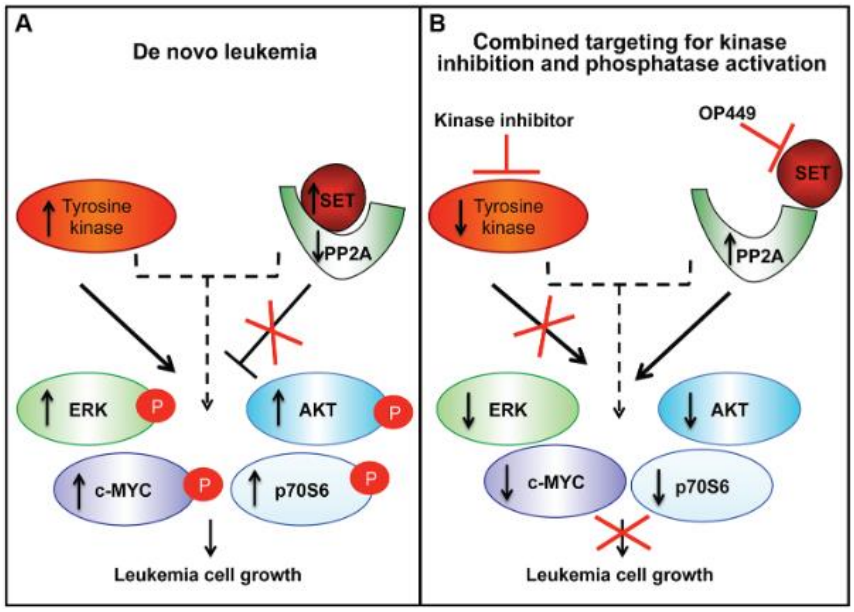

Figure 17: Représentation schématique de la combinaison réactivation de PP2A via l'antagonisme de SET et de l'inhibition de la tyrosine kinase. (A) SET est surexprimé dans les cellules leucémiques, ce qui entraîne une diminution de l'activité de la phosphatase PP2A et une perte de désactivation des kinases en aval. Les cellules leucémiques ont une activité tyrosine kinase accrue qui favorise la signalisation en aval. (B) Le ciblage combiné de SET et des kinases activées conduit à une inhibition plus prononcée de la croissance des cellules leucémiques de la lignée T-ALL. D'après(Richard et al*, 2016).*

Pour conclure, la possibilité d'utiliser des peptides bi-fonctionnels dans les CHC, comme moyen thérapeutique est une perspective concrète et réalisable dans les années à venir. Cette technologie ne doit pas se limiter aux traitements mais également au diagnostic et au pronostic. Elle devra s'intégrer dans la vision présente d'une future médecine, prédictive avec des traitements ciblée (Nault *et al*, 2018; Campani *et al*, 2023).

7 References

Adachi Y, Pavlakis GN & Copeland TD (1994) Identification and characterization of SET, a nuclear phosphoprotein encoded by the translocation break point in acute undifferentiated leukemia. *J Biol Chem* 269: 2258–2262

Adler S, Frank R, Lanzavecchia A & Weiss S (1994) T cell epitope analysis with peptides simultaneously synthesized on cellulose membranes: fine mapping of two DQ dependent epitopes. *FEBS Lett* 352: 167–170

Alberici L, Roth L, Sugahara KN, Agemy L, Kotamraju VR, Teesalu T, Bordignon C, Traversari C, Rizzardi G-P & Ruoslahti E (2013) *De Novo* Design of a Tumor-Penetrating Peptide. *Cancer Res* 73: 804–812

Alberts AS, Thorburn AM, Shenolikar S, Mumby MC & Feramisco JR (1993) Regulation of cell cycle progression and nuclear affinity of the retinoblastoma protein by protein phosphatases. *Proc Natl Acad Sci U S A* 90: 388–392

Andrini L, Marin GH, Inda AM, Bruzzoni-Giovanelli H, Garcia M, Errecalde J & Rebollo A (2020) Anti-tumoral Effect of a Cell Penetrating and Interfering Peptide Targeting PP2A/SET Interaction. *Folia Med (Plovdiv)* 62: 31–36

Arif M, Wei J, Zhang Q, Liu F, Basurto-Islas G, Grundke-Iqbal I & Iqbal K (2014) Cytoplasmic retention of protein phosphatase 2A inhibitor 2 (I2PP2A) induces Alzheimer-like abnormal hyperphosphorylation of Tau. *J Biol Chem* 289: 27677–27691

Arriazu E, Vicente C, Pippa R, Peris I, Martínez-Balsalobre E, García-Ramírez P, Marcotegui N, Igea A, Alignani D, Rifón J, *et al* (2020) A new regulatory mechanism of protein phosphatase 2A activity via SET in acute myeloid leukemia. *Blood Cancer J* 10: 3

Arrouss I, Nemati F, Roncal F, Wislez M, Dorgham K, Vallerand D, Rabbe N, Karboul N, Carlotti F, Bravo J, *et al* (2013) Specific Targeting of Caspase-9/PP2A Interaction as Potential New Anti-Cancer Therapy. *PLoS ONE* 8: e60816

Askoxylakis V, Zitzmann S, Mier W, Graham K, Krämer S, von Wegner F, Fink RHA, Schwab M, Eisenhut M & Haberkorn U (2005) Preclinical evaluation of the breast cancer cell-binding peptide, p160. *Clin Cancer Res Off J Am Assoc Cancer Res* 11: 6705–6712

Ayllón V, Martínez-A C, García A, Cayla X & Rebollo A (2000) Protein phosphatase 1α is a Ras-activated Bad phosphatase that regulates interleukin-2 deprivation-induced apoptosis. *EMBO J* 19: 2237–2246

Bagri A, Tessier-Lavigne M & Watts RJ (2009) Neuropilins in Tumor Biology. *Clin Cancer Res* 15: 1860–1864

Baharians Z & Schonthal AH (1998) Autoregulation of protein phosphatase type 2A expression. *JBiolChem* 273: 19019–19024

Banerjee S, Sengupta K, Dhar K, Mehta S, D'Amore PA, Dhar G & Banerjee SK (2006) Breast cancer cells secreted platelet-derived growth factor-induced motility of vascular smooth muscle cells is mediated through neuropilin-1. *Mol Carcinog* 45: 871–880

Bayarkhangai B, Noureldin S, Yu L, Zhao N, Gu Y, Xu H & Guo C (2018) A comprehensive and perspective view of oncoprotein SET in cancer. *Cancer Med* 7: 3084–3094

Bergna C, Marin GH, Maiz M, Bruzzoni Giovanelli H, Ponzinibbio C, Schinella G, Errecalde J & Rebollo A (2019) New forms of induction of apoptosis in aggressive lymphoma using peptides that interrupt the RAS / RAF interaction. *Ceylon Med J* 64: 46–51

Bidwell GL & Raucher D (2009) Therapeutic peptides for cancer therapy. Part I – peptide inhibitors of signal transduction cascades. *Expert Opin Drug Deliv* 6: 1033–1047

Binet JL, Auquier A, Dighiero G, Chastang C, Piguet H, Goasguen J, Vaugier G, Potron G, Colona P, Oberling F, *et al* (1981) A new prognostic classification of chronic lymphocytic leukemia derived from a multivariate survival analysis. *Cancer* 48: 198–206

Blanc JF, Debaillon-Vesque A, Roth G, Barbare JC, Baumann AS, Boige V, Boudjema K, Bouattour M, Crehange G, Dauvois B, *et al* (2021) Hepatocellular carcinoma: French Intergroup Clinical Practice Guidelines for diagnosis, treatment and follow-up (SNFGE, FFCD, GERCOR, UNICANCER, SFCD, SFED, SFRO, AFEF, SIAD, SFR/FRI). *Clin Res Hepatol Gastroenterol* 45: 101590

Braun GB, Sugahara KN, Yu OM, Kotamraju VR, Molder T, Lowy AM, Ruoslahti E & Teesalu T (2016) Urokinase-controlled tumor penetrating peptide. *J Control Release* 232: 188–95

Brautigan DL, Farrington C & Narla G (2021) Targeting protein phosphatase PP2A for cancer therapy: development of allosteric pharmaceutical agents. *Clin Sci* 135: 1545–1556

Bravi F, Bosetti C, Tavani A, Gallus S & La Vecchia C (2013) Coffee reduces risk for hepatocellular carcinoma: an updated meta-analysis. *Clin Gastroenterol Hepatol Off Clin Pract J Am Gastroenterol Assoc* 11: 1413-1421.e1

Bray F, Ferlay J, Soerjomataram I, Siegel RL, Torre LA & Jemal A (2018) Global cancer statistics 2018: GLOBOCAN estimates of incidence and mortality worldwide for 36 cancers in 185 countries. *CA Cancer J Clin* 68: 394–424

Bruix J, Sherman M, & Practice Guidelines Committee, American Association for the Study of Liver Diseases (2005) Management of hepatocellular carcinoma. *Hepatol Baltim Md* 42: 1208–1236

Bruzzoni-Giovanelli H, Alezra V, Wolff N, Dong CZ, Tuffery P & Rebollo A (2018) Interfering peptides targeting protein-protein interactions: the next generation of drugs? *Drug Discov Today* 23: 272–285

Cadier B, Bulsei J, Nahon P, Seror O, Laurent A, Rosa I, Layese R, Costentin C, Cagnot C, Durand-Zaleski I, *et al* (2017) Early detection and curative treatment of hepatocellular carcinoma: A cost-effectiveness analysis in France and in the United States. *Hepatol Baltim Md* 65: 1237–1248

Calin GA, di Iasio MG, Caprini E, Vorechovsky I, Natali PG, Sozzi G, Croce CM, Barbanti-Brodano G, Russo G & Negrini M (2000) Low frequency of alterations of the alpha (PPP2R1A) and beta (PPP2R1B) isoforms of the subunit A of the serine-threonine phosphatase 2A in human neoplasms. *Oncogene* 19: 1191–1195

Campani C, Zucman-Rossi J & Nault J-C (2023) Genetics of Hepatocellular Carcinoma: From Tumor to Circulating DNA. *Cancers* 15: 817

Campbell KS, Auger KR, Hemmings BA, Roberts TM & Pallas DC (1995) Identification of regions in polyomavirus middle T and small t antigens important for association with protein phosphatase 2A. *JVirol* 69: 3721–3728

Carlson SG, Eng E, Kim EG, Perlman EJ, Copeland TD & Ballermann BJ (1998) Expression of SET, an inhibitor of protein phosphatase 2A, in renal development and Wilms' tumor. *J Am Soc Nephrol JASN* 9: 1873–1880

Chen K-F, Yu H-C, Liu T-H, Lee S-S, Chen P-J & Cheng A-L (2010) Synergistic interactions between sorafenib and bortezomib in hepatocellular carcinoma involve PP2A-dependent Akt inactivation. *J Hepatol* 52: 88–95

Chen W, Arroyo JD, Timmons JC, Possemato R & Hahn WC (2005) Cancer-associated PP2A Aalpha subunits induce functional haploinsufficiency and tumorigenicity. *Cancer Res* 65: 8183–8192

Chen W, Possemato R, Campbell KT, Plattner CA, Pallas DC & Hahn WC (2004) Identification of specific PP2A complexes involved in human cell transformation. *Cancer Cell* 5: 127–136

Christensen DJ, Chen Y, Oddo J, Matta KM, Neil J, Davis ED, Volkheimer AD, Lanasa MC, Friedman DR, Goodman BK, *et al* (2011a) SET oncoprotein overexpression in B-cell chronic lymphocytic leukemia and non-Hodgkin lymphoma: a predictor of aggressive disease and a new treatment target. *Blood* 118: 4150–4158

Christensen DJ, Ohkubo N, Oddo J, Van Kanegan MJ, Neil J, Li F, Colton CA & Vitek MP (2011b) Apolipoprotein E and Peptide Mimetics Modulate Inflammation by Binding the SET Protein and Activating Protein Phosphatase 2A. *J Immunol* 186: 2535–2542

Cohen JA, Barkhof F, Comi G, Hartung H-P, Khatri BO, Montalban X, Pelletier J, Capra R, Gallo P, Izquierdo G, *et al* (2010) Oral fingolimod or intramuscular interferon for relapsing multiple sclerosis. *N Engl J Med* 362: 402–415

Cohen PT (1997) Novel protein serine/threonine phosphatases: variety is the spice of life. *Trends Biochem* 22: 245–251

Colella S, Ohgaki H, Ruediger R, Yang F, Nakamura M, Fujisawa H, Kleihues P & Walter G (2001) Reduced expression of the Aalpha subunit of protein phosphatase 2A in human gliomas in the absence of mutations in the Aalpha and Abeta subunit genes. *IntJCancer* 93: 798–804

Costentin CE, Layese R, Bourcier V, Cagnot C, Marcellin P, Guyader D, Pol S, Larrey D, De Lédinghen V, Ouzan D, *et al* (2018) Compliance With Hepatocellular Carcinoma Surveillance Guidelines Associated With Increased Lead-Time Adjusted Survival of Patients With Compensated Viral Cirrhosis: A Multi-Center Cohort Study. *Gastroenterology* 155: 431-442.e10

Costentin CE & Nahon P (2021) HCC risk prediction using biomarkers in non-cirrhotic patients following HCV eradication: Reassuring the patient or the doctor? *JHEP Rep* 3: 100320

Cristobal I, Garcia-Orti L, Cirauqui C, Cortes-Lavaud X, Garcia-Sanchez MA, Calasanz MJ & Odero MD (2012) Overexpression of SET is a recurrent event associated with poor outcome and contributes to protein phosphatase 2A inhibition in acute myeloid leukemia. *Haematologica* 97: 543–50

Cristóbal I, Manso R, Rincón R, Caramés C, Senin C, Borrero A, Martínez-Useros J, Rodriguez M, Zazo S, Aguilera O, *et al* (2014) PP2A inhibition is a common event in colorectal cancer and its restoration using FTY720 shows promising therapeutic potential. *Mol Cancer Ther* 13: 938–947

Cristóbal I, Rincón R, Manso R, Caramés C, Zazo S, Madoz-Gúrpide J, Rojo F & García-Foncillas J (2015) Deregulation of the PP2A inhibitor SET shows promising therapeutic implications and determines poor clinical outcome in patients with metastatic colorectal cancer. *Clin Cancer Res Off J Am Assoc Cancer Res* 21: 347–356

Dong CZ, Bruzzoni-Giovanelli H, Yu Y, Dorgham K, Parizot C, Zini JM, Brossas JY, Tuffery P & Rebollo A (2020) Identification of peptides interfering with the LRRK2/PP1 interaction. *PloS One* 15: e0237110

D'souza S, Lau KC, Coffin CS & Patel TR (2020) Molecular mechanisms of viral hepatitis induced hepatocellular carcinoma. *World J Gastroenterol* 26: 5759–5783

Duvoux C, Roudot-Thoraval F, Decaens T, Pessione F, Badran H, Piardi T, Francoz C, Compagnon P, Vanlemmens C, Dumortier J, *et al* (2012) Liver transplantation for hepatocellular carcinoma: a model including alpha-fetoprotein improves the performance of Milan criteria. *Gastroenterology* 143: 986–94 e3; quiz e14-5

Elahouel R, Blanc C, Carpentier G, Frechault S, Cascone I, Destouches D, Delbé J, Courty J & Hamma-Kourbali Y (2015) Pleiotrophin exerts its migration and invasion effect through the neuropilin-1 pathway. *Neoplasia N Y N* 17: 613–624

Enjoji S, Yabe R, Fujiwara N, Tsuji S, Vitek MP, Mizuno T, Nakagawa T, Usui T, Ohama T & Sato K (2015) The therapeutic effects of SET/I2PP2A inhibitors on canine melanoma. *J Vet Med Sci* 77: 1451–1456

Fallahi-Sichani M, Becker V, Izar B, Baker GJ, Lin J, Boswell SA, Shah P, Rotem A, Garraway LA & Sorger PK (2017) Adaptive resistance of melanoma cells to RAF inhibition via reversible induction of a slowly dividing de-differentiated state. *Mol Syst Biol* 13: 905

Fang H-Y, Stangl S, Marcazzan S, Carvalho MJB, Baumeister T, Anand A, Strangmann J, Huspenina JS, Wang TC, Schmid RM, *et al* (2022) Targeted Hsp70 fluorescence molecular endoscopy detects dysplasia in Barrett's esophagus. *Eur J Nucl Med Mol Imaging* 49: 2049–2063

Farrell AS, Allen-Petersen B, Daniel CJ, Wang X, Wang Z, Rodriguez S, Impey S, Oddo J, Vitek MP, Lopez C, *et al* (2014) Targeting inhibitors of the tumor suppressor PP2A for the treatment of pancreatic cancer. *Mol Cancer Res MCR* 12: 924–939

Finn RS, Qin S, Ikeda M, Galle PR, Ducreux M, Kim T-Y, Kudo M, Breder V, Merle P, Kaseb AO, *et al* (2020a) Atezolizumab plus Bevacizumab in Unresectable Hepatocellular Carcinoma. *N Engl J Med* 382: 1894–1905

Finn RS, Ryoo B-Y, Merle P, Kudo M, Bouattour M, Lim HY, Breder V, Edeline J, Chao Y, Ogasawara S, *et al* (2020b) Pembrolizumab As Second-Line Therapy in Patients With Advanced Hepatocellular Carcinoma in KEYNOTE-240: A Randomized, Double-Blind, Phase III Trial. *J Clin Oncol Off J Am Soc Clin Oncol* 38: 193–202

Fogal V, Richardson AD, Karmali PP, Scheffler IE, Smith JW & Ruoslahti E (2010) Mitochondrial p32 protein is a critical regulator of tumor metabolism via maintenance of oxidative phosphorylation. *Mol Cell Biol* 30: 1303–1318

Fogal V, Zhang L, Krajewski S & Ruoslahti E (2008) Mitochondrial/cell-surface protein p32/gC1qR as a molecular target in tumor cells and tumor stroma. *Cancer Res* 68: 7210–8

Frank R (2002) The SPOT-synthesis technique. Synthetic peptide arrays on membrane supports--principles and applications. *J Immunol Methods* 267: 13–26

Frank R & Overwin H (1996) SPOT synthesis. Epitope analysis with arrays of synthetic peptides prepared on cellulose membranes. *Methods Mol Biol Clifton NJ* 66: 149–169

Friedman SL, Neuschwander-Tetri BA, Rinella M & Sanyal AJ (2018) Mechanisms of NAFLD development and therapeutic strategies. *Nat Med* 24: 908–922

Galiger C, Dahlhaus M, Vitek MP, Debatin K-M & Beltinger C (2022) PPP2CA Is a Novel Therapeutic Target in Neuroblastoma Cells That Can Be Activated by the SET Inhibitor OP449. *Front Oncol* 12: 744984

Gaugain L, Cawston H, Dubois de Gennes C, Sanchez Alvares J, Nahon P, Mazaleyrat B & Le Dissez C (2023) Cost-utility analysis of atezolizumab with bevacizumab in untreated unresectable or advanced hepatocellular carcinoma in France. *PloS One* 18: e0280442

Gausepohl H, Boulin C, Kraft M & Frank RW (1992) Automated multiple peptide synthesis. *Pept Res* 5: 315–320

Geysen HM, Meloen RH & Barteling SJ (1984) Use of peptide synthesis to probe viral antigens for epitopes to a resolution of a single amino acid. *Proc Natl Acad Sci U S A* 81: 3998–4002

Ghosal K, Stathopoulos A, Thomas D, Phenis D, Vitek MP & Pimplikar SW (2013) The apolipoprotein-E-mimetic COG112 protects amyloid precursor protein intracellular domain-overexpressing animals from Alzheimer's disease-like pathological features. *Neurodegener Dis* 12: 51–58

Glenn GM & Eckhart W (1993) Mutation of a cysteine residue in polyomavirus middle T antigen abolishes interactions with protein phosphatase 2A, pp60c-src, and phosphatidylinositol-3 kinase, activation of c-fos expression, and cellular transformation. *JVirol* 67: 1945–1952

Glinka Y & Prud'homme GJ (2008) Neuropilin-1 is a receptor for transforming growth factor beta-1, activates its latent form, and promotes regulatory T cell activity. *J Leukoc Biol* 84: 302–310

Global Burden of Disease Liver Cancer Collaboration, Akinyemiju T, Abera S, Ahmed M, Alam N, Alemayohu MA, Allen C, Al-Raddadi R, Alvis-Guzman N, Amoako Y, *et al* (2017) The Burden of Primary Liver Cancer and Underlying Etiologies From 1990 to 2015 at the Global, Regional, and National Level: Results From the Global Burden of Disease Study 2015. *JAMA Oncol* 3: 1683–1691

Godet AN, Guergnon J, Galioot A, Falanga P-B, Colle J-H, Cayla X & Garcia A (2011) La famille des protéine phosphatases PP2A: Une cible stratégique pour les virus et pour la transformation tumorale. *médecine/sciences* 27: 1106–1111

Gong SJ, Feng XJ, Song WH, Chen JM, Wang SM, Xing DJ, Zhu MH, Zhang SH & Xu AM (2016) Upregulation of PP2Ac predicts poor prognosis and contributes to aggressiveness in hepatocellular carcinoma. *Cancer BiolTher* 17: 151–162

Gotz J, Probst A, Ehler E, Hemmings B & Kues W (1998) Delayed embryonic lethality in mice lacking protein phosphatase 2A catalytic subunit Calpha. *ProcNatlAcadSciUSA* 95: 12370–12375

Haesen D, Sents W, Lemaire K, Hoorne Y & Janssens V (2014) The Basic Biology of PP2A in Hematologic Cells and Malignancies. *Front Oncol* 4: 347

Hayashi MAF, Ducancel F & Konno K (2012) Natural Peptides with Potential Applications in Drug Development, Diagnosis, and/or Biotechnology. *Int J Pept* 2012: 1–2

He X, Li M, Yu H, Liu G, Wang N, Yin C, Tu Q, Narla G, Tao Y, Cheng S, *et al* (2020) Loss of hepatic aldolase B activates Akt and promotes hepatocellular carcinogenesis by destabilizing the Aldob/Akt/PP2A protein complex. *PLOS Biol* 18: e3000803

Hong T-M, Chen Y-L, Wu Y-Y, Yuan A, Chao Y-C, Chung Y-C, Wu M-H, Yang S-C, Pan S-H, Shih J-Y, *et al* (2007) Targeting Neuropilin 1 as an Antitumor Strategy in Lung Cancer. *Clin Cancer Res* 13: 4759–4768

Hung M-H, Chen Y-L, Chu P-Y, Shih C-T, Yu H-C, Tai W-T, Shiau C-W & Chen K-F (2016) Upregulation of the oncoprotein SET determines poor clinical outcomes in hepatocellular carcinoma and shows therapeutic potential. *Oncogene* 35: 4891–4902

Hunt H, Simon-Gracia L, Tobi A, Kotamraju VR, Sharma S, Nigul M, Sugahara KN, Ruoslahti E & Teesalu T (2017) Targeting of p32 in peritoneal carcinomatosis with intraperitoneal linTT1 peptide-guided pro-apoptotic nanoparticles. *J Control Release* 260: 142–153

International CLL-IPI working group (2016) An international prognostic index for patients with chronic lymphocytic leukaemia (CLL-IPI): a meta-analysis of individual patient data. *Lancet Oncol* 17: 779–790

Ioannou GN (2021) Epidemiology and risk-stratification of NAFLD-associated HCC. *J Hepatol* 75: 1476–1484

Ishitsuka A, Fujine E, Mizutani Y, Tawada C, Kanoh H, Banno Y & Seishima M (2014) FTY720 and cisplatin synergistically induce the death of cisplatin-resistant melanoma cells through the downregulation of the PI3K pathway and the decrease in epidermal growth factor receptor expression. *Int J Mol Med* 34: 1169–1174

Janghorban M, Farrell AS, Allen-Petersen BL, Pelz C, Daniel CJ, Oddo J, Langer EM, Christensen DJ & Sears RC (2014) Targeting c-MYC by antagonizing PP2A inhibitors in breast cancer. *Proc Natl Acad Sci U S A* 111: 9157–9162

Janssens V & Goris J (2001) Protein phosphatase 2A: a highly regulated family of serine/threonine phosphatases implicated in cell growth and signalling. *BiochemJ* 353: 417–439

Janssens V, Goris J & Van HC (2005) PP2A: the expected tumor suppressor. *CurrOpinGenetDev* 15: 34–41

Janssens V & Rebollo A (2012) The role and therapeutic potential of Ser/Thr phosphatase PP2A in apoptotic signalling networks in human cancer cells. *Curr Mol Med* 12: 268–87

Jia H, Bagherzadeh A, Hartzoulakis B, Jarvis A, Löhr M, Shaikh S, Aqil R, Cheng L, Tickner M, Esposito D, *et al* (2006) Characterization of a Bicyclic Peptide Neuropilin-1 (NP-1) Antagonist (EG3287) Reveals Importance of Vascular Endothelial Growth Factor Exon 8 for NP-1 Binding and Role of NP-1 in KDR Signaling. *J Biol Chem* 281: 13493–13502

Jiang S-W, Xu S, Chen H, Liu X, Tang Z, Cui Y & Liu J (2017) Pathologic significance of SET/I2PP2A-mediated PP2A and non-PP2A pathways in polycystic ovary syndrome (PCOS). *Clin Chim Acta Int J Clin Chem* 464: 155–159

Jin C, Bai L, Lin L, Wang S & Yin X (2018) Paclitaxel-loaded nanoparticles decorated with bivalent fragment HAb18 F(ab')2 and cell penetrating peptide for improved therapeutic effect on hepatocellular carcinoma. *Artif Cells Nanomedicine Biotechnol* 46: 1076–1084

Jin X, Ma X, Zhao D, Yang L & Ma N (2022) Immune microenvironment and therapeutic progress of recurrent hepatocellular carcinoma after liver transplantation. *Transl Oncol* 28: 101603

Jones S, Wang TL, Shih I, Mao TL, Nakayama K, Roden R, Glas R, Slamon D, Diaz LA Jr, Vogelstein B, *et al* (2010) Frequent mutations of chromatin remodeling gene ARID1A in ovarian clear cell carcinoma. *Science* 330: 228–231

Kalla C, Scheuermann MO, Kube I, Schlotter M, Mertens D, Dohner H, Stilgenbauer S & Lichter P (2007) Analysis of 11q22-q23 deletion target genes in B-cell chronic lymphocytic leukaemia: evidence for a pathogenic role of NPAT, CUL5, and PPP2R1B. *EurJCancer* 43: 1328–1335

Kamibayashi C, Estes R, Lickteig RL, Yang SI, Craft C & Mumby MC (1994) Comparison of heterotrimeric protein phosphatase 2A containing different B subunits. *JBiolChem* 269: 20139–20148

Kang HS & Choi I (2001) Protein Phosphatase 2A Modulates the Proliferation of Human Multiple Myeloma Cells via Regulation of the Production of Reactive Oxygen Intermediates and Anti-Apoptotic Factors. *Cell Immunol* 213: 34–44

Karjalainen K, Jaalouk DE, Bueso-Ramos CE, Zurita AJ, Kuniyasu A, Eckhardt BL, Marini FC, Lichtiger B, O'Brien S, Kantarjian HM, *et al* (2011) Targeting neuropilin-1 in human leukemia and lymphoma. *Blood* 117: 920–927

Kato R, Kaga C, Kunimatsu M, Kobayashi T & Honda H (2006) Peptide array-based interaction assay of solid-bound peptides and anchorage-dependant cells and its effectiveness in cell-adhesive peptide design. *J Biosci Bioeng* 101: 485–495

Katz C, Levy-Beladev L, Rotem-Bamberger S, Rito T, Rüdiger SGD & Friedler A (2011) Studying protein-protein interactions using peptide arrays. *Chem Soc Rev* 40: 2131–2145

Khew-Goodall Y & Hemmings BA (1988) Tissue-specific expression of mRNAs encoding alpha- and beta-catalytic subunits of protein phosphatase 2A. *FEBS Lett* 238: 265–268

Kong J, Li D, Zhang S, Zhang H, Fu Y, Qian B, Bei C, Tan S & Zhu X (2021) Okadaic acid promotes epithelial-mesenchymal transition of hepatocellular carcinoma cells by inhibiting protein phosphatase 2A. *J Cell Biochem* 122: 993–1002

Laakkonen P, Åkerman ME, Biliran H, Yang M, Ferrer F, Karpanen T, Hoffman RM & Ruoslahti E (2004) Antitumor activity of a homing peptide that targets tumor lymphatics and tumor cells. *Proc Natl Acad Sci* 101: 9381–9386

Laakkonen P, Porkka K, Hoffman JA & Ruoslahti E (2002) A tumor-homing peptide with a targeting specificity related to lymphatic vessels. *Nat Med* 8: 751–755

Lambrecht C, Ferreira GB, Omella JD, Libbrecht L, De Vos R, Derua R, Mathieu C, Overbergh L, Waelkens E & Janssens V (2020) Differential Proteomic Analysis of Hepatocellular Carcinomas from *Ppp2r5d* Knockout Mice and Normal (Knockout) Livers. *Cancer Genomics - Proteomics* 17: 669–685

Larrey E, Conti F & Allaire M (2022) A standardized immunosuppressive regimen for patients who received liver transplantations treated with atezolizumab-bevacizumab to avoid graft rejection? *Liver Transplant Off Publ Am Assoc Study Liver Dis Int Liver Transplant Soc* 28: 1262–1263

Lee Y-CA, Cohet C, Yang Y-C, Stayner L, Hashibe M & Straif K (2009) Meta-analysis of epidemiologic studies on cigarette smoking and liver cancer. *Int J Epidemiol* 38: 1497–1511

Li F-Q, Sempowski GD, McKenna SE, Laskowitz DT, Colton CA & Vitek MP (2006) Apolipoprotein E-derived peptides ameliorate clinical disability and inflammatory infiltrates into the spinal cord in a murine model of multiple sclerosis. *J Pharmacol Exp Ther* 318: 956–965

Li Y, Hu T, Chen T, Yang T, Ren H & Chen M (2018) Combination treatment of FTY720 and cisplatin exhibits enhanced antitumour effects on cisplatin-resistant non-small lung cancer cells. *Oncol Rep* 39: 565–572

Liang W-C, Dennis MS, Stawicki S, Chanthery Y, Pan Q, Chen Y, Eigenbrot C, Yin J, Koch AW, Wu X, *et al* (2007) Function Blocking Antibodies to Neuropilin-1 Generated from a Designed Human Synthetic Antibody Phage Library. *J Mol Biol* 366: 815–829

von Lindern M, van Baal S, Wiegant J, Raap A, Hagemeijer A & Grosveld G (1992) Can, a putative oncogene associated with myeloid leukemogenesis, may be activated by fusion of its 3' half to different genes: characterization of the set gene. *Mol Cell Biol* 12: 3346–3355

Lingasamy P & Teesalu T (2021) Homing Peptides for Cancer Therapy. In *Bio-Nanomedicine for Cancer Therapy*, Fontana F & Santos HA (eds) pp 29–48. Cham: Springer International Publishing

Liu Y, Wu X, Gao Y, Zhang J, Zhang D, Gu S, Zhu G, Liu G & Li X (2016) Aptamer-functionalized peptide H3CR5C as a novel nanovehicle for codelivery of fasudil and miRNA-195 targeting hepatocellular carcinoma. *Int J Nanomedicine* 11: 3891–3905

Llovet JM, Kelley RK, Villanueva A, Singal AG, Pikarsky E, Roayaie S, Lencioni R, Koike K, Zucman-Rossi J & Finn RS (2021) Hepatocellular carcinoma. *Nat Rev Primer* 7: 6

Llovet JM, Pinyol R, Kelley RK, El-Khoueiry A, Reeves HL, Wang XW, Gores GJ & Villanueva A (2022) Molecular pathogenesis and systemic therapies for hepatocellular carcinoma. *Nat Cancer* 3: 386–401

Luu T, Pham S & Deshpande S (1996) Automated multiple peptide synthesis: improvements in obtaining quality peptides. *Int J Pept Protein Res* 47: 91–97

Madeira A, Pommet JM, Prochiantz A & Allinquant B (2005) SET protein (TAF1beta, I2PP2A) is involved in neuronal apoptosis induced by an amyloid precursor protein cytoplasmic subdomain. *FASEB J Off Publ Fed Am Soc Exp Biol* 19: 1905–1907

Man S, Luo C, Yan M, Zhao G, Ma L & Gao W (2021) Treatment for liver cancer: From sorafenib to natural products. *Eur J Med Chem* 224: 113690

Mayer-Jaekel RE & Hemmings BA (1994) Protein phosphatase 2A--a 'menage a trois'. *Trends Cell Biol* 4: 287–291

McGlynn KA, Petrick JL & London WT (2015) Global epidemiology of hepatocellular carcinoma: an emphasis on demographic and regional variability. *Clin Liver Dis* 19: 223–238

Mohr R, Özdirik B, Lambrecht J, Demir M, Eschrich J, Geisler L, Hellberg T, Loosen SH, Luedde T, Tacke F, *et al* (2021) From Liver Cirrhosis to Cancer: The Role of Micro-RNAs in Hepatocarcinogenesis. *Int J Mol Sci* 22: 1492

Muttenthaler M, King GF, Adams DJ & Alewood PF (2021) Trends in peptide drug discovery. *Nat Rev Drug Discov* 20: 309–325

Nagao M, Shima H, Nakayasu M & Sugimura T (1995) Protein serine/threonine phosphatases as binding proteins for okadaic acid. *MutatRes* 333: 173–179

Nagata K, Saito S, Okuwaki M, Kawase H, Furuya A, Kusano A, Hanai N, Okuda A & Kikuchi A (1998) Cellular localization and expression of template-activating factor I in different cell types. *Exp Cell Res* 240: 274–281

Nagendra DC, Burke J III, Maxwell GL & Risinger JI (2012) PPP2R1A mutations are common in the serous type of endometrial cancer. *MolCarcinog* 51: 826–831

Nambotin SB, Lefrancois L, Sainsily X, Berthillon P, Kim M, Wands JR, Chevallier M, Jalinot P, Scoazec JY, Trepo C, *et al* (2011) Pharmacological inhibition of Frizzled-7 displays anti-tumor properties in hepatocellular carcinoma. *J Hepatol* 54: 288–299

Nasarre C, Roth M, Jacob L, Roth L, Koncina E, Thien A, Labourdette G, Poulet P, Hubert P, Crémel G, *et al* (2010) Peptide-based interference of the transmembrane domain of neuropilin-1 inhibits glioma growth in vivo. *Oncogene* 29: 2381–2392

Nault JC, Couchy G, Balabaud C, Morcrette G, Caruso S, Blanc JF, Bacq Y, Calderaro J, Paradis V, Ramos J, *et al* (2017) Molecular Classification of Hepatocellular Adenoma Associates With Risk Factors, Bleeding, and Malignant Transformation. *Gastroenterology* 152: 880–894

Nault J-C, Galle PR & Marquardt JU (2018) The role of molecular enrichment on future therapies in hepatocellular carcinoma. *J Hepatol* 69: 237–247

Nault J-C, Martin Y, Caruso S, Hirsch TZ, Bayard Q, Calderaro J, Charpy C, Copie-Bergman C, Ziol M, Bioulac-Sage P, *et al* (2020) Clinical Impact of Genomic Diversity From Early to Advanced Hepatocellular Carcinoma. *Hepatol Baltim Md* 71: 164–182

Nault J-C, Paradis V, Ronot M & Zucman-Rossi J (2022) Benign liver tumours: understanding molecular physiology to adapt clinical management. *Nat Rev Gastroenterol Hepatol* 19: 703–716

Nault J-C & Zucman-Rossi J (2011) Genetics of hepatobiliary carcinogenesis. *Semin Liver Dis* 31: 173–187

Neviani P, Santhanam R, Oaks JJ, Eiring AM, Notari M, Blaser BW, Liu S, Trotta R, Muthusamy N, Gambacorti-Passerini C, *et al* (2007) FTY720, a new alternative for treating blast crisis chronic myelogenous leukemia and Philadelphia chromosome-positive acute lymphocytic leukemia. *J Clin Invest* 117: 2408–2421

Neviani P, Santhanam R, Trotta R, Notari M, Blaser BW, Liu S, Mao H, Chang JS, Galietta A, Uttam A, *et al* (2005) The tumor suppressor PP2A is functionally inactivated in blast crisis CML through the inhibitory activity of the BCR/ABL-regulated SET protein. *Cancer Cell* 8: 355–368

Niland S & Eble JA (2019) Neuropilins in the Context of Tumor Vasculature. *Int J Mol Sci* 20: 639

Oaks J & Ogretmen B (2014) Regulation of PP2A by Sphingolipid Metabolism and Signaling. *Front Oncol* 4: 388

Orgad S, Brewis ND, Alphey L, Axton JM, Dudai Y & Cohen PT (1990) The structure of protein phosphatase 2A is as highly conserved as that of protein phosphatase 1. *FEBS Lett* 275: 44–48

Paasonen L, Sharma S, Braun GB, Kotamraju VR, Chung TD, She ZG, Sugahara KN, Yliperttula M, Wu B, Pellecchia M, *et al* (2016) New p32/gC1qR Ligands for Targeted Tumor Drug Delivery. *Chembiochem* 17: 570–5

Pang H-B, Braun GB, Friman T, Aza-Blanc P, Ruidiaz ME, Sugahara KN, Teesalu T & Ruoslahti E (2014) An endocytosis pathway initiated through neuropilin-1 and regulated by nutrient availability. *Nat Commun* 5: 4904

Pellet-Many C, Frankel P, Jia H & Zachary I (2008) Neuropilins: structure, function and role in disease. *Biochem J* 411: 211–226

Péneau C, Imbeaud S, La Bella T, Hirsch TZ, Caruso S, Calderaro J, Paradis V, Blanc J-F, Letouzé E, Nault J-C, *et al* (2022) Hepatitis B virus integrations promote local and distant oncogenic driver alterations in hepatocellular carcinoma. *Gut* 71: 616–626

Pippa R, Dominguez A, Christensen DJ, Moreno-Miralles I, Blanco-Prieto MJ, Vitek MP & Odero MD (2014) Effect of FTY720 on the SET-PP2A complex in acute myeloid leukemia; SET binding drugs have antagonistic activity. *Leukemia* 28: 1915–8

Poynard T, Peta V, Deckmyn O, Munteanu M, Moussalli J, Ngo Y, Rudler M, Lebray P, Pais R, Bonyhay L, *et al* (2019) LCR1 and LCR2, two multi-analyte blood tests to assess liver cancer risk in patients without or with cirrhosis. *Aliment Pharmacol Ther* 49: 308–320

Prud'homme GJ & Glinka Y (2012) Neuropilins are multifunctional coreceptors involved in tumor initiation, growth, metastasis and immunity. *Oncotarget* 3: 921–939

Rafferty J, Nagaraj H, P. McCloskey A, Huwaitat R, Porter S, Albadr A & Laverty G (2016) Peptide Therapeutics and the Pharmaceutical Industry: Barriers Encountered Translating from the Laboratory to Patients. *Curr Med Chem* 23: 4231–4259

Rahib L, Smith BD, Aizenberg R, Rosenzweig AB, Fleshman JM & Matrisian LM (2014) Projecting cancer incidence and deaths to 2030: the unexpected burden of thyroid, liver, and pancreas cancers in the United States. *Cancer Res* 74: 2913–2921

Rai KR, Sawitsky A, Cronkite EP, Chanana AD, Levy RN & Pasternack BS (1975) Clinical staging of chronic lymphocytic leukemia. *Blood* 46: 219–34

Rebollo A, Fliedel L & Tuffery P (2022) PEPscan: A Broad Spectrum Approach for the Characterization of Protein-Binder Interactions? *Biomolecules* 12: 178

Rebollo A, Savier E & Tuffery P (2021) Pepscan Approach for the Identification of Protein–Protein Interfaces: Lessons from Experiment. *Biomolecules* 11: 772

Reig M, Forner A, Rimola J, Ferrer-Fàbrega J, Burrel M, Garcia-Criado Á, Kelley RK, Galle PR, Mazzaferro V, Salem R, *et al* (2022) BCLC strategy for prognosis prediction and treatment recommendation: The 2022 update. *J Hepatol* 76: 681–693

Reineke U, Sabat R, Volk HD & Schneider-Mergener J (1998) Mapping of the interleukin-10/interleukin-10 receptor combining site. *Protein Sci Publ Protein Soc* 7: 951–960

Rich NE, Hester C, Odewole M, Murphy CC, Parikh ND, Marrero JA, Yopp AC & Singal AG (2019) Racial and Ethnic Differences in Presentation and Outcomes of Hepatocellular Carcinoma. *Clin Gastroenterol Hepatol Off Clin Pract J Am Gastroenterol Assoc* 17: 551-559.e1

Rich NE, Yopp AC, Singal AG & Murphy CC (2020) Hepatocellular Carcinoma Incidence Is Decreasing Among Younger Adults in the United States. *Clin Gastroenterol Hepatol Off Clin Pract J Am Gastroenterol Assoc* 18: 242-248.e5

Richard NP, Pippa R, Cleary MM, Puri A, Tibbitts D, Mahmood S, Christensen DJ, Jeng S, McWeeney S, Look AT, *et al* (2016) Combined targeting of SET and tyrosine kinases provides an effective therapeutic approach in human T-cell acute lymphoblastic leukemia. *Oncotarget* 7: 84214–84227

Ronne H, Carlberg M, Hu GZ & Nehlin JO (1991) Protein phosphatase 2A in Saccharomyces cerevisiae: effects on cell growth and bud morphogenesis. *MolCell Biol* 11: 4876–4884

Rosmorduc O, Chevreau C, Dielenseger P, Ederhy S, Goldwasser F, Grange J-D, Mortier L, Neidhardt-Berard M-E, Robert C, Scotté F, *et al* (2010) Bon usage du sorafénib chez les patients pris en charge pour un carcinome hépatocellulaire ou un cancer du rein. *Gastroentérologie Clin Biol* 34: 161–167

Ruediger R, Pham HT & Walter G (2001) Disruption of protein phosphatase 2A subunit interaction in human cancers with mutations in the A alpha subunit gene. *Oncogene* 20: 10–15

Ruvolo PP, Qui YH, Coombes KR, Zhang N, Ruvolo VR, Borthakur G, Konopleva M, Andreeff M & Kornblau SM (2011) Low expression of PP2A regulatory subunit B55alpha is associated with T308 phosphorylation of AKT and shorter complete remission duration in acute myeloid leukemia patients. *Leukemia* 25: 1711–1717

Sablina AA, Chen W, Arroyo JD, Corral L, Hector M, Bulmer SE, DeCaprio JA & Hahn WC (2007) The tumor suppressor PP2A Abeta regulates the RalA GTPase. *Cell* 129: 969–982

Saddoughi SA, Gencer S, Peterson YK, Ward KE, Mukhopadhyay A, Oaks J, Bielawski J, Szulc ZM, Thomas RJ, Selvam SP, *et al* (2013) Sphingosine analogue drug FTY720 targets I2PP2A/SET and mediates lung tumour suppression via activation of PP2A-RIPK1-dependent necroptosis. *EMBO Mol Med* 5: 105–121

Sangro B, Chan SL, Meyer T, Reig M, El-Khoueiry A & Galle PR (2020) Diagnosis and management of toxicities of immune checkpoint inhibitors in hepatocellular carcinoma. *J Hepatol* 72: 320–341

Santillan C, Chernyak V & Sirlin C (2018) LI-RADS categories: concepts, definitions, and criteria. *Abdom Radiol* 43: 101–110

Scatton O, Chiappini F, Liu XH, Riou P, Marconi A, Debuire B, Azoulay D & Lemoine A (2008) Generation and modulation of hepatocellular carcinoma circulating cells: a new experimental model. *J Surg Res* 150: 183–189

Scatton O, Chiappini F, Riou P, Marconi A, Saffroy R, Bralet MP, Azoulay D, Boucheix C, Debuire B, Uzan G, *et al* (2006) Fate and characterization of circulating tumor cells in a NOD/SCID mouse model of human hepatocellular carcinoma. *Oncogene* 25: 4067–4075

Schonthal AH (2001) Role of serine/threonine protein phosphatase 2A in cancer. *Cancer Lett* 170: 1–13

Scott JK & Smith GP (1990) Searching for peptide ligands with an epitope library. *Science* 249: 386–390

Seen S (2021) Chronic liver disease and oxidative stress - a narrative review. *Expert Rev Gastroenterol Hepatol* 15: 1021–1035

Sharma S, Kotamraju VR, Mölder T, Tobi A, Teesalu T & Ruoslahti E (2017) Tumor-Penetrating Nanosystem Strongly Suppresses Breast Tumor Growth. *Nano Lett* 17: 1356–1364

Simon-Gracia L, Hunt H, Scodeller P, Gaitzsch J, Kotamraju VR, Sugahara KN, Tammik O, Ruoslahti E, Battaglia G & Teesalu T (2016) iRGD peptide conjugation potentiates intraperitoneal tumor delivery of paclitaxel with polymersomes. *Biomaterials* 104: 247–257

Simon-Gracia L, Loisel S, Sidorenko V, Scodeller P, Parizot C, Savier E, Haute T, Teesalu T & Rebollo A (2022) Preclinical Validation of Tumor-Penetrating and Interfering Peptides against Chronic Lymphocytic Leukemia. *MolPharm* 19: 895–903

Simon-Gracia L, Savier E, Parizot C, Brossas JY, Loisel S, Teesalu T, Conti F, Charlotte F, Scatton O, Aoudjehane L, *et al* (2020) Bifunctional Therapeutic Peptides for Targeting Malignant B Cells and Hepatocytes: Proof of Concept in Chronic Lymphocytic Leukemia. *Adv Ther* 3

Singal AG, Lampertico P & Nahon P (2020) Epidemiology and surveillance for hepatocellular carcinoma: New trends. *J Hepatol* 72: 250–261

Singh K, Chaturvedi R, Asim M, Barry DP, Lewis ND, Vitek MP & Wilson KT (2008) The apolipoprotein E-mimetic peptide COG112 inhibits the inflammatory response to Citrobacter rodentium in colonic epithelial cells by preventing NF-kappaB activation. *J Biol Chem* 283: 16752–16761

Singh K, Chaturvedi R, Barry DP, Coburn LA, Asim M, Lewis ND, Piazuelo MB, Washington MK, Vitek MP & Wilson KT (2011) The apolipoprotein E-mimetic peptide COG112 inhibits NF-kappaB signaling, proinflammatory cytokine expression, and disease activity in murine models of colitis. *J Biol Chem* 286: 3839–3850

Smith GP (1985) Filamentous fusion phage: novel expression vectors that display cloned antigens on the virion surface. *Science* 228: 1315–1317

Sobral LM, Sousa LO, Coletta RD, Cabral H, Greene LJ, Tajara EH, Gutkind JS, Curti C & Leopoldino AM (2014) Stable SET knockdown in head and neck squamous cell carcinoma promotes cell invasion and the mesenchymal-like phenotype in vitro, as well as necrosis, cisplatin sensitivity and lymph node metastasis in xenograft tumor models. *Mol Cancer* 13: 32

Sugahara KN, Braun GB, de Mendoza TH, Kotamraju VR, French RP, Lowy AM, Teesalu T & Ruoslahti E (2015a) Tumor-penetrating iRGD peptide inhibits metastasis. *Mol Cancer Ther* 14: 120–128

Sugahara KN, Scodeller P, Braun GB, de Mendoza TH, Yamazaki CM, Kluger MD, Kitayama J, Alvarez E, Howell SB, Teesalu T, *et al* (2015b) A tumor-penetrating peptide enhances circulation-independent targeting of peritoneal carcinomatosis. *J Control Release* 212: 59–69

Sugahara KN, Teesalu T, Karmali PP, Kotamraju VR, Agemy L, Girard OM, Hanahan D, Mattrey RF & Ruoslahti E (2009) Tissue-Penetrating Delivery of Compounds and Nanoparticles into Tumors. *Cancer Cell* 16: 510–520

Sugahara KN, Teesalu T, Karmali PP, Kotamraju VR, Agemy L, Greenwald DR & Ruoslahti E (2010) Coadministration of a Tumor-Penetrating Peptide Enhances the Efficacy of Cancer Drugs. *Science* 328: 1031–1035

Sung H, Ferlay J, Siegel RL, Laversanne M, Soerjomataram I, Jemal A & Bray F (2021) Global Cancer Statistics 2020: GLOBOCAN Estimates of Incidence and Mortality Worldwide for 36 Cancers in 185 Countries. *CA Cancer J Clin* 71: 209–249

Switzer CH, Cheng RYS, Vitek TM, Christensen DJ, Wink DA & Vitek MP (2011) Targeting SET/I(2)PP2A oncoprotein functions as a multi-pathway strategy for cancer therapy. *Oncogene* 30: 2504–2513

Taniai M (2020) Alcohol and hepatocarcinogenesis. *Clin Mol Hepatol* 26: 736–741

Teesalu T, Sugahara KN, Kotamraju VR & Ruoslahti E (2009) C-end rule peptides mediate neuropilin-1-dependent cell, vascular, and tissue penetration. *Proc Natl Acad Sci* 106: 16157–16162

Teesalu T, Sugahara KN & Ruoslahti E (2013) Tumor-Penetrating Peptides. *Front Oncol* 3

Thièry JP, Blazsek I, Legras S, Marion S, Reynes M, Anjo A, Adam R & Misset JL (1999) Hepatocellular carcinoma cell lines from diethylnitrosamine phenobarbital-treated rats. Characterization and sensitivity to endothall, a protein serine/threonine phosphatase-2A inhibitor. *Hepatol Baltim Md* 29: 1406–1417

Tian L, Zhang X, Haesen D, Bravo J, Fominaya J, Choquet S, Zini JM, Loisel S, Waelkens E, Janssens V, *et al* (2018a) Identification of PP2A/Set Binding Sites and Design of Interacting Peptides with Potential Clinical Applications. *Int J Pept Res Ther* 24: 479–488

Tian L, Zhang X, Haesen D, Bravo J, Fominaya J, Choquet S, Zini JM, Loisel S, Waelkens E, Janssens V, *et al* (2018b) Identification of PP2A/Set Binding Sites and Design of Interacting Peptides with Potential Clinical Applications. *Int J Pept Res Ther* 24: 479–488

Torti D & Trusolino L (2011) Oncogene addiction as a foundational rationale for targeted anti-cancer therapy: promises and perils. *EMBO Mol Med* 3: 623–636

Tung HY, Alemany S & Cohen P (1985) The protein phosphatases involved in cellular regulation. 2. Purification, subunit structure and properties of protein phosphatases-2A0, 2A1, and 2A2 from rabbit skeletal muscle. *Eur J Biochem* 148: 253–263

Villanueva A (2019) Hepatocellular Carcinoma. *N Engl J Med* 380: 1450–1462

Vogelstein B, Papadopoulos N, Velculescu VE, Zhou S, Diaz LA & Kinzler KW (2013) Cancer Genome Landscapes. *Science* 339: 1546–1558

Wang G, Jia T, Xu X, Chang L, Zhang R, Fu Y, Li Y, Yang X, Zhang K, Lin G, *et al* (2016a) Novel miR-122 delivery system based on MS2 virus like particle surface displaying cell-penetrating peptide TAT for hepatocellular carcinoma. *Oncotarget* 7: 59402–59416

Wang J, Wang H, Li J, Liu Z, Xie H, Wei X, Lu D, Zhuang R, Xu X & Zheng S (2016b) iRGD-Decorated Polymeric Nanoparticles for the Efficient Delivery of Vandetanib to Hepatocellular Carcinoma: Preparation and in Vitro and in Vivo Evaluation. *ACS Appl Mater Interfaces* 8: 19228–19237

Wang L, Wang N, Zhang W, Cheng X, Yan Z, Shao G, Wang X, Wang R & Fu C (2022) Therapeutic peptides: current applications and future directions. *Signal Transduct Target Ther* 7: 48

Wang SS, Esplin ED, Li JL, Huang L, Gazdar A, Minna J & Evans GA (1998) Alterations of the PPP2R1B gene in human lung and colon cancer. *Science* 282: 284–287

Wang X, Wu F, Li G, Zhang N, Song X, Zheng Y, Gong C, Han B & He G (2018) Lipid-modified cell-penetrating peptide-based self-assembly micelles for co-delivery of narciclasine and siULK1 in hepatocellular carcinoma therapy. *Acta Biomater* 74: 414–429

Welzel TM, Graubard BI, Zeuzem S, El-Serag HB, Davila JA & McGlynn KA (2011) Metabolic syndrome increases the risk of primary liver cancer in the United States: a study in the SEER-Medicare database. *Hepatol Baltim Md* 54: 463–471

West DC, Rees CG, Duchesne L, Patey SJ, Terry CJ, Turnbull JE, Delehedde M, Heegaard CW, Allain F, Vanpouille C, *et al* (2005) Interactions of multiple heparin binding growth factors with neuropilin-1 and potentiation of the activity of fibroblast growth factor-2. *J Biol Chem* 280: 13457–13464

Wilson TR, Fridlyand J, Yan Y, Penuel E, Burton L, Chan E, Peng J, Lin E, Wang Y, Sosman J, *et al* (2012) Widespread potential for growth-factor-driven resistance to anticancer kinase inhibitors. *Nature* 487: 505–509

Wonder E, Simon-Gracia L, Scodeller P, Majzoub RN, Kotamraju VR, Ewert KK, Teesalu T & Safinya CR (2018) Competition of charge-mediated and specific binding by peptide-tagged cationic liposome-DNA nanoparticles in vitro and in vivo. *Biomaterials* 166: 52–63

Yang C-L, Qiu X, Lin J-Y, Chen X-Y, Zhang Y-M, Hu X-Y, Zhong J-H, Tang S, Li X-Y, Xiang B-D, *et al* (2021) Potential Role and Clinical Value of PPP2CA in Hepatocellular Carcinoma. *J Clin Transl Hepatol* 000: 000–000

Yang Y, Huang Q, Lu Y, Li X & Huang S (2012) Reactivating PP2A by FTY720 as a novel therapy for AML with C-KIT tyrosine kinase domain mutation. *J Cell Biochem* 113: 1314–22

Yau T, Park JW, Finn RS, Cheng A-L, Mathurin P, Edeline J, Kudo M, Han K-H, Harding JJ, Merle P, *et al* (2019) CheckMate 459: A randomized, multi-center phase III study of nivolumab (NIVO) vs sorafenib (SOR) as first-line (1L) treatment in patients (pts) with advanced hepatocellular carcinoma (aHCC). *Ann Oncol* 30: v874–v875

Yin J, Wen M, Cheng J, Hu L, Yang L, Chang X, Zhou Z, Li H, Liu Y & Li J (2022) A Patient With Failed Liver Transplantation After the Use of PD-1 Blockade Combined With Lenvaxen. *Front Med* 9: 712466

Yu G, Yan T, Feng Y, Liu X, Xia Y, Luo H, Wang J-Z & Wang X (2013) Ser9 phosphorylation causes cytoplasmic detention of I2PP2A/SET in Alzheimer disease. *Neurobiol Aging* 34: 1748–1758

Zan Y, Dai Z, Liang L, Deng Y & Dong L (2019) Co-delivery of plantamajoside and sorafenib by a multi-functional nanoparticle to combat the drug resistance of hepatocellular carcinoma through reprograming the tumor hypoxic microenvironment. *Drug Deliv* 26: 1080–1091

Zanuy D, Kotla R, Nussinov R, Teesalu T, Sugahara KN, Aleman C & Haspel N (2013) Sequence dependence of C-end rule peptides in binding and activation of neuropilin-1 receptor. *J Struct Biol* 182: 78–86

Zhang N, Dai L, Qi Y, Di W & Xia P (2013) Combination of FTY720 with cisplatin exhibits antagonistic effects in ovarian cancer cells: role of autophagy. *Int J Oncol* 42: 2053–2059

Zhang X, Brossas JY, Parizot C, Zini JM & Rebollo A (2018) Identification and characterization of novel enhanced cell penetrating peptides for anti-cancer cargo delivery. *Oncotarget* 9: 5944–5957

Zhang X-J, Hu LY, Hu Y, Yang X-T, Tang Y-Y, Tang YY, Li S & Zhu D (2020) Tumor-Penetrating Hierarchically Structured Nanomarker for Imaging-Guided Urinary Monitoring of Cancer. *ACS Sens* 5: 1567–1572

Zhao H, Wu M, Zhu L, Tian Y, Wu M, Li Y, Deng L, Jiang W, Shen W, Wang Z, *et al* (2018) Cell-penetrating Peptide-modified Targeted Drug-loaded Phase-transformation Lipid Nanoparticles Combined with Low-intensity Focused Ultrasound for Precision Theranostics against Hepatocellular Carcinoma. *Theranostics* 8: 1892–1910

Zucman-Rossi J, Villanueva A, Nault J-C & Llovet JM (2015) Genetic Landscape and Biomarkers of Hepatocellular Carcinoma. *Gastroenterology* 149: 1226-1239.e4

8 Annexes

Annexe 1: Classification moléculaire et immunitaire du CHC.

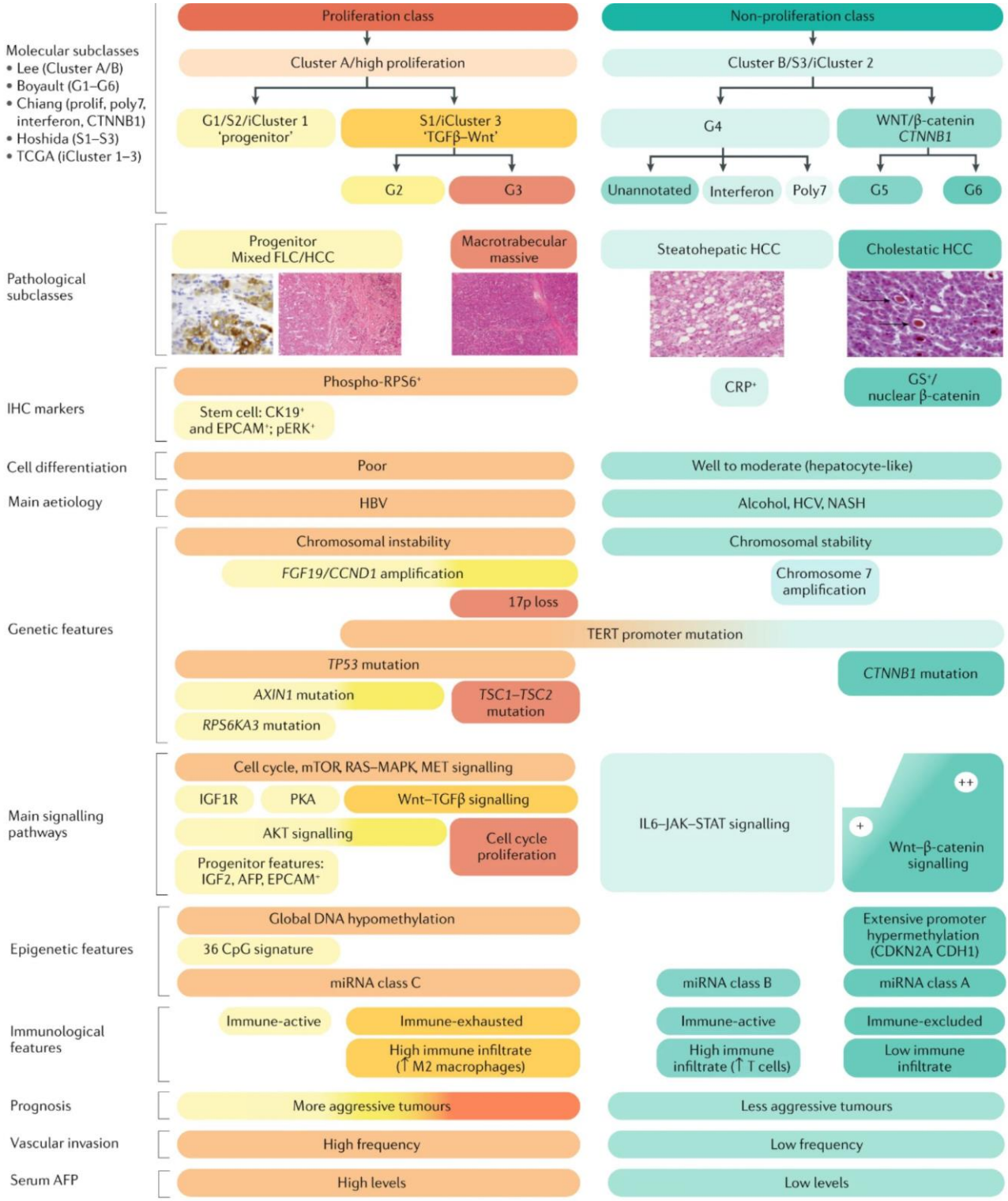

Les CHC peuvent etre classés en deux grands groupes moléculaires basés sur des phénotypes transcriptomiques : une classe prolifération et une classe non-prolifération. 1) La classe prolifération est caractérisée par des tumeurs à faible différenciation histologique, avec un taux d'invasion vasculaire élevée et augmentation niveaux de l'α- foetoprotéine (AFP). Cette classe peut être divisée en deux sous-classes : 1i) S1 ou iCluster 3 caractérisé par l'activation de Wnt/TGFβ, qui entraîne un phénotype d'épuisement immunitaire et 1ii) S2 ou iCluster 1, caractérisés par un phénotype de type progéniteur, avec l'expression de marqueurs de cellules souches (CK19, EPCAM) et activation des voies de signalisation IGF2 et EPCAM53. Les tumeurs associées au virus de l'hépatite B (VHB) présentent fréquemment une des voies classiques de prolifération cellulaire telles que les cascades PI3K/AKT/MTOR, RAS–MAPK, MET et IGF. En outre, sont associés à cette classe de fréquentes mutations de TP53, une instabilité chromosomique et une hypométhylation globale de l'ADN. 2) La classe de non prolifération est caractérisée des tumeurs moins agressives avec des différenciations histologiques faible à modérée, des faibles niveaux de d'AFP et des taux invasions vasculaires moins fréquentes. Ces tumeurs sont liées à des hépatites NASH, alcoolique et au virus de l'hépatite C (VHC). Des sous-groupes distincts ont été identifiés dans cette classe : 2i) la sous-classe WNT/β-catenin CTNNB1 qui présente des mutations CTNNB1 fréquentes et l'activation de la voie de signalisation WNT/β-catenin, qui entraîne un phénotype avec faible une infiltration immunitaire et 2ii) la sous-classe interféron qui présente une activation de la voie de signalisation IL6/JAK/STAT, s'accompagne d'un microenvironnement tumoral plus inflammatoire. Cette classe présente une stabilité chromosomique avec de fréquentes mutations du promoteur TERT. FLC, fibrolamellar carcinoma; IHC, immunohistochemistry; miRNA, microRNA; TCGA, The Cancer Genome Atlas. D'après Llovet et al*, 2021.*

Annexe 2: Mécanismes d'action des thérapies systémiques utilisées dans le carcinome hépatocellulaire

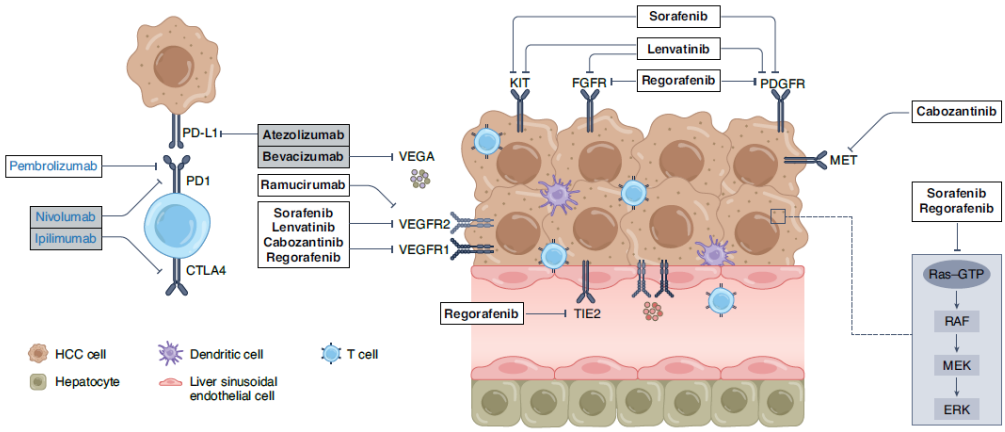

Représentation schématique des relations entre d'une part les TKI, les immunothérapies et les anticorps monoclonaux approuvés dans le CHC sur la base des données des essais de phase III et d'autre part les cellules tumorales, les cellules endothéliales sinusoïdales hépatiques et les lymphocytes. Les traitements en noir ont des résultats positifs basés sur des essais de phase III, soit avec une conception de supériorité (atezolizumab plus bevacizumab, sorafenib, régorafenib, cabozantinib et ramucirumab) soit avec une conception de non-infériorité (lenvatinib). Les traitements en bleu désignent d'autres médicaments approuvés par la FDA (Food and drug administration) sur la base d'essais de phase II non randomisés (pembrolizumab et nivolumab plus ipilimumab). Les cases grises indiquent les thérapies combinées. D'après (Llovet et al, 2022)

Annexe 3: Structure et classification des 21 acides aminés protéinogènes des eucaryotes

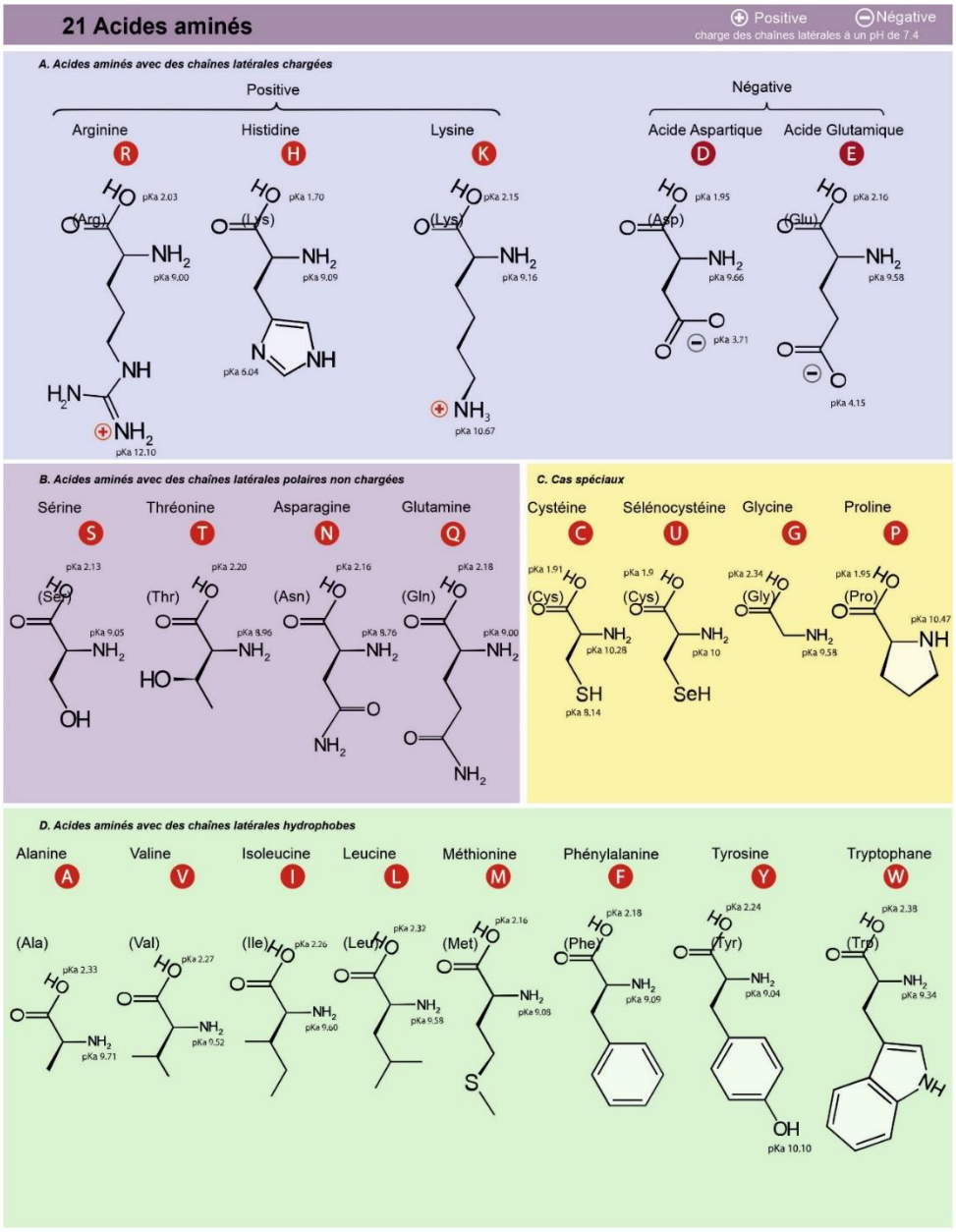

Par File:Amino Acids (Histidine Update 9-19-2014).svg: https://commons.wikimedia.org/wiki/User:Fred_the_Oysterderivative work: Chandres — Ce fichier est dérivé de : Amino Acids (Histidine Update 9-19-2014).svg:, CC BY-SA 3.0, https://commons.wikimedia.org/w/index.php?curid=113292945

Annexe 4: Peptides thérapeutiques approuvés depuis 2000 avec leurs cibles et leurs indications

Cible	Peptide	Année d' approbation	Indication(s)
Récepteur GLP-1	Exenatide	2005	Diabète sucré de type 2
	Liraglutide	2009	
	Lixisenatide	2013	
	Albiglutide	2014	
	Dulaglutide	2014	
	Semaglutide	2017	
Récepteur GLP-2	Teduglutide	2012	Malabsorption et syndrome de grêle court
Récepteur GC-C	Linaclotide	2012	Syndrome de l'intestin irritable avec constipation et constipation chronique idiopathique
Récepteur de la calcitonine	Pramlintide	2005	Diabète de type 1 ou 2
Récepteur du GnRH	Abarelix	2003	Cancer avancé de la prostate
	Degarelix	2008	
Fixation au site actif du protéasome 20S	Carfilzomib	2012	Myélome multiple
Protéine NOD2	Mifamurtide	2009	Ostéosarcome de haut grade, réséquable et non métastatique
Récepteur VIP1	Aviptadil	2009	Dysfonction érectile
Récepteur OT	Atosiban	2000	Accouchement prématuré imminent
	Carbetocin	2001	Hémorragie du post-partum
Récepteur TRH	Taltirelin	2000	Dégénération spinocérébelleuse
Récepteur MC	Bremelanotide	2019	Trouble du désir sexuel hypoactif
Récepteur PTH1	Teriparatide	2002	Ostéoporose
	Abaloparatide	2017	
Guanylate cyclase C	Plecanatide	2017	Constipation chronique idiopathique
NPR-A	Nesiritide	2001	Décompensation cardiaque aigue
Récepteur AT1	Angiotensine II	2017	Sepsis et choc septique
Beta2-récepteur	Icatibant	2008	Angioedeme hétéridaire aigue
Gp41	Enfuvirtide	2003	VIH-1 en combinaison de traitement
Récepteur GHRH	Tesamorelin	2010	Lipodystrophie du VIH
Canaux calcique de type N	Ziconotide	2004	Douleur chronique sévère
Récepteur de la thrombopoïétine	Romiplostim	2008	Purpura thrombopénique immun chronique
Récepteur de l'érythropoïétine humaine	Peginesatide	2012	Anémie de l'insuffisance rénale chronique
Surfactant pulmonaire	Lucinactant	2012	Prévention du syndrome de détresse respiratoire
CaSR	Etelcalcetide	2016	Hyperparathyroïdie secondaire
Récepteur MC1	Afamelanotide	2014	Prévention de la photo toxicité
Récepteur de la somatostatine	Pasireotide	2012	Syndrome de Cushing
	Lutetium Lu 177 dotatate	2018	Traitement des tumeurs neuroendocrines gastro-entero-pancréatiques avec récepteur de la somatostatine positif
	Edotreotide gallium Ga-68	2019	Diagnostic des tumeurs neuroendocrines avec récepteur de la somatostatine positif
Récepteur de la melanocortine-4	Setmelanotide	2020	Obésité

D'après Wang *et al*, 2022. Les peptides anticancéreux sont surlignés en jaune.

Annexe 5: Exemples de peptides et leurs applications en cours d'évaluation dans des essais cliniques

Phase d'essai clinique	Nom du peptide	Indication en cours d'investigation
IV	Avexitide	Hypoglycémie
	Calcitonin gene-related peptide	Migraine
	Corticorelin	Œdème cérébral, tumeur cérébrale
	Leptin	Lipodystrophie; obésité
	Thymalfasin	Cirrhose du foie, sepsis
III	Aclerastide	Ulcère du pied diabétique
	Albusomatropin	Déficit en hormone de croissance
	Anamorelin	Cachexie, cancer du poumon non à petites cellules
	G17DT	Différentes formes de cancer
	Insulin peglispro	Diabète
	Lenomorelin	Tumeurs malignes
	Selepressin	Choc, choc septique
	Somapacitan	Déficit de l'adulte en hormone de croissance
	Taspoglutide	Diabète de type
	Thymosin beta-4	Syndromes secs
	Tirzepatide	Diabète de type
	Ularitide	Décompensation cardiaque
	Vapreotide	Hémorragie digestive par rupture de varices oesophagiennes, hypertension portale, varices oesophagiennes
	Vosoritide	Achondroplasie
	Zoptarelin doxorubicin	Cancer de l'endomètre, cancer de prostate
II	Angiotensin -1-7	Anomalies des cellules sanguines périphériques de la lignée blanches
	Bombesin	cancer de prostate
	Cenderitide	Insuffisance cardiaque
	Deslorelin	Puberté précoce
	Gastric inhibitory polypeptide	Diabète de type
	MK-3207	Migraine
	Olcegepant	Migraine
	Pancreatic Polypeptide	Diabète de type
	Peptide YY (3-36)	Maladie métabolique, obésité
	Pirnabine	Constipation chronique idiopathique
	Somatoprim	Acromegalie
	Somatropin pegol	Déficit en hormone de croissance
	ThyrotropinC	Goitre bénin toxique et non-toxique, goitre, nodule thyroïdien
	TT-232	Adénocarcinome rénal
I	BPI-3016	Diabète de type
	NBI-6024	Diabète de type

D'après Wang *et al*, 2022. Les peptides anticancéreux sont surlignés en jaune.